Shengrui Wang · Zhihao Wu

DGT-based Measurement of Phosphorus in Sediment Microzones and Rhizospheres

Springer

DGT-based Measurement of Phosphorus in Sediment Microzones and Rhizospheres

Shengrui Wang · Zhihao Wu

DGT-based Measurement of Phosphorus in Sediment Microzones and Rhizospheres

Springer

Shengrui Wang
Chinese Research Academy
of Environmental Sciences
Beijing
People's Republic of China

Zhihao Wu
Chinese Research Academy
of Environmental Sciences
Beijing
People's Republic of China

ISBN 978-981-10-0720-0 ISBN 978-981-10-0721-7 (eBook)
DOI 10.1007/978-981-10-0721-7

Library of Congress Control Number: 2016934432

Printed on acid-free paper

This Springer imprint is published by Springer Nature
The registered company is Springer Science+Business Media Singapore Pte Ltd.

Preface

The Diffusion Gradients in Thin films (DGT) technique is an advanced sediment sampler, which can measure concentration and flux of pollutants in porewater on high spatial resolution. DGT has the functions as following, (1) in situ measurement; (2) time-averaged concentration; (3) the speciation of analyte (labile species); (4) bioavailability (effective concentration); (5) concentrations in solution and pore water in sediment/soil; (6) kinetic or thermodynamics parameter; (7) the measurement at high spatial resolution (<1 mm); (8) 2-dimensional concentration image; (9) DIFS (DGT-induced fluxes in sediment) model. However, the previous DGT papers have seldom researched P-release across sediment/water interface (SWI) or P-transfer across sediment/root interface, and the conventional research methods (linear distribution coefficient (K_d), a non-linear adsorption isotherm (Freundlich or Langmuir), or sequential extraction procedures) cannot perform in situ measurement of elements at environmental interface with high spatial resolution or reveal the "real" kinetic P-release or bioavailability at microzone. In this book, DGT and the related techniques have been developed in order to reveal the P-transfer and the kinetic exchange at SWI (Dianchi lake) or sediment/root interface (Erhai lake). Dianchi is an eutrophic lake and the extensive blue algal blooms have happened frequently since 1993. The nutrient level of Erhai lake is changing from mesotrophication to eutrophication in recent years. "Internal P-loading" in Dianchi lake, can engender P-release from the sediment and increase total dissolved P in overlying water and porewater regardless of "external P-loading." So, it is important to research the mechanism of "internal P-loading" and the geochemical reactions for P-release. The roots of aquatic plants play a key role for the uptake of appreciable quantities of nutrient from sediments. The new technique in the field of ecological engineering—the cultivation of aquatic plants has been used for the ecological restoration of lake eutrophication in Erhai lake. So, it is significant to research the P-uptake mechanism of roots and P-transfer across sediment/root interface. In this DGT research for lake interfaces, DGT and the related techniques have been developed in order to perform the following tasks: (1) the simultaneous measurement of P and the related elements (Fe and S(-II)) at fine scales at SWI,

(2) the numerical simulation of kinetic exchange of P across DGT/porewater/sediment interface, (3) the measurement of S(-II)- and Fe- microniches, (4) the DGT test at rhizosphere of aquatic plants, and (5) the assessment of mechanism of "internal P-loading" (Dianchi lake) or P taken up by roots (Erhai lake).

DGT technique and the related methods (the multi-layer-binding gel DGT, DIFS-DGT Induced Fluxes in Sediments, CID—computer imaging densitometry, LA-ICP-MS-laser ablation inductively coupled plasma mass spectrometry and DGT method for rhizosphere), were used to solve the following problems related to P-release and -transfer across SWI or sediment/root interface, including: (1) What geochemical reactions determine the "internal P-loading" and P-release in sediment; (2) How do the kinetic parameter and sediment-P pool determine P-release/-diffusion across DGT/porewater/sediment interface? (3) How are Fe- or S(-II)-microniche in sediment microzone measured for the prediction of the P-release or the coupled Fe-S(-II)-P reaction? (4) DGT's function to mimic P taken up by roots. Using DGT probes and the related methods, the above questions have been answered perfectly. This book consists of four parts, including the following contents: Part I The Basic Theory and Methodology, mainly introducing the basic theory of P-process at SWI in lake, the eutrophic problem; the DGT techniques used in this book (multi-layer-binding-gel DGT probe, DIFS, CID, LA-ICP-MS, DGT test method at SWI and rhizosphere), and the element uptake mechanism by plant root; Part II "Internal P-Loading" at SWI, mainly introduces the P-process at SWI of lake, the assessment of "internal P-loading," kinetic P-exchange across DGT/porewater/sediment, S(-II)- and Fe-microniches assessment for the prediction of P-release; Part III The P Behavior at the Sediment/Root Interface of Aquatic Plants, mainly introducing the DGT test in situ at rhizosphere and in rhizobox; and DGT as a surrogate to mimic P taken up by plant root; The Conclusion and Prospect (Chap. 9), mainly introducing the main conclusions about "internal P-loading" mechanism, geochemical reactions for P-release, the calculation for kinetic P-release at SWI, the assessment for "internal P-loading," Fe- and S(-II)-microniche for the prediction of the P-release and the coupled Fe-S(-II)-P reaction, the assessment of DGT as a surrogate to predict P-uptake by root and P-content in plant tissues, and the prospect for the sensing techniques such as: DGT-optode sandwich sensors for the images with multi-parameters in sediment microzone or rhizosphere.

The DGT investigate for lake interfaces in this book should reflect the latest research advances for P-transfer across SWI or sediment/root interface and assessment methods for "internal P-loading" of eutrophic lake, and may develop the new directions for the research of the mobility of P and other elements in lake interfaces or chemical images of solutes in sediments.

All chapters were subject to the peer-reviewing and revision processes. We would like to thank the following researchers because of their helps for the research or writing for this book, including: Prof. Hao Zhang in "Lancaster Environment Centre, Lancaster University" for the production of DGT assemblies and the suggestion for DGT research; Mingyue Hu, Linghao Zhao and Dongyang Sun in "Institute of National Research Center for Geoanalysis of China" for LA-ICP-MS analysis; Gengtian Ma in "the Institute of Geophysical and Geochemical

Exploration of China" for HR-ICP-MS analysis; Prof. Fengchang Wu, Lixin Jiao, Wenbin Liu, Yuanzhi Xu, Haichao Zhao, Yanping Li, Li Zhang, Yanli Yang, Junli Zhou and Zhaokui Ni in "Research Center of Lake Eco-environment, Chinese Research Academy of Environmental Sciences" for the experiment in Dianchi and Erhai lakes and writing; Prof. Mengchang He in "School of Environment, Beijing Normal University, Beijing, P. R. China" for the suggestion about writing this book.

The DGT research in this book was sponsored by the National Natural Science Foundation of China (No. U1202235), National High-level Personnel of Special Support Program (10000 people plan, No. 2012002001), the National Critical Patented Project for Water Pollution Control and Management (2012ZX07102-004), and the China Postdoctoral Science Foundation (2013M541002).

Please forgive us due to the time constraints for writing. If the reader has found anything that needs to be improved in the book, please propose the valuable suggestion

Beijing, People's Republic of China — Shengrui Wang
October 2015 — Zhihao Wu

Contents

List of Figures

List of Tables

Abstract

The P-process and the mechanism of P-transfer at sediment/water interface (SWI) based on DGT (Diffusive Gradients in Thin Films) technique at two lakes (Dianchi and Erhai lakes) are investigated in this book. In general, the main research content includes the basic theory and methodology of DGT technique for P-process in lake sediment; "internal P-loading" at SWI investigated by DGT technique (Dianchi lake); the P-behavior at the sediment/root interface of aquatic plants (Erhai lake); and the research conclusion and prospect for DGT technique. Using DGT technique and the related methods (the multi-binding-layer DGT for SWI, DIFS-DGT Induced Fluxes in Sediments, CID—computer imaging densitometry, LA-ICP-MS-laser ablation inductively coupled plasma mass spectrometry and DGT method for P-process at rhizosphere in lake), P-release mechanism and the quantification for "internal P-loading" of lake sediment, the kinetic P-exchange across DGT/porewater/sediment interface, sulfide image at fine scale for sulfide microniche and Fe-S(-II)-P geochemical reaction for P-release, Fe-image at fine scale for the verification of existence of Fe microniche and the prediction of P-release from Fe microniche, and DGT assembly for the measurement at rhizosphere, which is a surrogate for the assessment of P-uptake by aquatic plant root, can be investigated in detail. DGT technique, a powerful tool with multi-functions, and its significance for the research of P-transfer and kinetic process at sediment microzone and rhizosphere, has also been discussed and assessed.

Keywords Sediment/water interface (SWI) · Diffusive gradients in thin films (DGT) technique · Internal P-loading · DIFS-DGT-induced fluxes in sediments and soils · CID—computer imaging densitometry · LA-ICP-MS-laser ablation inductively coupled plasma mass spectrometry · Rhizosphere · Microniche

Part I
The Basic Theory and Methodology

Chapter 1
The Basic Theory of P-process at Sediment/Water Interface (SWI) in Lake

Element distributions in porewater provide the considerable information about the intensities of physical, chemical, and biological processes in sediments, while sediments are the principal sink/sources for metals, sulfide, or phosphorus in lake. In many studies, the sediment/water exchange has been proved to play a dominant role in the ecological cycle of phosphorus (P), sulfide (S), or metal. The measurement method for contaminants in sediments, and the assessment of P-release risk or sediment reactivity using DGT technique have been researched for the objectives of the determination of the extent to which the sediments are either a source or a sink for contaminants or the evaluation of the effects of these contaminants on the eutrophic status of water body. Moreover, DGT can also be used to mimic the element-uptake by plant root. In two Chinese lakes (Dianchi and Erhai lakes), the determination of multi-kinds of elements at the same location in sediment profile, the kinetic process of P at sediment/water interface (SWI), DGT image for S(-II) or Fe for the coupled reaction for P-release, the assessment of DGT as the proxy of root of aquatic plant for P-uptake, and the investigation of the mechanism of "internal P-loading" and P-transfer across sediment/root interface would be introduced in the next chapters. In this Chapter, the "internal P-loading," P-release mechanism, DGT technique for SWI of lake, and P-uptake by root investigated by DGT technique are summarized and discussed.

1.1 "Internal P-loading" and P-release Mechanisms in Lake Sediments

In China, there are a lot of lakes with the total reservoir capacity of 6.38×10^{11} m^3 and 2300 lakes have the area of more than 1 km^2 (Chinese Research Academy of Environmental Sciences 2014). Lakes are the main sources of water supply for inland water, and fifty percent of the drinking water source is from lakes. However,

S. Wang and Z. Wu, *DGT-based Measurement of Phosphorus in Sediment Microzones and Rhizospheres*, DOI 10.1007/978-981-10-0721-7_1

the water quality of fifty-seven percent of the state control key lakes and reservoirs belong to V class and substandard V class. Among those water bodies, in Taihu Lake, Dianchi Lake and Chao Lake, the extensive blue algal blooms have occurred frequently in recent years and the degeneration of aquatic ecosystem becomes serious. The lake pollution, especially lake eutrophication, has become the main problem in the field of lake environment (Chinese Research Academy of Environmental Sciences 2014).

Phosphorus (P) is the limiting factor for the lake eutrophication, and there are two kinds of the sources of P in lakes, including "external P-loading" and "internal P-loading." Even if the "external P-loading" is controlled, the "internal P-loading" can still influence the extent of lake eutrophication (Jin et al. 2008). The internal loading of lakes includes "internal P-loading" in water body (biological internal loading, especially algal) and in sediments. Sediment is the important pool for lake nutrients and the main source of the internal P-loading of lakes. The physico-chemical properties and the environmental process of P and related elements such as metals can have important influences on the P-release from sediments. So, the investigation of P-transfer and P-transformation across SWI plays an important role on the controlling lake eutrophication (David 1998).

P is an important nutrient element and is one of the limiting elements for the occurrence of algal blooms in lakes. In the eutrophic lake Dianchi (the southeast of China), the controlling methods for P eutrophication include the controlling technique for the P discharge into lake and the improvement of treatment methods for wastewater containing P. Despite the mentioned strategies for the control of P pollution, the extensive blue algal blooms have still occurred frequently in recent years and the algae biomass was 4.24×10^6 to 1.04×10^9 cell L^{-1} in 2013 (Chinese Research Academy of Environmental Sciences 2014). Dianchi Lake has failed to recover from eutrophic status partially because of P-release from the sediment ("internal P-loading"). The reason is that sediments are both the sink and the pool for P in water body and play an important role for P cycle in water ecological system in lakes. At SWI, the continuous transfer and transformation occur frequently. In certain environmental condition, P in sediments can be released into overlying water and have the important influence on water quality and eutrophic status in lakes. So, the understanding of the mechanism of "internal P-loading" is the important scientific problem for the controlling lake eutrophication and the restoration of ecological water system.

The interface between the sediment and the overlying water is the locus of activity which, in principal, determines most of the postdepositional static and dynamic behavior of the entire sediment down to depths at which the geothermal and geochemical diagenetic processes become substantial (Kennett 1982; Parsons and Sclater 1977; Hulbert et al. 2002). However, the knowledge of the interface characteristics and processes at SWI is so fragmentary that we can use it, at best, to create only a rudimentary description of the properties and environmental behavior at the interface and sediment. Both the observational data and the theoretical framework characterizing the interface and the environmental processes which occur there are deficient (Hulbert et al. 2002). P forms in sediments as inorganic

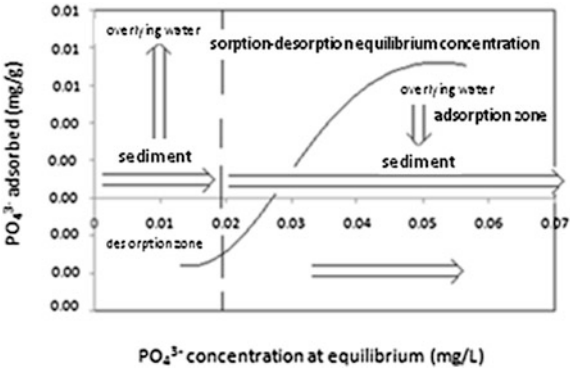

Fig. 1.1 The schematic graphic for the P sorption/desorption process across sediment/water interface (SWI) based on adsorption and desorption isotherm

(PO_4^{3-}, Pi) or organic (R-C-O-PO_3^{2-} of R-PO_3^{2-}, Porg) are associated with minerals (Fe–P, Al–P, or Ca–P) and the organic P. The remobilization of P from sediment was influenced by redox conditions, pH, P speciation in sediment, Fe (III) hydroxyoxide, and sulfate-reduction. Under anaerobic condition, soluble reactive phosphorus (SRP) can be released from inorganic P in sediments through the reduction of Fe (III) hydroxyoxide. The P-release from algae biomass or organic matter can also contribute to "internal P-loading." The P-release from bottom sediment into water column can engender "internal P-loading" (Cook et al. 2010; Wu et al. 2015a, b, c) and lake eutrophication (Palmer-Felgate et al. 2011). Moreover, researchers such as Roden and Edmonds (1997) and Ding et al. (2012) have revealed an indirect reduction mechanism for P-release, which is due to P-release from Fe (III) hydroxyoxide and the enhanced formation of insoluble FeS because of sulfide-reducing bacteria. "Internal P-loading" happens if the environmental conditions within sediments of a lake allow for P-release into the water column, thereby increases the TP (specifically available or reactive P (RP)) in the water column, regardless of the decrease of "external P-loading."

The schematic graphics for the sorption/desorption process or P-process across the sediment/water interface (SWI) are indicated in Figs. 1.1 and 1.2, in turn.

1.2 Diffusive Gradients in Thin Films (DGT) Technique and the Development Trend for the Application at SWI or Rhizosphere

DGT (diffusive gradients in thin films) technique is a passive sampling method, which has been applied widely in the fields of environmental science and analytical chemistry. This technique was invented by Davison et al. (1994) in Lancaster University and

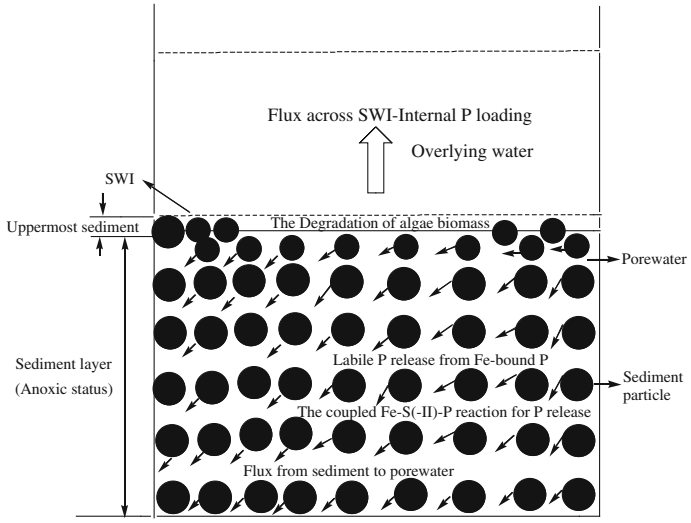

Fig. 1.2 The P-process at the sediment/water interface (SWI)

used for the test of trace metals in seawater initially. One year later, DGT was used for the measurement of trace metals at the high spatial resolution in sediments. The schematic graph for the DGT probe and piston devices is indicated in Fig. 1.3. DGT technique is developed based on DET (diffusive equilibration in thin films) technique, while DET technique was invented in 1991 (Davison et al. 1991). DET assembly consists of a thin film of hydrogel containing 95 % water in probe framework, which is inserted into sediments. Solute equilibration between the water within the gel and the porewater occurs. Normally, the DET or DGT probe can be retrieved after 24 h-deployment in sediments. Then, the DGT-binding gel or DET hydrogel can be eluted by elution solution, which is analyzed by instruments (Zhang et al. 1995; Fones et al. 2004). Initially, DET/DGT assembly can be used for the determination of solutes with high concentrations, including Fe and Mn (Fones et al. 2004; Davison et al. 1994), the major anions (Österlund et al. 2010) and major cations (Zhang and Davison 1999). But, DET technique is difficult to analyze elution solutions from small volumes of gel. The continued improvement in analytical technique, particularly inductively coupled plasma mass spectrometry (ICP-MS), made it possible to measure trace metals by DET in some studies (Docekalová et al. 2002; Morford et al. 2003; Leemakers et al. 2005). In the improved DGT assembly, one binding gel layer is introduced behind the diffusive layer of hydrogel, which allows trace solutes, such as metals to accumulate progressively with time, greatly improving the detection limits compared to DET.

The basis of the technique is fundamentally changed from the simple equilibration of DET to a dynamic measurement of a flux of the solute. DGT perturbs environment medium and removes solute. The subsequent measurement method determines the accumulated mass for the exposure area of DGT window in a given time, which is the time-averaged flux of DGT. The magnitude of flux depends on

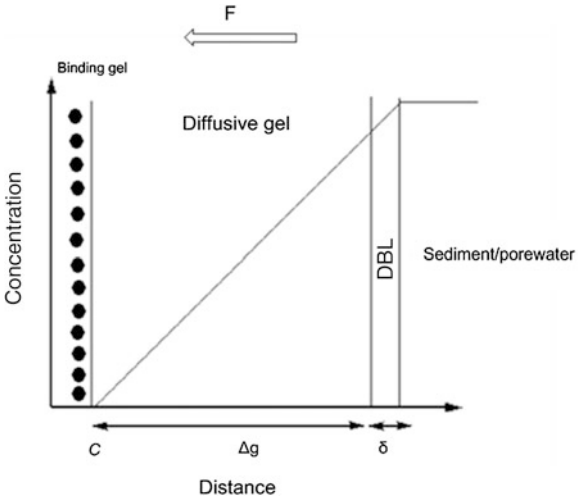

Fig. 1.3 The schematic graph for the DGT probe and piston devices (Reprinted from Arch. Environ. Con. Tox., published online (doi:10.1007/s00244-015-0184-1), Wu, Z.H., Jiao, L.X., Wang, S.R., Xu, Y.Z., Multi-metals Measured at Sediment–Water Interface (SWI) by Diffusive Gradients in Thin Films (DGT) Technique for Geochemical Research, copyright (2015), with the permission from Springer; Reprinted from Anal. Chim. Acta., 368, 243–253, Chang, L.Y., Davison, W., Zhang, H., Kelly, M., Performance characteristics for the measurement of Cs and Sr by diffusive gradients in thin films (DGT), copyright (1998), with the permission from Elsevier; Reprinted (adapted) with permission from (Environ. Sci. Technol., 45: 6080–6087, Williams, P.N., Zhang, H., Davison, W., Meharg, A.A., Norton, G.J., Organic matter—solid Phase interactions are critical for predicting Arsenic release and plant uptake in Bangladesh paddy soils), copyright (2011), American Chemical Society)

the response of dynamic response of the medium to the perturbation of solute removal. When DGT assembly is deployed in sediment/soil, it can give the information of solute supply. The dynamic interaction between DGT and sediment/soil can be explained by numerical model, which is helpful to a full and quantitative understanding of the theory of DGT test (Harper et al. 1998).

DGT can determine trace inorganic matter (metals, cations, and anions) in surface water (river, lake, and sea) and porewater in sediment/soil, which can be used for the research of bioavailability and environmental process. It has been widely used in the research institutions of the world and the reliable functions have been verified (User's guide to DGT technique 2003). DGT can determine 55 elements and among them, the measurement of 24 elements is accurate and reliable absolutely (Garmo et al. 2003). DGT has the functions as following: (1) in situ measurement; (2) time-averaged concentration; (3) the speciation of analyte (labile species); (4) bioavailability (effective concentration); (5) concentrations in solution and porewater in sediment/soil; (6) kinetic or thermodynamics parameter; (7) the measurement at high spatial resolution (<1 mm); (8) two-dimensional concentration image (Ding et al. 2012); and (9) DIFS (DGT-induced fluxes in sediments) model

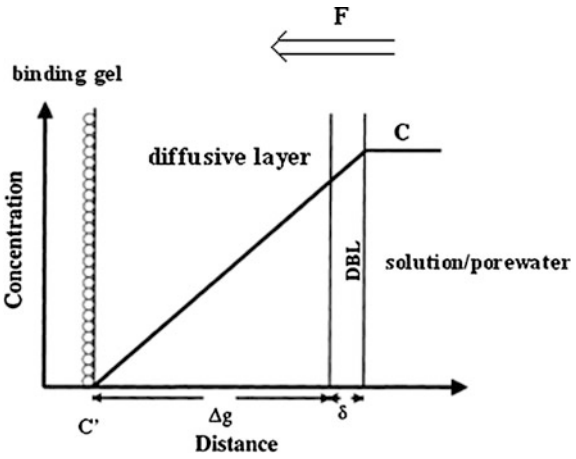

Fig. 1.4 The schematic graphic for concentration gradient in diffusion layer of DGT (Reprinted from Arch. Environ. Con. Tox., published online (doi:10.1007/s00244-015-0184-1), Wu, Z.H., Jiao, L.X., Wang, S.R., Xu, Y.Z., Multi-metals Measured at Sediment–Water Interface (SWI) by Diffusive Gradients in Thin Films (DGT) Technique for Geochemical Research, copyright (2015), with the permission from Springer)

(User's guide to DGT technique 2003). DGT is a passive sampling technique, which has been used for the measurement of trace elements in water and porewater in soil or sediment. It determines the solute mass which diffuses through diffusive gel and filter and forms the diffusive gradient. The solute can be bound by binding gel after it diffuses through diffusive gel. The binding gel behind the diffusive gel can remove solutes continuously and keep the concentration gradient during deployment time (Fig. 1.4). The designation of the structure of DGT enables the calculation of time-averaged flux (F) toward the DGT resin and the time-averaged concentration (C_{DGT}) in the interface of DGT/solution. The calculation equations are as follows:

$$F = M/At \tag{1.1}$$

$$C_{DGT} = M\Delta g/DAt \tag{1.2}$$

where deployment time is t; exposure area is A; the diffusive coefficient in diffusive layer is D; the thickness of diffusive layer is Δg (omitting the diffusive boundary layer-DBL); and the mass accumulated on binding gel is M. Typically, M is the measured solute mass after the gel elution. D can be determined by diffusion cell (Zhang and Davison 1999), and the D values of some solutes as the function of temperature can be found in one reference (User's guide to DGT technique 2003). Typically, Chelex-100 (Bio-Rad, Hercules, CA), AgI, and ferrihydrite gels in DGT devices can be used for the measurements of polyvalent metal cations, inorganic sulfide, and P, in turn (User's guide to DGT technique 2003).

For the measurement at the high spatial resolution by DGT probe, some methods have been used to determine metals or P, including slice and elution for binding gel and subsequent ICP-MS analysis (1 mm-resolution); PIXE (Davison et al. 1997) or Laser-ablation-ICP-MS (Santner et al. 2010; Warnken et al. 2004). The sulfide bound by AgI gel can be determined by gray-scan method (Teasdale et al. 1999).

The methods mentioned above can achieve the spatial resolution of 100 μm (PIXE, Laser-ablation-ICP-MS, and AgI gel).

When DGT is deployed in sediment, DGT as a sink for solute depletes the porewater adjacent to DGT window and the labile species in particles of sediment can supply for this depletion. The ratio of the average concentration at the DGT surface to the concentration in the bulk porewater, C_{soln}, measured by other techniques, is given as R. Three cases may arise related to the DGT-induced flux and the interfacial concentration (Fig. 1.5), including: (a) fully sustained ($R > 0.95$); (b) diffusion only ($R < 0.10$); and (c) partially sustained ($0.10 < R < 0.95$) (User's guide to DGT technique 2013). R is the indicator of the extent of the depletion of sediment solution concentration at the DGT/sediment interface.

"The environmental process at SWI" is the research focused in the field of sedimentology and aquatic science. So, it is necessary to research the element-transfer at SWI, the kinetic process of sorption/diffusion, the mechanism and source for element-release, and the effect of microorganism activity and physical perturbation on element-release at environmental interface. The dynamic condition of elements at SWI is significant, and the nonstable condition and the steep chemical gradient can be formed. The techniques for the accurate determination of the steep concentration profile are required because of the most importance of measuring accurate concentration gradient and flux at SWI. The composition of porewater in sediments is perhaps the most sensitive indicator of the types and the extent of reactions that take place between the pollutant-loaded sediment particle and the aqueous phase that contacts it (Förstner 2004). However, the porewater is customarily recovered from sediments by leaching (Förstner 2004; Ruban et al. 2001; Tessier et al. 1979),

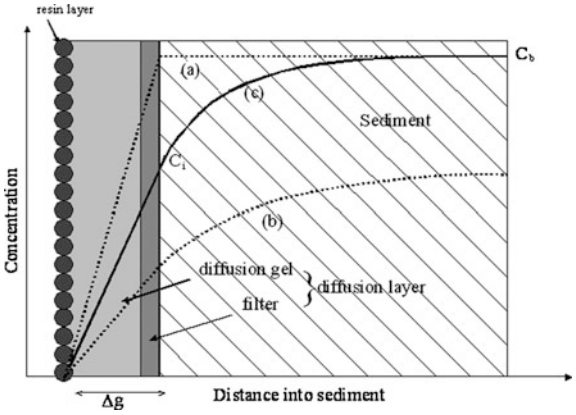

Fig. 1.5 The schematic graph for the representation of the concentration of labile element in a DGT piston and adjacent porewater during deployment. Fully sustained (*case a*), partially sustained (*case c*), or diffusion only (*case b*) by resupply from the solid phase in sediment (Reprinted from Environ. Pollu., 159: 1123–1128, Wu, Z.H., He, M.C., Lin, C.Y., In situ measurements of concentrations of Cd, Co, Fe and Mn in estuarine porewater using DGT, copyright (2011), with the permission from Elsevier)

centrifugation or squeezing (Bender et al. 1987), coring, and centrifugation (Hamilton-Taylor and Morris 1985) or sippers (Watson and Frickers 1990), and the measurement results using those methods are not perfect. Squeezing of sediment core can engender porewater passing through different layers of sediment where artificial reaction may occur. Centrifugation, in particular, often requires rigorous care to ensure all handling is carried out in an anoxic atmosphere. Dialysis peepers (centimeter to subcentimeter resolution) usually require typically days/weeks and often modify the redox state of the system during deployment.

DGT measurement can reflect the horizontal and vertical distribution at high spatial resolution of millimeter or submillimeter in sediment porewater (Zhang et al. 1995; Davison et al. 1997). The seasonal change of the chemical gradient of trace elements in porewater and the measurement at fine spatial scale can be used to determine the detailed site, the coupled reaction, and the microorganism activity (Wu et al. 2015a, b, c). DGT has been used for the measurement of multi-elements, and based on the measurement results, the microenvironmental condition, and the sediment property, the geochemical process of elements at SWI can be investigated. For example, Zhang et al. (2002) have investigated the geochemical reactions of Fe, Mn, Co, Ni, and As at SWI of Loch Duich off the west coast of Scotland; Naylor et al. (2004) have investigated the simultaneous release of Fe, Mn, Ni, Zn, and S(-II) in sediments at Fleetwood, Lancashire, United Kingdom, using the coupled Chelex/AgI-DGT probes. Gao et al. (2010) have investigated the mobility of ^{226}Ra using MnO_2-resin DGT in sediments of the Winterbeek. Monbet et al. (2008) have used DET and DGT for the investigation of DRP (dissolved reactive phosphorus) profiles in sediment porewater in two lagoons of the Gippsland Lakes (SE Australia) and the reactivity kinetics for P-release using dynamic numerical model. Chang et al. (1998) and Garmo et al. (2006) have investigated radioactive rare elements and lanthanide. Davison et al. (1997), Warnken et al. (2004), Santner et al. (2010), Ding et al. (2012, 2013), and Gao et al. (2015) have investigated the chemical images at ultra-high spatial resolutions of metals, sulfide, and P in sediment porewater. Ernstberger et al. (2002) have conducted the numerical calculation for the environmental process of metals at microinterface of DGT/sediment. The preparation methods for the binding gel with new types and the new measurement methods have also been developed in recent years (Lucas et al. 2012; Bennett et al. 2011; Panther et al. 2010, 2012; Dočekalová and Diviš 2005; Ding et al. 2012; Moorleghem et al. 2011).

The biogeochemical reaction in sediment porewater (adsorption and release) in sea, lake, and river can be investigated by element profiles and flux in sediment porewater profiles (Hamilton-Taylor and Morris 1985). Hydrogen sulfide in sediment can be engendered under anoxic conditions and by the microbially mediated reactions. Beside the large proportion of reoxidized H_2S, a part of sulfide reacts and metal sulfides such as pyrite (FeS_2) are formed in marine or estuarine environment. Moreover, other metals can also form metal sulfides and trace metals can be coprecipitated or adsorbed on minerals such as iron sulfides (Morse and Luther 1999; Rickard 1997).

The electron acceptors (O_2, SO_4^{2-}, Fe^{3+}, Mn^{4+}, and NO_3^-) play an important role in the oxidation process of organic matter in sediments (Zhang et al. 1995; Tessier 1992). The reduction of solid Fe or Mn oxides to the reduced and dissolved Fe^{2+} or Mn^{2+} can induce the release of other trace metals adsorbed or bound to them. The decomposition of labile organic matter can engender inorganic N, P, and metals. So, the biogeochemical reactions of organic matter can bring out the interrelated chemical gradients in the SWI under redox condition. The redox sensitive metals are commonly Fe and Mn (Fones et al. 2004). The oxidation species Mn^{3+} and Mn^{4+} can be formed under conditions of high pH and Eh. Mn^{2+} can be formed under low pH and Eh. Mn redox cycling responses to Eh conditions in sediment layer and Mn reduction are mainly by bacterial reduction of Mn oxides, which includes two types of reduction processes (indirect and direct) (Myers and Nealson 1993).

Lake sediments can act as both a sink and a source of P and are comprised of complex mineral aggregates, water, and in(organic) components. P can be sorbed to Fe, Mn, and Al hydroxyoxide minerals in sediments and be permanently or temporarily removed from water. The physical, chemical, and biological processes, inducing P-release from sediment, include desorption, ligand exchange, particle dissolution, mineralization, and the release from living cells (Christophoridis and Fytianos 2006). Physicochemical parameters such as temperature, pH, redox potential, nitrates, sulfates, bioturbation, and the presence of Ca, Mn, Fe, Al, and Mg have been found to control or play a role in P-release.

P exists in sediments as a soluble anion (orthophosphate, PO_4^{3-}), a precipitated phosphate salt, or as part of a mineral or organic compound. Possible phosphate minerals in lake sediments include stregnite [$FePO_4 \cdot 2H_2O$], vivianite [$Fe_3(PO_4)_2 \cdot 8H_2O$], hydroxyapatite [$Ca_5(PO_4)_3(OH)$], monelite [$CaHPO_4$], and variscite [$AlPO_4 \cdot 2H_2O$]. The redox reactive components in sediments in addition to pH fluctuations and equilibrium gradients are the primary chemical controls of P cycling in sediments.

The insoluble Fe (III) hydroxyoxide can be reduced to soluble Fe(II) and P can be released from the Fe-bound P into surrounding water (Bostrom and Pettersson 1982; Christophoridis and Fytianos 2006). The simultaneous release of DIP (PO_4^{3-}) and Fe^{2+} in equivalent concentrations under anoxic condition has been revealed by a benthic chamber in sediment layer in Gullmarsfjorden, Sweden (Sundby et al. 1986). An indirect P-release mechanism of the coupled reactions (Fe–S–P) has also been discovered by Roden and Edmonds (1997). This mechanism attributes the P-release from Fe (III) hydroxyoxide to the formation of insoluble FeS caused by sulfate-reducing bacteria. The measurement of P/Fe/sulfide at SWI and the investigation of P-transfer across SWI are important to reveal biogeochemical reactions. Moreover, in the microenvironment with the reactive organic matter, the geochemical behavior in this microzone is obviously different from bulk environment at the same depth in sediment (Stockdale et al. 2010). In a microscopic study of marine sediments, Johnson (1974) identified possible food sources with diameters ranging from 5 μm to 1.9 mm. Jørgensen (1977) estimates a

detrital particle scale range from 1 μm to several millimeters/centimeters. The microniche may exist in sediment microzone with such particles.

DGT measurement induces the minor disturbance to be controlled in sediments and the result of the measurement reflects the response of DGT to this disturbance. DGT measurement can derive the information about metal species in seawater (Davison et al. 1994), the remobilization flux with high spatial resolutions in sediments (Zhang et al. 1995), the DGT analysis at the ultra-high spatial resolution (100 μm) in microbial mat in sediments (Davison et al. 1997), and remobilization flux in sediments (Zhang et al. 1998). The main methods for the mentioned DGT tests are based on DGT theory and the subsequent measurement techniques are applied, such as PIXE (proton-induced X-ray emission), LA-ICP-MS (laser ablation inductively coupled plasma mass spectrometry), 2D slicing for binding gel, and mixed-binding gel and combined DGT probe. Based on the DGT experimental results, the environmental condition (pH and Eh) and the theory of biogeochemical reactions, and the remobilization process and release mechanism of metals, sulfide, and P in sediments can be investigated. DGT is an advanced passive sampling technique for the measurements of multi-kinds of labile elements in water, sediment, and soil. It has the advantages, such as (1) the simple instrument framework with multi-layers and easy to operate; (2) the quantification method to calculate time-averaged concentration (C_{DGT}) based on the mass accumulated on binding gel (M_{DGT}); (3) the sample contamination with very low level; and (4) high sensitivity (ultra-trace analysis) and dynamic measurement. DGT can accomplish the following tasks, including water quality monitoring (Sangi 1998; Munksgaard and Parry 2003); chemical speciation in solution (Li et al. 2005; Aung et al. 2008; Jansen et al. 2001); sediment geochemistry (Zhang et al. 2002; Fones et al. 2004); dynamic processes in waters (Levy et al. 2012; Garmo et al. 2006) and soils (Ernstberger et al. 2002, 2005), and bioavailability in waters (Nierop et al. 2002; Meylan et al. 2004; Roulier et al. 2008) and soils (Cattani et al. 2008).

The DGT method for plant rhizosphere in soils has been developed for the elements (metal or P) taken up by plant roots. Environmental risk assessment connected with heavy metal contamination in soils is not easy to research. For most ecological risk investigation, the toxicity of heavy metals is normally related to total content or mechanically extracted species (McLaughlin et al. 1998; Zhang et al. 2001). Though some legislation or guidelines for heavy metals in soil or sediment are based on the total content, the researchers have realized that some fractions in the total metal content are unavailable to plants, microorganisms, or soil fauna. The extraction method for soil or sediment divides the aquatic phase and the plant root or microorganisms and only free ion in soil/sediment solution can reflect the "real"-metal availability (Vulkan et al. 2000; Sauvé et al. 1996; McGrath et al. 1994; Zhang et al. 2001). However, the normal measurement in soil or sediment solution does not consider the element-release from solid phase to resupply the solution due to the depletion by root uptake. The method mentioned above cannot assess element bioavailability to plant effectively because many processes can influence the supply of element to plant, such as diffusional and convective transfer to root, the fresh root surface in sediment or soil due to plant growth, the rhizosphere microenvironment, and root exudates. DGT method for

rhizosphere is based on the diffusional transfer and the resupply from solid phase (Zhang et al. 2001). Labile element fraction can be released from sediment/soil, if root uptake is rapider than diffusional supply. Then, the depletion of element concentration in sediment/soil solution near the root surface can induce the element-transfer from solid into porewater. The element fraction in sediment/soil contributes to plant root uptake and can be transferred from solid into solution. The element fraction in solid phase is believed to be kinetically labile. Nutrients such as Fe, Cu, and Zn can be mobilized from solid into solution by plant root uptake due to the depletion in sediment/soil solution. The potential hazard of a soil/sediment with metals or P can be assessed by the characterization of soil/sediment/root properties. The resupply of elements from sediment pool other than porewater has been realized and the research on the intensity, quantity, and capacity in the initial 60 s in sediment/soil pool has been conducted (Barber 1995; Beckett 1964; Zhang et al. 2001).

The hazard assessment for contaminated soil/sediment has not been improved significantly because of the lack of a simple procedure to assess the kinetic release of element from soil/sediment and the supply to root. Extraction method for soil/sediment justly provides a mechanical classification of element fractions in sediment/soil (Tessier et al. 1979); however, this method is based on the reaction between chemical reagent and solid phase, rather than a real reflection of element lability. The placement DGT resin in soil/sediment can lower element concentration in porewater, and like root, the DGT assembly in soil/sediment can take up the element in soil/sediment (Skogley and Dobermann 1996; Lee et al. 1996; Zhang et al. 2001). Placement of DGT resin in soil/sediment lowers element concentration and it can mimic root uptake (Skogley and Dobermann 1996; Lee et al. 1996; Zhang et al. 2001). A layer of diffusion gel between the resin and the soil/sediment can allow ion and the complexes diffuse freely and limit the uptake rate. DGT calculation method ensures the precise flux and concentration. The DGT measurement for rhizosphere is based on kinetic rather than equilibrium principle (Davison et al. 1994; Zhang et al. 1998). DGT assembly can locally lower element concentrations in porewater and induce element supply from labile fractions and the reactive pool in solid phase (Zhang et al. 2001). The measurement in soil/sediment using DGT technique can derive a new parameter-effective concentration (C_E).

During the period for DGT devices deployment in soil/sediment, soluble labile elements are accumulated in the resin. The mass accumulated in resin-M can be measured. A full numerical model (1D or 2D) for DGT deployment in sediments with various properties has been invented and introduced in detail (Harper et al. 1998, 2000). The numerical model, named DIFS (DGT-induced fluxes in sediments), can be freely available in Web site: http://www.es.lancs.ac.uk/wdgroup/aquach.htm.

The effective concentration (C_E) is the hypothetical porewater concentration that would be needed to accumulate the observed amount of one element on the resin if there was only diffusional supply. The schematic graph of (C_E) related to (C_{DGT}) is indicated in Fig. 1.6.

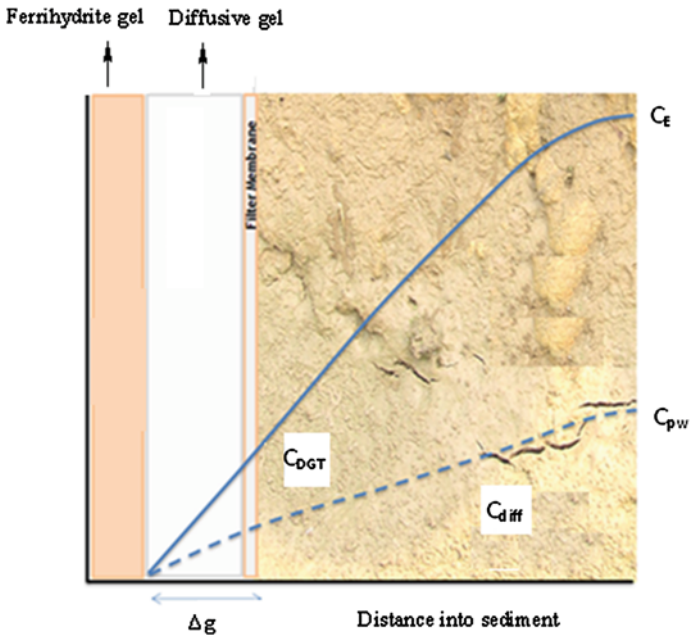

Fig. 1.6 The schematic graph of C_E related to C_{DGT} in soil/sediment solution (Reprinted (adapted) with permission from (Environ. Sci Technol, 45: 6080–6087, Williams, P.N, Zhang, H., Davison, W., Meharg, A.A., Norton, G.J., Organic matter—solid Phase interactions are critical for predicting Arsenic release and plant uptake in Bangladesh paddy soils), copyright (2011), American Chemical Society)

The effective concentration (C_E) differs from C_{DGT} with a factor that depends on the geometry of the device, deployment time, and soil tortuosity. The DGT measured concentration in a sediment C_{DGT} can be converted to (C_E) using Eq. (1.3).

$$C_E = C_{DGT}/R_{diff} \tag{1.3}$$

where R_{diff} is the ratio of C_{DGT} to the sediment solution concentration when supply to the DGT device is only by diffusion. It was calculated using the numerical model of the DGT-sediment system 2D DIFS (DGT-induced fluxes in sediments). It is freely available in two-dimensional form, via the Internet (http://www.es.lancs.ac.uk/wdgroup/aquach.htm).

Ds (the diffusion coefficient in sediment) was calculated using Eqs. (1.4-1.6):

$$\mathrm{Pc} = m/V \tag{1.4}$$

$$\phi = \mathrm{dp}/(\mathrm{Pc} + \mathrm{dp}) \tag{1.5}$$

$$\mathrm{Ds} = D_0/(1 - \ln \phi) \tag{1.6}$$

where m is the total mass of soil particles, V is the porewater volume in a given volume of soil, and dp is the density of the soil particles, which in this model was assumed to be 2.65 g cm^{-3}. The term D_0 refers to the diffusion coefficient in water. The ratio (R) of the DGT measured concentration (C_{DGT}) to the bulk concentration in soil solution (C_{sol}) reflects the extent to which there is dynamic resupply from the soil solid phase (Eq. 1.7):

$$R = C/C_{\mathrm{DGT\,sol}} \tag{1.7}$$

This DGT function has been used for the research of the uptake of metals or P and bioavailability. Mason et al. (2010) have investigated "available P" in soils of Australia using DGT technique, anion exchange resin membrane, and the traditional bicarbonate extraction method of Colwell. The research result indicated that the DGT method predicted plant (wheat) responsiveness to applied P more accurately than Colwell P and resin P, and the measured concentration in soils at the DGT surface, C_{DGT}, explained 74 % of the variation in response to both early dry matter and grain. Williams et al. (2012) have applied DGT in the rice paddy soils in "cancer village" in Southern China from industrial zones impacted by mining waste and assessed the Cd concentrations in rice grain. DGT piston tests (in situ and in laboratory) were conducted in the rice rhizosphere and the results indicated that laboratory- and field-deployed DGT assays and porewater measurements were linearly related to grain concentrations in all but the most contaminated samples where plant toxicity occurred. The laboratory DGT assay was the best predictor of grain Cd concentrations, accommodating differences in soil Cd, pollutant source, and the ratios of Cd/Zn.

1.3 The Uptake and Accumulation Mechanisms for Elements at the Rhizosphere of Aquatic Plant in Lake

The nutrient level of Erhai Lake (southeast of China) is changing from mesotrophication to eutrophication in recent years. The new technique in the field of ecological engineering, the cultivation of aquatic plants for the control of lake eutrophication, has been used for the ecological restoration of Erhai Lake. P can be removed by biomass and harvest. In the unharvested system, immobilization by sorption/precipitation is the other P-removal mechanism. Chemical and physical composition results in the efficiency of the removal process. The limiting nutrient concept has been developed to describe the photosynthesis and its stoichiometry. Redfield et al. (1963) have investigated the reaction of photosynthesis and given the Redfield ratios for composition of biomass, which are indicated as follows:

$$106\,CO_{2(a)} + 16\,NO_3^- + HPO_4^{2-} + 18H^+ + 122\,H_2O \leftrightarrow C_{106}H_{263}O_{110}N_{16}P + 138O_{2(a)} \quad (1.8)$$

The Redfield ratio is the indication for the judgment of whether N or P is potentially limiting for growth. The molar ratio of 16N:1P corresponded with about 7N:1P (mass ratio) is usually used as this judgment criterion. According to the theory introduced by Rast et al. (1989), in the short time (days), only inorganic species can be taken up by plants. Moreover, several environmental factors, including insolation, temperature, and biomass density, can also influence macrophyte growth. The main carbon source for submersed plants is dissolved carbon dioxide and carbonates can also be taken up by some macrophytes. Carbon hardly ever limits plant growth. The inorganic phosphate, (PO_4^{3-}, or one or its analogs, HPO_4^{2-} or $H_2PO_4^-$), is taken up by the primary producers, while nitrate (NO_3^-) or ammonia (NH_4^+) is taken up by macrophytes. P can be released as phosphate, nitrogen as ammonia, or nitrate during the degradation of organic matter.

Macrophytes can create a favorable environment with the chemical and biological processes for the P-uptake. Ligand exchange of soluble P with Al, Fe, Ca, and clay minerals is the main important P-removal process in macrophyte rhizosphere. The physicochemical properties of the sediment can influence the mobility and bioavailability of P in the rhizosphere. Eh and pH gradients play an important role on the mobility and the uptake of P in the rhizosphere. The phosphate-binding capacity can be increased due to the low pH and the protonation of Fe and Al surfaces. Moreover, under the low Eh, the reduction of Fe^{3+} to Fe^{2+} can induce the high P content in sediment solution. The mobility and bioavailability of P at root/porewater/sediment interface are influenced by organic ligand, P concentration, pCO_2, and PO_2 in the rhizosphere. The sediment chemistry in lakes can be changed by the oxygen release from aquatic macrophyte roots and the alternation of pH and oxidation–reduction reaction. The O_2 released from roots at scales from millimeter to micron at rhizosphere microzone can engenders Fe plagues surrounding the roots of macrophytes. The Fe plagues can reduce P-release intensity and P concentration in porewater, which is due to the P bound by Fe (III) hydroxyoxide (Christensen 1997; Christensen et al. 1998). The O_2 released from aquatic plant root can engender the oxidation of Fe^{2+} and form Fe (III) hydroxyoxide, which deposit on the root surface and enwrap the root. The reaction for the formation of Fe-plaque is as follows:

$$4Fe_2 + O_2 + 10H_2O = 4Fe(OH)_3 + 8H^+ \quad (1.9)$$

Armstrong (1978) and Gambrell and Patrick (1978) suggested that the formation of Fe-plaque on roots served as a sink for metals and was consequently a hindrance to nutrient uptake by wetland plants. The formation of Fe-plaque on roots of *Oryza sativa* (Lee et al. 2003), *Cymodocea serrulata* (Povidisa et al. 2009), *rhizophoraceae* (Machado et al. 2005), isoetid (SØndergaard and Lægaard 1977; Farmer 1985) and the effect on biogeochemical process in the rhizosphere have been researched. However, only few papers reported the quantitative research of plagues on aquatic

plant roots collected in field such as *Vallisneria americana michx*. and *Heteranthera dubia (Jacq.) macm*. (St-Cyr and Campbell 1996), *Littorella uniflora* (L.) *aschers*. and *Isoetes lacustris L.* (Christensen et al. 1998). Moreover, the oxidative status in macrophyte rhizosphere can protect against toxicity of metals because of the decrease of the reduced Fe or Mn contents in rhizosphere sediment (Armstrong 1979).

The free element ion is the main fraction for the uptake of elements by plant roots. When the element-transfer across root membrane is slower than diffusional transfer in sediment/porewater and the concentration of labile soluble element is high, the equilibrium status of the porewater is perturbed very little by root uptake and the concentration in plant tissue is related to free element ion in porewater adjusted due to the competitive binding effects of other ions (Luo et al. 2010). This case of "plant limiting uptake" can be simulated by the biotic ligand model (BLM). The dynamic plant uptake model (DPUM) (Lehto et al. 2006), a mathematical model, presented as Fig. 1.7 has been developed for the simulation of the element process at the sediment/porewater/root interface. The parameters for Fig. 1.7 are indicated in Tables 1.1 and 1.2. Soil parameters used in this model were measured under the similar conditions to those that DGT deployment for the prediction of root uptake. This model can be used to research "diffusion limitation" type for element-uptake, when transport across root membrane is faster than diffusion process and the free ion concentration in porewater is low (Luo et al. 2014). Like roots, DGT can locally deplete element concentrations in porewater and respond to

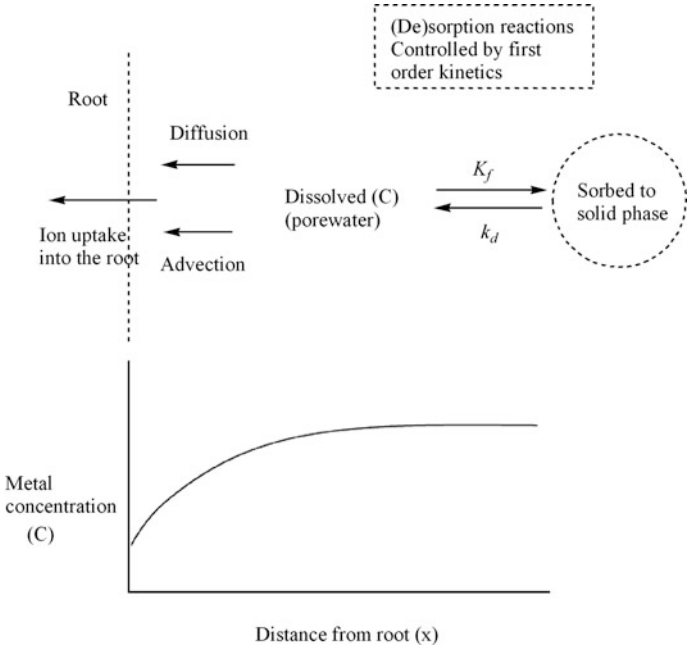

Fig. 1.7 The conceptual model about the DPUM (Reprinted from Plant and Soil, 282:227–238, Lehto, N.J., Davison, W., Zhang, H., Tych, W., Analysis of micro-nutrient behaviour in the rhizosphere using a DGT parameterised dynamic plant uptake model, copyright (2006), with the permission from Springer)

Table 1.1 Values and ranges of input and derived parameters used within the DPUM for simulating the uptake of zinc by two plants

Parameter	Description	*Thlaspi arvense*	*Thlaspi caerulescens*
Input parameters			
C_0	Initial soil solution concentration (mol cm^{-3})	10^{-10}	10^{-10}
D_0	Diffusion coefficient of the metal in water (cm^2 s^{-1})	5.87×10^{-6}	5.87×10^{-6}
$V0$	Rate of water movement in the soil toward the root (cm^2 s^{-1})	10^{-7} to 10^{-5}	10^{-7} to 10^{-5}
Pc	Particle concentration (g s^{-1})	2	2
T_{or}	Tortuosity	2.125	2.125
K_D	Solid-phase labile metal reservoir size (g s^{-1})	1–100,000	1–100,000
T_C	Soil response time (s)	1–100,000	1–100,000
I_{max}	Maximum flux of metal into the plant (mol cm^2 s^{-1})	1.11×10^{-13}	5×10^{-13}
Km	Michaelis–Menten coefficient 1 (mol cm^3)	6×10^{-9}	8×10^{-9}
Derived parameters			
$C_{s\_0} = C_0 \times K_D$	Initial solid-phase concentration (mol kg^{-1})	10^{-8} to 10^{-4}	10^{-8} to 10^{-4}
$D_s = D_0/T_{or}$	Diffusion coefficient of the metal in soil solution (cm^2 s^{-1})	2.76×10^{-6}	2.76×10^{-6}
$k_f = (1/T_c)$	Sorption rate constant (s^{-1})	$1–10^{-4}$	$1–10^{-4}$
$k_b = 1/(K_D \times P_c \times T_c)$	Desorption rate constant (s^{-1})	0.5–5×10^{-9}	0.5–5×10^{-9}

Reprinted from Plant and Soil, 282:227–238, Lehto, N.J., Davison, W., Zhang, H., Tych, W., Analysis of micro-nutrient behaviour in the rhizosphere using a DGT parameterised dynamic. Plant uptake model., copyright (2006), with the permission from Springer

Table 1.2 Initial and boundary conditions for the DPUM plant model

	Conditions for x, t	Location
Initial conditions		
$C(x, 0) = C_0$	$x_0 \le x \le x_N$	Soil
$C_s(x, 0) = C_0 \times K_D$	$x_0 \le x \le x_N$	Soil
Boundary conditions		
$C(0, t) = I_{max} \times C_i/(K_m + C_i)$	$\forall t$	Root–Soil interface
$\nabla C(x_N, t) = 0$	$\forall t$	Furthest point in sediment
$\nabla C_s(x_0, t) = 0$	$\forall t$	Solid phase at root–soil interface
$\nabla C_s(x_0, t) = 0$	$\forall t$	Solid phase at furthest point in sediment

Reprinted from Plant and Soil, 282:227–238, Lehto, N.J., Davison, W., Zhang, H., Tych, W., Analysis of micro-nutrient behaviour in the rhizosphere using a DGT parameterised dynamic plant uptake model., copyright (2006), with the permission from Springer

element resupplied from labile species in soil/sediment solution and labile element pool in solid phase. The size of the solid-phase reservoir and the rate at which the solid-phase reservoir responds to element depletion in the solution phase are important to determine the soil solution concentration at which the plant uptake kinetics begin to limit the uptake of the element. DGT technique has been used for the root/soil system, including Zn taken up by *Lepidium sativum* (Zhang et al. 2004); Cu taken up by *Lepidium heterophyllum* (Zhang et al. 2001); and Ni and Cd taken up by Radish (Luo et al. 2014). These papers indicate DGT is likely to behave as a reliable surrogate for the element-transfer and element-release processes that affect plant uptake.

1.4 Summary

This chapter introduced the theory of "internal P-loading" in eutrophic lakes, DGT theory and methods for measurement and element-release assessment at SWI in lake, and the element-transfer and uptake mechanism in rhizosphere of aquatic plants. Nutrient loading to lake systems can be from external or internal sources. Where "external P-loading" has contributed to the internal P-store in the reservoir, the reduction in external supply through management can increase the importance of "internal P-loading" from the sediment (Van der Molen and Boers 1994). The processes influencing phosphorus release from the sediment have been extensively summarized. The physicochemical processes and the properties of sediments influence the P-release and include: temperature, pH, redox potential, element in sediments: Fe, sulfide/sulfate, Al, Ca and OM, P fractions, and chlorophyll a (Chl a). Fe-reduction and P-release from Fe-bound P is the main reason for P-release from lake sediments. Ca- and Al-bound P are nonavailable. Organic P is partly available, and the exact nature of this complex fraction is not precisely known. The coupled Fe–S–P geochemical process is the minor sediment-P-release mechanism. DGT as a passive sampler has been used widely in water, soil, sediment, and rhizosphere. The DGT device passively accumulates labile species from solution; while deployed in situ and therefore the contamination problems associated with the conventional water collection and filtration procedures are eliminated. The theory behind DGT technique is based on the diffusional characteristics of elements in a hydrogel and an element-binding resin. Specifically, the technique utilizes a hydrogel layer to control the diffusive transport of elements in solution to a binding resin. In addition, since the resin used in DGT is selective for labile species, it provides a proxy for the bioavailability of elements in solution. The usage of DGT assembly in sediment has provided the new in situ method for the measurement of metals, P, and S(-II), which is the base for geochemical reactions for P-release. Moreover, DGT calculation method, element-release/element-diffusion process across DGT/sediment interface, DGT parameters, new DGT techniques for element image in sediment microzone, a numerical model (DIFS) for the diffusion/sorption/desorption process during DGT deployment in sediment, and

DGT deployment in the rhizosphere as the simulation method for metal-uptake by root system have also been introduced. The ecological restoration of eutrophic lakes by aquatic vegetation has been investigated by many researchers. The roots of aquatic plants play a key role for the uptake of appreciable quantities of nutrient from sediments. In order to reveal the element-uptake and the transfer mechanism across sediment/root interface, the influencing factors of the physicochemical properties of the sediment on the mobility and bioavailability of elements in the rhizosphere, the Fe plague surrounding the root, and the mathematical model of micronutrient uptake by plant have been introduced and commented.

References

Armstrong W (1978) Root aeration in the wetland condition. In: Hook DD, Crawford RMM (eds) Plant life in anaerobic environments. Ann Harbor Science Publishers Inc., Ann Harbor, MI, pp 269–297

Armstrong W (1979) Aeration in higher plants. Adv Bot Res 7:225–332

Aung NN, Nakajima F, Furumai H (2008) Trace metal speciation during dry and weather flow in the Tama River, Japan, by using diffusive gradients in thin films (DGT). J Environ Monitor 10:219–230

Barber SA (1995) Soil nutrient bioavailability: a mechanistic approach. Wiley, New York

Beckett PHTJ (1964) The immediate Q/I relations of labile potassium in the soil. Soil Sci 15:9–23

Bender M, Martin W, Hess J, Sayles F, Ball L, Lambert C (1987) A whole core squeezer for interfacial pore-water sampling. Limnol Oceanogr 32:1214–1225

Bennett WW, Teasdale PR, Panther JG, Welsh DT, Jolley DF (2011) Speciation of dissolved inorganic arsenic by diffusive gradients in thin films: selective binding of As-III by 3-mercaptopropyl-functionalized silica gel. Anal Chem 83:8293–8299

Bostrom B, Pettersson K (1982) Different patterns of phosphorus release from lake-sediments in laboratory experiments. Hydrobiologia 91–2:415–429

Cattani I, Spalla S, Beone GM, Del Rea AAM, Boccelli R, Trevisan M (2008) Characterization of mercury species in soils by HPLC-ICP-MS and measurement of fraction removed by diffusive gradient in thin films. Talanta 74:1520–1526

Chang LY, Davison W, Zhang H, Kelly M (1998) Performance characteristics for the measurement of Cs and Sr by diffusive gradients in thin films (DGT). Anal Chim Acta 368:243–253. (Reprinted from Anal Chim Acta 368:243–253, Chang LY, Davison W, Zhang H, Kelly M (1998) Performance characteristics for the measurement of Cs and Sr by diffusive gradients in thin films (DGT), copyright (1998), with the permission from Elsevier)

Chinese Research Academy of Environmental Sciences (2014) The report on the survey of "internal loading character" and assessment of release risk of N and P in the whole Dianchi Lake, 2014 (unpublished, in Chinese)

Christensen KK (1997) Differences in iron, manganese, and phosphorus binding in freshwater sediment vegetated with Littorella uniflora and benthic microalgae. Water Air Soil Pollut 99:265–273

Christensen KK, Jensen HS, Andersen FO, Wigand C, Holmer M (1998) Interferences between root plaque formation and phosphorus availability for isoetids in sediments of oligotrophic lakes. Biogeochemistry 43(2):107–128

Christophoridis C, Fytianos K (2006) Conditions affecting the release of phosphorus from surface lake sediments. J Environ Qual 35(4):1181–1192

Cook PLM, Holland DP, Longmore AR (2010) Effect of a flood event on the dynamics of phytoplankton and biogeochemistry in a large temperate Australian lagoon. Limnol Oceanogr 55:1123–1133

David LC (1998) The role of phosphorus in the eutrophication of receiving water: a review. J Environ Qual 27:261–266

Davison W, Grime GW, Morgan J, Clarke K (1991) Distibution of dissolved iron in sediment pore waters at submillimetre resolution. Nature 352:323–324

Davison W, Zhang H, Grime G (1994) In situ speciation measurements of trace components in natural waters using thin-film gels. Nature 367:546–548

Davison W, Fones G, Grime GW (1997) Dissolved metals in surface sediments and a microbial mat at 100 mm resolution. Nature 387:885–888

Ding SM, Sun MQ, Xu D, Jia F, He XA, Zhang CS (2012) High-resolution simultaneous measurements of dissolved reactive phosphorus and dissolved sulfide: the first observation of their simultaneous release in sediments. Environ Sci Technol 46:8297–8304

Ding SM, Wang Y, Xu D, Zhu CG, Zhang CS (2013) Gel-based coloration technique for the submillimeter-scale imaging of labile phosphorus in sediments and soils with diffusive gradients in thin films. Environ Sci Technol 47:7821–7829

Dočekalová H, Diviš P (2005) Application of diffusive gradient in thin films technique (DGT) to measurement of mercury in aquatic systems. Talanta 65:1174–1178

Dočekalová H, Clarisse O, Salomon S, Wartel M (2002) Use of constrained DET probe for a high-resolution determination of metals and anions distribution in the sediment pore water. Talanta 57:145–155

Ernstberger H, Davison W, Zhang H, Tye A, Young S (2002) Measurement and dynamic modelling of trace metal mobilization in soils using DGT and DIFS. Sci Total Environ 36:349–354

Ernstberger H, Zhang H, Tye A, Young S, Davison W (2005) Desorption kinetics of Cd, Zn, and Ni measured in soils by DGT. Environ Sci Technol 39(6):1591–1597

Farmer AM (1985) The occurrence of vesicular-arbuscular mycorrhiza in isoetid-type submerged aquatic macrophytes under naturally varying conditions. Aquat Bot 21:245–249

Fones GR, Davison W, Hamilton-Taylor J (2004) The fine-scale remobilization of metals in the surface sediment of the North-East Atlantic. Cont Shelf Res 24:1485–1504

Förstner U (2004) Traceability of sediment analysis. Trac-Trend Anal Chem 23(3):217–236

Gambrell RP, Patrick WH (1978) Chemical and microbiological properties of anaerobic soils and sediments. In: Hook DD, Crawford RMM (eds) Plant life in anaerobic environments. Ann Harbor Science Publishers Inc., Ann Harbor, MI, pp 375–423

Gao Y, Lesven L, Gillan D, Sabbe K, Billon G, De Galan S, Elskens M, Baeyens W, Leermakers M (2009) Geochemical behavior of trace elements in sub-tidal marine sediments of the Belgian coast. Mar Chem 117:88–96

Gao Y, Baeyens W, De Galan S, Poffijn A, Leermakers M (2010) Mobility of radium and trace metals in sediments of the Winterbeek: application of sequential extraction and DGT techniques. Environ Pollut 158:2439–2445

Gao Y, van de Velde S, Williams PN, Baeyens W, Zhang H (2015) Two-dimensional images of dissolved sulfide and metals in anoxic sediments by a novel diffusive gradients in thin film probe and optical scanning techniques. Trac-Trend Anal Chem 66:63–71

Garmo ØA, Røyset O, Steinnes E, Flaten TP (2003) Performance study of diffusive gradients in thin films for 55 elements. Anal Chem 75:3573–3580

Garmo ØA, Lehto NJ, Zhang H, Davison W, Røyset O, Steinnes E (2006) Dynamic aspects of DGT as demonstrated by experiments with lanthanide complexes of a multidentate ligand. Environ Sci Technol 40:4754–4760

Hamilton-Taylor J, Morris EB (1985) The dynamics of iron and manganese in surface sediments of a seasonally anoxic lake. Archiv Für Hydrobiologie-Supplement 72:135–165

Harper MP, Davison W, Zhang H, Tych W (1998) Kinetics of metal exchange between solids and solutions in sediments and soils interpreted from DGT measured fluxes. Geochim Cosmochim Acta 62:2757–2770

Harper M, Davison W, Tych W (2000) DIFS-a modelling and simulation tool for DGT induced trace metal remobilisation in sediments and soils. Environ Modell Softw 15:55–66

Hulbert MH, Bennett RH, Baerwald RJ, Long RL, Curry KJ (2002) Observations of the sediment-water interface: marine and fresh water environments. Mar Georesour Geotechnol 20 (4):255–274

Jansen B, Kotte MC, Wijk AJV, Verstraten JM (2001) Comparison of diffusive gradients in thin films and equilibrium dialysis for the determination of Al, Fe(III) and Zn complexed with dissolved organic matter. Sci Total Environ 277:45–55

Jin XC, Jiang X, Wang Q (2008) Seasonal changes of P adsorption/desorption characteristics at the water sediment interface in Meiliang Bay, Taihu Lake, China. Acta Scientiae Circumstantiae 28(1):24–30 (in Chinese)

Johnson RG (1974) Particulate matter at the sediment-water interface in coastal environments. J Mar Res 32:313–330

Jørgensen BB (1977) Bacterial sulfate reduction within reduced microniches of oxidized marine-sediments. Mar Biol 41:7–17

Kennett JP (1982) Marine geology. Prentice-Hall, Englewood Cliffs

Lee DY, Chiang PH, Houng KH (1996) Determination of bioavailable cadmium in paddy fields by chelating resin membrane embedded in soils. Plant Soil 181:233–239

Leemakers M, Gao Y, Gabelle C, Lojen B, Ouddane B, Wartel M, Baeyens W (2005) Determination of high resolution porewater profiles of trace metals in sediments of the Rupel River (Belgium) using DET and DGT techniques. Water Air Soil Pollut 166:265–286

Lehto NJ, Davison W, Zhang H, Tych W (2006) Analysis of micro-nutrient behaviour in the rhizosphere using a DGT parameterised dynamic plant uptake model. Plant Soil 282:227–238 (Reprinted from Plant Soil 282:227–238, Lehto NJ, Davison W, Zhang H, Tych W (2006) Analysis of micro-nutrient behaviour in the rhizosphere using a DGT parameterised dynamic plant uptake model, copyright (2006), with the permission from Springer)

Levy JL, Zhang H, Davison W, Galceran J, Puy J (2012) Kinetic signatures of metals in the presence of Suwannee River fulvic acid. Environ Sci Technol 46:3335–3342

Li WJ, Zhao HJ, Teasdale PR, John R, Wang FY (2005) Metal speciation measurement by diffusive gradients in thin films technique with different binding phases. Anal Chim Acta 533:193–202

Lucas A, Rate A, Zhang H, Salmon SU, Radford N (2012) Development of the diffusive gradients in thin films technique for the measurement of labile Gold in natural waters. Anal Chem 84:6994–7000

Luo J, Zhang H, Zhao FJ, Davison W (2010) Distinguishing diffusional and plant control of Cd and Ni uptake by hyperaccumulator and nonhyperaccumulator plants. Environ Sci Technol 44:6636–6641

Luo J, Cheng H, Ren JH, Davison W, Zhang H (2014) Mechanistic insights from DGT and soil solution measurements on the uptake of Ni and Cd by radish. Environ Sci Technol 48:7305–7313

Machado W, Gueiros BB, Lisboa-Filho SD, Lacerda LD (2005) Trace metals in mangrove seedlings: role of iron plaque formation. Wet Ecol Manage 13(2):199–206

Mason S, McNeill A, McLaughlin MJ, Zhang H (2010) Prediction of wheat response to an application of phosphorus under field conditions using diffusive gradients in thin-films (DGT) and extraction methods. Plant Soil 337(1):243–258

McGrath SP, Chang AC, Page AL, Witter EL (1994) Land application of sewage sludge: scientific perspectives of heavy metal loading limits in Europe and the United States. Environ Rev 2:108–118

McLaughlin MJ, Smolders E, Merckx R (1998) In soil chemistry and ecosystem health. Special Publication no. 52, Soil Science Society of America: Madison, WI, pp 233–277

Meylan S, Odzak N, Behra R, Sigg L (2004) Speciation of copper and zinc in natural freshwater: comparison of voltammetric measurements, diffusive gradients in thin films (DGT) and chemical equilibrium models. Anal Chim Acta 510:91–100

Monbet P, Mckelvie ID, Worsfold PJ (2008) Combined gel probes for the in situ determination of dissolved reactive phosphorus in porewaters and characterization of sediment reactivity. Environ Sci Technol 42:5112–5117

Moorleghem CV, Six L, Degryse F, Smolders E, Merckx R (2011) Effect of organic P forms and P present in inorganic colloids on the determination of dissolved P in environmental samples by the diffusive gradient in thin films technique, ion chromatography, and colorimetry. Anal Chem 83:5317–5323

Morford J, Kalnejais L, Martin W, François R., Karle I-M (2003) Sampling marine porewaters for Mn, Fe, U, Re and Mo: modifications on diffusional equilibration thin film gel probes. J Exp Mar Biol Ecol 285:85–103

Morse JW, Luther GW III (1999) Chemical influences on trace metal-sulfide interactions in anoxic sediments. Geochim Cosmochim Acta 63:3373–3378

Munksgaard NC, Parry DL (2003) Monitoring of labile metals in turbid coastal seawater using diffusive gradients in thin-films. J Environ Monitor 5:145–149

Myers CR, Nealson KH (1993) Biological and chemical mechanisms of manganese reduction in aquatic and sediment systems: transport and transformation of contaminations near the sediment-water interface. In: DePinto JV, Lick W, Paul JF (eds), Lewis, pp 205–223

Naylor C, Davison W, Motelica-Heino M, Van Den Berg GA, Van Der Heijdt LM (2004) Simultaneous release of sulfide with Fe, Mn, Ni and Zn in marine harbour sediment measured using a combined metal/sulfide DGT probe. Sci Total Environ 328:275–286

Nierop KGJ, Jansen B, Vrugt JA, Verstraten JM (2002) Copper complexation by dissolved organic matter and uncertainty assessment of their stability constants. Chemosphere 49:1191–1200

Österlund H, Faarinen CM, Widerlund A, Rodushkin L, Ingri J, Baxter D (2010) Simultaneous measurements of As, Mo, Sb, V and W using a ferrihydrite diffusive gradients in thin films (DGT) device. Anal Chim Acta 682:59–65

Palmer-Felgate EJ, Mortimer RJG, Krom MD, Jarvie HPR, Williams JR, Spraggs E, Stratford CJ (2011) Internal loading of phosphorus in a sedimentation pond of a treatment wetland: effect of a phytoplankton crash. Sci Total Environ 409:2222–2232

Panther JG, Teasadle PR, Bennett WW, Welsh DT, Zhao HJ (2010) Titanium dioxide-based DGT technique for in situ measurement of dissolved reactive phosphorus in fresh and marine waters. Environ Sci Technol 44:9419–9424

Panther JG, Bennett WW, Teasdale PR, Welsh DT, Zhao HJDGT (2012) Measurement of dissolved Aluminum species in waters: comparing Chelex-100 and Titanium dioxide-based adsorbents. Environ Sci Technol 46:2267–2275

Parsons B, Sclater JG (1977) An analysis of the variation of ocean floor bathymetry and heat flow with age. J Geophys Res 82:803–827

Povidisa K, Delefosse M, Holmer M (2009) The formation of iron plaques on roots and rhizomes of the seagrass *Cymodocea serrulata* (R. Brown) Ascherson with implications for sulphide intrusion. Aquat Bot 90(4):303–308

Rast W, Smith VH, Thornton JA (1989) Characteristics of eutrophication. In: Ryding SO, Rast W (eds) The control of eutrophication of lakes and reservoirs. Man and the Biosphere Series, vol 1. UNESCO, Paris, pp 37–64

Redfield AC, Ketchum BH, Richards FA (1963) The influence of organisms on the composition of sea water. In: Hill MN (ed) The sea, 2. Wiley, New York, pp 177–192

Rickard D (1997) Kinetics of pyrite formation by the H_2S oxidation of iron(II) monosulfide in aqueous solutions between 25 and 125 °C: the rate equation. Geochim Cosmochim Acta 61:115–134

Roden EE, Edmonds JW (1997) Phosphate mobilization in iron-rich anaerobic sediments: microbial Fe(III) oxide reduction versus iron-sulfide formation. Arch Hydrobiol 139(3):347–378

Roulier JL, Tusseau-Vuillemin MH, Coquery M, Geffard O, Garric J (2008) Measurement of dynamic mobilization of trace metals in sediments using DGT and comparison with bioaccumulation in *Chironomus riparius*: first results of an experimental study. Chemosphere 70:925–932

Ruban V, Lopez-Sanchez JF, Pardo P, Rauret G, Muntau H, Quevauviller P (2001) Harmonized protocol and certified reference material for the determination of extractable contents of phosphorus in freshwater sediments-a synthesis of recent works. Fresen J Anal Chem 370: 224–228

Sangi MR (1998) Trace metal determination in river water by diffusive gradients in thin-films. PhD thesis, The University of Otago, New Zealand

Santner J, Prohaska T, Luo J, Zhang H (2010) Ferrihydrite containing gel for chemical imaging of labile phosphate species in sediments and soils using diffusive gradients in thin films. Anal Chem 82:7668–7674

Sauvé S, Cook N, Hendershot WH, McBride MB (1996) Linking plant tissue concentrations and soil copper pools in urban contaminated soils. Environ Pollut 94:153–157

Skogley EO, Dobermann A (1996) Synthetic ion-exchange resins: soil and environmental studies. J Environ Qual 25:13–24

SØndergaard M, Lægaard S (1977) Vesicular±arbuscular mycorrhiza in some aquatic vascular plants. Nature 268:232–233

St-Cyr L, Campbell PGC (1996) Metals (Fe, Mn, Zn) in the root plaque of submerged aquatic plants collected in situ: relations with metal concentrations in the adjacent sediments and the root tissue. Biogeochemistry 33:45–76

Stockdale A, Davison W, Zhang H (2010) Formation of iron sulfide at faecal pellets and other microniches within suboxic surface sediment. Geochim Cosmochim Acta 74:2665–2676

Sundby B, Anderson LG, Hall POJ, Iverfeldt A, Vanderloeff MMR, Westerlund SFG (1986) The effect of oxygen on release and uptake of cobalt, manganese, iron and phosphate at the sediment-water interface. Geochim Cosmochim Acta 50(6):1281–1288

Teasdale PR, Hayward S, Davison W (1999) In situ, high-resolution measurement of dissolved sulfide using diffusive gradients in thin films with computer-imaging densitometry. Anal Chem 71:2186–2191

Tessier A (1992) Sorption of trace elements on natural particles in oxic environments: environmental Particles. In: Buffle J, van Leeuwen HP (eds), Lewis, pp 425–453

Tessier A, Campbell PGC, Bisson M (1979) Sequential extraction procedure for the speciation of trace metals. Anal Chem 51(7):844–851

User's guide to DGT technique (2003) DGT Research Ltd. Available at: http://www.dgtresearch.com. Accessed 24 May 2009

Van der Molen D, Boers P (1994) Influence of internal loading on phosphorus concentration in shallow lakes before and after reduction of the external loading. Hydrobiologia 275(276): 379–389

Vulkan R, Zhao FJ, Barbosa-Jefferson V, Preston S, Paton GI, Tipping E, McGrath SP (2000) Environ Sci Technol 34:5115–5121

Warnken K, Zhang H, Davison W (2004) Performance characteristics of suspended particulate reagent-iminodiacetate (SPR-IDA) as a binding agent for diffusive gradients in thin films (DGT). Anal Chim Acta 508:41–51

Watson PG, Frickers TE (1990) A multilevel, in situ pore water sampler for use in intertidal sediments and laboratory microcosms. Limnol Oceanogr 35(6):1381–1389

Williams PN, Zhang H, Davison W, Zhao SZ, Lu Y, Dong F, Zhang L, Pan Q (2012) Evaluation of in situ DGT measurements for predicting the concentration of Cd in Chinese field-cultivated rice: impact of soil Cd: Zn ratios. Environ Sci Technol 46:8009–8016

Wu ZH, Wang SR, He MC (2015a) Element remobilization, "internal P-loading" and sediment-P reactivity researched by DGT (diffusive gradients in thin films) technique. Environ Sci Pollut R 22:16173–16183

Wu ZH, Wang SR, Jiao LX (2015b) Geochemical behavior of metals-sulfide-phosphorus at SWI (sediment/water interface) assessed by DGT (Diffusive gradients in thin films) probes. J Geochem Explor 156:145–152

Wu ZH, Jiao LX, Wang SR, Xu YZ (2015c) Multi-metals Measured at sediment–water interface (SWI) by Diffusive Gradients in Thin Films (DGT) Technique for Geochemical Research. Arch Environ Con Tox. doi:10.1007/s00244-015-0184-1 (online published) (Reprinted from

Arch Environ Con Tox, published online (doi:10.1007/s00244-015-0184-1), Wu ZH, Jiao LX, Wang SR, Xu YZ (2015) Multi-metals measured at sediment–water interface (SWI) by Diffusive Gradients in Thin Films (DGT) Technique for geochemical research, copyright (2015), with the permission from Springer)

Zhang H, Davison W (1999) Diffusional characteristics of hydrogels used in DGT and DET techniques. Anal Chim Acta 398:329–340

Zhang H, Davison W, Miller S, Tych W (1995) In situ high-resolution measurements of fluxes of Ni, Cu, Fe, and Mn and concentrations of Zn and Cd in porewaters by DGT. Geochim Cosmochim Acta 59:4181–4192

Zhang H, Davison W, Gadi R, Kobayashi T (1998) In situ measurement of dissolved phosphorus in natural waters using DGT. Anal Chim Acta 370:29–38

Zhang H, Zhao F-J, Sun B, Davison W, Mcgrath SP (2001) A new method to measure effective soil solution concentration predicts Copper availability to plants. Environ Sci Technol 35:2602–2607

Zhang H, Davison W, Mortimer RJG, Krom MD, Hayes PJ, Davies IM (2002) Localised remobilization of metals in a marine sediment. Sci Total Environ 296:175–187

Zhang H, Lombi E, Smolders E, Mcgrath S (2004) Kinetics of Zn release in soils and prediction of Zn concentration in plants using diffusive gradients in thin films. Environ Sci Technol 38:3608–3613

Chapter 2
Problem Introduction, Research Idea, and Studying Zone

Due to "internal P-loading" for lake eutrophication, it is important to quantify the P-release intensity at SWI for the restoration of contaminated lake (Förstner et al. 1994). So, the environmental behavior and biogeochemistry of P, Fe, and S in sediments should be understood (Shaw et al. 1990). The chemical property in sediment porewater has been verified as the sensitive indicator of the biogeochemical reaction happening between water and sediment particle (Zhang et al. 2002; Fones et al. 2004; Wu et al. 2011, 2014, 2015a, b, c, d). The bioavailability and mobility for P or meals can be investigated by conventional methods, such as a linear distribution coefficient (K_d), a nonlinear adsorption isotherm (Freundlich or Langmuir), sequential extraction procedures, or other procedures and analytical methods (Hamilton-Taylor and Morris 1985; Cutter and Oatts 1987; Barbanti et al. 1994; Golterman 2004; Kopáček et al. 2005; Wilson et al. 2008; Lin et al. 2009; Shilla et al. 2009; Wang et al. 2009). Compared with "bulk" analysis methods, the diffusive gradients in thin films (DGT) technique (Davison et al. 1994, 2000) is an advanced method for DGT profile/image of trace elements in sediment porewater (Zhang et al. 2002; Fones et al. 2004; Wu et al. 2011, 2014, 2015a, b, c, d), geochemical process (Naylor et al. 2004; Ding et al. 2012), kinetic exchange at the DGT/sediment microzone (Harper et al. 1998; Ernstberger et al. 2002), and microniche research (Widerlund and Davison 2007). The root of aquatic plant is important for P-cycling, and the kinetic P-uptake at root/sediment interface plays a key role in lake restoration (Nuttall 1985). The mobility and bioavailability of P in the rhizosphere are influenced by the physicochemical properties of sediments (Christensen 1997; SØndergaard and Lægaard 1977; Farmer 1985). DGT test in root microenvironments can act as an indicator for element availability and the element taken up by root (Lehto et al. 2006; Mason et al. 2010).

In this chapter, we introduced the eutrophic problem in lake sediments (Dianchi and Erhai lakes), which should be revealed and assessed by DGT technique, and the layout of DGT and the related techniques has been discussed for the research of P-transfer across environmental interfaces, including DGT measurement for P, S(-II),

S. Wang and Z. Wu, *DGT-based Measurement of Phosphorus in Sediment Microzones and Rhizospheres*, DOI 10.1007/978-981-10-0721-7_2

and Fe, the software and program for P-transfer in sediment microzone, the analytical method for element 2D-distribution in sediment microzone, and DGT's function to research P-bioavailability and P-transfer across sediment/root interface. Moreover, the studying zones for DGT at SWI (Dianchi Lake) or sediment/root interface (Erhai Lake) were also introduced.

2.1 Problem Introduction

DGT is the analytical tool and research method for the profile character, the remobilization character, and the geochemical reaction mechanisms, and it has been widely used in all kinds of water bodies (lake, sea, and river). However, DGT has seldom been used for the geochemical character of P at SWI of lakes (Monbet et al. 2008; Ding et al. 2012), and the mechanism of "internal P-loading" should be revealed more thoroughly. Moreover, the previous researchers have never assessed "internal P-loading" in eutrophic lake comprehensively, and only one or two kinds of DGT probes have been investigated. Lake sediment is significant for the nutrient cycle, the reason of which is that it is the internal pool and source for plant root and benthic alga. The soluble nutrient released from sediment porewater can supply P. Under the anaerobic condition, the reduction of Fe(III) hydroxyoxide may lead to the release of soluble reactive P (SRP) associated with mineral phases (Palmer-Felgate et al. 2011). The anoxic condition promotes the reduction of insoluble Fe(III) hydroxyoxide to soluble Fe(II), resulting in the P-release from the sediments and into the surrounding water (Böstrom and Pettersson 1982; Christophoridis and Fytianos 2006). For example, Sundby et al. (1986) found that inorganic P (DIP, PO_4^{3-}) and Fe^{2+} were released simultaneously in equivalent concentrations as oxygen concentrations approached near zero in a benthic chamber in the sediments of Gullmarsfjorden, Sweden. The last reason and the decomposition of algae/organic matter may cause "internal P-loading" of lake (Cook et al. 2010). Roden and Edmonds (1997) suggested an indirect reduction pathway, attributing P-release from Fe(III) hydroxyoxide due to sulfate-reducing bacteria which enhance the formation of insoluble FeS.

So, it is important to measure the concentration/flux of P/Fe/S involved in the geochemical process of P, which can be used for the mechanism of "internal P-loading." When the lake environment permits P-release from sediment into water phase, total dissolved P (TDP) level in water can be elevated and "internal P-loading" appears, regardless of "external P-loading." For example, Dianchi Lake is a lake with eutrophic status in southeast of China (Wu et al. 2015c, d). "Internal P-loading" is one important factor for P-cycle at SWI. So, it is important to research P-release mechanism and the mechanism of "internal P-loading." Lake sediment, composed of complex minerals, porewater, as well as inorganic and organic compounds, can act as both a sink and a source of P (Christophoridis and Fytianos 2006). Temperature, pH, redox potential, nitrate, sulfate, bioturbation, algae bloom,

as well as the presence of Ca, Mn, Fe, Al, and Mg have been found to be able to control P-release (Kleeberg and Dudel 1997). The adsorption of P on $Al(OH)_3$ or the precipitation process of hydroxylapatite or fluorapatite ($Ca_5(PO_4)_3(OH,F)$) is the main reason for P-sequestration at SWI.

The sediment has been identified as the important pool for P in a lot of aquatic ecosystems (Lebo 1991; Conley et al. 1995; Paludan and Morris 1999; Zwolsman 1994; Zhang and Huang 2007). Thus, the P-release across the SWI through adsorption–desorption processes and coprecipitation–dissolution reactions plays a key role in controlling the dissolved phosphate concentrations in the overlying waters and porewaters (Froelich et al. 1982; Froelich 1988). Understanding the kinetic P-release between the sediment and porewater interface is significant for assessing the release risk and the P-mobility in lake sediments. Some researchers have focused on the linear distribution coefficient (K_d) or the nonlinear adsorption isotherm (Freundlich or Langmuir) to investigate the P distribution at SWI; other researchers have investigated the sequential extraction method for P-fractionation in sediments for assessing the bioavailable P in the sediment or potential P-release (Wilson et al. 2008; Shilla et al. 2009; Wang et al. 2009; Lin et al. 2009). Commonly, the adsorption–desorption studies are performed in dilute suspensions, whereas the sequential extraction procedures can systematically alter the chemical environment (Ernstberger et al. 2002).

The recently developed skill (Davison et al. 1994)—diffusive gradients in thin films (DGT) technique—has been used to measure in situ concentrations and fluxes of elements in the sediment/soil/water. It operates through introducing a localized sink that induces a diffusion flux to the DGT resin. The quantity measured directly is the mass of one element accumulated by the sink (the binding gel) during DGT deployment. These in situ DGT measurements depend on the element concentrations in sediment porewater and the resupply from the solid phases. Thus, the in situ evaluation for rate constants of the element release from the solid phase and capacities of element reservoir in the solid pool can be reached.

The macrophytes such as *Zizania caduciflora* or *Myriophyllum aquaticum* are distributed widely in the lakes or rivers in China, such as Erhai Lake (the southeast of China). The technique for wetland treatment project to control "internal P-loading" has advantages for the ecological restoration of lake eutrophication. The water quality in lakes or rivers can be largely improved by macrophyte roots (Blindow et al. 1993; Barko et al. 1991; Gu et al. 2001; Brix and Schierup 1989; McNabb 1976; O'Dell et al. 1995; Canfield and Hoyer 1992; Leslie et al. 1983). Redox potential, pH, pCO_2, PO_2, and element concentrations in the proximity of macrophyte root determine the mobility and bioavailability of elements in rhizosphere (Hinsinger and Courchesne 2008). Aquatic plants in lake systems can effectively alter the chemistry of rhizosphere sediment by O_2 released from roots. The rhizosphere oxidation and the formation of Fe-plaque on roots of aquatic plants led to the accumulation of metals such as iron, zinc, and arsenic in rhizosphere (Otte et al. 1991; Kirk and Bajita 1995). Oxidation of ferrous iron to its ferric form would

lead to precipitation of Fe(III) hydroxyoxide in the rhizosphere (Otte et al. 1989), which in turn engenders a decreasing concentration gradient of dissolved iron toward the plant roots. These gradients would lead to the diffusion of iron, arsenic, and zinc in the direction of the roots. Assuming the uptake of the elements by roots is slower than supply through diffusion, an increase in the concentrations of all three elements would be expected to occur in the solid phase of the rhizosphere (Doyle and Otte 1997). Armstrong (1978) and Gambrell and Patrick (1978) suggested that the formation of Fe-plaque on roots served as a sink for elements and was consequently a hindrance to nutrient uptake by wetland plants. DGT technique for the measurement in the rhizosphere sediment can act as a predictor for the element taken up by plant root. The ferrihydrite-sorbent binding gel installed in DGT assembly is highly selective for labile P in sediment porewater. The diffusive gel layer in DGT assembly limits the largest flux of labile P from the sediment porewater into binding gel. This kind of induced flux of DGT is similar to that of P taken up by plant root. The Fick's law calculation ensures the accurate DGT concentration. DGT concentration depends on the soluble P in sediment porewater, and the resupply rate of P desorbed from sediment solid into porewater.

At the SWI of eutrophic lakes, the eutrophic element, P, redox sensitive elements, Fe and S, undergo complex exchanges and cogeochemical reactions, which control the eutrophic status and P-release risk. So, some questions should be answered, including: (1) What does the geochemical reaction determine the P-release and "internal P-loading" character in the vertical direction of sediment microzones? (2) How do kinetic parameters and sediment pools determine P-release/P-diffusion across the DGT/sediment interface? (3) How are S(-II)- or Fe-microniches analyzed and assessed at fine spatial scales in order to predict P-release risk? (4) Whether can the P-transfer and P-uptake in root of aquatic plant be assessed by DGT parameter? (5) Can DGT with multi-functions achieve the last measurement and assessment? The DGT techniques and the related methods with multi-functions for the two case studies (Dianchi and Erhai lakes) introduced in the next sections "Chap. 3" can solve the last questions.

2.2 The Research Idea and the General Design for DGT Research

DGT has been widely applied in the water body worldwide, as a powerful tool for the measurement of multi-elements and the research of environmental process at SWI. In this research, two problems should be answered: The first is the mechanism of P-release in sediment and the assessment for P-release intensity in eutrophic Dianchi Lake and the second is the P-uptake mechanism and P-transfer across sediment/root interface in Erhai Lake. DGT can be applied as a chemical sensor or a

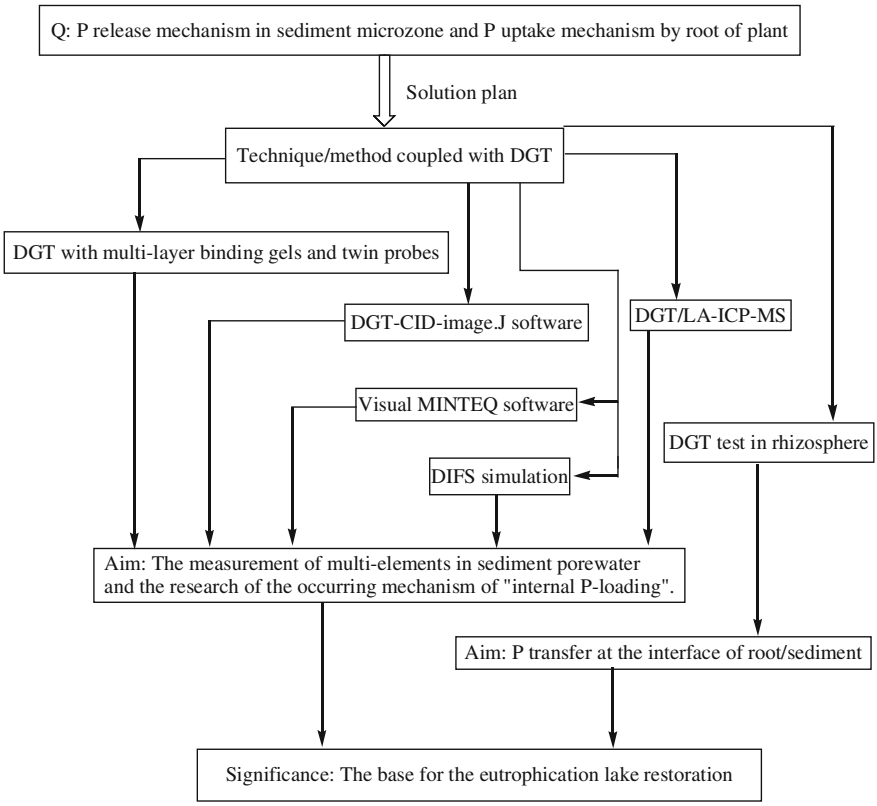

Fig. 2.1 The schematic graph of the general design for DGT research

passive sampler in the complex microenvironment (SWI) and the sediment/root microzone), and the other technique/method can be applied coupled with DGT technique in order to derive valuable data at fine spatial scales, environmental phenomenon, and the mechanism about P-transfer in sediment microzone or root/sediment interface. The schematic graph for the general design for DGT research is shown in Fig. 2.1. For the aim of the research for P-release mechanism and the related geochemical mechanism (Dianchi Lake), DGT probe with multilayer-binding gels and twin DGT probes have been developed for the simultaneous measurement of Fe/P/S elements in sediment porewater. The geochemical reactions were investigated, and the "internal P-loading" (Dianchi lake) was quantified. In order to quantify kinetic exchange of P and P-release/P-diffusion across DGT/sediment microzone, it is needed to develop numerical model to derive kinetic parameters and diagraph of P-exchange process as the functions of time/distance, and 1D-DIFS (DGT-induced fluxes in sediments) can be researched for input parameters, the operation of DIFS model, the discussion of output parameters and diagraphs, the mechanism for kinetic parameters controlling the

change character of DIFS curves, and P-release characters in sediment microzones. Due to the coupled biogeochemical process of Fe–S–P in sediment porewater, it is needed to research solubility of Fe-sulfide and Visual MINTEQ software can be used to achieve this aim; sulfide microniche determines the distribution of soluble inorganic sulfide in sediment porewater and influences the P-release from Fe-bound P; AgI-CID technique and ImageJ 1.38e software can be used to research sulfide microniche distribution character and the coupled Fe–S–P mechanism for P-release. Labile Fe-distribution in sediment microzone is the main factor for P-release from Fe-bound P, and LA-ICP-MS can be used for the analysis of labile Fe-bound by SPR-IDA gel in DGT probe. Based on chemical image of DGT-Fe in sediment microzone, Fe-distribution character and the prediction of P-release in "hot spots" in chemical image can be researched. The above-mentioned method/technique can be used to reveal P-release mechanism in sediment microzone and "internal P-loading," thoroughly. Moreover, in order to research P-transfer and P-uptake at the interface of sediment and the rhizosphere of aquatic plants in Erhai Lake, DGT piston can be used for the tests in situ or in rhizobox to achieve the last aim; the derived C_E value can be used to provide a major step forward in assessing hazards posed by P in eutrophic lake sediments. Finally, P-process at SWI or sediment/root interface and the release mechanism in microzone can be revealed, which is the base for the designation of the restoration of the eutrophic lake using in situ technology such as Al dose to prevent P-release or the ecological engineering technique of aquatic plants.

2.3 Studying Zones in Dianchi and Erhai Lakes

Dianchi Lake (102°37′59.76″–102°45′55.07″E, 24°40′38.89″–25°1′21.39″N) is the sixth largest freshwater lake of China at the foot of the Western Hills in southwest of Kunming city of Yunnan Province (southwest China). Dianchi Lake consists of two parts, which are the internal lake and the outer lake. The total area of Dianchi Lake is 306.3 km^2, with a length of 39 km (N–S), a width of 13 km (E–W), an average depth of about 5 m, and a total water capacity of 1.593 billion m^3. The different areas of Dianchi Lake are eutrophic in the various degrees. In 2009, the average total phosphorus (TP) concentrations in sediments are 2–3 g kg^{-1} (0–5 cm), 1–2 g kg^{-1} (5–10 cm), and 1–2 g kg^{-1} (10–20 cm) in turn. The average contents of metal-bound P and organic P (OP) are about 17.57–48.82 % and 20–30 % of those of TP, respectively. The contents of OM in sediments are 8.24–677 g kg^{-1} (0–5 cm), 4.5–590 g kg^{-1} (5–10 cm), and 7.07–649.03 g kg^{-1} (10–20 cm), respectively. The content of TN in sediments (0–20 cm) is 4.91 g kg^{-1}. Extensive blue algal blooms have happened frequently in recent years, and biomass of alga is 4.402×10^6–1.102×10^9 cell l^{-1} (Chinese Research Academy of Environmental Sciences 2014). Despite reduced "external P-loading," Dianchi Lake has failed to recover from eutrophic status partially due to the P-release from

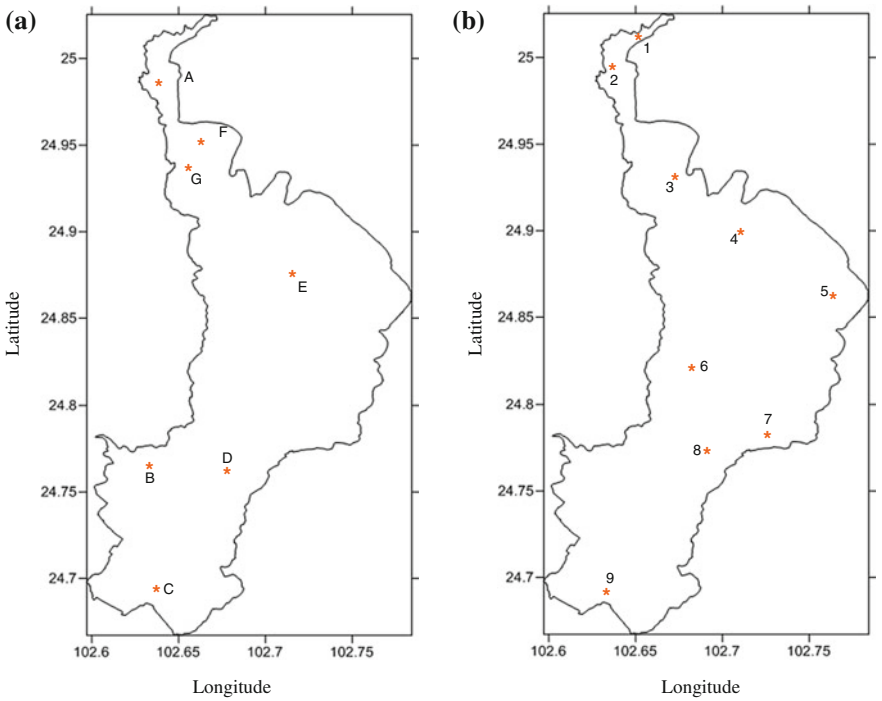

Fig. 2.2 Sampling sites for DGT probe tests and DIFS test at Dianchi Lake. **a** Seven sites (*A–G*) for DGT probes; **b** nine sites (*1–9*) for DIFS test. (Reprinted from Water Air Soil Pollut, 225:2188–2194, Wu, Z.H., Wang, S.R., Jiao, L.X., Wu, F.C., The simultaneous measurement of phosphorus, sulfide, and trace metals by Ferrihydrite/AgI/Chelex-100 DGT (Diffusive Gradients in Thin Films) probe at sediment/water interface (SWI) and remobilization assessment, copyright (2015), with the permission from Springer; Reprinted from J. Geochem. Explor., 156: 145–152., Wu, Z.H., Wang, S.R., Jiao, L.X., Geochemical behavior of metals-sulfide-phosphorus at SWI (sediment/water interface) assessed by DGT (Diffusive gradients in thin films) probes, copyright (2015), with the permission from Elsevier)

the sediment ("internal P-loading"). The sampling locations (Dianchi Lake) for DGT probe test are indicated in Fig. 2.2a (Wu et al. 2014, 2015d). The sampling locations for P-DIFS test (Dianchi Lake) are indicated in Fig. 2.2b. The longitudes and latitudes for all sampling sites are listed in Table 2.1 (Wu et al. 2014, 2015c, d).

Erhai Lake (100°5′E–100°17′E, 25°35′N–25′58′N) is situated at Dali Bai Autonomous Prefecture in Yunnan Province (China) and the second largest lake in Yunnan Plateau. The shape of this lake is like an ear with the length of 43 km and the width of 8.4 km. The lake has a surface area of 249 km^2 with the maximum water depth of 21.5 m. The storage capacity is 2.88×10^9 m^3, and the water

Table 2.1 Sampling locations of DGT tests in Dianchi Lake. (Seven sites (A–G) for DGT probe test; nine sites (1–9) for DGT–DIFS test)

Site	Longitude	Latitude	Site	Longitude	Latitude
	E	N		E	N
A	102°38′34″	24°59′30″	1	102.67	25.02
B	102°37′48″	24°46′24″	2	102.63	24.99
C	102°38′12.149″	24°41′22.542″	3	102.68	24.93
D	102°41′24.463″	24°47′52.517″	4	102.73	24.91
E	102°43′40.84″	24°52′27.39″	5	102.77	24.87
F	102°39′45.54″	24°57′1.01″	6	102.68	24.86
G	102°40′55.99″	24°52′27.39″	7	102.74	24.8
			8	102.72	24.78
			9	102.62	24.69

Reprinted from Water Air Soil Pollut, 225:2188–2194, Wu, Z.H., Wang, S.R., Jiao, L.X., Wu, F.C., The simultaneous measurement of phosphorus, sulfide, and trace metals by Ferrihydrite/AgI/Chelex-100 DGT (Diffusive Gradients in Thin Films) probe at sediment/water interface (SWI) and remobilization assessment, copyright (2015), with the permission from Springer; Reprinted from J. Geochem. Explor., 156: 145–152., Wu, Z.H., Wang, S.R., Jiao, L.X., Geochemical behavior of metals-sulfide-phosphorus at SWI (sediment/water interface) assessed by DGT (Diffusive gradients in thin films) probes, copyright (2015), with the permission from Elsevier

residence time is 2.75 years. The nutrient level of Erhai Lake is changing from mesotrophication to eutrophication in recent years. The location for DGT test in situ and in rhizobox for P taken up by plant root is shown in Fig. 2.3.

2.4 Summary

This chapter reported the environmental problem of Dianchi and Erhai lakes in the southwest of China. The "internal P-loading" in Dianchi Lake and two aquatic plants (*Zizania caduciflora* and *Myriophyllum aquaticum*) for the ecological restoration in Erhai Lake have been introduced. To reveal the mechanism of "internal P-loading" (Dianchi Lake) and P-uptake mechanism by plant roots (Erhai Lake), DGT and related techniques should be developed and applied. The DGT technique for lake sediment and rhizosphere should be designed to illustrate the environmental problem related to lake eutrophication. In order to lay out the DGT research program for the P-transfer across SWI or sediment/root interface, a series of DGT probes with new types, LA-ICP-MS, CID, 1D/2D-DIFS, Visual MINTEQ and ImageJ 1.38e softwares, and DGT test in rhizosphere have been arranged to achieve DGT profile/image at fine scale, DGT image of S(-II) or P, kinetic P-release at DGT/porewater/sediment interface, P-transfer across root/sediment interface for the quantification of "internal P-loading," geochemical reactions for P-release, sulfide or Fe microniche for P-release, and the DGT function as a surrogate of plant

Fig. 2.3 The site for DGT test in rhizosphere of aquatic plants at Erhai Lake. *Open triangle* the site of the experimental base for aquatic plants in Erhai (Institute of Hydrobiology, Chinese Academy)

root for P-uptake. The logical stratification of the components (all sorts of DGT techniques) making up the general design for DGT research has been discussed. Moreover, DGT test locations for probe, piston, and DIFS in Dianchi Lake and DGT test in rhizosphere in Erhai Lake were also introduced.

References

Armstrong W (1978) Root aeration in the wetland condition. In: Hook DD, Crawford RMM (eds) Plant life in anaerobic environments. Ann Harbor Science Publishers Inc., Ann Harbor, MI, pp 269–297

Barbanti A, Bergamini MC, Frascari F, Miserocchi S, Rosso G (1994) Critical aspects of sedimentary phosphorus chemical fractionation. Environ Qual 23(5):1093–1102

Barko JW, Gunnison D, Carpenter SR (1991) Sediment interactions with submersed macrophyte growth and community dynamics. Aquat Bot 41:41–65

Blindow I, Andersson G, Haregy A (1993) Long-term pattern of alternative stable states in two shallow eutrophic lakes. Freshwater Biol 30:1159–1167

Böstrom B, Pettersson K (1982) Different patterns of phosphorus release from lake-sediments in laboratory experiments. Hydrobiologia 91–2:415–429

Brix H, Schierup HH (1989) The use of aquatic macrophytes in water-pollution control. Ambio Stockh 18:100–107

Canfield DE, Hoyer MV (1992) Aquatic macrophytes and their relation to the limnology of Florida lakes. Final Report Submitted to the Bureau of Aquatic Plant Management, Florida Department of Natural Resources, Tallahassee, FL, pp 596

Chinese Research Academy of Environmental Sciences (2014) The survey and the investigation of "internal loading character" of Dianchi Lake (Chinese)

Christensen KK (1997) Differences in iron, manganese, and phosphorus binding in freshwater sediment vegetated with Littorella uniflora and benthic microalgae. Water Air Soil Pollut 99:265–273

Christophoridis C, Fytianos K (2006) Conditions affecting the release of phosphorus from surface lake sediments. J Environ Qual 35(4):1181–1192

Conley DJ, Smith WM, Cornwell JC, Fisher TR (1995) Transformation of particle-bound phosphorus at the land sea interface. Estuar Coast Shelf Sci 40:161–176

Cook PLM, Holland DP, Longmore AR (2010) Effect of a flood event on the dynamics of phytoplankton and biogeochemistry in a large temperate Australian lagoon. Limnol Oceanogr 55:1123–1133

Cutter GA, Oatts TJ (1987) Determination of dissolved sulfide and sedimentary sulfur speciation using gas chromatography-photoionization detection. Anal Chem 59:717–721

Davison W, Zhang H, Grime G (1994) In situ speciation measurements of trace components in natural waters using thin-film gels. Nature 367:546–548

Davison W, Fones G, Harper M, Teasdale P, Zhang H (2000) Dialysis, DET and DGT: in situ diffusional techniques for studying water, sediment and soils. In: Buffle J, Horvai G (eds) In situ monitoring of aquatic systems: chemical analysis and speciation. Wiley, Chichester, pp 495–570

Ding S, Sun MQ, Xu D, Jia F, He XA, Zhang CS (2012) High-resolution simultaneous measurements of dissolved reactive phosphorus and dissolved sulfide: the first observation of their simultaneous release in sediments. Environ Sci Technol 46:8297–8304

Doyle MO, Otte ML (1997) Organism-induced accumulation of iron, zinc and arsenic in wetland soils. Environ Pollut 96(1):1–11

Ernstberger H, Davison W, Zhang H, Tye A, Young S (2002) Measurement and dynamic modelling of trace metal mobilization in soils using DGT and DIFS. Sci Total Environ 36:349–354

Farmer AM (1985) The occurrence of vesicular arbuscular mycorrhiza in isoetid-type submerged aquatic macrophytes under naturally varying conditions. Aquat Bot 21:245–249

Fones GR, Davison W, Hamilton-Taylor J (2004) The fine-scale remobilization of metals in the surface sediment of the North-East Atlantic. Cont Shelf Res 24:1485–1504

Förstner U, Calmano W, Hong J, Kersten M (eds) (1994) Effects of redox variations on metal speciation: implications on sediment quality criteria assessment. The Royal Society of Chemistry, London, pp 83–102

Froelich PN (1988) Kinetic control of dissolved phosphate in natural rivers and estuaries: a primer on the phosphate buffer mechanism. Limnol Oceanogr 33:649–668

Froelich PN, Bender ML, Luedtke NA, Heath GR, DeVries T (1982) The marine phosphorus cycle. Am J Sci 282:474–511

Gambrell RP, Patrick WH (1978) Chemical and microbiological properties of anaerobic soils and sediments. In: Hook DD, Crawford RMM (eds) Plant life in anaerobic environments. Ann Harbor Science Publishers Inc., Ann Harbor, MI, pp 375–423

Golterman HL (eds) (2004) The chemistry of phosphate and nitrogen compounds in sediments. Kluwer, Dordrecht, The Netherlands

Gu B, DeBusk T, Dierberg FE, Chimney M, Pietro K, Aziz T (2001) Phosphorus removal from Everglades agricultural area runoff by submerged aquatic vegetation/limerock treatment technology: an overview of research. Water Sci Technol 44:101–108

Hamilton-Taylor J, Morris EB (1985) The dynamics of iron and manganese in surface sediments of a seasonally Anoxic Lake. Archiv Für Hydrobiologie-Supplement 72:135–165

Harper MP, Davison W, Tych W, Zhang H (1998) Kinetics of metal exchange between solids and solutions in sediments and soils interpreted from DGT measured fluxes. Geochim Cosmochim AC 62:2757–2770

Hinsinger P, Courchesne F (2008) Biogeochemistry of metals and metalloids at the soil-root interface. In: Violante A, Huang PM, Gadd GM (eds) Biophysico-chemical processes of heavy metals and metalloids in soil environments. Wiley-Interscience, Hoboken, NJ, pp 268–311

Kirk GJD, Bajita JB (1995) Root-induced iron oxidation, pH changes and zinc solubilization in the rhizosphere of lowland rice. New Phytol 131:129–137

Kleeberg A, Dudel GE (1997) Changes in extent of phosphorus release in a shallow lake (Lake GroDer Miiggelsee; Germany, Berlin) due to climatic factors and load. Mar Geol 139:61–75

Kopáček J, Borovec J, Hejzlar J, Ulrich KU, Norton SA, Amirbahman A (2005) Aluminum control of phosphorus sorption by lake sediments. Environ Sci Technol 39:8784–8789

Lebo ME (1991) Particle-bound phosphorus along an urbanized coastal plain estuary. Mar Chem 34:225–246

Lehto NJ, Davison W, Zhang H, Tych W (2006) Analysis of micro-nutrient behaviour in the rhizosphere using a DGT parameterised dynamic plant uptake model. Plant Soil 282:227–238

Leslie AJ, Nall LE, Van Dyke JM (1983) Effects of vegetation control by grass carp on selected water-quality variables in four Florida lakes. Trans Am Fish Soc 112:777–787

Lin CY, Wang ZG, He MC, Li YX, Liu RM, Yang ZF (2009) Phosphorus sorption and fraction characteristics in the upper, middle and low reach sediments of the Daliao river systems, China. J Hazard Mater 170:278–285

Mason S, McNeill A, McLaughlin MJ, Zhang H (2010) Prediction of wheat response to an application of phosphorus under field conditions using diffusive gradients in thin-films (DGT) and extraction methods. Plant Soil 337(1):243–258

McNabb CD (1976) The potential of submersed vascular plants for reclamation of wastewater. In: Tourbier J, Pearson RW (eds) Biological control of water pollution. The University Press, Philadelphia, PA, pp 120–132

Monbet P, Mckelvie ID, Worsfold PJ (2008) Combined gel probes for the in situ determination of dissolved reactive phosphorus in porewaters and characterization of sediment reactivity. Environ Sci Technol 42:5112–5117

Naylor C, Davison W, Motelica-Heino M, Van Den Berg GA, Van der Heijdt LM (2004) Simultaneous release of sulfide with Fe, Mn, Ni and Zn in marine harbor sediment measured using a combined metal/sulfide DGT probe. Sci Total Environ 328:275–286

Nuttall PM (1985) Uptake of phosphorus and nitrogen by *Myriophyllum aquaticum* (velloza) Verdc. growing in wastewater treatment system. Aus J Mar Res 36:493–507

O'Dell KM, Van Arman J, Welch BH, Hill SD (1995) Changes in water chemistry in a macrophyte-dominated lake before and after herbicide treatment. Lake Res Manage 11(4): 311–316

Otte ML, Rozema J, Koster L, Haarsma MS, Broekman RA (1989) Iron plaque in roots of *Aster tripolium* L.: interaction with zinc uptake. New Phytol 111:309–317

Otte ML, Dekkers MJ, Rozema J, Broekman RA (1991) Uptake of arsenic by *Aster tripolium* in relation to rhizosphere oxidation. Can J Bot 69:2670–2677

Palmer-Felgate EJ, Mortimer RJG, Krom MD, Jarvie HPR, Williams JR, Spraggs E, Stratford CJ (2011) Internal loading of phosphorus in a sedimentation pond of a treatment wetland: effect of a phytoplankton crash. Sci Total Environ 409:2222–2232

Paludan C, Morris JT (1999) Distribution and speciation of phosphorus along a salinity gradient in intertidal marsh sediments. Biogeochemistry 45:197–221

Roden E, Edmonds JW (1997) Phosphate mobilization in iron-rich anaerobic sediments: microbial Fe(III) oxide reduction versus iron-sulfide formation. Arch Hydrobiol 139(3):347–378

Shaw T, Gieskes JM, Jahnke RA (1990) Early diagnosis in differing depositional environments: the response of transition metals in pore water. Geochim Cosmochim Acta 54:1233–1246
Shilla DA, Asaeda T, Kalibbala MM (2009) Phosphorus speciation in Myall lake sediment, NSW, Australia. Wetlands Ecol Manage 17:85–91
SØndergaard M, Lægaard S (1977) Vesicular arbuscular mycorrhiza in some aquatic vascular plants. Nature 268:232–233
Sundby B, Anderson LG, Hall POJ, Iverfeldt A, Vanderloeff MMR, Westerlund SFG (1986) The effect of oxygen on release and uptake of cobalt, manganese, iron and phosphate at the sediment-water interface. Geochim Cosmochim AC 50(6):1281–1288
Wang S, Jin XC, Zhao HC, Wu FC (2009) Phosphorus release characteristics of different trophic lake sediments under simulative disturbing conditions. J Hazard Mater 161:1551–1559
Widerlund A, Davison W (2007) Size and density distribution of sulfide-producing microniches in lake sediments. Environ Sci Technol 41:8044–8049
Wilson TA, Norton SA, Lake BA, Amirbahman A (2008) Sediment geochemistry of Al, Fe, and P for two historically acidic, oligotrophic Maine lakes. Sci Total Environ 404:269–275
Wu ZH, He MC, Lin CY (2011) In situ measurements of concentrations of Cd Co, Fe and Mn in estuarine porewater using DGT. Environ Pollu 159:1123–1128
Wu ZH, Wang SR, Jiao LX, Wu FC (2014) The simultaneous measurement of phosphorus, sulfide, and trace metals by Ferrihydrite/AgI/Chelex-100 DGT (diffusive gradients in thin films) probe at sediment/water interface (SWI) and remobilization assessment. Water Air Soil Pollut 225:2188–2194. (Reprinted from Water Air Soil Pollut, 225:2188-2194, Wu, Z.H., Wang, S.R., Jiao, L.X., Wu, F.C., The simultaneous measurement of phosphorus, sulfide, and trace metals by Ferrihydrite/AgI/Chelex-100 DGT (Diffusive Gradients in Thin Films) probe at sediment/water interface (SWI) and remobilization assessment, copyright (2015), with the permission from Springer)
Wu ZH, Wang SR, He MC, Wu FC (2015a) The measurement of metals by diffusive gradients in thin films (DGT) at sediment/water interface (SWI) of bay and remobilization assessment. Environ Earth Sci 73(10):6283–6295
Wu ZH, He MC, Wang SR, Ni ZK (2015b) The assessment of localized remobilization and geochemical process of 14 metals at sediment/water interface (SWI) of Yingkou coast (China) by diffusive gradients in thin films (DGT). Environ Earth Sci 73(10):6081–6090
Wu ZH, Wang SR, He MC (2015c) Element remobilization, "internal P-loading" and sediment-P reactivity researched by DGT (diffusive gradients in thin films) technique. Environ Sci Pollut R. doi:10.1007/s11356-015-4736-8
Wu ZH, He MC, Wang SR (2015d) Multi-metals measured at sediment/water interface (SWI) by diffusive gradients in thin films (DGT) technique for geochemical research. Arch Environ Con Tox. doi:10.1007/s00244-015-0184-1 (online published)
Wu ZH, Wang SR, Jiao LX (2015e) Geochemical behavior of metals-sulfide-phosphorus at SWI (sediment/water interface) assessed by DGT (Diffusive gradients in thin films) probes. J Geochem Explor 156:145–152. (Reprinted from J. Geochem. Explor., 156: 145-152., Wu, Z. H., Wang, S.R., Jiao, L.X., Geochemical behavior of metals-sulfide-phosphorus at SWI (sediment/water interface) assessed by DGT (Diffusive gradients in thin films) probes, copyright (2015), with the permission from Elsevier)
Zhang JA, Huang XL (2007) Relative importance of solid-phase phosphorus and iron on the sorption behavior of sediments. Environ Sci Technol 41:2789–2795
Zhang H, Davison W, Mortimer RJG, Krom MD, Hayes PJ, Davies IM (2002) Localised remobilization of metals in a marine sediment. Sci Total Environ 296:175–187
Zwolsman JJG (1994) Seasonal variability and biogeochemistry of phosphorus in the Scheldt Estuary, southwest Netherlands. Estuar Coast Shelf S 39:227–248

Chapter 3
The Research Methodology

For DGT research for P in lake sediment, there is only one paper (Monbet et al. 2008; Zhang et al. 1998), which simply investigated the DGT-P profiles, P-release characters, or kinetic P-release at two sites of lakes. The related elements (Fe and S (-II)) and "internal P-loading" in lakes have not been measured or discussed in these papers. The kinetic P-release was investigated only at a few sites by DGT/DET profiles (Monbet et al. 2008). The result of this research (Monbet et al. 2008) cannot be used to assess the P-release in whole lakes, and the sediment P-pool (exchangeable and loosely sorbed P) for K_D in numerical simulation may not be the "real" P-pool. The Fe-microniche-related flux of in sediment microzone and the coupled Fe–S(-II)–P reaction may also engender P-release. Aquatic plant root can absorb P and restore lake ecology. However, there is no paper reporting the P-uptake mechanism by root or Fe-microniche image for P-release prediction. So, it is needed to develop DGT probe technique, numerical model, DGT image technique, and DGT test in sediment or rhizosphere for the investigation of P-transfer and P-release process. In this chapter, the DGT and related techniques for the P-research at lake sediment or rhizosphere have been introduced, including the measurement of P and related elements (S(-II) and Fe) in sediment profile, P-kinetic exchange between sediment and water, chemical image of S(-II) or Fe measured by CID or LA-ICP-MS techniques, P-transfer across sediment/root interface, and the test method for physicochemical properties of sediment and water. Based on the DGT test method and theory for lake sediment, the DGT measurement results and P-transfer across SWI or sediment/root can be introduced and discussed in the Chaps. 4 and 7.

S. Wang and Z. Wu, *DGT-based Measurement of Phosphorus in Sediment Microzones and Rhizospheres*, DOI 10.1007/978-981-10-0721-7_3

3.1 The Design for DGT Probe and Piston

In order to measure Fe/P/S at the same location of SWI simultaneously, the DGT probe with multilayer-binding gels and the twin DGT probes were designed. The conformation of DGT probes with multilayer-binding gels is indicated in Fig. 3.1 (Wu et al. 2014, 2015d). The twin probes arranged back-to-back (ferrihydrite probe vs. AgI/Chelex-100 probe) were used for the measurement of three elements at sites A, C, and F (Fig. 3.2); the other kind of twin probes (ferrihydrite probe vs. Chelex-100 probe) was used for the measurement of P and Fe at sites B, D, and E (Fig. 3.2); Ferrihydrite/AgI/Chelex-100 probe (three binding layers) was used for three elements at site G (Fig. 3.2). Moreover, at site H, SPR-IDA DGT probe was used for the chemical image of labile Fe in sediment porewater. At sites (1–9) (Fig. 2.2 in Chap. 2), ferrihydrite DGT pistons were used for the DGT-DIFS test for the simulation calculation of release/diffusion at DGT/sediment microzone and assessment of kinetic P-release. The DGT probe with one framework and one open window (1.8 × 15 cm) and the DGT piston with window diameter (1.8 cm) with 0.78-mm-thick diffusive gel were used for the mentioned tests. The multilayer-binding-gel DGT probes and twin probes were designed based on the methods introduced by references (Wu et al. 2014, 2015c, d). In this research, the single-binding gel (Chelex-100 or ferrihydrite), AgI/Chelex100, and ferrihydrite/AgI/Chelex-100 DGTs were equipped for the DGT tests at seven sites (A–G). With regard to the DGT probe (0.39 mm diffusive gel) test at sites F and G in May, 2013, Δg (diffusive layer thickness) of Fe was 0.53 mm, Δg of labile sulfide was 0.93 mm, and Δg of labile P was 1.53 mm, for ferrihydrite/AgI/Chelex-100 DGT probe; Δg of labile Fe was 0.53 mm and Δg of labile sulfide was 0.93 mm, for AgI/Chelex-100 DGT probe; and Δg of labile P was 0.53 mm, for ferrihydrite DGT probe. In the case of the probe (0.78 mm diffusive gel) test from sites A to E in September, 2013, Δg of labile Fe was 0.92 mm and Δg of labile sulfide was 1.32 mm, for AgI/Chelex100 DGT probe; Ag of labile Fe or P was both 0.92 mm, for Chelex-100 or ferrihydrite DGT probe.

3.2 The Test Method for DGT Piston and Probe in Sediments of Dianchi Lake and the Subsequent Procedures

The DGT probes mentioned above were used for the DGT profiles at seven sites (A–G). The DGT types and sediment sites (A-G) have been listed in the Sect. 3.1. At site H, suspended particulate reagent (iminodiacetate) (SPR-IDA) DGT probe was used for chemical image of labile Fe. The deployment method for DGT probes were introduced in references (Wu et al. 2011, 2014, 2015c, d). The deployment times were 36 h at sites (A–E), 24 h at sites (F and G), and 48 hat site H, in turn. The temperatures at SWIs were 22 °C at sites (A–E), 26 °C at sites (F and G), and 17 °C at site H, in turn. The schematic graph for DGT probe deployment at SWI is indicated in Fig. 3.2.

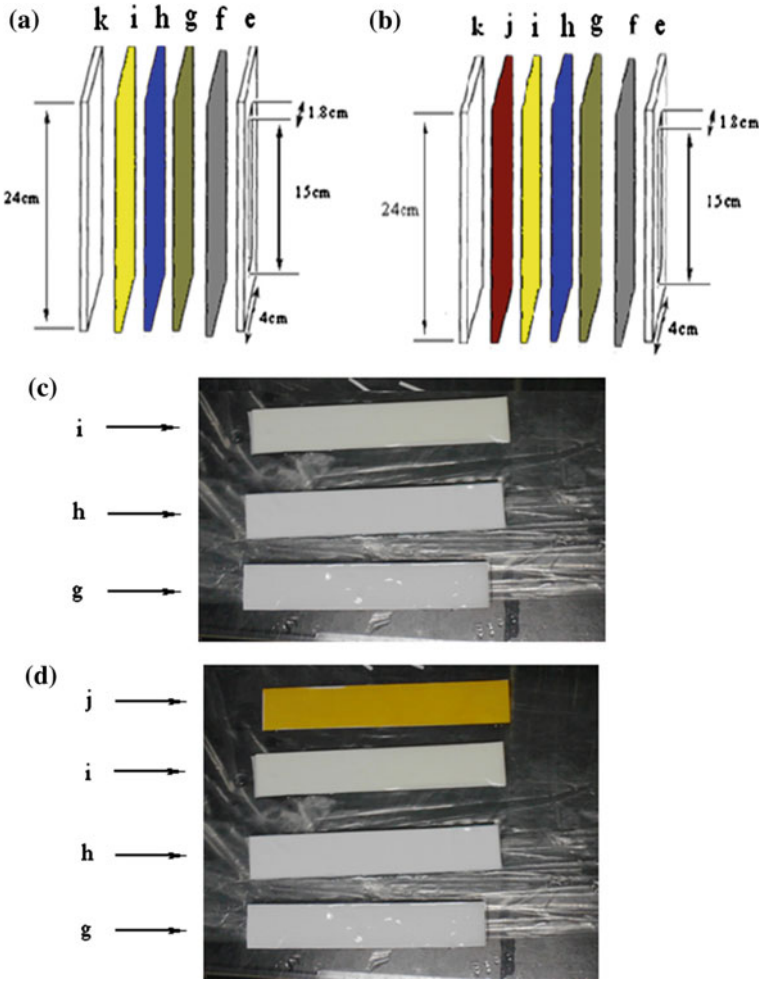

Fig. 3.1 The conformation of DGT probes with multi-layer-binding gels. **a** AgI/Chelex-100-DGT probe; **b** ferrihydrite/AgI/Chelex-100-DGT probe; *e* Top retaining plate with a window; *f* Filter; *g* Diffusive gel; *h* Chelex-100 gel; *i* AgI gel; *j* Ferrihydrite gel; *k* Backing plate; **c** the picture of *g*, *h,* and *i* of (**a**); **d** the picture of *g*, *h*, *i,* and *j* of (**b**). (Reprinted from Water Air Soil Pollut, 225:2188–2194, Wu, Z.H., Wang, S.R., Jiao, L.X., Wu, F.C., The simultaneous measurement of phosphorus, sulfide, and trace metals by Ferrihydrite/AgI/Chelex-100 DGT (Diffusive Gradients in Thin Films) probe at sediment/water interface (SWI) and remobilization assessment, copyright (2015), with the permission from Springer; Reprinted from J. Geochem. Explor.,156:145–152., Wu, Z.H., Wang, S.R., Jiao, L.X., Geochemical behavior of metals-sulfide-phosphorus at SWI (sediment/water interface) assessed by DGT (Diffusive gradients in thin films) probes, copyright (2015), with the permission from Elsevier)

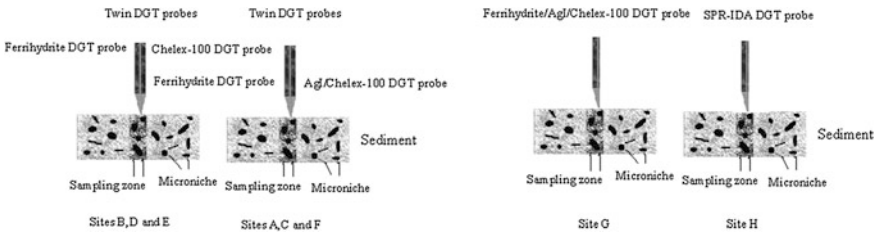

Fig. 3.2 The schematic graph for deployment method of DGT probes with multi-types

Table 3.1 Diffusive coefficients of Fe, P, and S(-II) in diffusion gel and elution factor

Element	Diffusive coefficient ($\times$ cm^{-2} s^{-1})				Elution factor (%)
	26 °C	22 °C	24 °C	17 °C	
Fe	6.28×10^{-6}	5.63×10^{-6}		4.87×10^{-6}	80
P	6.21×10^{-6}	5.57×10^{-6}	5.89×10^{-6}		100
S	1.85×10^{-5}	1.66×10^{-5}			

Reprinted from Water Air Soil Pollut 225:2188–2194, Wu, Z.H., Wang, S.R., Jiao, L.X., Wu, F. C., The simultaneous measurement of phosphorus, sulfide, and trace metals by Ferrihydrite/AgI/Chelex-100 DGT (Diffusive Gradients in Thin Films) probe at sediment/water interface (SWI) and remobilization assessment, copyright (2015), with the permission from Springer; Reprinted from Environ. Sci. Pollut. R., published online, DOI:10.1007/s11356-015-4736-8, Wu, Z.H., Wang, S.R., He, M.C., Element remobilization, "internal P-loading" and sediment-P reactivity researched by DGT (diffusive gradients in thin films) technique, copyright (2015), with the permission from Springer

The diffusion coefficients for Fe, P, and S(-II) in diffusion gel are indicated in Table 3.1 (Wu et al. 2014, 2015c).

After deployment, the subsequent test for DGT probes was conducted according to the methods introduced in references (Zhang et al. 2002; Widerlund and Davison 2007; Ding et al. 2012; Naylor et al. 2004; Wu et al. 2014, 2015a, b, c, d). Chelex-100 and ferrihydrite gel strips were sliced at vertical resolution of 2 mm, every segments of Chelex-100 or ferrihydrite gels were eluted by1 M HNO_3 or 0.25 M H_2SO_4 for Fe or P, and both the elution times were 24 h. The elution coefficients for P and Fe were listed in Table 3.1. Then, the elution solutions were diluted for HR-ICP-MS analysis (ELEMENT XR, Thermo Scientific) and ^{103}Rh was used as the internal element. Standard material GSD-9 (Institute of Geophysical and Geochemical Exploration of China) was used for the QC of the P- and Fe-analyses. DGT concentration/flux can be calculated based on mass accumulated on DGT resin, Eqs. (3.1, 1.1, and 1.2).

$$M = C_E\left(V_{gel} + V_{acid}\right)/f_e \tag{3.1}$$

where V_{gel} is the volume of gel strip; V_{acid} is the volume of elution solution; and fe is elution coefficient.

After test in surface sediment for P-DIFS simulation at nine sediment sites (1–9), the ferrihydrite DGT piston underwent the same procedures of the retrieval of DGT resin, the elution of ferrihydrite gel, and analysis for P by molybdenum blue methods (User's guide to DGT technique 2003).

When it comes to AgI gel and SPR-IDA gel analysis, these contents will be introduced in Sects. 3.4 and 3.5.

3.3 The DGT Method (in Situ or in Rhizobox) for the P-Uptake Process by Roots of Aquatic Plants in Erhai Lake

The in situ DGT test in the rhizosphere was conducted in the site (Fig. 2.3 in Chap. 2) in the experimental base for aquatic plants in Erhai Lake (Institute of Hydrobiology, Chinese Academy). Aquatic plants play an important role in the nutrient removal by creating a favorable environment due to the complex chemical, biological, and physical processes and P-uptake by roots. DGT has been proved to be an in situ surrogate of plant root to mimic element-uptake (metals or P) in soil porewater (Zhang et al. 2001; Williams et al. 2012). So, the test method for DGT piston at sediment/root interface and the calculation method should be introduced.

3.3.1 The in situ DGT Test

For the research aim of DGT's function as the proxy of root for the P-uptake and the in situ DGT test in rhizosphere of aquatic plants, the subsequent experiment procedures were introduced, including the following steps:

1. The selection of aquatic plants for DGT test in rhizosphere. Ten locations in Erhai lake (Fig. 2.3 in Chap. 2), each with at least three aquatic plants *(Zizania caduciflora* or *Myriophyllum verticillatum)* and water depth in the range of 1.0–1.5 m, were chosen as test sites. These plants were located near the bank of Erhai Lake, where the water area is wide with gentle flow. *Zizania caduciflora* grew well with about 40 cm height aboveground part, and the distance among each location was more than 10 m. *Myriophyllum verticillatum* grew well with at least 15-cm-length stem, and the distance among each location was about 5 m.
2. DGT test in rhizosphere of aquatic plants. The ferrihydrite-DGT pistons with the diffusive gel thickness of 0.78 mm and window area of 2.54 cm^2 were assembled and pretreated according to the method in references (Zhang et al. 1998; User's guide to DGT technique 2003). Then, the long rod with the DGT piston fixed to the tip of it was inserted into the rhizosphere of two kinds of aquatic plants, both at the depth of 3.0 cm under SWI. The same operation was

conducted in each plant rhizosphere. The initial time and temperature in rhizosphere were recorded.

3. After 24 h, the rods with DGT pistons were retrieved and the DGT resin gels were eluted as the method introduced in Sect. 3.2. Then, each plant with whole root/stem/leaf and sediment was sampled and kept in ice box for subsequent procedures.
4. DGT concentration determination. The elution solution was determined for P by ICP-MS or molybdenum blue methods (SEPA 2002; Wu et al. 2015c, d). The DGT-P concentration was calculated according to Eqs. (3.1, 1.1 and 1.2).
5. The treatment method for porewater and sediment. The soluble reactive P (SRP) in porewater, the particle density (P_c) of sediment particle, sediment porosity (ϕ_s), and the effective diffusion coefficient in the sediment porewater (D_s), total P-content, and P-fractions in sediment can be determined using the method introduced in Sect. 3.4.
6. The treatment method for root/stem/leaf and P measurement. Plant tissues were washed free of sediment by water; then, the plant was divided into root, leaf, and stem; and the fresh weights were determined. The plants in each site or rhizobox were divided into root/stem/leaf parts, and the root in sediment was washed out by water and 40-μm mesh carefully. Then, the blotting paper was used to blot up the water on root surface, and the fresh weight of root in each site (in situ DGT test) or rhizobox was recorded. Then, the roots were tiled on the PMMA dish, scanned by SNAP SCAN 1236 (AGFA company, Germany), and analyzed by WINRHIZO root analyzing software (Regent Instruments Inc, Canada). Based on this technique, the roots of two kinds of macrophytes were divided into separate groups according to root diameters. The roots excluding rhizome were divided into groups, $d < 2$ mm, $2 < d < 3$ mm, and $d > 3$ mm. The root surface areas according to diameter classifications were analyzed, and the total root surface areas for plants in each site were calculated. The roots according to the diameter classification and rhizomes in each site were oven-dried at 80 °C until a constant weight was reached, and the dry weights of them were recorded. The total weight of roots and rhizomes in each site were calculated and recorded. Then, the last root samples were pulverized into flours and mixed uniformly. The stem and leaf samples in each site were also washed, dried, weighted, pulverized, and mixed, respectively. All plant samples (root/stem/leaf) (0.5 g) were digested using H_2SO_4-HNO_3-$HClO_4$ method introduced by reference (Lao 1988). Then, P-contents in digestion solutions for plant tissues (root/stem/leaf) were measured by molybdenum blue colorimetry method. The P-content in plant tissues can be calculated by P-mass divided by tissue dry weight. The blank sample and standard materials (Laver-GBW 10023, Tea leaf-GBW08513 and Carrot-GBW10047) (National Sharing platform for Reference Material) were also processed and determined by this method, and *LOD* and recovery were listed in Table 3.2.
7. The calculation of C_E and P-transfer across sediment/root interface. C_E, the effective concentration, includes both concentration in sediment porewater and the resupply from sediment particle, which is corresponded with the same mass accumulated in DGT resin in case (b) (Fig. 1.5 in Chap. 1) "diffusion-only" case.

Table 3.2 Quality control for analysis of aquatic plants

Standard material	Recovery (%) $n = 5$	Duplicate sample RSD (%) $n = 9$	Standard value (mg kg^{-1})	LOD (mg kg^{-1})
GBW10023	92 ± 9	7.2 ± 2	5850	
GBW08513	103 ± 8	8.5 ± 4	1480	
GBW10047	88 ± 9	9.1 ± 3	2300	4

C_{DGT} measurement provides a derived concentration of C_E, which is based on the research of element diffusional processes in rhizosphere (Williams et al. 2012). When plant uptake locally lowers sediment concentration, C_E can be related to root uptake. This transport-limited root uptake type is the worst case because the element can be supplied from both solution concentration and sediment particle and C_E can be used to assess the potential hazard for the measured sediment. The 2D-DIFS model (DGT-induced fluxes in sediments) has been invented for the calculation of R_{diff} (Sochaczewski et al. 2007). For the R_{diff} calculation in the "diffusion-only" case, the input parameters distribution ratio (K_d) and soil response time (T_c) were 10^{-10} (cm^3 g^{-1}) and 10^{10} (s), in turn (Sochaczewski et al. 2007). According to Eqs. (1.4–1.6), P_c, ϕ, and D_s can be calculated and they are input into the user's interface of 2D-DIFS (Fig. 3.3), together with DGT parameters, and R_{diff} value can be output. Finally, C_E can be calculated by Eq. (1.3). Based on measurement results of DGT, porewater, and plants, the linear relations between C_{DGT}, C_E, labile P in porewater, and P-contents in root/shoot/leaf were researched, and the uptake mechanism by root, P-transfer across root/porewater/sediment interface, and the prediction of DGT for P concentration in plant tissues can be investigated.

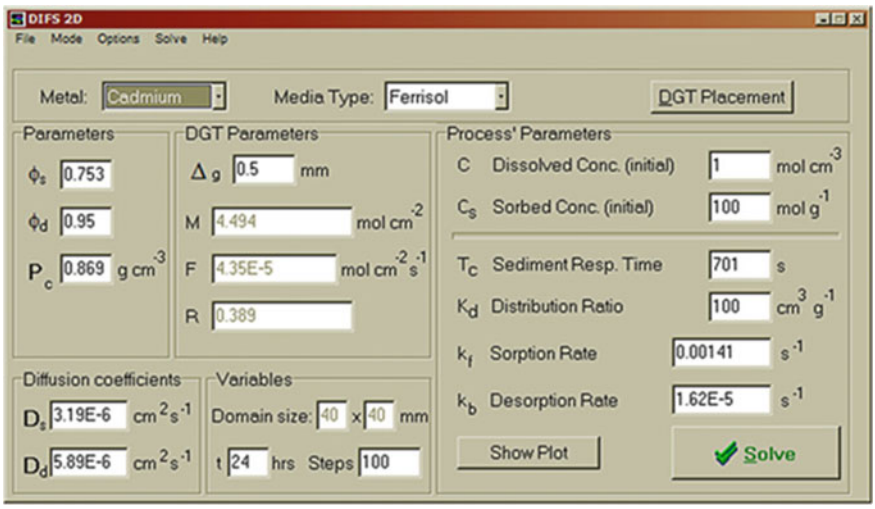

Fig. 3.3 The user's interface of 2D-DIFS model

3.3.2 The DGT Test in Rhizobox

To illuminate the DGT test in rhizobox for the investigation of P taken up by roots of aquatic plants cultivated in rhizobox, the conformation and functions of the rhizobox, and the experiment method for DGT test should be introduced as the following contents.

1. The conformation and function of the rhizobox. The rhizobox (Fig. 3.4) used in DGT test contained three sections of sediments, which were the bottom layer (M), the middle layer (L), and the high layer (K), with the lengths of 8, 30, and 15 cm, in turn. Between M and L (mesh B), there was one nylon mesh (d = 28 μm). There were two fiberglass meshes (d = 2 mm) between K and L (mesh C), and at the bottom of M (mesh A). Three circular holes were in the middle of fiberglass mesh (mesh C). The diameters of the middle hole and the other two near the middle hole were 3 and 1 cm, in turn. Meshes A and C only permitted water exchange and did not allow particles pass through; Mesh B divided M and L layers, only permitted the growth of the plant in L layer, and the rhizosphere was formed in L layer. Mesh B also allowed element and water exchange between two sides of this mesh. The conformation of the rhizobox favored the DGT test and the measurement of the monitoring sondes. The sampling hole with the inside diameter of 2.0 cm and waterproof cover was in the side of L layer in the rhizobox. The sampling hole was used for the placement of DGT piston and the retrieval of sediment sample. There were two rulers with the miniunit of mm at the vertical and horizontal directions adhered to the rhizobox, which can be used for the accurate position of the monitoring sondes, DGT piston, and sediment sampling. There were two lugs at the top of the rhizobox. After the plant was cultivated in the rhizobox, it was fastened to the cross beam of the floating flat (Fig. 3.5) in Erhai Lake.
2. The sampling device. The sampling device for the sediment in rhizobox was a plastic injector without needle with the inner diameter of 2 cm. The sampling device can be put into the sampling hole in the L layer of the rhizobox to extract wet sediment.
3. The monitoring sondes. The monitoring sondes included the portable 5-star-pH/Eh electrode probe (Thermo Orion, USA) and one soil temperature sensor (Precise Instrument Company, Wuxi, China). They were inserted into two circular holes in mesh C for the determination of pH/Eh/temperature.
4. The floating flat. The plant in rhizobox was cultivated in the floating flat in lake. The floating flat (Fig. 3.5) was situated on the experimental base for aquatic plants in Erhai (Institute of Hydrobiology, Chinese Academy). The floating flat was 300 m away from Erhai bank. The walls, which were fixed into the sediment bottom, divided the separate water in floating flat from the surrounding lake water. The steel girders traversed each unit with the square shape (4 × 4 m) in floating flat, and water depth was 4 m. The ropes connected two lugs at the top of the rhizobox and the steel girders.

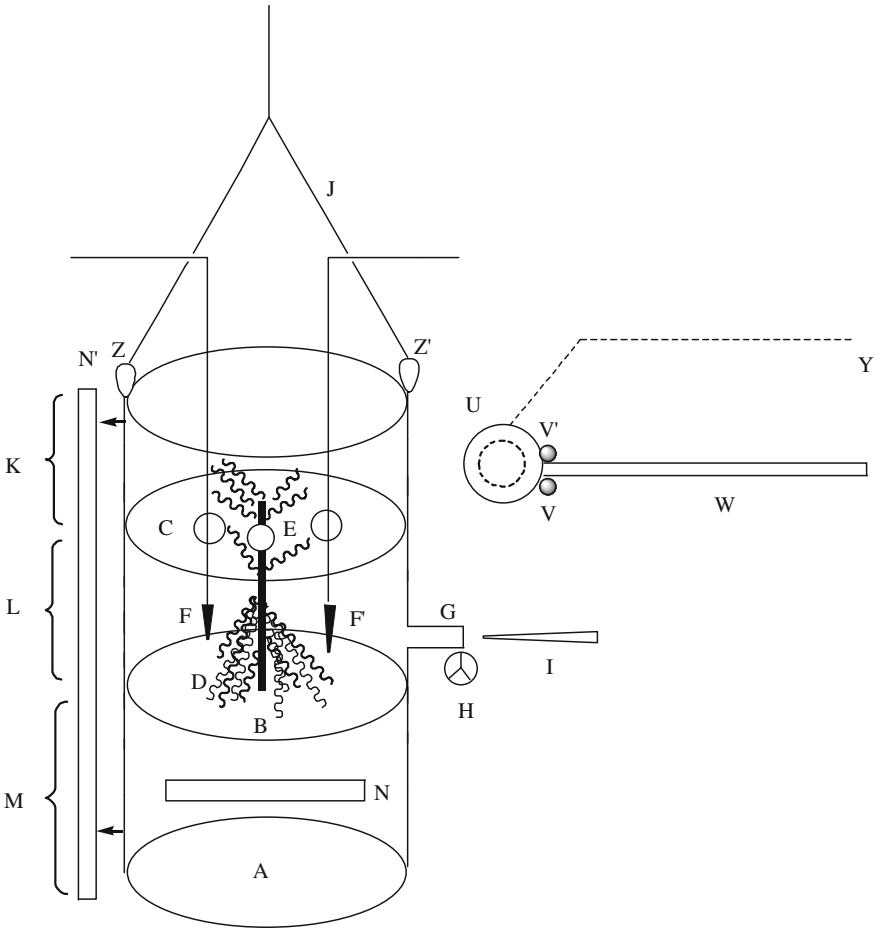

Fig. 3.4 The schematic graph for the conformation of rhizobox and auxiliary device. *A* The mesh A at the bottom of M layer in rhizobox (d = 1 mm); *B* The mesh B between L and M layer in rhizobox (d = 28 μm); *C* The mesh C between K and L layer in rhizobox (d = 1 mm) with the three circle holes (one for aboveground part of plant—F, and the other two for the monitoring sondes—*E* and E′). *D* The rhizosphere of plant in L layer. *G* The sampling hole. *H* The waterproof cover for *G*. *I* The sampling device—a plastic injector. *J* The rope for fixation of the rhizobox into crossbeam of the floating flat. *K* The top layer of rhizobox. *L* The middle layer of rhizobox for belowground part of plant. *M* The bottom layer of rhizobox-sediment layer without roots. *N* and *N′* The two rulers in vertical and horizontal directions. *U* The circular clamp for fastening DGT piston. *W* The ruler for insertion of DGT into root. *X* The button in the end of *W* for the control of *V* and *V′*. *Y* The fine line connected with DGT edge

5. The procedure for the cultivation of aquatic plants. The cultivation method for two aquatic plants *(Zizania caduciflora* or *Myriophyllum verticillatum)* includes the collection of plants, the procedure for mixing sediment and sand, and filling the

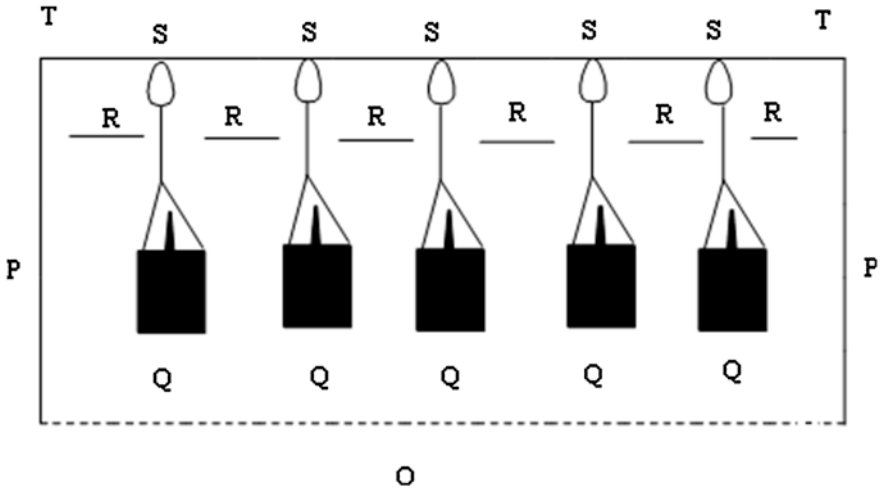

Fig. 3.5 The schematic graph of the floating flat. *O* The bottom of Erhai Lake; *P* The well of floating flat; *Q* The rhizobox with plants; *R* The water level; *S* The rings for fixation of rhizobox; *T* The crossbeam in the top of the floating flat

rhizobox with sediment + sand, and the cultivation of aquatic plants in rhizobox in floating flat. *Zizania caduciflora* plant with the entire rhizome was collected from sediment at depth of 30 cm. The aboveground part was 20 cm length, and each plant had the similar weight of 120.4 ± 10 g. *Myriophyllum verticillatum* plant was collected from sediment at depth of about 20 cm. The above ground part was 15 cm length, and each plant had the similar weight of 10.2 ± 1.1 g. After wash, the plants were soaked in water for 1d. The fertile sediments and sands were naturally dried; then, sediment and sand particles were crushed and passed through 2 mm or 100 μm screen, in turn. The sediment (TP: 1805 or 4000 g kg^{-1}, dw) and sand (240 or 80 g kg^{-1},dw) were mixed according to a series of weight ratios. The total weight for sediment + sand in each rhizobox was 23 kg. Furthermore, 10 kg H_2O was added in each rhizobox (Fig. 3.4) and let the saturation of sediment for 4d. The plant was reared in the layer L in the rhizobox and aboveground part (20 or 15 cm length) passed through the circular hole in mesh C. The belowground part was 10 cm length. The rhizobox was put into the floating platform, and the distance between the top of the rhizobox and water surface was 0.5 m. The plant in rhizobox grew for at least 4 months.

After the cultivation for 4 months, the rhizobox was taken out. The monitoring sondes for Eh/pH/temperature were put into the rhizosphere through two circular holes in mesh C. The ferrihydrite DGT piston with diffusive gel thickness of 0.78 mm was fixed onto the ruler (Fig. 3.4). The sampling hole was opened, and the DGT piston was put into the rhizosphere using the ruler. Then, the sampling hole was closed, and the rhizobox was put into the water, again. After 24 h, the rhizobox

was retrieved and data for Eh/pH/temperature were recorded. The sampling hole was opened, DGT was retrieved, and sediment sample was collected by the sampling device. The plastic injector with sediment was kept in one icebox, and DGT resin was retrieved. The plant in the rhizobox was also collected and kept in icebox. The subsequent procedures for DGT, sediment and plant, and C_E value were conducted according to Sect. 3.3.1. Then, based on measurement results of DGT, sediments, porewater, and plants, the linear relations of C_{DGT}, C_E, labile P in porewater, and P-contents in root/shoot/leaf were researched, and the P-uptake mechanism by root in rhizobox, P-transfer across root/porewater/sediment, and the prediction for P concentration in plant tissues by DGT measurement can be investigated.

3.4 The Computer Programs for DGT (DIFS, Visual MINTEQ, and Image J.1.38 E Softwares) and the Operation/Experiment Methodology

To investigate the response of the DGT test to the kinetic exchange of labile elements between the solid phase and water, a one-dimensional (1D)-DIFS model (Ernstberger et al. 2002; Wu et al. 2015c) has been developed to assess the sediment reactivity. When ferrihydrite DGT piston is deployed in sediments, ferrihydrite resin strongly binds labile P, which diffuses through the diffusion layer. The sorption/desorption/diffusion processes induced through the DGT piston at the DGT/porewater/sediment interface are indicated in Fig. 3.6. These processes lead to the formation of a linear concentration gradient in the diffusion layer. The gradient depends on the thickness of the diffusion layer (Δg) and the interfacial concentration of labile P species (C_i), which determines the flux ($F(t)$) of labile P toward the ferrihydrite gel according to Fick's first law in Eq. (3.2):

$$F(t) = \phi_d D_d \tag{3.2}$$

where ϕ_d is the porosity of the diffusion gel (0.95), D_d is the diffusion coefficient of the labile P in the diffusion layer ($cm^2\ s^{-1}$), $C_i(t)$ is the concentration at DGT surface, and Δg is diffusion layer thickness (cm).

The ratio between C_{DGT} and the independently determined C_{soln} (initial sediment porewater concentration) provides R parameter which offers a criterion for the depletion extent of sediment porewater at the DGT/sediment interface (Eq. 3.3):

$$R = \frac{C_{DGT}}{C_{soln}} \tag{3.3}$$

The DIFS model quantifies the dependence of R on the resupply of labile P from solid particle to porewater, that is, related to the diffusion transfer to the DGT

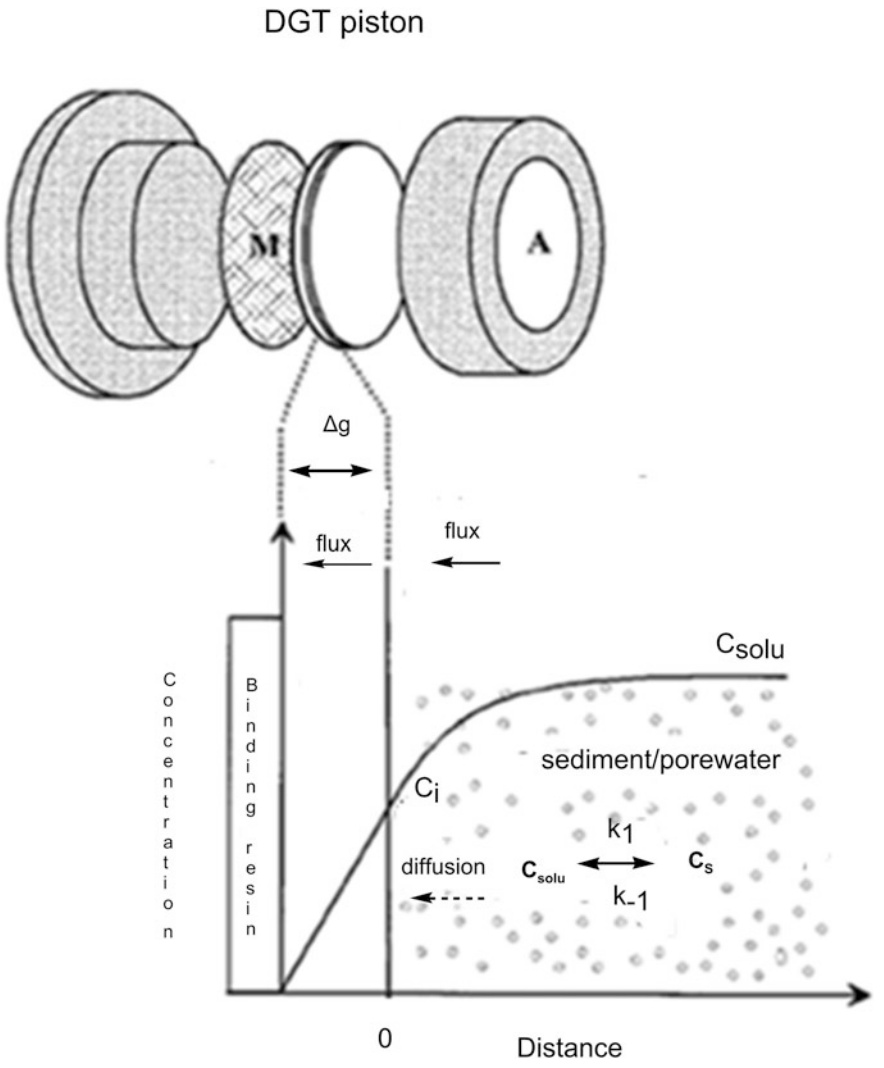

Fig. 3.6 The schematic graph of the sorption/desorption/diffusion processes induced through the DGT piston at the DGT/porewater/sediment interface (Reprinted from Environ. Sci. Pollut. R., published online, doi:10.1007/s11356-015-4736-8, Wu, Z.H., Wang, S.R., He, M.C., Element remobilization, "internal P-loading" and sediment-P reactivity researched by DGT (diffusive gradients in thin films) technique, copyright (2015), with the permission from Springer)

interface and across the diffusion layer to the binding gel through solving a pair of linked partial differential equations (Eqs. 3.4 and 3.5), describing the *dissolved/sorbed* concentrations of labile P in the sediment/porewater or DGT diffusion layer.

$$\frac{\partial C}{\partial t} = -k_1 C + K_{-1} P_c C_s + D_s \tag{3.4}$$

$$\frac{\partial C_s}{\partial t} == -K_{-1} C_s - K_{-1} C_s \tag{3.5}$$

K_d (Eq. 3.6) and the response time (T_c) (Eq. 3.7) are used for quantifying adsorption/desorption kinetics in the sediment/porewater.

$$K_d = \frac{C_s}{C_{soln}} = \frac{K_1}{Pc \times K_{-1}} \tag{3.6}$$

$$T_C = \frac{1}{K_1 + K_{-1}} \tag{3.7}$$

T_c defines the time for the partitioning components of K_d to reach 63 % of their equilibrium value. DIFS needs data for C_{DGT}, C_{soln} (C_0), soil porosity (ϕ_s), diffusion layer porosity (ϕ_d), diffusion layer thickness (Δg), particle concentration (P_c), effective diffusion coefficient in the sediment (D_s), diffusion coefficient in the diffusion layer (D_d), and deployment time (T). Two of the three parameters, K_d, T_c, and R, are determined as input parameters, and DIFS calculates the other one. k_{-1}(adsorption rate constant)/k_1(desorption rate constant) is derived through Eqs. (3.6 and 3.7). Distributions of P concentrations across the DGT/porewater/sediment interface are calculated for any deployment time/distance.

Considering the redox state of surface sediments and the high concentration of P in the sediment porewater of Dianchi Lake, a sequential extraction method with five steps introduced in Sect. 3.6 was used in this study for the five P-fractionations, including NH_4Cl-P, BD-P, $NaOH_{25}$-P, HCl-P, and $NaOH_{85}$-P. According to the DGT probe research in anoxic sediment (Chap. 4) at Dianchi Lake, the DGT-P/-Fe profiles (Fig. 4.3 in Chap. 4) indicated the corresponding detailed and broad character of the corelease of labile Fe and P, which verified the main P-release from Fe-bound P through the reduction of Fe (III) hydroxyoxide in the sediments. The Fe-bound P-release mechanism in the anoxic sediment of Dianchi Lake was also consistent with the result of the two references for sediment-P-researches (Böstrom and Pettersson 1982; Christophoridis and Fytianos 2006). Anoxic conditions promote the reduction of insoluble Fe (III) hydroxyoxide to soluble Fe(II), resulting in P-release from the sediment into the surrounding water (Sundby et al. 1986; Böstrom and Pettersson 1982; Christophoridis and Fytianos 2006). The liable P-pool in sediments of Dianchi Lake was the total content of the NH_4Cl-P and BD-P-fractions because nine sediments (sites 1–9) were all in anoxic states. The total content of NH_4Cl-P and BD-P stands for the loosely sorbed P and Fe-bound P phases (Wu et al. 2015c). In this study, the total content of NH_4Cl-P and BD-P was used for K_d in DIFS simulation.

The physicochemical parameters for sediment and P-DIFS were also determined and calculated using the methods recommended in references (Wu et al. 2015c).

Table 3.3 Particle density (P_c), sediment porosity (porsed), diffusion gel porosity (pordif), effective diffusion coefficient in the sediment (D_s), and diffusion coefficient in diffusion gel (D_d)

Site	K_d (cm^3g^{-1})	P_c (g cm^{-3})	D_d (cm^2 s^{-1})	D_s (cm^2 s^{-1})	Pordif	Porsed
1	232.9	0.1367	5.89	7.65	0.95	0.95
2	299.2	0.0934	5.89	7.87	0.95	0.97
3	168.4	0.2119	5.89	7.29	0.95	0.93
4	354.8	0.2225	5.89	7.25	0.95	0.92
5	172.6	0.2813	5.89	7.00	0.95	0.90
6	148.3	0.1281	5.89	7.69	0.95	0.95
7	1536	0.1293	5.89	7.68	0.95	0.95
8	328.8	0.2031	5.89	7.33	0.95	0.93
9	134.7	0.1639	5.89	7.51	0.95	0.94

Table 3.4 Output parameters of the P-DIFS simulation during the DGT test

Site	T_c(s)	K_{-1}(d^{-1})	K_{-1}(d^{-1})
1	498	5.28	168.08
2	2603	1.15	32.05
3	1777	1.33	47.30
4	6994	0.15	12.20
5	56,060	0.03	1.51
6	332	13.03	247.60
7	33	13.13	2609.02
8	13,140	0.10	6.48
9	382	9.79	216.15

Particle density (P_c), sediment porosity (ϕ_s), and effective diffusion coefficient in the sediment (D_s) and the output parameters are listed in Tables 3.3 and 3.4. The procedure for labile P in sediment porewater was conducted in a designed glove box that was purged with nitrogen (O_2 concentration < 1 %) at all times during the process. *Pc* and ϕ_s were measured and calculated according to the recommended method. Effective diffusion coefficient in the sediment (D_s) can be calculated using Eq. (3.8):

$$D_s = \frac{D_0}{1 - 2\ln\phi_s} \tag{3.8}$$

where ϕ_s is the sediment porosity and *Do* is the diffusion coefficient (8.30×10^{-6} cm^2 s^{-1}) of labile P in water (24 °C).

The surface sediments (8 cm thickness and 1 kg weight) with overlying water (3 cm thickness) were sampled from nine sites (1–9) of Dianchi Lake (Fig. 2.2 in Chap. 2). Then, they were put into separate containers in incubators at the same temperature (24 °C) of sampling stations. DGT pistons were deoxygenated for 18 h through placing them in a clean container with solution of 0.01 mol L^{-1} NaCl (ultra pure) bubbled with N2. DGT pistons with the DGT windows facing downward were

pushed gently into sediments at depth of −4.0 cm. DGT pistons began to adsorb labile P from porewater. After 24 h, DGT pistons were pulled out from sediments and dismantled. The ferrihydrite resin was retrieved and eluted by 0.25 M H_2SO_4, and the elution solutions were determined by molybdenum blue method for labile P (Wu et al. 2015c). Then, DGT-P concentration was calculated for the subsequent P-DIFS simulation according to the method for 1D-DIFS model introduced above. The detailed introduction for the numerical model for DIFS simulation is present in references (User's guide to DGT technique 2013; Ernstberger et al. 2002; Wu et al. 2015c).

The DGT values at peaks of DGT-S(-II) and -Fe profiles were input into the user's interface of Visual MINTEQ program to output parameters to assess the solubility of Fe-sulfide minerals (Naylor et al. 2004; Wu et al. 2014, 2015d). DOS program MINTEQA2 is the former generation of software of Visual MINTEQ and was originally coded by EPA-US (Environmental Protection Agency). The Visual MINTEQ program could be found on Web site in the year 2000 and was very different from the former type of the software MINTEQA2 and its code. The equilibrium and speciation for soluble inorganic materials in solutions in natural water body can be simulated and calculated by Visual MINTEQ program. This program has been awarded the copyright. The VR (the Swedish Research Council and MISTRA) and MISTRA (the Foundation for Strategic Environmental Research) have supported Visual MINTEQ program. This software can be downloaded in the Web site: http://hem.bredband.net/b108693/download.html. Figure 3.7 indicates the user's interface of Visual MINTEQ.

ImageJ 1.38e software is a public domain Java image processing and analysis program inspired by NIH Image for the Macintosh, which can be downloaded in the

Fig. 3.7 The user's interface of Visual MINTEQ

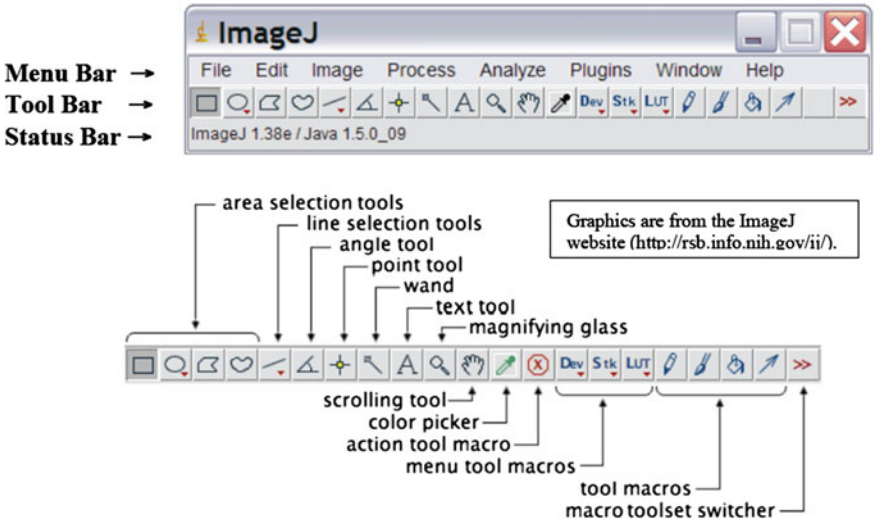

Fig. 3.8 The user's interface of Image J 1.38e software

Web site: http://rsb.info.nih.gov/ij/download.html. For the grayscale image of AgI gel derived by a flatbed scanner (OpticBook 3600), the numerical analysis for grayscale distribution, grayscale profile, area analysis, and shape and number of particles can be finished by image J. software. Based on the derived results, DGT-S(-II) profiles, 2D images for DGT concentration distribution, and the quantification for sulfide-microniche can be researched. The user interface of Image J. 1.38 e software is indicated in Fig. 3.8.

3.5 The Computer Imaging Densitometry (CID) Technique for the Analysis of Sulfide-Microniches and DGT-S(-II) Profile

In anoxic sediments, insoluble metal-sulfide minerals can deposit by diagenetic reaction or remobilization. Fe-sulfide minerals include hematite and mackinawite, which are the common metal-sulfide minerals and stand for the main deposition type of sulfide. The change of sulfide concentration in sediment porewater gives the information about biogeochemistry, which is a factor for controlling the concentration and toxicity of soluble trace metals. Sulfide-microniche in sediments is related to reactive organic matter and ore mineral (Widerlund and Davison 2007). In order to conduct the DGT determination of labile sulfide in sediment porewater, DGT-sulfide-concentration profile, 2D image of DGT sulfide, and the analysis of sulfide-microniche distribution, it is needed to conduct the AgI-DGT test in standard solution, grayscale analysis, elution experiment for AgI gel, and the calibration

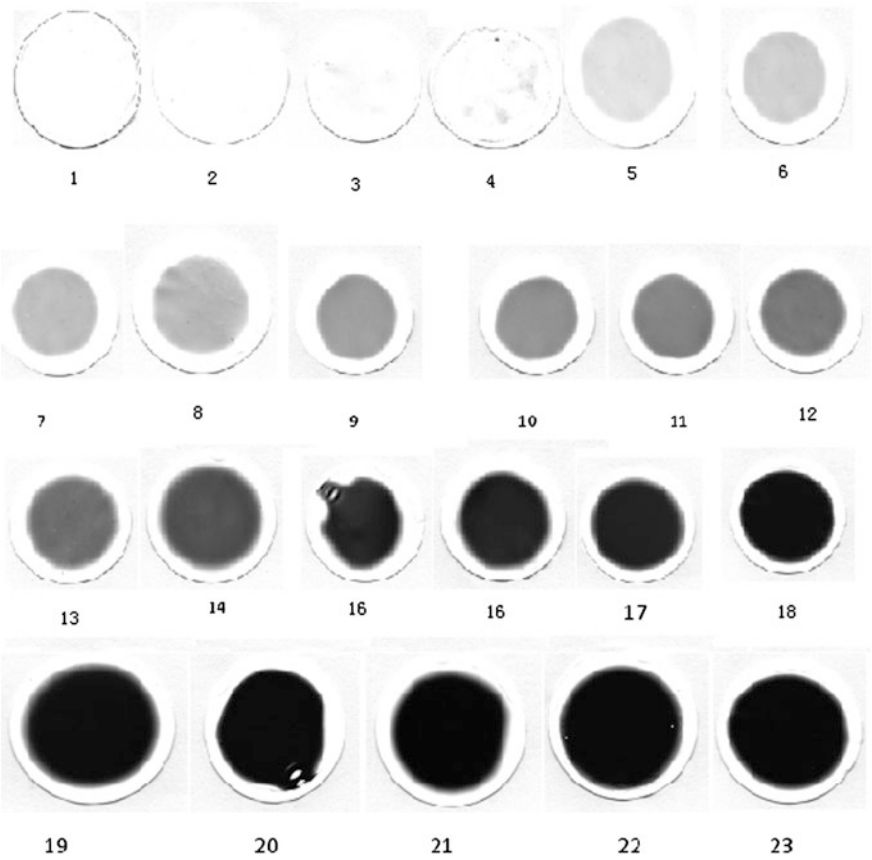

Fig. 3.9 The grayscale images of 23 standard AgI gels for the calculation of calibration curve

equation for greyscale vs. eluted sulfide mass (μg cm^{-2}), grayscale analysis for AgI-gel strip in DGT probe, DGT-S(-II) profile, 2D image, and image of sulfide-microniche.

Figure 3.9 is the grayscale image of 23 AgI gels after the deployment of them in a series of standard S(-II) solutions, which can be used to derive calibration equation for grayscale analysis. After 23 AgI-DGT pistons were deployed in standard sulfide solutions (pH = 8.14) for 25 h (T = 26 °C), 23 gels were dried and then scanned by a flatbed scanner (OpticBook 3600) at a resolution of 600 dpi, corresponding to a vertical image resolution of ∼ 0.042 mm, giving grayscale targeted image files format (Tiff).

According to CID technique, the grayscale intensity of the scanned images (0–255) was analyzed with Image J. 1.38 e software. Then, the purge-and-trap method for elution of sulfide from the binding gel and methylene blue colorimetric technique for the determination of mass of sulfide accumulated on AgI gel (Teasdale

et al. 1999) was conducted, and the calibration curve (greyscale intensity-(x) vs. sulfide-(y) (μg cm^{-2})) of DGT standard AgI gels deployed in a various of sulfide solutions was calculated, which was indicated as equation (Eq. (3.9)):

$$\begin{aligned} y &= 242.22399 - 250.85488 \exp(-0.40146x) \\ R^2 &= 0.9976 \end{aligned} \tag{3.9}$$

where y is the grayscale intensity of AgI gel and x is S(-II) accumulated on AgI gel (μg cm^{-2}). For the AgI-DGT in this book, a limit of detection (LOD) (3SD) of 0.11 μg cm^{-2} was thus estimated.

In order to get the DGT-S(-II) profile and image at fine spatial scales at SWI, AgI/Chelex-100 or Ferrihydrite/AgI/Chelex-100 DGT probes can be used for the measurement of S(-II) at SWI of Dianchi lake; after the deployment, AgI gel was retrieved and underwent the subsequent procedures of gel-drying, grayscale scan, gel-grayscale analysis by ImageJ 1.38e software, the 2D-image drawing, and the quantification for sulfide-microniche.

3.6 Laser Ablation Inductively Coupled Plasma Mass Spectrometry (LA-ICP-MS) Technique for Gel Analysis

In order to analyze labile Fe at the high 2D (2-dimensional) spatial resolutions in sediment porewater, this book reported the analysis of labile Fe-bound by SPR-IDA gel in DGT probe at high spatial resolutions by LA-ICP-MS instrument. The main experimental procedures included the following: DGT piston deployment in ^{115}In (internal element) standard solution, DGT piston deployment in Fe standard solutions, LA-ICP-MS analysis for labile Fe bound by DGT piston resin, the calculation of calibration curve, the test for SPR-IDA DGT probe at SWI, the measurement of Fe in SPR-IDA gel in DGT probe by LA-ICP-MS, and the 2D-image for the distribution of DGT-Fe.

The DGT probe with one framework and one open window (1.8 × 15 cm) for the test in sediments and the DGT piston with window diameter (1.8 cm) for the test in standard solutions to derive the calibration equation of LA-ICP-MS analysis were used as DGT assemblies. They both contained one filter (0.45 μm pore size and 0.13 mm thickness), one diffusive gel (APA2, 5 nm pore size and 0.39 mm thickness), and one binding layer (SPR-IDA type with the thickness of 0.40 mm), which were made by DGT Research Ltd. (Lancaster University, UK). DGT assembly with APA2 diffusive gel (5 nm-pore size) can measure the labile species (free metal ions, inorganic metal complexes, and small organic metal complexes). Suspended particulate reagent (iminodiacetate) has a bead size of 0.2 μm and a high affinity for many metal cations (Stockdale et al. 2009) and 2D image at submillimeter scales.

The first procedure is the deployment of DGT piston and probe in ^{115}In (internal element) standard solution. The variations of laser energy during the line scan ablation, plasma unsteadiness, matrix effect, and sample heterogeneity can degrade the analytical precision by LA-ICP-MS (Warnken et al. 2004). In this study, ^{115}In was chosen as the internal element for gel ablation through preloading ^{115}In onto the SPR-IDA resin of DGT before it was used for tests in sediments or Fe standard solutions. To minimize contamination in all samples, DGT framework, glass slides, glass plates, centrifuge tubes, and containers were acid-washed (10 % HNO_3) followed by numerous rinses with ultrapure water (Milli-Q, < 18.2 MΩ cm). NaCl and $(NH_4)_2SO_4{\cdot}FeSO_4$ were ultrapure grade, and ultrapure grade HNO_3 was used for acid baths and other acid solutions (1 mol L^{-1}). Indium in 2 % HNO_3 (SPEX Company, USA) is used for ^{115}In standard solution. Eighty-four DGT pistons and three probes (I, II, and III) were deoxygenated prior to deployment by purging in N_2 for 24 h in 4L containers filled with 0.01 M NaCl in ultrapure water. Then, each seven DGT pistons were deployed in one well-stirred standard solution for 24 h (17 °C) with 30 μg L^{-1} ^{115}In and 0.01 mol L^{-1} NaCl at pH = 6. Twelve containers with ^{115}In solutions were used for all DGT pistons. Three DGT probes (I, II, and III) were also conducted for the same operation in three containers. The volume of each container was 8L, and all solutions were deoxygenated with high-purity nitrogen before and during DGT deployment. No obvious changes in concentrations of dissolved ^{115}In were detected in all solutions during the DGT deployment. According to DGT theory (Warnken et al. 2004), the mass accumulated on per area of SPR-IDA gel in DGT sampler (M/A) in each container was same. After the deployment, the resin segments (1.8 × 2 mm) in different positions (n = 11) in the DGT probe (I) were peeled and used for elution using 1 mol L^{-1} HNO_3; the elution solutions of 11 resin strips were determined by ICP-MS, and RSD for M/A values (Eqs. 1.1 and 3.2) was 1.9 %. DGT resins in three DGT pistons in each container were also peeled for elution using 1 mol L^{-1} HNO_3, and the *RSD* of M/A values of 36 piston resins in 12 containers was 2.1 %. The good precisions of M/A for DGT pistons or DGT probe reflected the even distribution of ^{115}In in gel strips. Then, the other four DGT pistons from each container (12 containers) and the other two probes (II and III) preloaded with ^{115}In were deoxygenated for subsequent tests.

The second procedure is the deployment of DGT pistons in Fe standard solutions. After the operation described in the first procedure, each four DGT pistons preloaded with ^{115}In standard were immediately used for the deployment in 8L well-stirred $(NH_4)_2SO_4{\cdot}FeSO_4$ solution containing 0.01 NaCl at pH = 5.0 at 17 °C for 48 h. The concentrations of Fe^{2+} solutions in all containers (n = 12) ranged from 0 to 4000 μg L^{-1} and pH were adjusted using HNO_3 to 5.0. Each four pistons were deployed in each container. Each solution is deoxygenated with the high-pure nitrogen before and during DGT deployment. To minimize the loss of Fe^{2+} through oxidation and precipitation, the solutions were prepared with the ultrapure water purged with high-purity nitrogen. No obvious changes of the concentrations of dissolved Fe^{2+} were detected in all solutions during the DGT deployment. After the retrieval of four DGT pistons from each container, three SPR-IDA gels in three DGT pistons were eluted using 1 mol L^{-1} HNO_3 for 24 h. The elution solution was

determined by ICP-MS (Element 2) for ^{56}Fe and ^{115}In to quantify M/A values on the resin gel. In each container, the RSD (^{56}Fe) of three resins (M/A values) was 1.8 %, and the average M/A value for each container (n = 12) was used for calibration equation of LA-ICP-MS analysis. The RSD (^{115}In) of M/A values for all 72 piston resins (36 piston resins described in the first procedure and the other 36 piston resins in this procedure) was 2.8 %, indicating the accurate ^{115}In mass accumulated on piston resins and the exchange between the preloaded ^{115}In in DGT resin and the Fe^{2+} ions in standard solution in this procedure can be neglected.

The final SPR-IDA gel in DGT piston in each container (n = 12) with Fe standard solution was placed between two glass slides and dried using a vacuum drier at 40 °C for 2d. The surface of the dried SPR-IDA gel was flat. Then, it was fixed onto an acid-washed polycarbonate plate using a standard double-sided tape (Warnken et al. 2004) for LA-ICP-MS analysis.

The third procedure is the deployment of DGT probe at SWI, and the line-scan analysis by LA-ICP-MS for the ^{56}Fe-distribution bound by SPR-IDA gel in DGT piston or probe. After deoxygenation (Zhang et al. 2002), two DGT probes (II and III) preloaded with internal ^{115}In were inserted vertically back-to-back into the SWI of one sediment core (Wu et al. 2015d), and the deployment time was 48 h. The length of DGT probes in sediment was 13 cm. After the deployment, twin probes were retrieved. One DGT probe (II) was opened, and the SPR-IDA gel was retrieved. The resin segments (1.8 × 2 mm) (n = 11) in this DGT probe (II) at the same positions of the other DGT probe (I) as described in the mentioned method above were peeled and used for elution using 1 M HNO_3. The ^{115}In concentrations in elution solutions of 11 resin segments were determined by ICP-MS. The *RSD* of M/A values (^{115}In) for 22 resin strips in those two probes (I and II) mentioned above was 2.4 %, indicating the even ^{115}In distribution in the whole gel strips of DGT probes and the exchange of ^{115}In bounded by SPR-IDA resin and metal ions such as ^{56}Fe in sediment porewater can be neglected. Altogether, the *RSD* of all M/A values (^{115}In) in 72 piston resins and 22 probe resin strips was 3.2 %. The high capacity of SPR-IDA resin of ∼ 1.0 mequiv mL^{-1} (wet SPR-IDA) ensured the accurate test of ^{56}Fe without influencing the preloaded ^{115}In in SPR-IDA resin.

After deployment at SWI, the SPR-IDA gel strip (1.8 × 15.0 cm) in the other DGT probe (III) was also retrieved, put between two perspex sheets, and was dried for 2d (40 °C) in a vacuum drier. The two flat perspex sheets ensured the dried SPR-IDA gel strip were flat without any crack. Then, it was fixed onto an acid-washed polycarbonate plate using one standard double-sided tape (Warnken et al. 2004) for the subsequent LA-ICP-MS analysis.

Laser ablation was accomplished with a NWR193 (ESI, USA) laser ablation system coupled to an ELEMENT2 (Finnigan, Thermo Electron Corporation, Germany) ICP-MS to record ^{115}In and ^{56}Fe cps (counts per second) signals. A high-resolution ICP mass spectrometer equipped with a magnetic sector mass spectrometer (ELEMENT2, Thermo Fisher Scientific) was used for the determination of ^{56}Fe. For the acquisition of the data, the ELEMENT2 was equipped with a Meinhard-type nebulizer and a Scott-type spray chamber. Isotopes typically used for the determination were ^{56}Fe and ^{115}In, which were measured in the

Table 3.5 The main instrumental parameters for LA-ICP-MS analysis

ICP-MS (Element 2)		LA (NWR 193)	
Cooling gas flow	16 L min^{-1}	Laser wavelength	193 nm
Auxiliary gas flow	0.73 L min^{-1}	Ablation rate	10 Hz
Auxiliary gas flow	0.85 L min^{-1}	Spot size	150 μm
RF power	1200 W	Carrier gas (He) flow	0.65 L min^{-1}
Sample cone	1.0 mm	Line scan	300 μm s^{-1}
Skimmer cone	0.7 mm		
Resolution	Medium		

medium-resolution mode (MR), $m/\Delta m$ = 4000. Laser ablation analyses were performed with a NWR193 (ESI, USA) laser ablation system, Q switched Nd:YAG (193 nm), high-precision X–Y stages, ActiveView software, and 7 mJ/pulse output laser energy. The dried gel sample was placed inside the ablation cell, and a laser beam was focused on the surface of the sample.

For the dried SPR-IDA gel, the continuous line-scan mode was performed at a scanning speed of 300 μm s^{-1}, a beam diameter of 150 μm, an interline distance of 20 μm, and a repetition rate of 10 Hz. The laser energy level was set to 80 %. The readout time for a single ICP-MS reading was 0.328 s. The instrumental parameters used for LA-ICP-MS analysis are presented in Table 3.5. The precision of $^{56}Fe/^{115}In$ cps ratio (seven line-scan ablations) for each dried SPR-IDA disk (standard gel 2, 4, 6 or 8) was < 9.0 % during 0.5 h-laser ablation. So, the ^{115}In distribution was even in SPR-IDA gel surface, and cps signal was stable. The resin gels were sufficiently dried prior to analysis and that the tuning parameters (Table 3.5) during laser ablation yielded a stable plasma, free from significant molecular oxide or doubly charged ion interference (Warnken et al. 2004). The advantage of internal ^{115}In standard is the normalization data and the correction for long-term drift during the 32-h ablation process for the resin strip of DGT probe.

The size of surface area of SPR-IDA strip in DGT probe deployed at SWI for LA-ICP-MS analysis was 1.409 cm (width) × 12.614 cm (length) and one line scan (1.409 cm) for LA-ICP-MS analysis in the horizontal direction output 81 pairs of cps data for the ratio of $^{56}Fe/^{115}In$ cps. The spatial resolutions of line scan for Fe-measurements were 174 × 170 μm (width × length). It should be noted that the actual spatial resolution for labile Fe in DGT resin was lower than that of laser ablation due to the lateral diffusion of Fe in the diffusive layer during DGT deployment (Warnken et al. 2006). There were 742 scan lines and 60,102 pairs of data for resin strip analysis. The images of the line-scan analysis for SPR-IDA gel are indicated in Fig. 3.10. The picture of the dried SPR-IDA gel strip in DGT probe for LA-ICP-MS analysis is indicated in Fig. 3.11. According to the line-scan analysis and instrument parameters (Table 3.5), the output cps (^{56}Fe and ^{115}In) of each standard disk gel was used for the calculation of the ratio of $^{56}Fe/^{115}In$ cps. The calibration equation (Table 3.6) was established by the linear fit of $^{56}Fe/^{115}In$ signal ratio vs. the mass of Fe accumulated on per area in the resin (μg cm^{-2}) (12

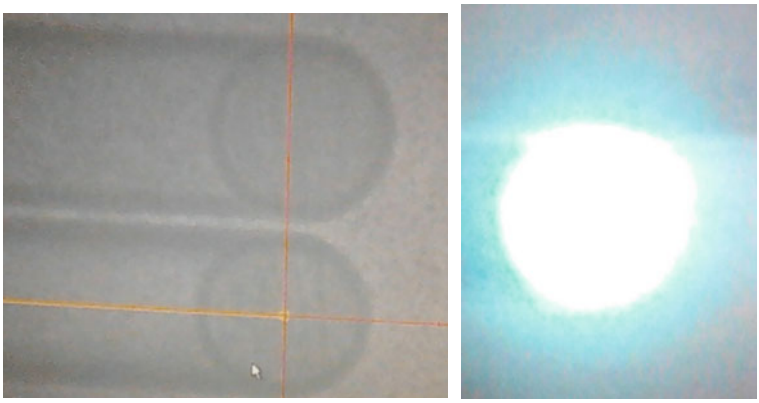

Fig. 3.10 The line scan in SPR-IDA gel by laser ablation

gel standards). The linear working range (0–64.71 μg cm^{-2}) could satisfy the determination of labile Fe-fractions in sediment porewater. Standard reference materials: NIST SRM 610, 612, and 615 (Ca as internal element, Max Planck Institute-MPI, Germany) and SRP-IDA disk gels (standards 2, 4, 6, and 8, ^{115}In as internal element) were used for analytical quality control (QC). Certified values of NIST SRM 610, 612, and 615 (silicate glass) (downloaded from http://georem.mpch-mainz.gwdg.de/sample_query.asp), and RSD (n = 7) for each standard (SRM NIST or DGT gel standards) are indicated in Table 3.6. The limit of detection (LOD) (3SD) (n = 7) for DGT gel analysis is 9.56 ng cm^{-2}. For a typical

Table 3.6 The analytical quality control (QC), certified values for NIST SRM standards, the calibration equation, and LOD for LA-ICP-MS analysis

Sample	Mean mass		Certified value (mg kg^{-1})	RSD (%)	Calibration equation[a]	LOD (ng cm^{-2})
	μg cm^{-2}	mg kg^{-1}				
Standard gel 2	0.227 ± 0.013			7.2	$y = 0.788x - 0.069$	9.56
					$R^2 = 0.998$	
Standard gel 4	0.915 ± 0.074			8.2		
Standard gel 6	5.651 ± 0.401			8.6		
Standard gel 8	13.01 ± 0.95			8.8		
SRM 610		472.4 ± 27.4	481	5.8		
SRM 612		55.31 ± 3.59	51	6.5		
SRM 615		18.8 ± 1.02	18.8	7.1		

[a]y is mass accumulated on per area (M/A) in SPR-IDA gel (pg cm^{-2}); x is the Fe-signal intensity (^{57}Fe cps/^{115}In [c]ps)

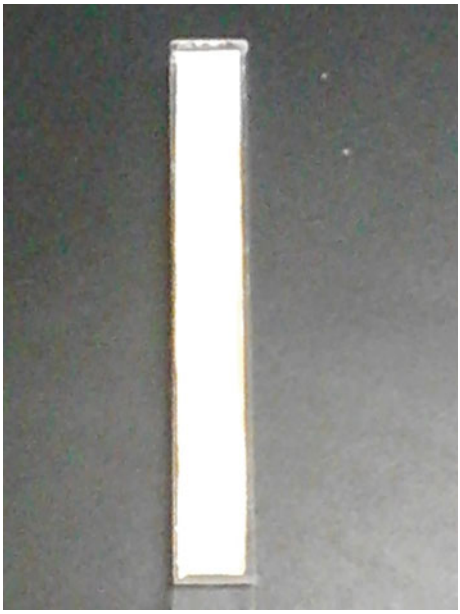

Fig. 3.11 The dried SPR-IDA gel strip in DGT probe for LA-ICP-MS analysis

DGT piston with 0.39 mm diffusive gel and 48-h deployment in natural water/porewater, a LOD of 0.59 μg L^{-1} can be estimated. Based on the result of LA-ICP-MS analysis and the calculated C_{DGT} (Fe), the C_{DGT} (Fe) distribution image (2D) at submillimeter scales was acquired through software surfer 11 (http://www.golden.com). The lengths (depths) of the whole DGT-Fe-image in the overlying water and the sediment layer were 0.994 and 11.620 cm, in turn. The width of the whole C_{DGT} (Fe) image was 1.409 cm. Four figures (images) were chosen for the investigation of Fe-release characters in different sediment microzones (Figs. 6.2 and 6.5 in Chap. 6).

3.7 The Analysis Methods for Physicochemical Properties of Lake Sediments

In two seasons (May and September) in 2013 and May in 2014, undisturbed sediment cores and overlying water at seven sites (A–H) in Dianchi Lake were collected using Jenkin corers (length: 80 cm, diameter: 10 cm). In May, 2013, surface sediments (0 ~ −8 cm) at nine sites (1–9) were also collected using Ekman grab samplers. Water samples were collected in acid-cleaned polyethylene (PE) bottles. Then, the sediments and water samples were immediately brought into the laboratory. Sediment cores and surface sediments for DGT tests were immediately stored in incubators (MIR-262, Panasonic Company) at the sampling temperature before and

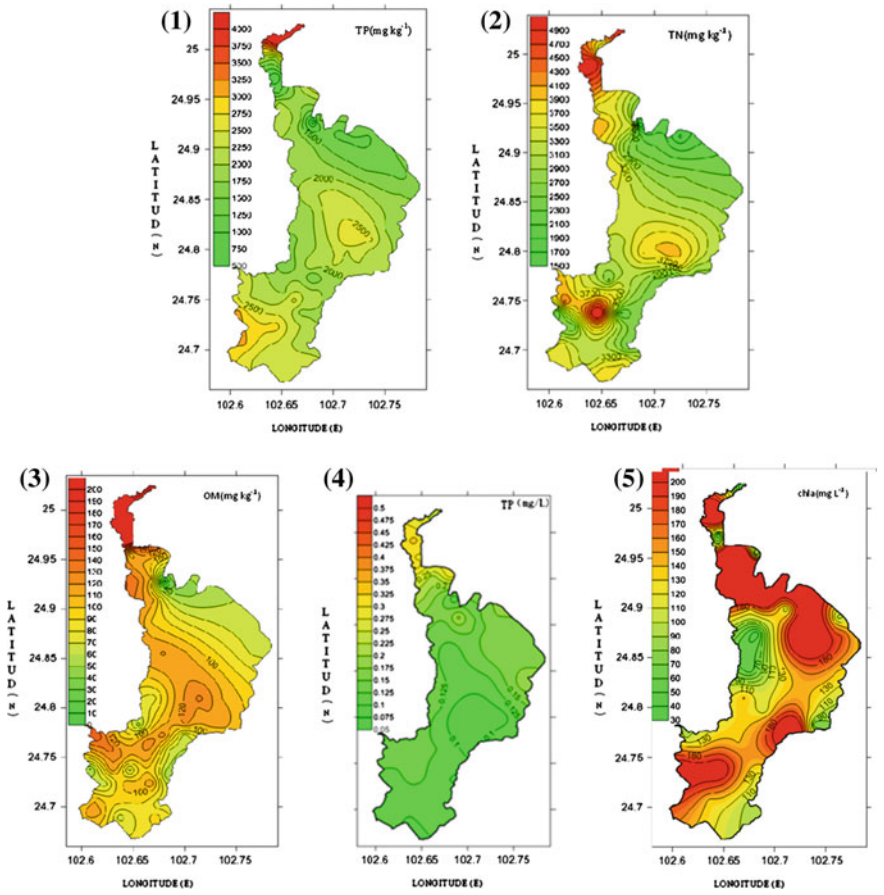

Fig. 3.12 The distribution graph of TP, TN, and OM in surface sediment (0 ~ −8 cm), and TP and Chla in surface water at Dianchi Lake in 2013. *1* TP; *2* TN; *3* OM; *4* TP; *5* Chla. (Reprinted from J. Geochem. Explor. 156:145–152., Wu, Z.H., Wang, S.R., Jiao, L.X., Geochemical behavior of metals-sulfide-phosphorus at SWI (sediment/water interface) assessed by DGT (Diffusive gradients in thin films) probes, copyright (2015), with the permission from Elsevier)

during DGT tests. Subcores and surface sediments were stored at −20 °C in iceboxes for subsequent analysis. Water sample was stored at 4 °C in iceboxes.

The distribution of organic matter content (OM), total phosphorus (TP), and total nitrogen (TN) in surface sediments, as well as the TP and Chlorophyll-*a* (Chl-*a*) contents in the water of the whole Dianchi Lake, was processed and determined according to the methods in references (Wu et al. 2014, 2015c, d), and the results of them are indicated in Fig. 3.12.

The sequential extraction procedure for P in the sediments was conducted using the method that Hieltjes and Lijklema (1980) and Psenner and Pucsko (1988) recommended. The physicochemical properties of the sediment (eight sites: A–H)

Table 3.7 Physicochemical properties of the sediment (eight sites: A–H): TP, TN, Fe, OM, and AVS

Site	TP (mg kg^{-1})	TN (mg kg^{-1})	Fe (mg kg^{-1})	OM (mg kg^{-1})	AVS (μmol g^{-1})
A	2800	4209	22,815	203	1.608
B	2284	3755	21,113	131	1.221
C	1922	2700	23,138	99	1.093
D	2011	3109	28,230	108	1.508
E	1524	2408	28,121	103	1.552
F	2300	2900	22,800	199	1.018
G	2400	3000	22,615	202	1.048
H	1559	2408	15,812	103	1.552

Table 3.8 Physicochemical properties of the sediment (eight sites: A–H): P-fractions

Site	TP (μg g^{-1})	P(NH_4Cl) (μg g^{-1})	P(BD) (μg g^{-1})	P($NaOH_{25\ ^\circ C}$) (μg g^{-1})	P(HCl) (μg g^{-1})	P($NaOH_{85^\circ C}$) (μg g^{-1})
A	2800	129	199	961	604	907
B	2284	21	122	249	1032	860
C	1922	32	117	615	1058	100
D	2011	54	134	553	680	590
E	1524	55	57	454	493	465
F	2300	59	113	482	890	756
G	2400	105	125	490	883	797
H	1559	55	257	354	493	365

Table 3.9 Physicochemical properties of the sediment (eight sites: A–H): the average total dissolved phosphorus (TDP) in porewater (0−5 cm)

Site	DTP (μg L^{-1})	Recovery (%)
A	2054	90.07
B	599	
C	488.9	
D	490.3	
E	759.8	
F	410	
G	898	

are listed in Tables 3.7, 3.8, and 3.9. The average TDP (total dissolved phosphorus) in porewater (0 ∼ −5 cm) of the eight sediments (sites A–H) determined by the centrifugation (Yang et al. 2010) and molybdenum blue methods (Standards of National Environmental Protection Department 2002) is listed in Table 3.9. The physicochemical properties of the sediment and water (nine sites: 1–9) for DIFS are listed in Table 3.11. The phosphorus extracted of nine sites (1–9) is indicated in Fig. 3.13. ORION STAR instrument (Thermo Electron Corporation, USA) was

Table 3.10 Physicochemical properties of the sediment (eight sites: A–H): The result of QC (analytical quality control) for sediment analysis

	Recovery (%)	RSD (%)
Fe	104.8	
Al	103.9	
Ca	97.5	
TN		3.45
TP		3.52
AVS		7.58
OM		7.02

used to determine the Eh and pH (Ave. ± SD) in sediment porewater. The profiles (pH and Eh) of sediment porewater at seven sites (A–H) are indicated in Fig. 3.14. The properties of water including conductivity and dissolved oxygen were determined using an electrode probe (HACH sensION156, USA). The result of analytical quality control (QC) is listed in Tables 3.9 and 3.10 for sediment, porewater, and water. Standard material (So-1(F48)) was used for the QC of the Fe-analysis in sediment (Li et al. 1995). Standard material GSS2 (Institute of Geophysical and Geochemical Exploration of China) was used for the QC of the P analysis in sediment/water/porewater. The physicochemical parameters for sediment and P-DIFS were also determined and calculated using the methods recommended in references (Wu et al. 2015c). Particle density (P_c), sediment porosity (ϕ_s), and effective diffusion coefficient in the sediment (D_s) are listed in Table 3.3.

3.8 The Main Scientific Problem and Technological Difficulty to Be Solved

The "internal P-loading" can increase the TDP (total dissolved P) in lake water by the P-release from sediment into overlying water. It can happen regardless of the control of "external P-loading." Sediment can be a major P-sink in lake by sedimentation process across epilimnion/hypolimnion/lake bottom. In some conditions, P can be recycled or released from bottom sediments (Böstrom and Pettersson 1982), which can still engender lake eutrophication. The mechanism of P-release from Fe-bound P in anoxic sediment has been revealed firstly by Einsele (1936) and Mortimer (1941), and the significant correlation was found between the P and Fe released from sediment. An indirect reduction mechanism, the P-release form Fe (III) hydroxyoxide due to sulfate reducing bacteria and the formation of soluble FeS, has been verified by Roden and Edmonds (1997). In general, P-solubility in sediment porewater is caused by the biogeochemical reactions of minerals or amorphous materials under conditions of pH, redox potential, and ionic strength (Maine et al. 1992). Those materials involving in P-release include the association of phosphate with iron, aluminum, and calcium, and the adsorptive nature of

Table 3.11 The physicochemical properties of the sediment and water (nine sites: 1–9) for DIFS

Sampling site	1	2	3	4	5	6	7	8	9
Water depth (m)	3.2	3.8	4.3	4.5	4	6.2	3.8	3.3	3
Water									
TDP(μg L^{-1})	301	312	232	153	137	124	102	98	109
pH	7.89	8.18	8.25	8.09	7.86	7.5	8.19	8.03	8.15
DO (mg L^{-1})	5.97	6.97	7.82	8.82	8.09	9.93	9.08	8.88	7.53
Conductivity (μs cm^{-1})	1126	909	899	919	1043	1098	952	904	939
Sediment									
pH	7.56 ± 0.12	7.83 ± 0.09	7.61 ± 0.12	7.42 ± 0.23	7.53 ± 0.33	7.64 ± 0.07	7.74 ± 0.08	7.84 ± 0.11	7.47 ± 0.21
Eh(mv)	-90.05 ± 7.20	-78.47 ± 8.78	-89.09 ± 6.05	-80.18 ± 8.02	-65.08 ± 5.23	-86.04 ± 4.98	-98.98 ± 7.08	-70.77 ± 10.64	-80.56 ± 4.55
TOC(dw%)	3.09	3.59	2.88	2.43	2.58	1.99	2.08	2.22	2.88
Fe_{total}(mg kg^{-1} dw)	19,626	8039	9033	8974	9086	10,320	11,096	13,098	14,329
Al_{total}(mg kg^{-1} dw)	6896	5873	4896	3975	4896	4564	3329	5807	3869
Ca total(mg kg^{-1} dw)	9335	11,089	11,021	11,281	14,175	10,033	9335	12,141	9733
TP(mg kg^{-1})	4412	1646	1354	1244	1550	1646	1927	1675	1032

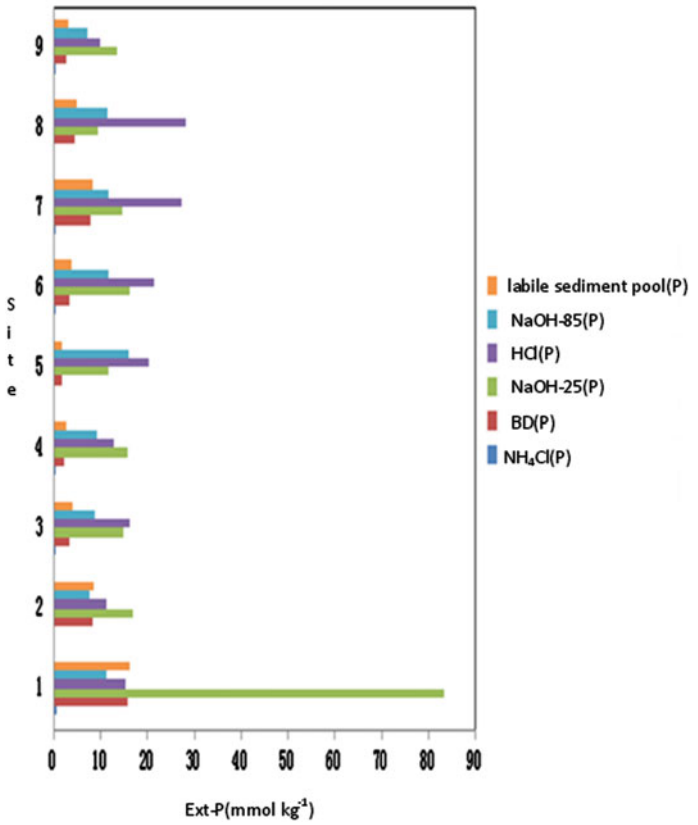

Fig. 3.13 Extracted P in surface sediments (sites 1–9) of Dianchi Lake for DGT-DIFS test

carbonates and clays (Jensen and Andersen 1992). Laboratory sorption experiments for P-exchange and P-flux for bed sediment (House et al., 1995; Jarvie et al. 2008), sequential extraction for P-bioavailability or mobility in sediment, and porewater profiles in sediment cores (House 2003; Farmer et al. 1994; Moore and Reddy 1994; Harper et al. 1998) have already been investigated. Concentration profiles at depth in sediment for trace metals or elements in lakes, rivers, or marines have been investigated to infer flux at SWI (Klinkhammer et al. 1982) and digenetic reactions involving release or adsorption of elements in sediments (Shaw et al. 1990).

Dianchi Lake has failed to recover from eutrophication partially due to P-release from the sediment ("internal P-loading"). In order to restore Dianchi Lake from eutrophication status, it is needed to understand mechanism of "internal P-loading" in sediment using the in situ technique. Compared with "bulk" analysis methods, the newly developed DGT (diffusive gradients in thin films) technique (Davison et al. 1994, 2000) is an advanced method for DGT profiles of trace elements in sediment porewater (Zhang et al. 2002; Fones et al. 2004), geochemical process

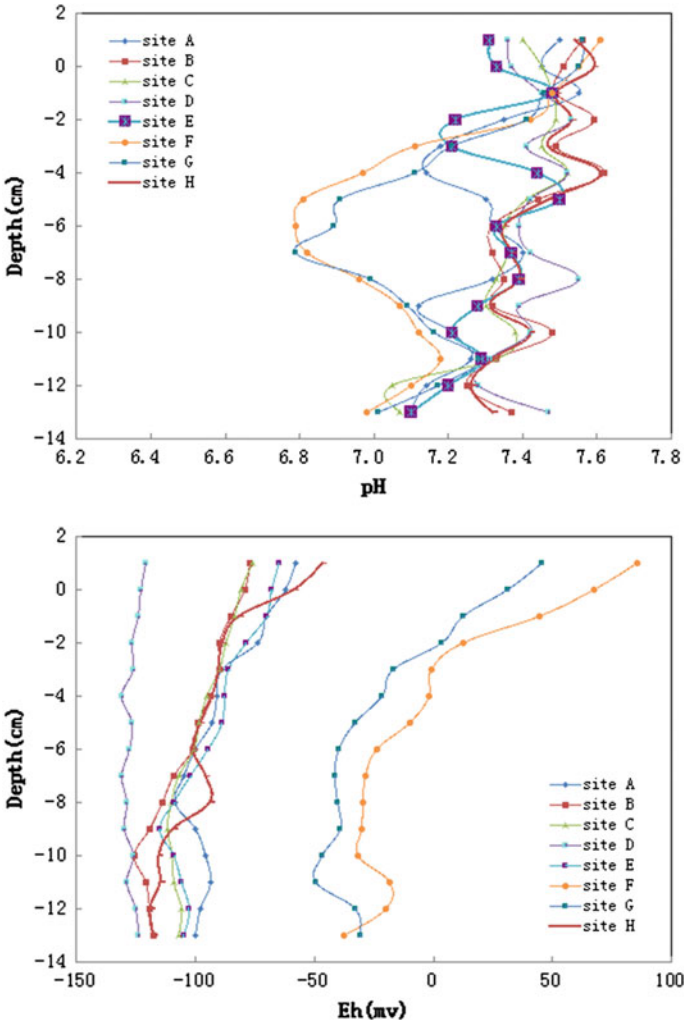

Fig. 3.14 Profiles of redox potential and pH in sediment porewater of seven sites (A–H) for DGT probes

(Ding et al. 2012; Naylor et al. 2004), kinetic exchange at DGT/sediment microzone (Harper et al. 1998; Ernstberger et al. 2002), and microniche research (Widerlund and Davison 2007).

In order to research P-release mechanism using DGT technique, it is important to measure three elements (Fe/P/S(-II)) or Fe/P at the same location in sediment. However, the previous DGT techniques seldom determine two kinds of elements at the same location in sediments. The multilayer-binding-gel DGT and twin DGT probes can finish this task and derive Fe, P, and S(-II) concentration profiles or

images at the same location at SWI. Based on the character of DGT-Fe/P/S(-II) profiles/images, P-release from Fe-bound P and the coupled Fe–S–P-biogeochemical reaction for P-release can be researched in detail, and the mechanism of "internal P-loading" can be revealed. Moreover, "internal P-loading" in Dianchi Lake can also be quantified using Fick's law and DGT-P profiles. In order to investigate the kinetic exchange of P across DGT/porewater/sediment, DIFS and DGT pistons were used to study capacities in sediment-P-pool, rate constants of the P-release, and how those two factors determine the DIFS curves reflecting P-release character in sediment microzones. In order to determine the minor mechanism of coupled Fe–S–P-biogeochemical reaction, DGT-CID technique was used for the measurement of DGT-S(-II)-profile and sulfide-microniche image. Then, based on DGT-Fe/P/S(-II)-profile and sulfide-microniche image, the P-release through the coupled Fe–S–P-biogeochemical reaction in sediment microzone can be researched. The mechanisms of P-release have been found in DGT research by DGT profiles of P/Fe and DGT-S(-II) image, which was discussed in "Chap. 4 and Chap. 5 in Sect. 5.2." How to predict P-release in sediment microzone? In "Chap. 6 in Sect. 6.2," DGT/LA-ICP-MS has been developed to derive DGT-Fe-chemical image, and P-release from Fe-"hot spots" (microniches) can be predicted. Altogether, through DGT and related methods/technique, the mechanism of "internal P-loading," the quantification of "internal P-loading," the biogeochemical reactions for P-release mechanism, DIFS model for P-release/P-diffusion at DGT/sediment interface, sulfide–microniche, and Fe-image for P-release mechanism can be researched deeply and comprehensively.

The lake eutrophication mechanism and the aquatic vegetation for the ecological restoration of lake have been investigated intensively. P-bioavailability and P-mobility should be investigated to reveal the supply process of both solution and sediment particle. In order to achieve this aim, P-specie in sediment solution and operationally defined P-fractions in sediment solid were the main research methods. When plant adsorption is rapid compared with diffusional supply in sediment porewater, a proportion of P in sediment particle is available and can supply this depletion in sediment porewater. The transfer from solid phase into solution in the rhizosphere sediment was due to the root uptake and subsequent P-depletion in sediment porewater (McLaughlin et al. 1998; Zhang et al. 2001). So, the labile P-fraction in sediment particle should be quantified to investigate P resupply from sediment into porewater and the plant uptake. However, the realistic procedure to assess the rate and extent combined with P-desorption from sediment solid and supply to plant root is absent. Extraction method (Hieltjes and Lijklema 1980; Psenner and Pucsko 1988) justly makes a classification of P-fractions in sediment and relies on the arbitrary responds to chemical reagents. So, this method cannot reflect the real P-lability. DGT can mimic P-uptake by plant root, lower P concentrations in sediment solution, and respond to P resupplied from liable species in solution and reactive P-fractions in sediment-P-pool. In Erhai Lake, DGT technique was used in rhizosphere sediment for the measurement of DGT flux and concentration, which can be related to P adsorption by plant root. Moreover, P-transfer/P-biogeochemical process in rhizosphere sediment and DGT's function to predict P-content in plant tissues can be investigated.

3.9 Summary

Sediments play an important role in overall P-cycling in shallow lake ecosystem, acting both as a sink and a source of P due to continuous transport of chemical species across the SWI. Most of the P stored within sediment has the potential to be remobilized and released back to the overlying water column by physical, geochemical, and microbial processes. P-release due to the reduction of Fe^{3+} under anoxic condition increases the P concentration in water column. Sequestration of P by $Al(OH)_3$ (s) and precipitation of Ca-P in sediment can be considered as P-sink. Restoration of eutrophic waters has become a research focus in recent years, and recovery of aquatic vegetation in the water bodies is an important component of the issue. The mobility and bioavailability of P in the rhizosphere are influenced by changes in the physicochemical properties of the sediment, and the uptake mechanism by roots of aquatic plant is important for the ecological restoration of eutrophic lake. DGT and the related methods should be developed to solve the last questions of "internal P-loading" mechanism and the quantification for P-uptake by aquatic plants. In this section, the general experimental method and calculation method for DGT technique have been designed, including: the design of DGT devices of piston and probe, CID technique, Visual MINTEQ software for Fe-sulfide solubility, DIFS simulation for P-kinetic process, LA-ICP-MS analysis, and DGT test method in sediment/root interface (in situ or in rhizobox). The detailed experiment and calculation methods were introduced in detail. Moreover, the method for analysis of physicochemical properties of lake SWI is also introduced. The elaborate design of DGT method and the related techniques for lake sediment and rhizosphere should be the base for the research of biogeochemical process of P in sediment for P-release mechanism, the quantification of "internal P-loading," the chemical image at fine spatial scale, and the proxy function of DGT for P-uptake by root in the next sections.

References

Böstrom B, Pettersson K (1982) Different patterns of phosphorus release from lake-sediments in laboratory experiments. Hydrobiologia 91–2:415–429

Christophoridis C, Fytianos K (2006) Conditions affecting the release of phosphorus from surface lake sediments. J Environ Qual 35(4):1181–1192

Davison W, Zhang H, Grime G (1994) In situ speciation measurements of trace components in natural waters using thin-film gels. Nature 367:546–548

Davison W, Fones G, Harper M, Teasdale P, Zhang H (2000) Dialysis, DET and DGT: in situ diffusional techniques for studying water, sediment and soils. In: Buffle J, Horvai G (eds) In situ monitoring of aquatic systems: chemical analysis and speciation. Wiley, Chichester, pp 495–570

Ding S, Sun MQ, Xu D, Jia F, He XA, Zhang CS (2012) High-resolution simultaneous measurements of dissolved reactive phosphorus and dissolved sulfide: the first observation of their simultaneous release in sediments. Environ Sci Technol 46:8297–8304

Einsele W (1936) Uber die Beziehungen der Eisenkreislaufes zum Phosphorkreislauf im eutrophen. See Arch Hydrobiol 29:664–686
Ernstberger H, Davison W, Zhang H, Tye A, Young S (2002) Measurement and dynamic modelling of trace metal mobilization in soils using DGT and DIFS. Sci Total Environ 36:349–354
Farmer JG, Baileywatts AE, Kirika A, Scott C (1994) Phosphorus fractionation and mobility in Loch Leven. Aquat Conserv Mar Freshwater Ecosyst 4(1):45–56
Fones GR, Davison W, Hamilton-Taylor J (2004) The fine-scale remobilization of metals in the surface sediment of the North-East Atlantic. Cont Shelf Res 24:1485–1504
Harper MP, Davison W, Tych W, Zhang H (1998) Kinetics of metal exchange between solids and solutions in sediments and soils interpreted from DGT measured fluxes. Geochim Cosmochim AC 62:2757–2770
Hieltjes AHM, Lijklema L (1980) Fractionation of inorganic phosphates in calcareous sediments. J Environ Qual 9:405–407
House WA (2003) Geochemical cycling of phosphorus in rivers. Appl Geochem 18:739–745
House R, Rousseau DM, Thomas-Hunt M (1995) The Meso paradigm: a framework for the integration of micro and macro organizational behavior. Res Organ Behav 17:71–114
Javie HP, Mortimer RJG, Palmer-Felgate EJ, Quinton KS, Harman SA, Carbo P (2008) Measurement of soluble reactive phosphorus concentration profiles and fluxes in river-bed sediments using DET gel probes. J Hydrol 350:261–273
Jensen HS, Andersen FO (1992) Importance of temperature, nitrate, and ph for phosphate release from aerobic sediments of 4 shallow, eutrophic lakes. Limnol Oceanogr 37(3):577–589
Klinkhammer GP, Heggie DT, Graham DT (1982) Metal diagenesis in oxic marine sediments. Earth Planet Sci Lett 61:211–219
Lao JG (1988) The measurement of P in plant. The manual for soil agro-chemistrical analysis. Agricultural Publishing House, Beijing, pp 644–647
Li XD, Barry JC, Michael HR, Iain T (1995) Sequential extraction of soils for multielement analysis by ICP-AES. Chem Geol 124:109–123
McLaughlin MJ, Smolders E, Merckx R (1998) In soil chemistry and ecosystem health; special publication no. 52. Soil Science Society of America, Madison, pp 233–277
Monbet P, Mckelvie ID, Worsfold PJ (2008) Combined gel probes for the in situ determination of dissolved reactive phosphorus in porewaters and characterization of sediment reactivity. Environ Sci Technol 42:5112–5117
Moore PA, Reddy KR (1994) Role of Eh and pH on phosphorus geochemistry in sediments of Lake Okeechobee. Florida J Environ Qual 23:955–964
Mortimer CH (1941) The exchange of dissolved substances between mud and water in lakes. Ecology 29:280–329
Naylor C, Davison W, Motelica-Heino M, Van Den Berg GA, Van der Heijdt LM (2004) Simultaneous release of sulfide with Fe, Mn, Ni and Zn in marine harbor sediment measured using a combined metal/sulfide DGT probe. Sci Total Environ 328:275–286
Psenner R, Pucsko R (1988) Phosphorus fractionation: advantages and limits of the method for the study of sediment P origins and interactions. Arch Hydrobiol Beih Ergebn Limnol 30:43–59
Roden E, Edmonds JW (1997) Phosphate mobilization in iron-rich anaerobic sediments: microbial Fe(III) oxide reduction versus iron-sulfide formation. Arch Hydrobiol 139(3):347–378
SEPA (State Environmental Protection Administration of China) (2002) Monitor and analysis method of water and wastewater. Chinese Environmental Science, Beijing
Shaw T, Gieskes JM, Jahnke RA (1990) Early diagnosis in differing depositional environments: the response of transition metals in pore water. Geochim Cosmochim Acta 54:1233–1246
Sochaczewski L, Tych W, Davison B, Zhang H (2007) 2D DGT induced fluxes in sediments and soils (2D DIFS). Environ. Modell. Softw. 22(1):14–23
Standards of National Environmental Protection Department (2002) Analysis methods for the examination water and wasterwater, 4th edn. Chinese Environmental Sciences, Beijing

Stockdale A, Davison W, Zhang H (2009) Micro-scale biogeochemical heterogeneity in sediments: a review of available technology and observed evidence. Earth-Sci Rev 92:81–97

Sundby B, Anderson LG, Hall POJ, Iverfeldt A, Vanderloeff MMR, Westerlund SFG (1986) The effect of oxygen on release and uptake of cobalt, manganese, iron and phosphate at the sediment-water interface. Geochim Cosmochim AC 50(6):1281–1288

Teasdale PR, Hayward S, Davison W (1999) In situ, high-resolution measurement of dissolved sulfide using diffusive gradients in thin films with computer-imaging densitometry. Anal Chem 71:2186–2191

User'guide to DGT technique (2003) DGT Research Ltd. Available at: http://www.dgtresearch.com/. Accessed 24 May 2009

Warnken KW, Zhang H, Davison W (2004) Analysis of polyacrylamide gels for trace metals using diffusive gradients in thin films and laser ablation inductively coupled plasma mass spectrometry. Anal Chem 76:6077–6084

Warnken KW, Zhang H, Davison W (2006) Accuracy of the diffusive gradients in thin-films technique: diffusive boundary layer and effective sampling area considerations. Anal Chem 78 (11):3780–3787

Widerlund A, Davison W (2007) Size and density distribution of sulfide-producing microniches in lake sediments. Environ Sci Technol 41:8044–8049

Williams PN, Zhang H, Davison W, Zhao SZ, Lu Y, Dong F, Zhang L, Pan Q (2012) Evaluation of in situ DGT measurements for predicting the concentration of Cd in Chinese field-cultivated rice: impact of soil Cd: Zn ratios. Environ Sci Technol 46:8009–8016

Wu ZH, He MC, Lin CY (2011) In situ measurements of concentrations of Cd Co, Fe and Mn in estuarine porewater using DGT. Environ Pollu 159:1123–1128

Wu ZH, Wang SR, Jiao LX, Wu FC (2014) The simultaneous measurement of phosphorus, sulfide, and trace metals by Ferrihydrite/AgI/Chelex-100 DGT (diffusive gradients in thin films) probe at sediment/water interface (SWI) and remobilization assessment. Water Air Soil Pollut 2014, 225:2188–2194 (Reprinted from Water Air Soil Pollut, 225:2188–2194, Wu ZH, Wang SR, Jiao LX, Wu FC, The simultaneous measurement of phosphorus, sulfide, and trace metals by Ferrihydrite/AgI/Chelex-100 DGT (Diffusive Gradients in Thin Films) probe at sediment/water interface (SWI) and remobilization assessment, copyright (2015), with the permission from Springer)

Wu ZH, Wang SR, He MC, Wu FC (2015a) The measurement of metals by diffusive gradients in thin films (DGT) at sediment/water interface (SWI) of bay and remobilization assessment. Environ Earth Sci 73(10):6283–6295

Wu ZH, He MC, Wang SR, Ni ZK (2015b) The assessment of localized remobilization and geochemical process of 14 metals at sediment/water interface (SWI) of Yingkou coast (China) by diffusive gradients in thin films (DGT). Environ Earth Sci 273(10):6081–6090

Wu ZH, Wang SR, He MC (2015c) Element remobilization, "internal P-loading" and sediment-p reactivity researched by DGT (diffusive gradients in thin films) technique. Environ Sci Pollut R 22:16173–16183 (Reprinted from Environ Sci Pollut R, published online, doi:10.1007/s11356-015-4736-8, Wu ZH, Wang SR, He MC, Element remobilization, "internal P-loading" and sediment-P reactivity researched by DGT (diffusive gradients in thin films) technique, copyright (2015), with the permission from Springer)

Wu ZH, Wang SR, Jiao LX (2015d) Geochemical behavior of metals-sulfide-phosphorus at SWI (sediment/water interface) assessed by DGT (Diffusive gradients in thin films) probes. J Geochem Explor 156:145–152 (Reprinted from J Geochem Explor, 156: 145–152., Wu ZH, Wang SR, Jiao LX, Geochemical behavior of metals-sulfide-phosphorus at SWI (sediment/water interface) assessed by DGT (Diffusive gradients in thin films) probes, copyright (2015), with the permission from Elsevier)

Yang YG, Hea ZL, Lin Y, Stoffella PJ (2010) Phosphorus availability in sediments from a tidal river receiving runoff water from agricultural fields. Agr Water Manage 97:1722–1730

Zhang H, Davison W, Gadi R, Kobayashi T (1998) In situ measurement of dissolved phosphorus in natural waters using DGT. Anal Chim Acta 370:29–38

Zhang H, Zhao F-J Sun B, Davison W, Mcgrath SP (2001) A new method to measure effective soil solution concentration predicts Copper availability to plants. Environ Sci Technol 35:2602–2607

Zhang H, Davison W, Mortimer RJG, Krom MD, Hayes PJ, Davies IM (2002) Localised remobilization of metals in a marine sediment. Sci Total Environ 296:175–187

Part II
"Internal P-Loading" at SWI of Dianchi Lake

Chapter 4
The "Internal P-Loading" at SWI Assessed by DGT Technique

There are only a few DGT/DET papers focusing on P-release at SWI in lake (Javie et al. 2008; Monbet et al. 2008). One paper (Monbet et al. 2008) reported the DET and DGT techniques to determine sediment porewater profiles of the dissolved reactive phosphorus (DRP) in two lagoons of the Gippsland Lakes (SE Australia) during summer. DIFS model has been developed for the calculation of T_c (response time), K_1 (adsorption coefficient) and K_{-1} (desorption coefficient), and the diffusion/adsorption/desorption process, which can be used to assess sediment reactivity and resupply ability (Monbet et al. 2008). However, DIFS model for sediment profile in this paper only used NH_4Cl-P fraction in sediment-P-pool to calculate K_d in numerical calculation. In fact, BD-P fraction in sediment stands for Fe-bound P and P-remobilization from Fe-bound P is the main mechanism for P-release in anoxic sediment. When it comes to deep sediment layer, the labile P pool in sediment defined as NH_4Cl-P (Monbet et al. 2008) cannot stand for the "real" P pool. In Chap. 4, based on the eutrophic characters and DGT techniques introduced in "Chap. 3 in Part I," the multi-kinds of DGT probes for the measurement of P/Fe/S(-II) at SWI and the numerical simulation using DGT–DIFS method are introduced. The quantification for "internal P-loading" of lake sediments, the P-release mechanism, and the P-release/-diffusion at the interface of DGT/porewater/sediment can be investigated and assessed using DGT profile/image and 1D-DIFS calculation. DGT-Fe- and DGT-P-profiles can be used to research Fe- or P-remobilization character in sediment porewater, indicating the corresponded character of them in broad and detailed DGT curves at the same depth in the sampling site. Then, based on the DGT profile character of labile Fe and P, P-release mechanism can be deduced and "internal P-loading" can be quantified. DGT piston test and 1D-DIFS can quantify the P-process at DGT/sediment interface using the derived DGT parameters and the kinetic curves. An investigation method for the "internal P-loading" of lake sediments and the kinetic release character of P at sediment microzone has been established.

S. Wang and Z. Wu, *DGT-based Measurement of Phosphorus in Sediment Microzones and Rhizospheres*, DOI 10.1007/978-981-10-0721-7_4

4.1 Fe-Remobilization and the Solubility Assessment for Fe-Sulfide Mineral

DGT-Fe/S/P-profiles at sites (A–E) were measured in September 2013 (the end of one algae bloom); the DGT profiles of three elements at sites (F and G) were also measured in May 2013 (during the process of the other algae bloom). Figure 4.1a, b indicates the diffusion and binding process of three (a, ferrihydrite/AgI/chelex-100 DGT) or two (b, AgI/chelex-100 DGT) kinds of Fe/S/P elements during the DGT measurement. By using multilayer-binding-gel DGT probes, three kinds of elements can be determined at the same depth in sediment layer.

Figure 4.2 indicated the picture of the deployment of DGT probes at SWI. The DGT-Fe/P-profiles at those sites (A–G) are indicated in Fig. 4.3. Both DGT-Fe and

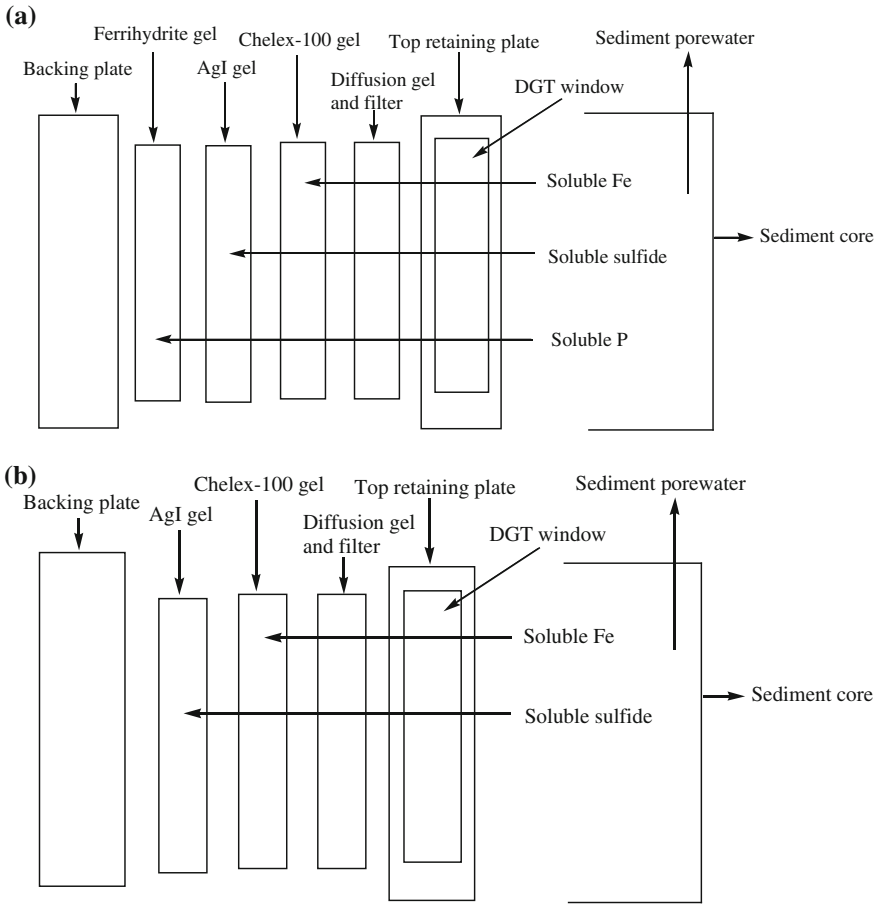

Fig. 4.1 The schematic graphics for the process of diffusion and binding process during the deployment of **a** ferrihydrite/AgI/chelex-100 DGT or **b** AgI/chelex-100 DGT

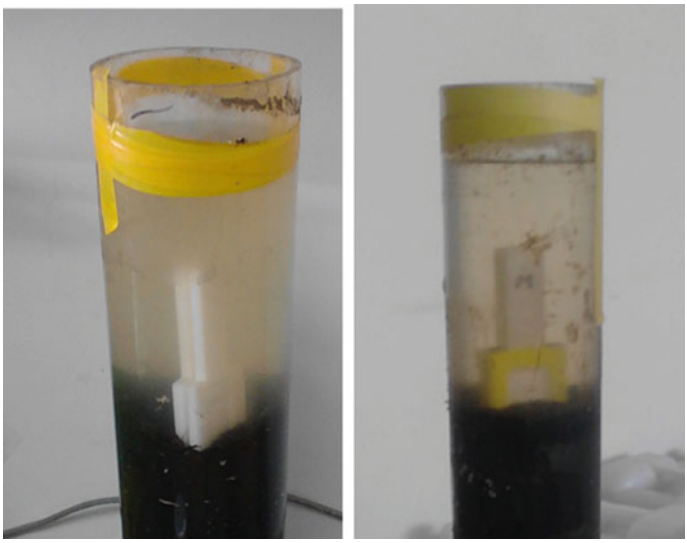

Fig. 4.2 The picture of the deployment of DGT probes at SWI

DGT-P-profiles indicated the distinct remobilization character, which was related to the physicochemical properties and environment conditions of Eh-pH at SWI. The DGT-S(-II)-profiles at sites A, C, F, and G indicated distinct sulfate-reductive process (Fig. 5.3 in Chap. 5). Based on the corresponded characters of DGT-P/S(-II)/P, sediment reactivity, release risk/mobility, the remobilization of Fe and P, biogeochemical reactions, and "internal P-loading" can be researched and assessed.

Figure 4.3 indicates seven profiles (sites A–G) of the DGT-Fe-concentration, which reflect the different characters of redox process in the sediment. According to the standard for the redox status of sediment that Vershinn and Rozanov (1982) recommended, two sites in May (sites F and G) belonged to weak reduction (0–200 mv) states, whereas five sites in September (sites A–E) belonged to reduction (0 to −200 mv) states (Fig. 3.14). All profiles of seven sites at two seasons indicated the distinct Fe-reduction (Fe-R) zones in the anoxic sediments. The decomposition of algae biomass in the uppermost sediment layer can release Fe (Fones et al. 2004) because of the intensive algae bloom justly before September and high content of chlorophyll A (Chla) in the area of north of Dianchi Lake (Wu et al. 2015a, b). The distinct peaks at −0.70 cm (1307 μg L^{-1}) and −1.30 cm (1516 μg L^{-1}) at site A and the peak at −0.30 cm (1835 μg L^{-1}) at site E reflected this decomposition of algae biomass. Below this depth and from −2.00 to −13.00 cm in sediments, the seven sites of two seasons all displayed many distinct peaks at sites A (−2.90, −3.30, −4.30, −4.70, −5.10, −6.70, and −7.50 cm), B (−2.30, −4.70, −6.10, −6.90, −8.30, 10.70, −11.50, −12.10, and −12.90 cm), F (−3.70, −5.30, −6.90, −7.70, and −8.30 cm), and G (−4.70, −6.90, −9.30, −10.30 cm, 4791 μg L^{-1}, −11.50, and −12.30 cm). The Fe curves also had continuous increases at sites C, D, and E, which verified the intensive Fe-R process

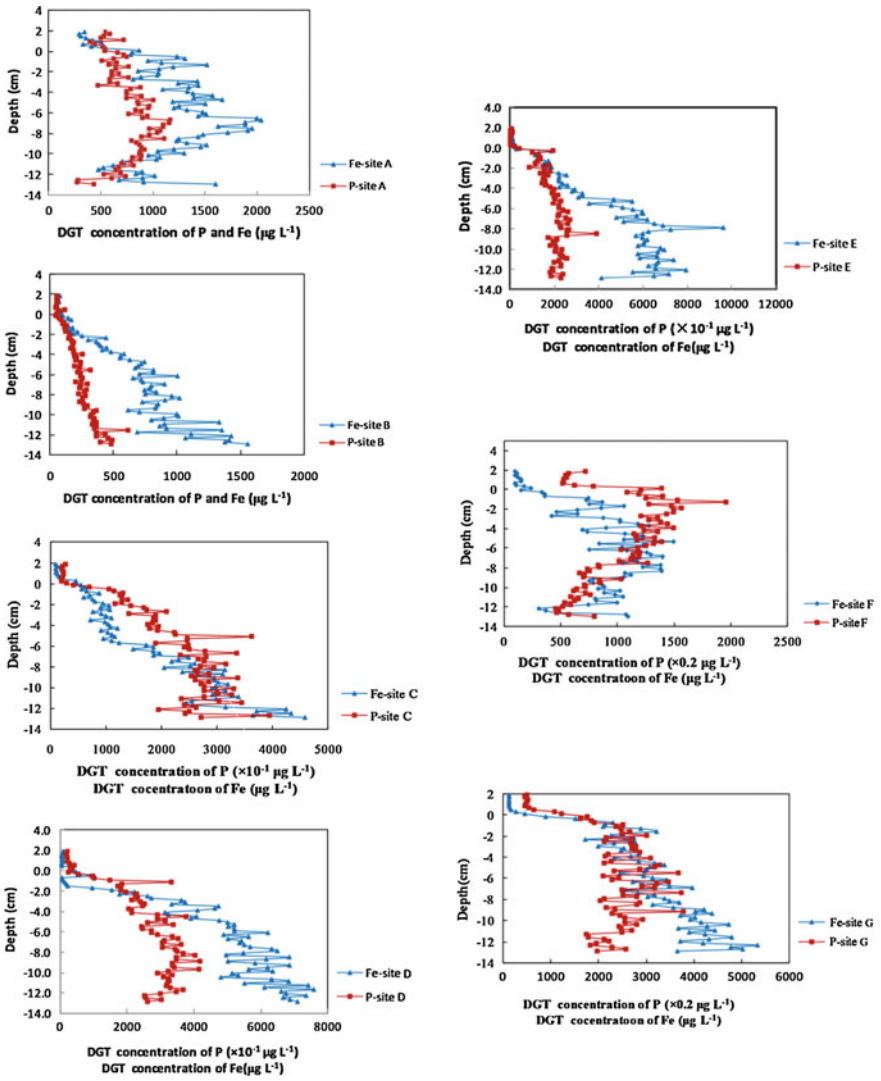

Fig. 4.3 DGT concentration profiles of labile Fe and P at seven sites (A–G) for DGT probes (Reprinted from Water Air Soil Pollut, 225:2188–2194, Wu, Z.H., Wang, S.R., Jiao, L.X., Wu, F. C., The simultaneous measurement of phosphorus, sulfide, and trace metals by Ferrihydrite/AgI/Chelex-100 DGT (Diffusive Gradients in Thin Films) probe at sediment/water interface (SWI) and remobilization assessment, copyright (2015), with the permission from Springer; Reprinted from Environ. Sci. Pollut. R., published online, doi:10.1007/s11356-015-4736-8, Wu, Z.H., Wang, S.R., He, M.C., Element remobilization, "internal P-loading" and sediment-P reactivity researched by DGT (diffusive gradients in thin films) technique, copyright (2015), with the permission from Springer)

(the reductive process of Fe (III) hydroxyoxide) (Wu et al. 2015b; Zhang et al. 2002). Moreover, the low values of the profiles at sites A (−11.50 cm) and F (−4.10, −6.10, −9.30, −12.10 cm) were because of the formation of FeS (Wu et al. 2015b; Krom et al. 2002).

Due to the high content of Fe in sediments at seven sites (Table 3.7 in Chap. 3), the large nonpoint sources such as agriculture, the reductive status of sediment porewater (Fig. 3.14 in Chap. 3), the effect of alga bloom, and high temperature in two seasons, all DGT-Fe-profiles in Dianchi Lake indicated larger concentrations in sediment porewater and more intensive reductive process than those of DGT-Fe researches in Yingkou Bay (Wu et al. 2011) and Loch Duich (Zhang et al. 2002). In particular, at zones D and E, the largest DGT-Fe-concentrations in profiles can exceed 7000 μg L^{-1}.

To assess the degree of saturation with respect to Fe–sulfide, ion activity product (IAP) and saturation index (SI) were calculated according to Eqs. (4.1 and 4.2) (Naylor et al. 2004; Davison 1991; Gustafsson 1999; Wu et al. 2015a) by Visual MINTEQ ver. 3.0 software (Gustafsson 1999). These calculations of IAP and SI can strictly be applied to the porewaters immediately adjacent to the DGT device. Depending on the rate of supply from the solid phase, bulk porewater concentrations of Fe and sulfide could be larger (Naylor et al. 2004).

$$\mathrm{IAP} = \left[\mathrm{Fe}^{2+}\right]\left[\mathrm{HS}^{-}\right]\gamma\mathrm{Fe}^{2+}\gamma\mathrm{HS}^{-}\left(\mathrm{H}^{+}\right)^{-1} \tag{4.1}$$

where $[Fe^{2+}]$ and $[HS^{-}]$ are activities of Fe^{2+} and HS^{-}, in turn; γFe^{2+} and γHS^{-} are activity factors of Fe^{2+} and HS^{-}, in turn.

$$\mathrm{SI} = \log(\mathrm{IAP}/K_{\mathrm{so}}) \tag{4.2}$$

where IAP is ion activity products, and K_{so} is solubility constant.

Based on DGT-Fe/S(-II)-profiles at sites A, C, F, and G (Figs. 4.3 and 4.4) and concentrations of Fe/S(-II) at the depths of Fe-peaks, pH, ionic strength, and temperature were input into the interface of software (Visual MINTEQ ver. 3.0), and then, log IAP and SI corresponded with amorphous FeS (am) and mackinawite were calculated and the indices were listed in Table 4.1.

According to these calculations, there was no FeS(am) production at four sites since SI values were always below 0. When it came to mackinawite, at site A, SI at −7.50 cm was small positive, which indicated a little "oversaturation" at this depth, while other values of SI at all peaks of two sites were negative. However, some peaks at −1.30, −2.90, −3.30, −4.30, −4.70, −6.70, −9.10, and −12.90 cm (site A), at −4.30, −6.10, −7.10, −7.70, −8.30, −9.70, −10.90, and −12.50 cm (site C), and at −9.30, −10.30, −11.50, and −12.30 cm (site G) were a little "undersaturation" because of little negative values. Due to the lower concentration determined by DGT than bulk concentration (Naylor et al. 2004), the last Fe-peaks with little negative SI values in sediment porewater at three sites with respect to sulfide may be at "saturation" status.

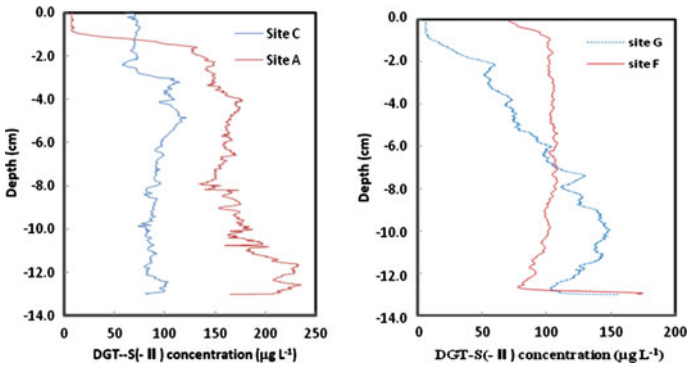

Fig. 4.4 DGT-S(-II) concentration profiles at 4 sites (A, C, F, and G) for DGT probes (Reprinted from Environ. Sci. Pollut. R., published online, doi:10.1007/s11356-015-4736-8, Wu, Z.H., Wang, S.R., He, M.C., Element remobilization, "internal P-loading" and sediment-P reactivity researched by DGT (diffusive gradients in thin films) technique, copyright (2015), with the permission from Springer)

4.2 P-Remobilization and "Internal P-Loading"

In general, the inorganic or organic P can be sorbed to metal oxides at neutral pH in the sediment, and the reduction and subsequent solubilization of these oxides can significantly affect P-release into the overlying water and porewater. In this book, the DGT-P/-Fe-profiles, the eutrophic status, Eh-pH condition, and sediment chemistry at the seven sites at two seasons were compared and studied to deduce the P-release mechanism and assess the "internal P-loading" of sediment in Dianchi Lake. All DGT-P-concentrations in overlying water were lower than those in sediment (Table 4.2 and Fig. 4.3). The mean DGT concentration, the mean DGT flux, and the mean mass accumulated on per unit area of binding gel of DGT probes at seven sites (A–G) in Dianchi Lake are listed in Table 4.2. The main mechanisms for the "internal P-loading" of sediments reflected by DGT probe are indicated in Fig. 4.5. The breakdown of algae biomass in the uppermost sediment layer, the P-release from Fe-bound P in sediment particle to porewater in anoxic sediment, and the upward P-flux across SWI were the main mechanisms for "internal P-loading" of Dianchi Lake.

Firstly, the DGT-P-profiles at sites B–E (0 to −1.90 cm) and those at site F (0.00 to −1.00 cm) and G (0.00 to −1.30 cm) all indicated the distinct increment (all six sites) or peaks in the uppermost layer of sediments. Considering the blue algae blooms in two seasons, the reason of the P-release in this zone was the breakdown of algae biomass that accumulated in the uppermost sediment layer (Cook et al. 2010). Moreover, the microbial degradation of algae biomass (Palmer-Felgate et al. 2011) or the heterotrophic respiration of algae in the uppermost sediment layer can reduce the DO concentration and lead to a redox-dependent P-release from the sediment.

Table 4.1 Ion activity product (IAP) and saturation indices (SIs) of Fe–sulfides at some Fe peaks of the DGT-measured profiles (sites A, C, F, and G)

Site	Depth/cm	Fe-concentration (μg L^{-1})	Sulfide concentration (μg L^{-1})	Log IAP	SI (FeS)	SI (Mackinawite)
A	−0.7	1307	9.69	−4.805	−1.875	−1.205
	−1.3	1517	83.67	−3.949	−1.019	−0.349
	−2.9	1426	146.32	−3.863	−0.932	−0.263
	−3.3	1434	148.07	−3.922	−0.991	−0.322
	−4.3	1569	170.59	−3.748	−0.818	−0.148
	−4.7	1661	166.49	−3.712	−0.782	−0.112
	−6.7	2034	157.08	−3.632	−0.701	−0.032
	−7.5	1947	150.58	−3.58	−0.649	0.02
	−9.1	1512	165.17	−3.871	−0.941	−0.271
	−12.9	1599	214.08	−3.779	−0.849	−0.179
C	−4.3	1210	106.32	−3.674	−0.743	−0.074
	−6.1	1860	97.04	−3.874	−0.944	−0.274
	−7.1	2494	90.73	−3.829	−0.899	−0.229
	−7.7	2604	89.9	−3.996	−1.066	−0.396
	−8.3	3149	84.87	−3.953	−1.023	−0.353
	−8.7	3111	90.09	−4	−1.069	−0.4
	−9.7	3205	79.67	−3.949	−1.019	−0.349
	−10.9	3394	82.87	−3.92	−0.99	−0.32
	−12.1	4253	81.68	−4.229	−1.299	−0.629
	−12.5	4343	100.66	−3.974	−1.043	−0.374
	−12.9	4594	93.85	−4.095	−1.165	−0.495
F	−3.7	1280	135.52	−4.084	−1.128	−0.484
	−5.3	1496	137.07	−4.298	−1.341	−0.698
	−6.9	1399	139.67	−4.286	−1.329	−0.686
	−7.7	1380	139.96	−4.163	−1.206	−0.563
	−8.3	1392	135.22	−4.088	−1.132	−0.488
G	−4.7	3392	73.35	−4.364	−1.408	−0.764
	−6.9	3970	105.28	−4.027	−1.07	−0.427
	−9.3	4374	140.48	−3.9	−0.943	−0.3
	−10.3	4733	145.07	−3.792	−0.836	−0.192
	−11.5	4792	133.77	−3.807	−0.85	−0.207
	−12.3	5342	115.29	−3.971	−1.015	−0.371

Figure 4.6 indicated the algae biomass that was deposited on surface sediments of Dianchi Lake. The cyanobacterial bloom in freshwater systems significantly affects nutrient cycling at SWI during the decomposition process (Seitzinger 1991; Xie et al. 2003; Lehman 2011; Trojanowska and Izydorczyk 2012).

Secondly, the corresponding broad and detailed features (increment, high value, and peak) between the DGT-P- and DGT-Fe-profiles at all seven sites (Fig. 4.3) occurred frequently, which were because of the reductive dissolution of Fe-bound P (Mortimer 1971; Krom 1981; Jensen et al. 1995; Palmer-Felgate et al. 2011; Smith

Table 4.2 Mean DGT concentration, mean DGT flux, and mean mass accumulated on per unit area of binding gel in sediment of DGT probes at seven sites (A–G) in Dianchi Lake

Site/element	C (μg L^{-1})	M/A	F
Site A			
DGT-Fe	1238	3.535 μg cm^{-2}	7.58×10^{-5} μg cm^{-2} s^{-1}
DGT-P	796.1	6246 ng cm^{-2}	4.820×10^{-2} ng cm^{-2} s^{-1}
DGT-S(-II)	153.1	2.518 μg cm^{-2}	1.94×10^{-5} μg cm^{-2} s^{-1}
Site B			
DGT-Fe	696.7	5.525 μg cm^{-2}	4.26×10^{-5} μg cm^{-2} s^{-1}
DGT-P	250.1	1962 ng cm^{-2}	1.514×10^{-2} ng cm^{-2} s^{-1}
Site C			
DGT-Fe	1961	15.55 μg cm^{-2}	1.20×10^{-4} μg cm^{-2} s^{-1}
DGT-P	230.1	1810 ng cm^{-2}	1.397×10^{-2} ng cm^{-2} s^{-1}
DGT-S(-II)	88.34	1.453 μg cm^{-2}	1.12×10^{-5} μg cm^{-2} s^{-1}
Site D			
DGT-Fe	4563	36.19 μg cm^{-2}	2.79×10^{-4} μg cm^{-2} s^{-1}
DGT-P	278	2181 ng cm^{-2}	1.683×10^{-2} ng cm^{-2} s^{-1}
Site E			
DGT-Fe	4521	35.86 μg cm^{-2}	2.77×10^{-4} μg cm^{-2} s^{-1}
DGT-P	197.6	1550 ng cm^{-2}	1.196×10^{-2} ng cm^{-2} s^{-1}
Site F			
DGT-Fe	910	9.21 μg cm^{-2}	1.078×10^{-4} μg cm^{-2} s^{-1}
DGT-P	208.7	2.123 μg cm^{-2}	2.445×10^{-5} μg cm^{-2} s^{-1}
DGT-S(-II)	101.9	1.596 μg cm^{-2}	2.005×10^{-5} μg cm^{-2} s^{-1}
Site G			
DGT-Fe	3254	33.32 μg cm^{-2}	3.856×10^{-4} μg cm^{-2} s^{-1}
DGT-P	505.5	1.773 μg cm^{-2}	2.052×10^{-2} ng cm^{-2} s^{-1}
DGT-S(-II)	92.26	1.586 μg cm^{-2}	1.835×10^{-5} μg cm^{-2} s^{-1}

2009). Furthermore, DGT-P-concentrations had the good linear correlation ($R > 0.75$) with those of DGT-Fe in the whole profiles at sites (B–E), which also indicated the cogeochemical reaction of Fe and P (Wu et al. 2015a). Distinct characters in different layers of sediment porewater profiles can verify the P-release from Fe-bound P through the detailed comparison of the DGT-P- and DGT-Fe-profiles. At site A, the DGT-P-profile indicated the intensive P-release from −0.50 cm (749 μg L^{-1}) to −8.50 cm (1108 μg L^{-1}) with the average value of 826 μg L^{-1} and the less intensive P-release from −8.70 cm (799 μg L^{-1}) to the end of the profile with an average value of 719 μg L^{-1}. The DGT-P-profiles of sites B, C, D, and E all indicated a continuous and intensive P-release character from −1.90 cm to the end of profiles except for a few low values in profiles. At site F, the average values of the DGT concentration in different zone of the vertical profile were 245.3 μg L^{-1} (0.00 to –1.00 cm), 290.8 μg L^{-1} (−1.00 to −3.50 cm), 243.8 μg L^{-1} (−3.70 to −7.50 cm), and 136.3 μg L^{-1} (−7.70 to −12.90 cm). The

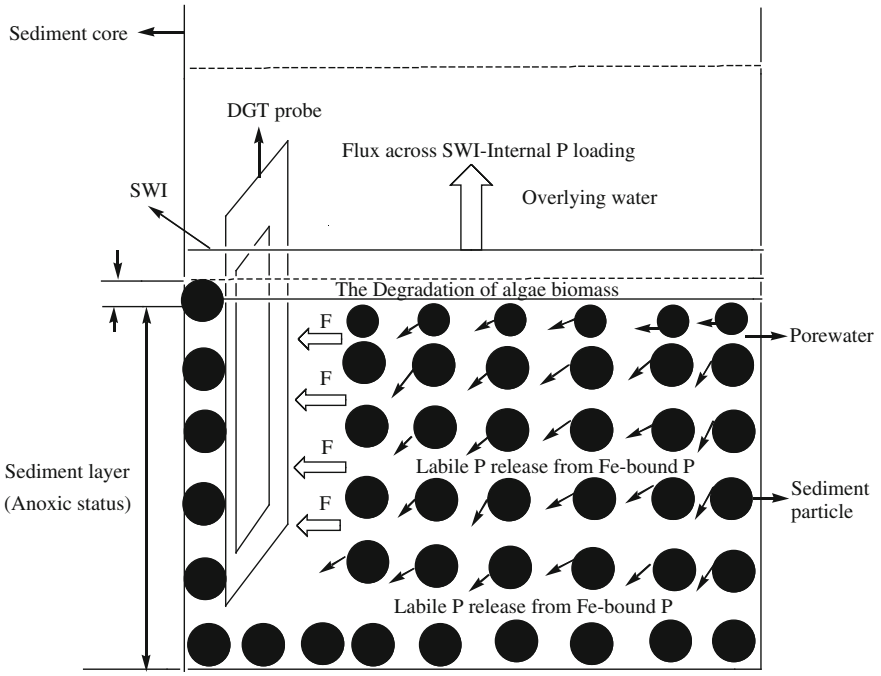

Fig. 4.5 The schematic graphic for the main mechanisms of the "internal P-loading" in lake sediments researched by DGT probe

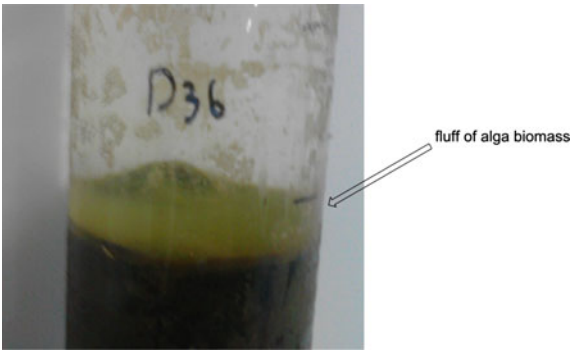

Fig. 4.6 The photographs of the fluff of alga biomass in uppermost sediments in the sediment core (Reprinted from Environ. Sci. Pollut. R., published online, doi:10.1007/s11356-015-4736-8, Wu, Z.H., Wang, S.R., He, M.C., Element remobilization, "internal P-loading" and sediment-P reactivity researched by DGT (diffusive gradients in thin films) technique, copyright (2015), with the permission from Springer)

P-release mainly occurred in the first three zones. At site G, the average values of the DGT concentration in different zones of the vertical profile were 415.7 μg L^{-1} (0.00 to −1.30 cm), 538.4 μg L^{-1} (−1.50 to −8.10 cm), and 485.1 μg L^{-1} (−8.30 to −12.90 cm). The high temperature, low Eh in sediment porewater profiles, and eutrophication status of Dianchi Lake favored the Fe-R and microbial activity, which can lead to an intensive P-release from sediments.

The less intensive release feature of the DGT-P-profiles below −8.70 or −7.70 cm and the low DGT-P-values at the end of profile at sites A or F, the low values at −5.70 cm (189.2 μg L^{-1}) and −12.10 cm (194.7 μg L^{-1}) of the profile at site C, the low value of DGT-P at the end of the profile of site D, the low value of 170.7 μg L^{-1} at −8.90 cm of site E, and the low value of 348.8 −μg L^{-1} (−11.30 cm) at site G were because of the adsorption of P on $Al(OH)_3$ or the precipitation of hydroxylapatite or fluorapatite ($Ca_5(PO_4)_3(OH,F)$) (Kopáček et al. 2005; Miot et al. 2009; Palmer-Felgate et al. 2011).

At site A, two peaks at −10.50 cm (882 μg L^{-1}) and −11.10 cm (813 μg L^{-1}) of DGT-P-profile were at the same depths of two low Fe values (1033 and 619 μg L^{-1}) in the DGT-Fe-profile, which were at the microzones of the FeS(s) formation with large sulfide concentrations of 188 μg L^{-1} (−10.50 cm) and 186 μg L^{-1} (−11.10 cm) in the anoxic sediment. The image (Fig. 4.7) of two segments at −10.50 and −11.10 cm at depths in sulfide image of AgI gel (0.2 × 1.8 cm) indicated a large amount of sulfide microniches (Widerlund and Davison 2007). The mechanisms of P-release at the last two depths at site A were sulfate reduction, formation of insoluble FeS, and associated P-release from Fe-bound P (Oehmi et al. 1997; Ding et al. 2012).

Thirdly, sites A–E were chosen for calculation of "internal P-loading" of Dianchi Lake because of the intensive algae bloom in the late summer and the five sites (A–E) standing for the regions that have areas of 10, 40, 56, 100, and 100 km^2

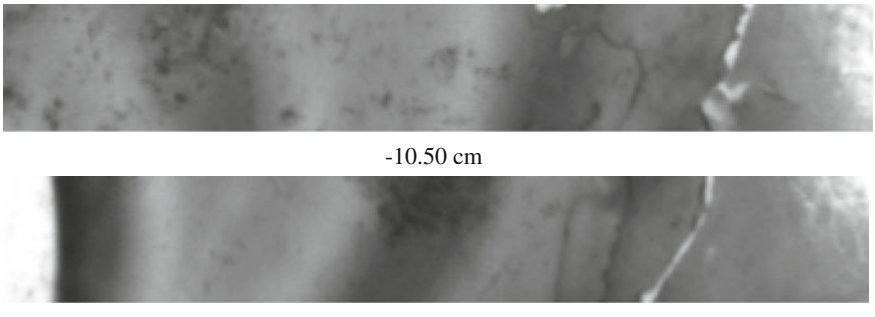

Fig. 4.7 The grayscale images (0.2 × 1.8 cm) of the segment at −10.50 and −11.10 cm at depths in AgI gel (0.2 × 1.8 cm) with black spots, indicating sulfide microniches in the sediment (Reprinted from Environ. Sci. Pollut. R., published online, doi:10.1007/s11356-015-4736-8, Wu, Z.H., Wang, S.R., He, M.C., Element remobilization, "internal P-loading" and sediment-P reactivity researched by DGT (diffusive gradients in thin films) technique, copyright (2015), with the permission from Springer)

(zones A–E). Based on Fick's 1st law of diffusion and the method in the references (Berner 1980; Ullman and Aller 1982), the diffusive fluxes across SWI in five zones were 130.1 μg m^{-2} d^{-1} (A), 103.2 μg m^{-2} d^{-1} (B), 133.5 μg m^{-2} d^{-1} (C), 188.2 μg m^{-2} d^{-1} (D), and 148.8 μg m^{-2} d^{-1} (E). Based on diffusive flux across SWI, the "internal P-loading" with the value of 17.01 t a^{-1} was derived, which was approximately 2.6 % of the total "entering P-loading" (648 t a^{-1}) of Dianchi Lake (Table 4.3). The agriculture nonpoint source contributed to 56 % of the total "entering P-loading" in the whole lake (Chinese Research Academy of Environmental Sciences 2014). The "internal P-loading" and flux across SWI in other lakes and gulfs in the world are listed in Table 4.4 (Denis and Grenz 2002; Fan et al. 2002; Javie et al. 2008; Li et al. 2010).

Fourthly, the sequences of DGT-P-concentration (0 to −8 cm) and the total content of P(NH_4Cl) + P(BD) of surface sediments at all seven sites were as the following: A(807 μg L^{-1}) > G(520 μg L^{-1}) > F(255 μg L^{-1}) > D(245 μg L^{-1}) > C(198 μg L^{-1}) > B(187 μg L^{-1}) > E(182 μg L^{-1}) or A(328 μg g^{-1}) > G (230 μg g^{-1}) > D (188 μg g^{-1}) > F(172 μg g^{-1}) > C(149 μg g^{-1}) > B(143 μg g^{-1}) > E(112 μg g^{-1}), respectively. Generally, the sequence of DGT-P-concentration was consistent with that of the total content of NH_4Cl-P and BD-P which reflected the

Table 4.3 Diffusive flux across SWI and "internal P-loading" of Dianchi Lake

Site	Area (km^2)	F (μg m^{-2} d^{-1})	Internal loading (t $year^{-1}$)
A	10	130.1	0.475
B	40	103.2	1.507
C	56	133.5	2.729
D	100	188.2	6.869
E	100	148.8	5.431
Total	306		17.01

Reprinted from Environ. Sci. Pollut. R., published online, doi:10.1007/s11356-015-4736-8, Wu, Z.H., Wang, S.R., He, M.C., Element remobilization, "internal P-loading" and sediment-P reactivity researched by DGT (diffusive gradients in thin films) technique, copyright (2015), with the permission from Springer

Table 4.4 Diffusive flux across SWI and "internal P-loading" of other lake and sea area in the world

Site	Area (km^2)	F (μg m^{-2} d^{-1})	Internal loading (t $year^{-1}$)
luoma Lake (Fan et al. 2002)	253	354	11.29
Gulf of Lions (Denis et al. 2002)	16000	527	2900
Belton Bridge stream (Javie et al. 2008)		−66	
Stretford Brook (Javie et al. 2008)		−496	
Xianghu Lake (Li et al. 2010)		480	

Reprinted from Environ. Sci. Pollut. R., published online, doi:10.1007/s11356-015-4736-8, Wu, Z.H., Wang, S.R., He, M.C., Element remobilization, "internal P-loading" and sediment-P-reactivity researched by DGT (diffusive gradients in thin films) technique, copyright (2015), with the permission from Springer

main mechanism of P-release that Fe-bound P in sediment controls. Large point sources such as municipal effluent into zone A were corresponded with the largest TP content/total content of NH_4Cl-P + BD-P in sediment and the largest porewater concentration (Chinese Research Academy of Environmental Sciences 2014). The reverse sequence of sites F and D may be attributed to the effect of $CaCO_3/Al(OH)_3$ on the desorption/sorption of P in sediment (Kopáček et al. 2005; Dong et al. 2011). Moreover, the high content of $P(NaOH_{85°c})$-organic P in Dianchi sediment (Table 3.8 in Chap. 3) may also be the potential release source in sediment (Smith et al. 2009).

4.3 P-DIFS Simulation and Sediment-P Reactivity

To quantify the kinetic exchange at the DGT/porewater/sediment interface and assess sediment-P reactivity, nine sites (1–9) in Danchi Lake (Fig. 2.2 in Chap. 2) were chosen for the DGT–DIFS test in May 2013. According to the DGT–DIFS method introduced in "Chap. 3 in Part I," after the parameters in Table 4.5 were input into 1D-DIFS model, DIFS simulation derived *Tc*, K_{-1}, and K_1 (Table 4.6), as well as the curves of *R* and the *dissolved* concentration (Figs. 4.8 and 4.9) during the DGT test in surface sediments. K_d and *R* values were chosen as input parameters of DIFS simulation. According to the research result in Sect. 4.2, P-release from Fe-bound P in anoxic sediments of Dianchi Lake was verified and the similar research results were also found in two references (Smith 2009; Palmer-Felgate et al. 2011).

Compared with the P-DIFS research result of Monbet et al. (2008), the T_c values at Dianchi Lake (33–56060 s) in this chapter were much lower than those at Victoria Lake (UK) (4128–183400 s) and Wellington Lake (UK) (55–149400 s); K_{-1} values in this paper in the range (0.03–13.13 d^{-1}) were also lower than those at Victoria Lake (0.3–21 d^{-1}) and Wellington Lake (0.6–1558 d^{-1}). The adsorption parameters in this DIFS test were in the range (1.51–2609 d^{-1}), which were larger than those at Victoria Lakes (UK) (0.3–21 d^{-1}) and Wellington Lakes (UK) (0.6–1558 d^{-1}). According to other references, the adsorption rate constants in estuarine sediments were in the range of 0.1–294 d^{-1} (Appan and Wang 2000) and 0.5–1.5 d^{-1} (Slomp et al. 1998). *R* values in Dianchi Lake were in the range (0.189–0.743), which were larger than those at Victoria Lake (0–0.40) and a little lower than those at Wellington Lake (0.40–1.00).

The *R* curves (Fig. 4.8) in this book can be classified into three cases: "fast resupply" (site 7), "intermediate rate of resupply" (sites 1, 2, 3, 6, and 9), and "slow rate of resupply" (sites 4, 5, and 8). All *R* curves initially increased continuously into high values (sites 7, 1, 2, 3, 6, and 9) or peaks (sites 4, 5, and 8) in less than two hours. The *R* value at site 7 belonged to "fast resupply." After the high value was attained, a plateau was maintained with only a little drop after 10 h. The large K_d (1536 cm^3 g^{-1}) and low *Tc* (33 s) characterized this case. A distinct resupply sustained an effectively constant flux, but was insufficient to fully satisfy the DGT demand. On the contrary, the *R* curves at sites 4, 5, and 8 (slow rate of resupply)

Table 4.5 Input and output parameters of the model of P-diffusion simulation (P-DIFS simulation) for the sites (1–9) in Dianchi Lake (China). Input parameters and C_{DGT} of the P-DIFS simulation during the DGT test

Site	R	K_d ($cm^3\ g^{-1}$)	Pc ($g\ cm^{-3}$)	Dd ($cm^2\ s^{-1}$)	Ds ($cm^2\ s^{-1}$)	Pordif	Porsed	C_0 ($nmol\ mL^{-1}$)	dg (cm)	C_{DGT} ($nmolmL^{-1}$)
1	0.513	232.9	0.1367	5.89	7.65	0.95	0.95	70.29	0.092	36.06
2	0.428	299.2	0.0934	5.89	7.87	0.95	0.97	29.13	0.092	12.47
3	0.451	168.4	0.2119	5.89	7.29	0.95	0.93	24.03	0.092	10.84
4	0.353	354.8	0.2225	5.89	7.25	0.95	0.92	7.97	0.092	2.81
5	0.189	172.6	0.2813	5.89	7	0.95	0.9	11.19	0.092	2.11
6	0.459	148.3	0.1281	5.89	7.69	0.95	0.95	25.87	0.092	11.87
7	0.743	1536	0.1293	5.89	7.68	0.95	0.95	5.45	0.092	4.05
8	0.291	328.8	0.2031	5.89	7.33	0.95	0.93	15.06	0.092	4.38
9	0.47	134.7	0.1639	5.89	7.51	0.95	0.94	23.53	0.092	11.06

Table 4.6 Input and output parameters of the model of P-diffusion simulation (P-DIFS simulation) for the sites (1–9) in Dianchi Lake (China). Output parameters of the P-DIFS simulation during the DGT test

Site	T_C (s)	K_{-1} (d^{-1})	K_1 (d^{-1})
1	498	5.28	168.08
2	2603	1.15	32.05
3	1777	1.33	47.3
4	6994	0.15	12.2
5	56060	0.03	1.51
6	332	13.03	247.6
7	33	13.13	2609.02
8	13140	0.1	6.48
9	382	9.79	216.15

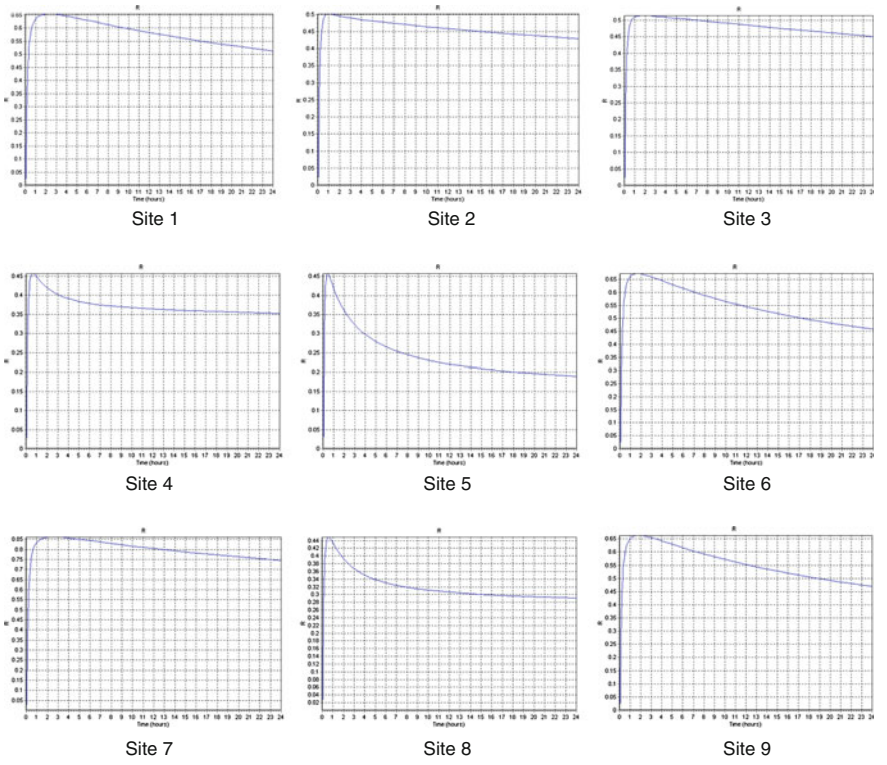

Fig. 4.8 *R* value against deployment time (*T*) of sediments (sites 1–9) during DGT–DIFS simulation

indicated a distinct peak in less than 1-h DGT deployment and a swift decrease after that peak. A continuous decline of *R* indicated the solid phase had an effectively little resupply from the solid phase. In this case, the porewater concentration depleted rapidly as P continuously diffused to the resin gel. The rate of desorption

can only sustain a low level of resupply. The low desorption rate constants (0.03–0.15 d^{-1}) at sites 4, 5, and 8 verified the last reason. The R of this case cannot exceed 0.40. Otherwise, the fast resupply from the sediment particle may mask the generated peak. The R values of sites 1, 2, 3, 6, and 9 belonged to the "intermediate rate of resupply" case in the range of 0.40–0.60.

Dissolved concentration curves (Fig. 4.9) of the "slow rate of resupply" case (sites 4, 5, and 8) indicated a distinct depletion of labile P-concentration from the diffusive layer and into the sediment with the distance of more than 1.0 cm. In particular at site 5, the distance of depletion was 2.5 cm, which may be because of the largest Tc (56060 s), the lowest R (0.189), and the lowest K_{-1} (0.03 d^{-1}). The DIFS concentration curves at site 7 (fast resupply) indicated that the slight depletion over deployment time and depletion distance was approximately 0.30 cm, which was because of the largest sediment-P pool with K_d (1536 cm^3 g^{-1}) and the desorption parameter (13.13 d^{-1}) of nine sediments. Meanwhile, the sites 1, 2, 3, 6, and 9 belonged to the "intermediate rate of resupply" case with the depletion distance of no more than 1.0 cm. The depletion of the dissolved P-concentration

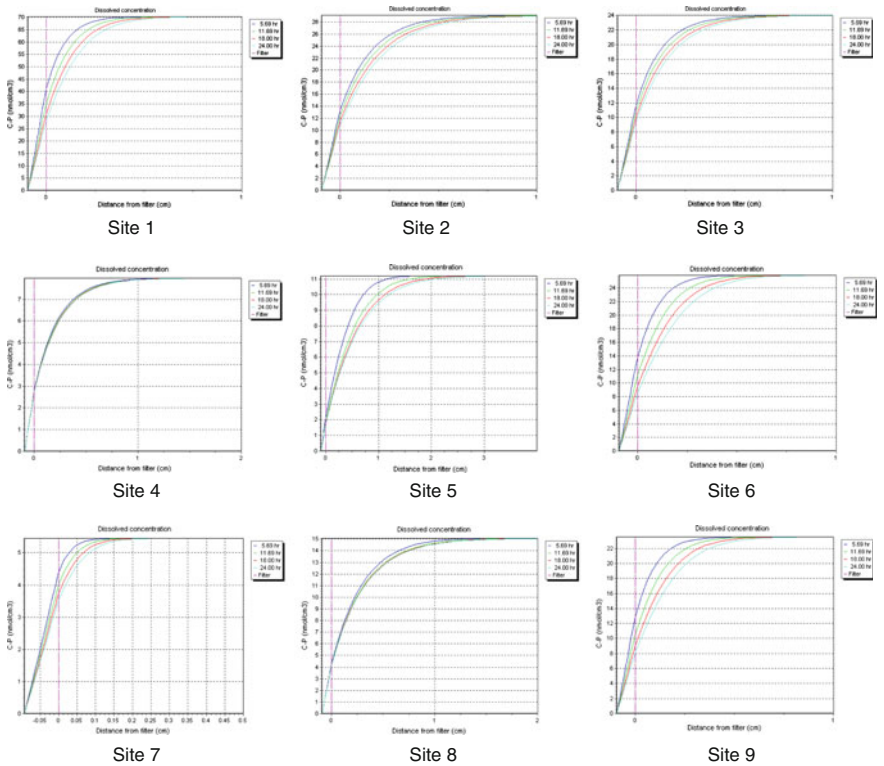

Fig. 4.9 The *dissolved* concentrations against the distance/time of nine sediments during DGT–DIFS test. The *dissolved* concentration (*C-P*) is the labile P-concentration in porewater (distance > 0) and diffusion layer (distance < 0)

was more distinct than that of sorbed P-concentration at short times (5.69 h) because of the small particulate reservoir (K_d = 172.6 cm^3 g^{-1}) and the largest *Tc* (56060 s) at site 5 of all nine sites. The DGT-P (Table 4.5) of surface sediments at two sites (1 and 2) still indicated high DGT concentrations in porewater and P-release risk with a low K_d because of the abundant contents of NH_4Cl-P and BD-P (Fig. 3.13 in Chap. 3) in surface sediments with a reductive status.

4.4 Summary

In this chapter, diffusive gradients in thin films (DGT) technique and DGT-induced flux in sediments (DIFS) model have been researched in order to (1) measure the profile or image of labile P, Fe, and sulfide in the sediment porewater in Dianchi Lake (China) using multi-kinds of DGT probes; (2) assess the occurring mechanism of "internal P-loading" through DGT profiles; and (3) assess the kinetic process across the DGT/porewater/sediment interface using DIFS model. According to DGT profile character of labile P and Fe at seven sites (A–G), the P-release mechanism was investigated. The major mechanism was the distinct P-release from Fe-bound P during the reduction of Fe oxide in the reductive sediment layers at all sites. The minor mechanisms were the algae biomass decomposition in the uppermost sediment layer at sites (B–G) and the coupled Fe–S–P geochemical reaction at the two depths of site A. The "internal P-loading" in Dianchi Lake was estimated at 17.01 t a^{-1} and accounted for 2.6 % of the total "entering P-loading" (648 t a^{-1}). Kinetic parameter *Tc* (33–56060 s), distribution coefficient K_d (134.7–1536 cm^3 g^{-1}), resupply parameter *R* (0.189–0.743), curve changes of the *dissolved* concentration, as well as those of *R* at the DGT/porewater/sediment interface in nine sites (1–9) were derived through DIFS simulation. This research indicates DGT/DIFS should be a valuable method to evaluate "internal P-loading" and sediment reactivity in sediment microzone in lakes.

References

Appan A, Wang H (2000) Sorption isotherms and kinetics of sediment phosphorus in a tropical reservoir. J Environ Eng 126:993–998

Berner RA (ed) (1980) Early diagenesis: a theoretical approach. Princeton University Press, Princeton

Chinese Research Academy of Environmental Sciences (2014) The survey and the investigation of "internal loading character" of Dianchi Lake (Chinese)

Cook PLM, Holland DP, Longmore AR (2010) Effect of a flood event on the dynamics of phytoplankton and biogeochemistry in a large temperate Australian lagoon. Limnol Oceanogr 55:1123–1133

Davison W, Grime GW, Morgan J, Clarke K (1991) Distibution of dissolvediron in sedement pore waters at submillimetre resolution. Nature 352:323–324

Denis L, Grenz C (2002) Spatial variability in oxygen and nutrient fluxes at the sediment-water interface on the continental shelf in the Gulf of Lions (NW Mediterranean). Oceanol Acta 26:373–389

Ding S, Sun MQ, Xu D, Jia F, He XA, Zhang CS (2012) High-resolution simultaneous measurements of dissolved reactive phosphorus and dissolved sulfide: the first observation of their simultaneous release in sediments. Environ Sci Technol 46:8297–8304

Dong LM, Yang ZF, Liu XH (2011) Phosphorus fractions, sorption characteristics, and its release in the sediments of Baiyangdian Lake, China. Environ Monit Assess 179:335–345

Fan CX, Zhang L, Yang LY, Huang WY, Yu PZ (2002) Simulation of internal loading of nitrogen and phosphorus in a lake. Oceanologia et Limnologia Sinica 33(4):370–378 (in Chinese)

Fones GR, Davison W, Hamilton-Taylor J (2004) The fine-scale remobilization of metals in the surface sediment of the North-East Atlantic. Cont Shelf Res 24:1485–1504

Gustafsson JP (1999) Visual MINTEQ 3.0 user guide, http://hem.bredband.net/b108693/download.html

Krom MD, Berner RA (1981) The diagenesis of phosphorus in a nearshore marine sediment. Geochim Cosmochim AC 45:207–216

Krom MD, Mortimer RJG, Hayes SWP, Davies IM, Davison W, Zhang H (2002) In-situ determination of dissolved iron production in recent marine sediments. Aquat Sci 64:282–291

Lehman JT (2011) Nuisance cyanobacteria in an urbanized impoundment: interacting internal phosphorus loading, nitrogen metabolism, and polymixis. Hydrobiologia 661:277–287

Li YZ, Xia BC, Zhang JY, Li CH, Zhu WZ (2010) Assessing high resolution oxidation-reduction potential and soluble reactive phosphorus variation across vertical sediments and water layers in Xinghu Lake: a novel laboratory approach. J Environ Sci 22:982–990

Javie HP, Mortimer RJG, Palmer-Felgate EJ, Quinton KS, Harman SA, Carbo P (2008) Measurement of soluble reactive phosphorus concentration profiles and fluxes in river-bed sediments using DET gel probes. J Hydrol 350:261–273

Jensen HS, Mortensen PB, Andersen Rasmussen FLE, Jensen A (1995) Phosphorus cycling in a coastal marine sediment, Aarhus Bay, Denmark. Limnol Oceanogr 40:908–917

Kopáček J, Borovec J, Hejzlar J, Ulrich KU, Norton SA, Amirbahman A (2005) Aluminum control of phosphorus sorption by lake sediments. Environ Sci Technol 39:8784–8789

Miot J, Benzerara K, Morin G, Bernard S, Beyssac O, Larquet E (2009) Transformation of vivianite by anaerobic nitrate-reducing iron-oxidizing bacteria. Geobiology 7:373–384

Monbet P, Mckelvie ID, Worsfold PJ (2008) Combined gel probes for the in situ determination of dissolved reactive phosphorus in porewaters and characterization of sediment reactivity. Environ Sci Technol 42:5112–5117

Mortimer CH (1971) The exchange of dissolved substances between mud and water in lakes. Ecology 29:280–329

Naylor C, Davison W, Motelica-Heino M, Van Den Berg GA, Van der Heijdt LM (2004) Simultaneous release of sulfide with Fe, Mn, Ni and Zn in marine harbor sediment measured using a combined metal/sulfide DGT probe. Sci Total Environ 328:275–286

Oehmi NJ, Luben TJ, Ostrofsky ML (1997) Spatial distribution of acid-volatile sulfur in the sediments of Canadohta Lake, PA. Hydrobiologia 345:79–85

Palmer-Felgate EJ, Mortimer RJG, Krom MD, Jarvie HPR, Williams JR, Spraggs E, Stratford CJ (2011) Internal loading of phosphorus in a sedimentation pond of a treatment wetland: Effect of a phytoplankton crash. Sci Total Environ 409:2222–2232

Seitzinger SP (1991) The effect of pH on the release of phosphorus from Potomac estuary sediments: implications for blue-green algal blooms. Estuarine, Coastal Shelf S. 33:409–418

Slomp CP, Malschaert JFP, Van Rassphorst W (1998) The role of adsorption in sediment-water exchange of phosphate in North Sea continental margin sediments. Limnol Oceanogr 43:532–846

Smith LG (2009) Missiquoi bay sediment phosphorus cycling: the role of organic phosphorus and seasonal redox fluctuations. Master Thesis, The University of Vermont, Vermont, USA

Trojanowska AA, Izydorczyk K (2012) Phosphorus fractions transformation in sediments before and after cyanobacterial bloom: implications for reduction of eutrophication symptoms in Dam reservoir. Water, Air, and Soil Pollut 211:287–298

Ullman WJ, Aller RC (1982) Diffusion coefficients in nearshore marine sediments. Limnol Oceanogr 27:552–556

Vershinn AV, Rozanov AG (1982) On the problem of Eh measurement by the Pt electrode and estimation of oxidation reduction conditions in marine media. Geokhimiya 1:121–128

Widerlund A, Davison W (2007) Size and density distribution of sulfide-producing microniches in lake sediments. Environ Sci Technol 41:8044–8049

Wu ZH, He MC, Lin CY (2011) In situ measurements of concentrations of Cd Co, Fe and Mn in estuarine porewater using DGT. Environ Pollu 159:1123–1128

Wu ZH, Wang SR, He MC (2015a) Element remobilization, “internal P-loading” and sediment-P reactivity researched by DGT (diffusive gradients in thin films) technique. Environ Sci Pollut R 22:16173–16183. (Reprinted from Environ Sci Pollut R, published online, doi:10.1007/s11356-015-4736-8, Wu ZH, Wang SR, He MC, Element remobilization, “internal P-loading” and sediment-P reactivity researched by DGT (diffusive gradients in thin films) technique, copyright (2015), with the permission from Springer)

Wu ZH, Wang SR, Jiao LX (2015b) Geochemical behavior of metals-sulfide-phosphorus at SWI (sediment/water interface) assessed by DGT (Diffusive gradients in thin films) probes. J Geochem Explor 156:145–152

Xie LQ, Xie P, Tang HJ (2003) Enhancement of dissolved phosphorus release from sediment to lake water by Microcystis blooms—an enclosure experiment in a hyper-eutrophic, subtropical Chinese lake. Environ Pollu 122(3):391–399

Zhang H, Davison W, Mortimer RJG, Krom MD, Hayes PJ, Davies IM (2002) Localised remobilization of metals in a marine sediment. Sci Total Environ 296:175–187

Chapter 5
The Coupled Fe–S–P Biogeochemical Mechanism for P-Release and Sulfide Microniche in Sediments Assessed by DGT–CID Technique (Dianchi Lake)

The DGT sampler containing a diffusive gel layer and a binding layer (AgI gel) (Teasdale et al. 1999) can be used for the measurement of S(-II) in sediment porewater. When DGT was deployed in sediment, soluble sulfide species can diffuse through diffusive layer and react with $AgI_{(s)}$ in the binding gel. Then, the black $Ag_2S_{(s)}$ is formed in the binding gel. The sulfide accumulated in the binding gel can be determined and calculated by the grayscale density of binding gel, CID (computer imaging densitometry) technique, and ImageJ 1.38e software. The sulfide flux diffusing from sediment porewater to DGT resin can be determined by this method. 2D image of P and S(-II) with high resolution in sediment porewater has been determined by Ding et al. (2012), and ZrO–AgI binding layer, the CID technique, the 2D slicing for the binding gel, and microcolorimetric analysis method have been used for this research. The phenomena of the corelease of P and S(-II) have been observed in 2D images. These combined Fe–S–P geochemical reactions, which engender P-release in sediment porewater, can be investigated by this technique. Widerlud and Davison (2007) used DGT–CID technique for the research of sulfide-microniche-distribution character in sediments of seasonal anoxic England lake and the mechanism of sulfide microniche. However, the previous DGT-S(-II) researches only investigated S(-II) image or S(-II) and P images. For P-release risk, the coupled Fe–S(-II)–P reaction is judged by DGT-S(-II) and DGT-P images at the same location, and there was a lack of Fe-profile or image at the same location to reveal this reaction. In order to reveal this geochemical reaction with DGT profile or image of three elements, in this chapter, Fe/S(-II)/P elements at same location in one same sampling site at SWI of Dianchi Lake were measured by the double-binding-layer DGT and twin DGT probes. AgI gel in one DGT probe and CID can derive 2D distribution of DGT-S(-II) concentration. Based on DGT-S(-II) image, the distribution character of sulfide microniches can be assessed and the coupled reaction of Fe–S–P for P-release mechanism can be researched according to the character of DGT profiles of Fe and P and sulfide microniche image at the

S. Wang and Z. Wu, *DGT-based Measurement of Phosphorus in Sediment Microzones and Rhizospheres*, DOI 10.1007/978-981-10-0721-7_5

same location in sediment layer. Moreover, based on DGT-S(-II) image and ImageJ 1.38e software, the distribution character of sulfide microniche in sediment in Dianchi Lake was quantified and assessed.

5.1 The Distribution Character of Sulfide Microniche and Biogeochemical Mechanism in Sediments Based on DGT–CID Technique

Microniche, which can exist in localized zones of high organic matter in anoxic sediments, has been termed 100 years ago. However, the microniche at high spatial resolutions has been measured only in recent years (Stockdale et al. 2010). For the microscopic research of sediments, the microniche size was in the ranges of 5 μm–1.9 mm (Johnson 1974) or 1 μm to several millimeters/centimeters (Jørgensen 1977). Under particular conditions in sediment microzone, such microniche can exist. The formation mechanism for sulfide microniche in sediment has been simulated by 3D reaction-transport model developed specifically for spherical microniches (Stockdale et al. 2010). The effects of organic matter (OM) degradation, particle porosity, and niche lifetime on the dissolved sulfide and iron concentrations, and the formation of FeS were also researched in this paper. DGT–CID method has been used to measure sulfide microniche at spatial resolution of 85 μm and assess the distribution character of sulfide microniche in sediment cores in lake. In this paper, three sulfide microniches reflected by AgI gel are indicated in Fig. 5.1.

In this chapter, DGT–CID technique with resolution of 42 μm was used for sulfide microniche assessment. The niche areas reported in this test were considered as apparent areas (Widerlud and Davison 2007), operationally defined by the spatial resolution (42 μm) obtained after diffusion through diffusive layer, and depending on the niche-DGT distance. The apparent surface area of a microniche was measured by ImageJ 1.38e software according to the standard method recommended by Widerlud and Davison (2007). The parameters for the assessment of sulfide microniche character were grayscale intensity, circularity, area, and peak flux, which were determined by ImageJ 1.38e software. Grayscale images-S(-II) at sites F and G, as well as 2D images at sites A and C with spatial resolution of 42 μm, are presented in Figs. 5.2 and 5.3. Microniche images derived by DGT–CID at sites A, C, F, and G with spatial resolution of 42 μm are indicated in Fig. 5.4 for the assessment of sulfide microniches. The DGT-S(-II) concentration profiles at sites A, C, F, and G are indicated in Fig. 4.4 (Chap. 4). The parameters used for assessing sulfide microniche character were circularity, area, peak flux, and R_{JM} (i.e., the ratio between microniche-related sulfide flux from n niches and the total horizontal net flux of sulfide). These parameters were defined in accordance with the method introduced by Widerlund and Davison (2007), which is listed in Eqs. (5.1 and 5.2).

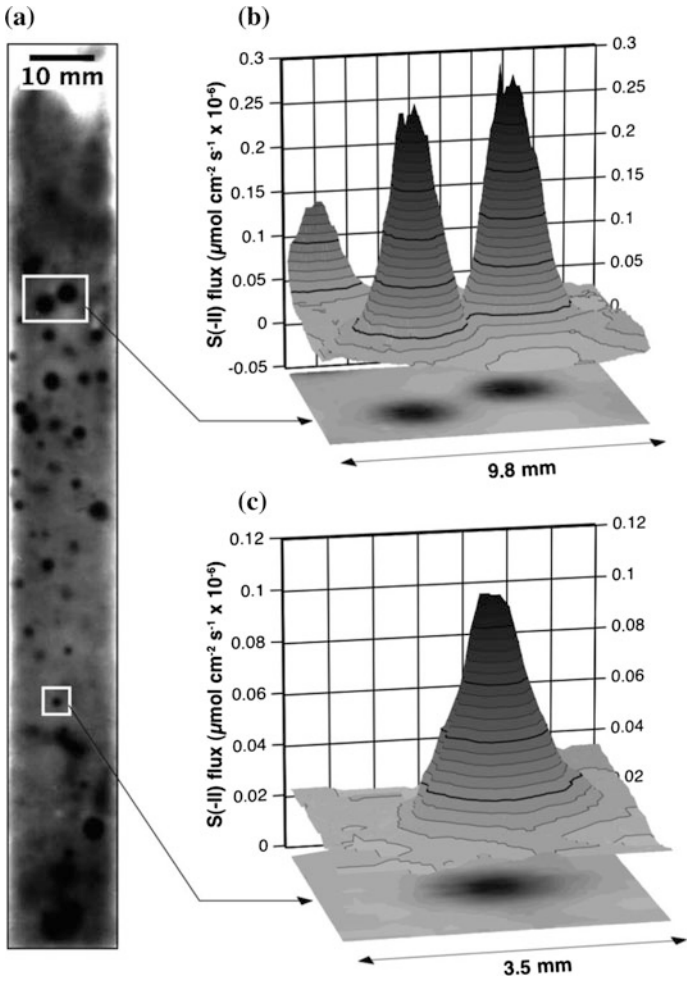

Fig. 5.1 **a** Scanned grayscale image of a gel with 53 microniches covering 6.9 % of the gel surface area (gel size 17.2 × 141.6 mm). **b** Three-dimensional plot of two circular microniches, with horizontal S(-II) maximum fluxes of $\sim 0.3 \times 10^{-6}$ μmol cm^{-2} s^{-1} and a background flux of $\sim 0.05 \times 10^{-6}$ μmol cm^{-2} s^{-1}. **c** Three-dimensional plot of a circular microniche, with a horizontal S(-II) maximum flux of $\sim 0.1 \times 10^{-6}$ μmol cm^{-2} s^{-1} and a background flux of $\sim 0.02 \times 10^{-6}$ μmol cm^{-2} s^{-1} (Reprinted (adapted) with the permission from Environ. Sci. Technol., 41: 8044–8049, Widerlund, A., Davison, W., Size and density distribution of sulfide-producing microniches in lake sediments, copyright (2007), American Chemical Society)

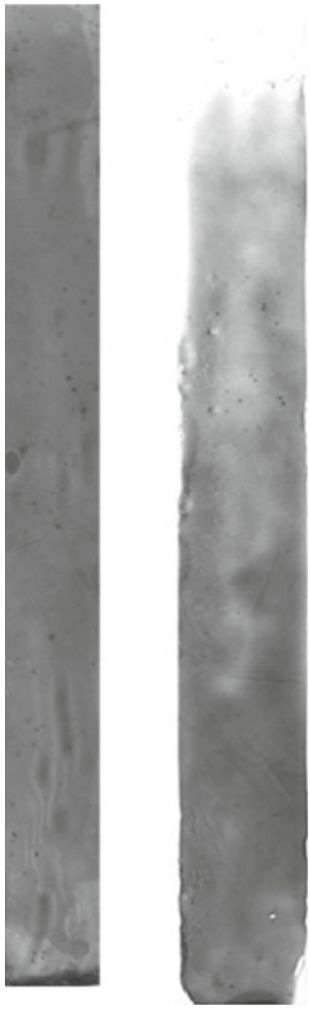

Fig. 5.2 Grayscale images-S (-II) of sites F and G

The microniche characters of four zones at sites A, C, F, and G are indicated in Table 5.1.

The parameter of circularity for the assessment of sulfide microniche character (Widerlund and Davison 2007) is indicated as Eq. (5.1).

$$C = 4\pi(A/P^2) \tag{5.1}$$

where A is the area of the niche and P is its perimeter. A circularity value of 1.0 indicates a perfect circle, while a value approaching 0 indicates an increasingly elongated polygon.

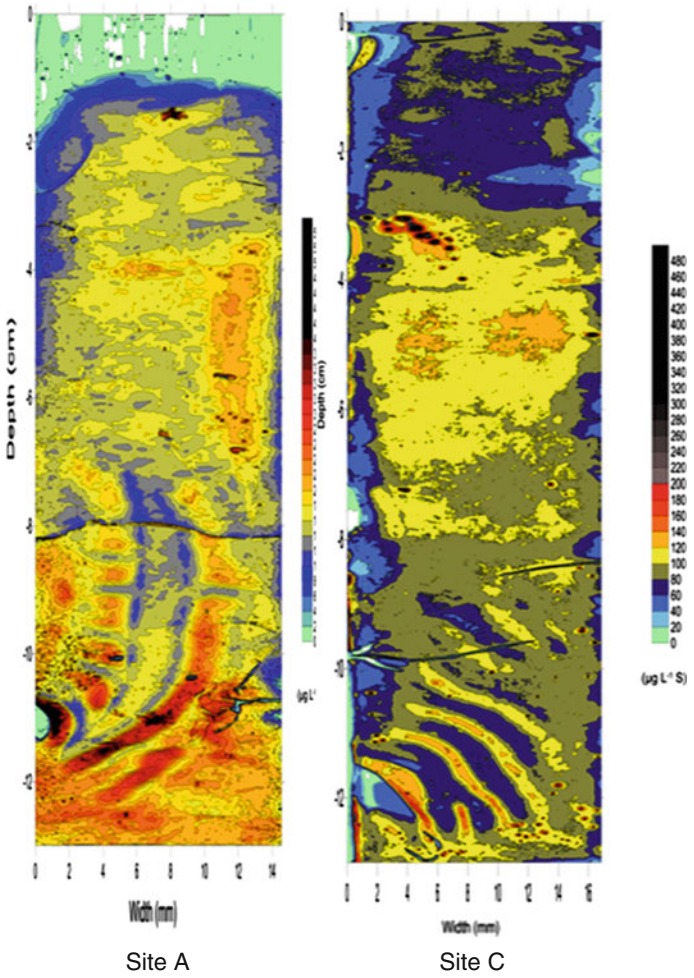

Fig. 5.3 2D images at sites A and C with spatial resolution of 42 μm

R_{JM} (the ration between microniche-related sulfide flux from n niches and the total horizontal net flux of sulfide) is indicated as Eq. (5.2).

$$R_{\mathrm{JM}} = \frac{\sum_{i=1}^{n} J_i^{\mathrm{peak}} \times A_i^{\mathrm{peak}}}{\sum_{i=1}^{n} J_{\mathrm{average}}^{\mathrm{bg}} \times A^{\mathrm{gel}} + J_i^{\mathrm{peak}} \times A_i^{\mathrm{peak}}} \tag{5.2}$$

where (μg cm^{-2} s^{-1}) is the microniche peak sulfide flux for peak i, (μg cm^{-2} s^{-1}) is the average of the background flux of sulfide at the base of n niches in a gel, (cm^2) is the microniche area for peak i, and (cm^2) is the total area of AgI gel.

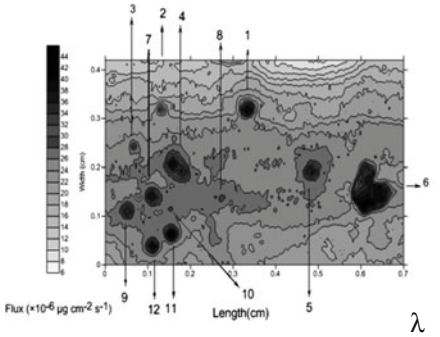
Flux (×10-6 μg cm-2 s-1)
Length(cm)
Width (cm)

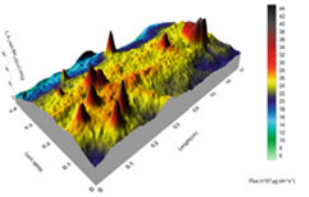

λ

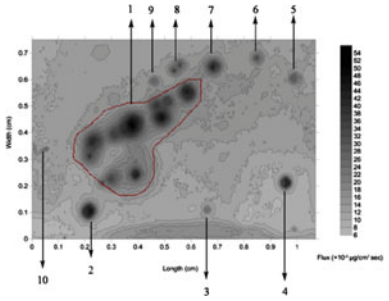
Length (cm)
Width (cm)

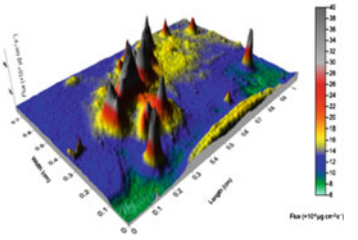

μ

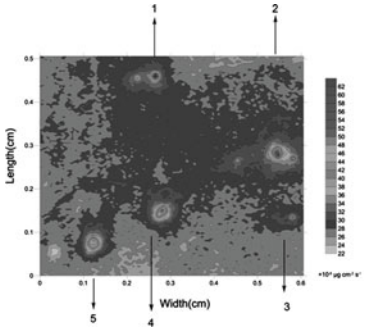
Length(cm)
Width(cm)

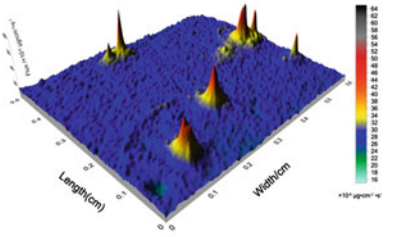
Length(cm)
Width/cm

ψ

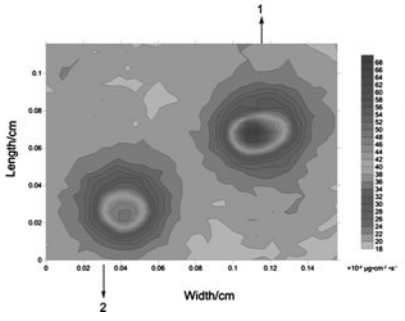
Length/cm
Width/cm

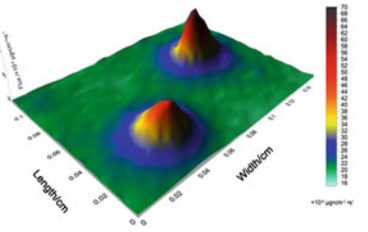
Length/cm
Width/cm

τ

◀ **Fig. 5.4** Microniche images at sites A, C, F, and G derived by DGT–CID. λ-Niche images (2D) for the assessment of a group of microniches in the left of AgI gel at a depth of approximately −6.50 cm in sediment at site A; μ-niche images (2D) for the assessment of a group of microniches in the right of AgI gel at a depth of approximately −3.20 cm in sediment at site C; ψ-niche images (2D) for the assessment of five niches at the left of AgI gel of at a depth of almost −7.00 cm at site F; and τ-niche images (2D) for the assessment of two niches at the left of AgI gel at a depth of almost −6.70 cm at site G

Sulfide microniche peak flux was obtained by subtracting the background flux surrounding a niche from the maximum flux of the niche, and represents a horizontal (1D) net flux of dissolved sulfide from a microniche (Widerlund and Davison 2007).

There were 12 microniches in the left of CID image (λ) at the depth of about −6.50 cm in sediment layer at site A. The microniches (2, 3, 8, 9, 10, 11, and 12) had the circularity of 1, indicating a preface circle. The total area of 12 microniches was 0.0135 cm^2 (4.58 % of total area of selected zone). The calculated $\sum_{i=1}^{n} J_i^{peak} \times A_i^{peak}$ was 5.59×10^{-8} μg s^{-1} with R_{JM} of 0.68 %.

There was a group of 10 microniches in the right of CID image (μ) at the depth of about −3.20 cm in sediment at site C. The largest microniche (niche 6) with the area of 0.06 cm^2 had the niche peak flux of 1.01×10^{-5} μg cm^{-2} s^{-1}. The other niches surrounded this niche, among which were niches 1, 5, 7, and 10 with the shape of a preface circle. For image (μ), the calculated $\sum_{i=1}^{n} J_i^{peak} \times A_i^{peak}$ was 6.90×10^{-7} μg s^{-1} with R_{JM} value of 4.02 %.

There were 5 microniches at the left of microzone (ψ) at site F at a depth of about −7.00 cm. The R_{JM} value is 1.59 % with the total niche area of 0.0106 cm^2. There were 2 microniches (microzone τ) at the left of AgI gel at site G at depth of about −6.70 cm. The total area of two niches was 0.003 cm^2 with a R_{JM} value of 14.26 %.

The localized sulfide formation in four microzones may be due to the oxidation of OM, algae biomass, fecal pellets, and pyrite at the edge of niches. The undisturbed sediment cores were used for DGT test. If algae were added into sediment layers as the method introduced by Widerlud and Davison (2007), the niche peaks with little flux, such as niches 2, 8, and 10 at image (λ) and 7 and 10 at image (μ), may be changed into the larger fluxes, and the values of $\sum_{i=1}^{n} J_i^{peak} \times A_i^{peak}$ and R_{JM} can also increased compared with undisturbed sediments.

This study revealed the existence of localized sulfide microniches in lake sediment. The dynamics of the biogeochemical occurring in microniches with larger flux exceeding the background value are important to reveal the biogeochemical process and the distribution character of sulfide. The sediment reactivity, the size and shape of the detrital organic particles, microbial activity, and burrowing organisms may influence the formation of sulfide microniche. Moreover, the formation of sulfide microniche is also affected by the sulfide sink, the availability of Fe, and the precipitation of FeS mineral (Motelica-Heino et al. 2003; Hamilton-Taylor et al. 1985; Widerlud and Davison 2007).

Table 5.1 Assessment results of microniche images (λ, μ, ψ, and τ) at sites A, C, F, and G derived by DGT–CID

Microniche	Niche area/cm^2	Circularity	Peak flux/μg cm^{-2} s^{-1}	R_{JM}
Microzone λ				0.68 %
1	7.17×10^{-4}	0.973	4.08×10^{-6}	
2	1.79×10^{-5}	1	1.33×10^{-6}	
3	1.43×10^{-4}	1	1.63×10^{-6}	
4	2.00×10^{-3}	0.818	4.09×10^{-6}	
5	1.00×10^{-3}	0.863	3.42×10^{-6}	
6	6.00×10^{-3}	0.671	4.54×10^{-6}	
7	1.00×10^{-3}	0.993	3.64×10^{-6}	
8	3.58×10^{-5}	1	1.13×10^{-6}	
9	8.06×10^{-4}	1	3.20×10^{-6}	
10	3.58×10^{-5}	1	1.33×10^{-6}	
11	9.3×10^{-4}	1	4.89×10^{-6}	
12	7.71×10^{-4}	1	3.97×10^{-6}	
Microzone μ				4.02 %
1	8.60×10^{-4}	1	4.65×10^{-6}	
2	4.00×10^{-3}	0.908	8.12×10^{-6}	
3	2.00×10^{-3}	0.909	5.24×10^{-6}	
4	9.7×10^{-4}	0.933	3.64×10^{-6}	
5	4.66×10^{-4}	1	2.67×10^{-6}	
6	6.00×10^{-2}	0.204	1.01×10^{-5}	
7	3.58×10^{-5}	1	1.23×10^{-6}	
8	1.00×10^{-3}	0.993	7.86×10^{-6}	
9	3.00×10^{-3}	0.952	8.94×10^{-6}	
10	7.17×10^{-5}	1	1.13×10^{-6}	
Microzone ψ				1.59 %
1	0.002036	0.588, 1, 1	1.49×10^{-5}	
2	0.0043	1, 1, 1, 1, 1, 1, 0.527	1.36×10^{-5}	
3	0.00027	1, 0.993	9.9×10^{-6}	
4	0.002	0.841	1.20×10^{-5}	
5	0.002	0.821	6.80×10^{-6}	
Microzone τ				14.26 %
1	0.002	0.954	2.23×10^{-5}	
2	0.001	0.957	1.62×10^{-5}	

In this paper, the DGT–CID technique can reveal the sulfide microniche at an ultra-resolution of 0.042 mm in sediment microzone. However, the peeper method for sulfide image can only achieve the resolution of 1 cm. The sulfide image derived by Teasdale et al. (1999) can only indicate the significant lateral heterogeneity of sulfide in sediment at Conder River estuary (United Kingdom). In this research, the heterogeneous distribution of sulfide microniche at two dimensions

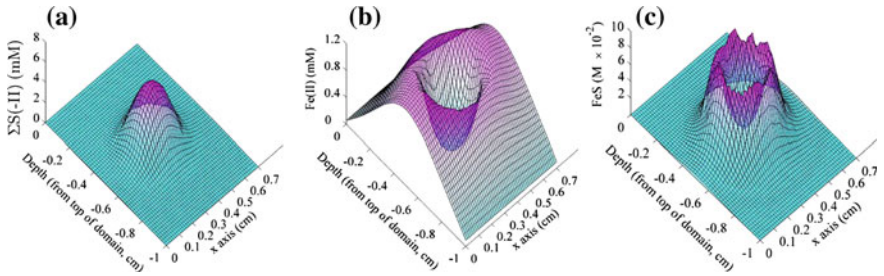

Fig. 5.5 Total sulfide (ΣS(-II)) (**a**), Fe^{2+} (**b**), and FeS (**c**) concentrations across the *x*-axis of the modeled domain after 24 h (y-coordinate was the center of the microniche). The microniche had a porosity of 0.7, an OM degradation rate constant of 9.6×10^{-6} s^{-1}, and an OM concentration of 5 M (representing 21.6 μmol of OM in 14.4 mm^{-3}, volume specific dry mass) (Reprinted from Geochim. Cosmochim. AC, 74: 2665–2676, Stockdale, A., Davison, W., Zhang, H., Formation of iron sulfide at faecal pellets and other microniches within suboxic surface sediment., copyright (2010), with the permission from Elsevier)

(Figs. 5.2 and 5.3) in sediment at Dianchi Lake (China) can be observed by DGT–CID method. The sulfide concentration (Figs. 5.2, 5.3, and 4.4 in Chap. 4) at SWI increased generally from the overlying water down to the deeper in sediments.

The existence of sulfidic microenvironment with distinct concentration peaks (dark hot spots) in some microzones in bulk sediment with sulfide is indicated in Figs. 5.2, 5.3, and 4.7 (Chap. 4). The sulfide hot spots were engendered by the discretely aggregated sulfate-reducing bacteria and the organic matter such as the fecal pellets, which can be assimilated by the bacteria (Widerlund and Davison 2007). The organic material and sulfate-reducing bacteria can be discovered in recently deposited or highly permeable sediments and cretaceous rocks (Devries and Wang 2003). The 2D distribution of the biogeochemistry of sulfur and sulfide metal (Fe, As, Cd, Cu, Hg, Pb, Sb, Zn) in sediment microzones due to biogeochemical reactions, especially Fe around the sulfide microniche peaks (Widerlund and Davison 2007; Stockdale et al. 2010) can be revealed. A similar heterogeneity at two dimensions can possibly exist with concentration and speciation in sediment porewater. Moreover, the ecological risk assessment according to bulk sediment and porewater needs to be improved because of the heterogeneous distribution of sulfide in sediment microzone. The mechanism and model simulation for sulfide microniche have been researched by Stockdale et al. (2010). Figure 5.5 indicates the microniche distribution of total sulfide (ΣS(-II)), Fe^{2+}, and FeS) in sediment porewater.

5.2 The Coupled Fe–S–P Process for P-Release Mechanism in Sediment Microzone

Over thirty years, lake environmental deterioration induced by algae blooms in the water body has been a significant aquatic problem all over the world, and the nutrient cycling attracts the extensive attention worldwide due to its direct effect on

lake eutrophication. The "internal P-loading" and other pollutants from the sediment can continuously engender lake eutrophication after the reduction of "external P-input." Sediment plays an important role in lake eutrophication due to its capacity to absorb or release various pollutants from or into the overlying water. The substance turnover and nutrient exchange across SWI are due to complex physical, chemical, and biological interactions. P, Fe, and sulfur are essential nutrients for living organisms and have an impact on lake eutrophication. P has a significant effect on eutrophication and algae bloom in lake ecosystem. Fe, the redox-sensitive element, plays an important role in the oxidation of organic matter and the formation of phytoplankton bloom during Fe-R process. Soluble sulfide is toxic and influences metal solubility. Moreover, the interactions among the geochemical reaction involving P, S, and Fe can influence their availability and mobility, especially for P-release from sediment. It is well known that P remobilization in sediment is mainly controlled by the reduction of Fe(III) hydroxide and the subsequent P-release from Fe-bound P. Sulfate reduction to S(-II) can control Fe^{2+} solubility in anoxic sediment by the formation of insoluble iron–sulfide precipitates (FeS/FeS_2), which indirectly control P-release and availability. Investigation on the dynamic process among Fe, P, and S is important to reveal their biogeochemical fates and endogenous effect on lake eutrophication. Furthermore, the algae decomposition may have a profound effect on the sediment and water quality, which would consequently influence the ecology and biogeochemical cycling. Roden (1997) suggested an indirect reduction pathway, which attributed P-release from Fe(III) hydroxide to sulfate-reducing bacteria that enhances the formation of soluble FeS.

Until now, the research of the cycling of P, Fe, and S at the SWI has been limited because of the lack of in situ measurement methods for multi-elements at fine scale in sediment layer. Most conventional methods are based on invasive ex situ sampling methods such as the collection of sediment sample from SWI followed by slicing and centrifugation, which can change environmental conditions of sediment and cause large original analytical errors. DGT assembly—a dynamic sampler for sediment based on Fick's first law—can minimize the last problems, such as analyte contamination and analyte speciation change during sampling process and measurement. DGT allows the in situ measurement of multi-solutes at the high spatial resolution, which enables the interpretation of biogeochemical reactions related to P, Fe, and S(-II). DGT has been used for the profile and image of metals, P or S(-II) for the biogeochemical reactions. In order to reveal the coupled Fe–S(-II)–P reaction in sediment, Ding et al. (2012) have used ZrO–AgI-mixing-binding-gel DGT probe for the measurement of 2D images of S(-II) and P at the same locations in Taihu Lake (China), which verified the P-release mechanism mentioned above by the simultaneous appearance of S(-II) and P microniche at the same locations in 2D-images. The images of DGT-S(-II) and DGT-P in this paper are indicated in Fig. 5.6. However, this paper did not conduct DGT-Fe measurement. In Chap. 4, DGT-S(-II) image DGT-Fe- and DGT-P-profiles were determined at same location at sampling sites. DGT concentrations in Fe-, S(-II)- and P-profiles and DGT images of sulfide microniche were compared with each other. At site A, two peaks

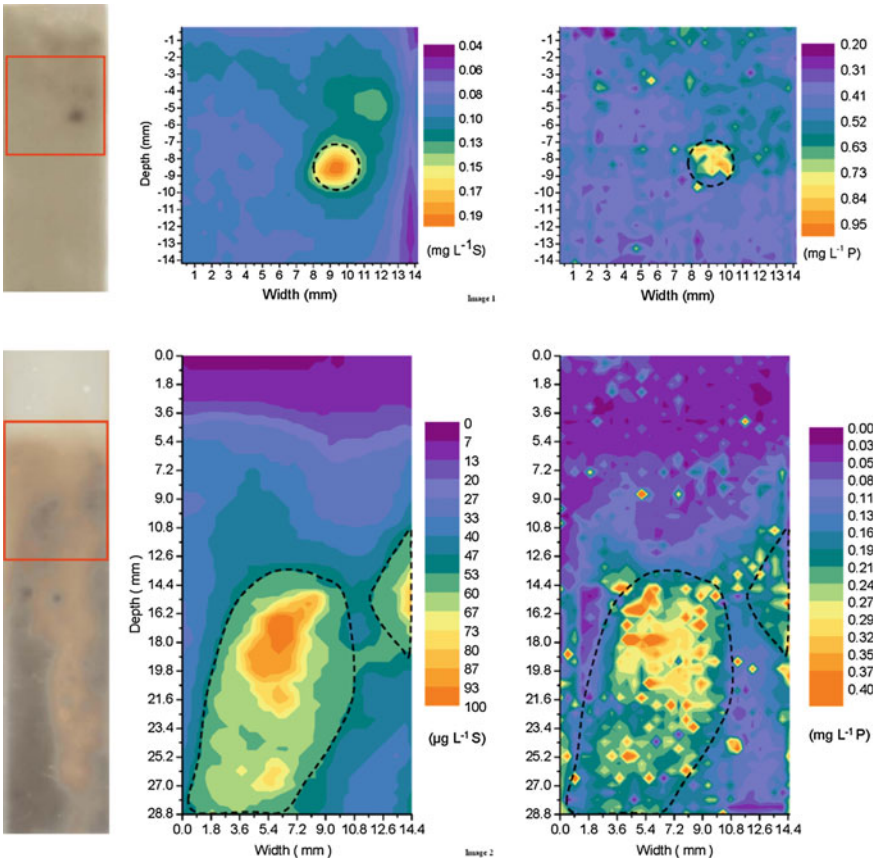

Fig. 5.6 The images of DGT-S(-II) and DGT-P in one reference. Two-dimensional concentration distribution images of the dissolved sulfide and DRP (C_{DGT}) from the in situ deployments of the ZrO–AgI DGT probes in two of the sediment profiles taken in Lake Taihu. The *left* images show color changes on the binding gels after retrieval. The spatial resolutions are 0.169 mm × 0.169 mm and 0.45 mm × 0.45 mm for the images of dissolved sulfide and DRP, respectively (Reprinted (adapted) with the permission from Environ. Sci. Technol., 46: 8297–8304, Ding, S., Sun, M. Q., Xu, D., Jia, F., He, X. A., Zhang, C. S., High-resolution simultaneous measurements of dissolved reactive phosphorus and dissolved sulfide: The first observation of their simultaneous release in sediments, copyright (2007), American Chemical Society)

at −10.50 cm (882 μg L^{-1}) and −11.10 cm (813 μg L^{-1}) of DGT-P-profile were at the same depths of two low Fe values (1033 and 619 μg L^{-1}) in the DGT-Fe-profile, which were corresponded with the microzones of the FeS(s) formation with high sulfide concentrations of 188 μg L^{-1} (−10.50 cm) and 186 μg L^{-1} (−11.10 cm) in the anoxic sediment. The images (Fig. 4.6 in Chap. 4) of the segments at −10.50 and −11.10 cm in sulfide images of AgI gel (0.2 × 1.8 cm) indicated the existence of a large amount of sulfide microniches (Widerlud

and Davison 2007). The mechanisms of P-release at the last two depths at site A were sulfate reduction, the formation of insoluble FeS, and the associated P-release from Fe-bound P (Gachter et al. 2003; Giordani et al. 1996; Ding et al. 2012).

5.3 Summary

In this Chapter, DGT probes with AgI gel were used for determination of dissolved labile sulfide (S (-II)) at SWI in Dianchi Lake (China). The retrieved AgI gel was analyzed for sulfide profile/image with a spatial resolution of 0.042 mm by CID (computer imaging densitometry) technique. DGT-S(-II) profiles at four sites (A, C, F, and G) indicated the sulfate reduction process in anoxic sediment, which was coupled to Fe-R process. Based on S(-II)/P images (in the cited paper: Ding et al. 2012), or Fe/P-profiles and S(-II) image (in this Chapter), the mechanism for the coupled Fe–S(-II)–P geochemical reaction for P-release in sediment microzone can be revealed. Sulfide microniche characters (size, shape, density, and niche peak flux) of S (-II) images were assessed by the parameters derived by ImageJ 1.38e software. The distribution character of microniche zones verified the heterogeneity of sulfide in porewater at vertical/lateral dimensions, caused by the spatially discrete aggregates of sulfate-reducing bacteria and the reactive organic matter (fecal pellets) in anoxic microenvironment. The microniches at four microzones indicated that the localized elevated sulfide formed as a result of the oxidation of reactive organic matter, decaying organisms, algae aggregates, fecal pellets, and the localized pyrite at the edges of the niches. DGT–CID technique should be a valuable method to measure sulfide microniche in sediment microzone for the geochemical research such as sulfate reduction, the formation of FeS(s), and the related P-release due to coupled Fe–S(-II)–P reaction.

References

Devries C, Wang F (2003) In situ two-dimensional high-resolution profiling of sulfide in sediment interstitial waters. Environ Sci Technol 37:792–797

Ding S, Sun MQ, Xu D, Jia F, He XA, Zhang CS (2012) High-resolution simultaneous measurements of dissolved reactive phosphorus and dissolved sulfide: the first observation of their simultaneous release in sediments. Environ Sci Technol 46:8297–8304 (Reprinted (adapted) with permission from Environ Sci Technol, 46:8297–8304, Ding S, Sun MQ, Xu D, Jia F, He XA, Zhang CS, High-resolution simultaneous measurements of dissolved reactive phosphorus and dissolved sulfide: the first observation of their simultaneous release in sediments, copyright (2007) American Chemical Society)

Gachter R, Muller B (2003) Why the phosphorus retention of lakes does not necessarily depend on the oxygen supply to their sediment surface. Limnol Oceanogr 48(2):929–933

Giordani G, Bartoli M, Cattadori M, Viaroli P (1996) Sulphide release from anoxic sediments in relation to iron availability and organic matter recalcitrance and its effects on inorganic phosphorus recycling. Hydrobiologia 329(1–3):211–222

Hamilton-Taylor J, Morris EB (1985) The dynamics of iron and manganese in surface sediments of a seasonally anoxic lake. Archiv Für Hydrobiologie-Supplement 72:135–165

Johnson RG (1974) Particulate matter at the sediment-water interface in coastal environments. J Mar Res 32:313–330

Jørgensen BB (1977) Bacterial sulfate reduction within reduced microniches of oxidized marine-sediments. Mar Biol 41:7–17

Motelica-Heino M, Naylor C, Zhang H, Davison W (2003) Simultaneous release of metals and sulfide in Lacustrine sediment. Environ Sci Technol 37:4374–4381

Roden E, Edmonds JW (1997) Phosphate mobilization in iron-rich anaerobic sediments: microbial Fe(III) oxide reduction versus iron-sulfide formation. Arch Hydrobiol 139(3):347–378

Stockdale A, Davison W, Zhang H (2010) Formation of iron sulfide at faecal pellets and other microniches within suboxic surface sediment. Geochim Cosmochim AC 74:2665–2676 (Reprinted from Geochim Cosmochim AC 74:2665–2676, Stockdale A, Davison W, Zhang H, Formation of iron sulfide at faecal pellets and other microniches within suboxic surface sediment, copyright (2010), with the permission from Elsevier)

Teasdale PR, Hayward S, Davison W (1999) In situ, high-resolution measurement of dissolved sulfide using diffusive gradients in thin films with computer-imaging densitometry. Anal Chem 71:2186–2191

Widerlund A, Davison W (2007) Size and density distribution of sulfide-producing microniches in lake sediments. Environ Sci Technol 41:8044–8049 (Reprinted (adapted) with permission from (Environ Sci Technol 41:8044–8049, Widerlund A, Davison W, Size and density distribution of sulfide-producing microniches in lake sediments), copyright (2007), American Chemical Society)

Chapter 6
The P-release Risk Predicted by Chemical Image of Fe in Sediment Porewater Measured by DGT/LA-ICP-MS and Fe-Microniches

There are only a few papers having reported DGT technique coupled laser ablation ICP-MS for the microzone element analysis. Warnken et al. (2004) have invented microzone metal analysis using suspended particulate reagent iminodiacetate (SPR-IDA) binding gel with particle diameter of 0.2 μm and laser ablation ICP-MS instrument. Santner et al. (2010) have measured P in DGT-binding gel using ferrihydrite gel made by $FeCl_3 \cdot 6H_2O$ and line-scan mode of laser ablation ICP-MS (UP-193-ELAN-DRCe). Gao et al. (2015) reported the simultaneous release of metals (Fe, Mn, Co, and Ni) and sulfide at the same areas in chemical images, which were derived by DGT/laser ablation ICP-MS and DGT-CID techniques. In this chapter, LA-ICP-MS was used to measure SPR-IDA gel. The pretreatment method for DGT gel and ablation mode for LA-ICP-MS analysis have been improved. Based on DGT-Fe image at a submillimeter spatial resolution at SWI of Dianchi Lake derived by the long-time ablation analysis, the distribution character of DGT-Fe-concentration in 2D directions at fine scale was researched. The research result indicated the heterogenous distribution of Fe in sediment porewater and the geochemical reactions for Fe-microniches. Moreover, the quantification method for DGT-Fe-flux, the distribution character of Fe-"hot spots" and Fe-microniches, and the mechanisms for Fe-microniches were assessed, and the release of P and trace metals from Fe-microniches can also be predicted.

6.1 The Measurement Method for Fe at SWI Using SPR-IDA DGT and LA-ICP-MS with High Spatial Resolutions

In recent years, laser ablation inductively coupled plasma mass spectrometry (LA-ICP-MS) has been developed for the quantitative imaging of elements in biological tissues (Seltzer and Berry 2005; Wu et al. 2009) and geological samples

S. Wang and Z. Wu, *DGT-based Measurement of Phosphorus in Sediment Microzones and Rhizospheres*, DOI 10.1007/978-981-10-0721-7_6

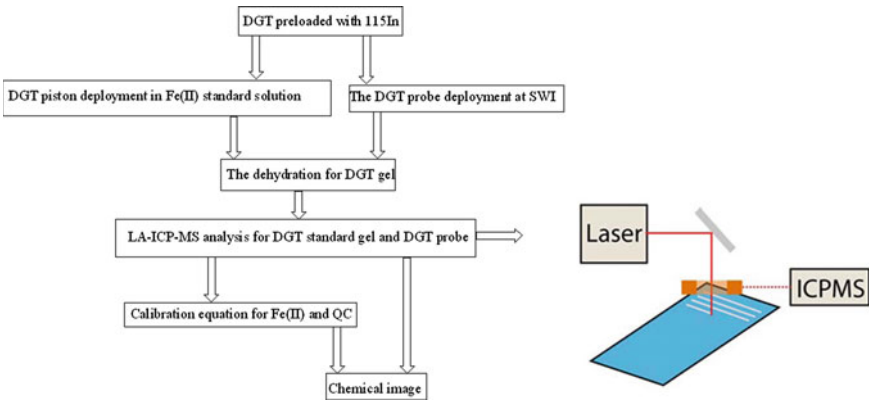

Fig. 6.1 The procedure for the LA-ICP-MS analysis for labile Fe bounded by SRP-IDA gel

(Liu et al. 2008). LA-ICP-MS has the advantages of high sensitivity, high spatial resolution, and ease of sample preparation (Scarpelli et al. 2015). In this chapter, DGT probe with SPR-IDA binding gel was used for the measurement of labile Fe at SWI of Dianchi Lake (China) and the LA-ICP-MS instrument at spatial resolutions (174 × 170 μm) for laser ablation was used for the determination of Fe bound by SPR-IDA gel. The procedure for the LA-ICP-MS analysis for labile Fe bounded by SRP-IDA gel is shown in Fig. 6.1. The objectives of this investigation were to (1) research line-scan method for LA-ICP-MS to measure labile Fe bound by DGT resin, (2) investigate the distribution character of C_{DGT}(Fe) or DGT flux in the Fe-microniches in two dimensions (2D), and (3) research the mechanism for Fe-microniches and the corelease of Fe and P or trace metals in the sediment microzones.

DGT probe with one framework and one open window (1.8 × 15 cm) for SWI and DGT piston with the window diameter (1.8 cm) for standard solutions were used as DGT assemblies. In this research, DGT samples contained one cellulose nitrate filter (0.45 μm pore size and 0.13 mm thickness), one diffusive gel (APA2 type, 5 nm pore size, and 0.39 mm thickness), and one binding layer (SPR-IDA type with the thickness of 0.40 mm), and they were made by DGT Research Ltd. (Lancaster University, UK). The preparation method for SPR-IDA and diffusive gels was recommended by Warnken et al. (2004) and Scally et al. (2006). A stock solution of polyacrylamide comprising 15 vol% acrylamide and 0.3 vol% agarose-based cross-linker (DGTResearch, UK) was used. The diffusive gels were prepared by adding 70 μL of ammonium persulfate 10 % (w/v) initiator and 25 μL of TEMED (*N*,*N*,*N*′,*N*′-tetramethylethylenediamine) catalyst to each 10 mL of stock solution (Scally et al., 2006). The resin gel solution was made by mixing the stock solution with 7 % of suspended iminodiacetate resin (CETAC, Omaha, NE; 0.2 μm bead size). This is referred to as the colloidal resin (Davison et al. 1997). Gels were

hydrated in ultra-pure water (Millipore Milli-Q, known here as MQ) for 24 h to allow them to expand to a stable volume prior to assembling the probes. Suspended particulate reagent iminodiacetate (SPR-IDA) has a bead size of 0.2 μm and a high affinity for many metal cations (Stockdale et al. 2009). Gels that contain homogeneous distributions of binding components can be analyzed at a high resolution by LA-ICP-MS or PIXE (Stockdale et al. 2009).

The Chelex-100 resin beads are too large for chemical image with the resolution of 100 μm. So, the suspended particulate reagent iminodiacetate (SPR-IDA) resin beads (0.2 μm) have been developed to achieve this aim. SPR-IDA has a bead size of 0.2 μm and a high affinity (a permanent sink) for many metal cations (Stockdale et al. 2009; Warnken et al. 2004), which can be used for chemical image at high spatial resolutions. Considering the concentration range (10–4200 μg L^{-1}) in sediment porewater, the binding capacity of the ~1.0 mequiv mL^{-1} (wet SPR-IDA) for this experiment can satisfy this test. DGT assembly with APA2 diffusive gel can measure the labile species (free metal ions, inorganic metal complexes, and small organic metal complexes).

The detailed pretreated method for DGT gel and analysis method for LA-ICP-MS has been introduced in Sect. 3.7 (Chap. 3). This method can be summarized in the flow diagram (Fig. 6.1). The spatial resolutions for laser ablation are 174 × 170 μm. It should be noted that the actual spatial resolution for labile Fe in DGT resin was lower than that of laser ablation due to the lateral diffusion of Fe in the diffusive layer during DGT deployment (Warnken et al. 2006).

Based on the result of LA-ICP-MS analysis and the calculated C_{DGT}(Fe), the C_{DGT}(Fe) distribution image (2D) was acquired through software—Surfer 11 (http://www.golden.com). The lengths (depths) of the whole DGT-Fe image in the overlying water and the sediment were 0.994 and 11.620 cm, in turn. The width of the whole DGT-Fe image was 1.409 cm. Four figures (images) were chosen for the investigation of Fe-release characters in different sediment microzones. In this research, in order to investigate the large C_{DGT}(Fe) more than 1000 μg L^{-1}, which was linked to highly localized Fe-R reaction and Fe-microniches at a scale of 1 mm or submillimeter and was at least 3 times larger than the background values, the term "hot spot" was used to define these spots with C_{DGT}(Fe) > 1000 μg L^{-1} distributed in chemical images. Four figures (Figs. 6.2, 6.3, 6.4, and 6.5) with a lot of "hot spots" were chosen to quantify the localized Fe-microniche flux and the distribution character in sediment microzone. Figure 6.2 (at depths between 0 and −49.98 mm), Fig. 6.3 (at depths between −50.15 and −64.26 mm), Fig. 6.4 (at depths between −84.15 and −99.96 mm), and Fig. 6.5 (at depths between −100.13 and −116.11 mm) indicated 2D distribution of C_{DGT}-Fe in sediment porewater. There were 12 zones in the four images. The vertical 1D C_{DGT}(Fe) profile of the whole DGT probe converted from 2D C_{DGT}(Fe) data is presented in Fig. 6.6. In this chapter, the exact position of one spot in chemical image can be indicated as (x mm, y mm) at horizontal axis (x) and vertical axis (y), i.e., width and length.

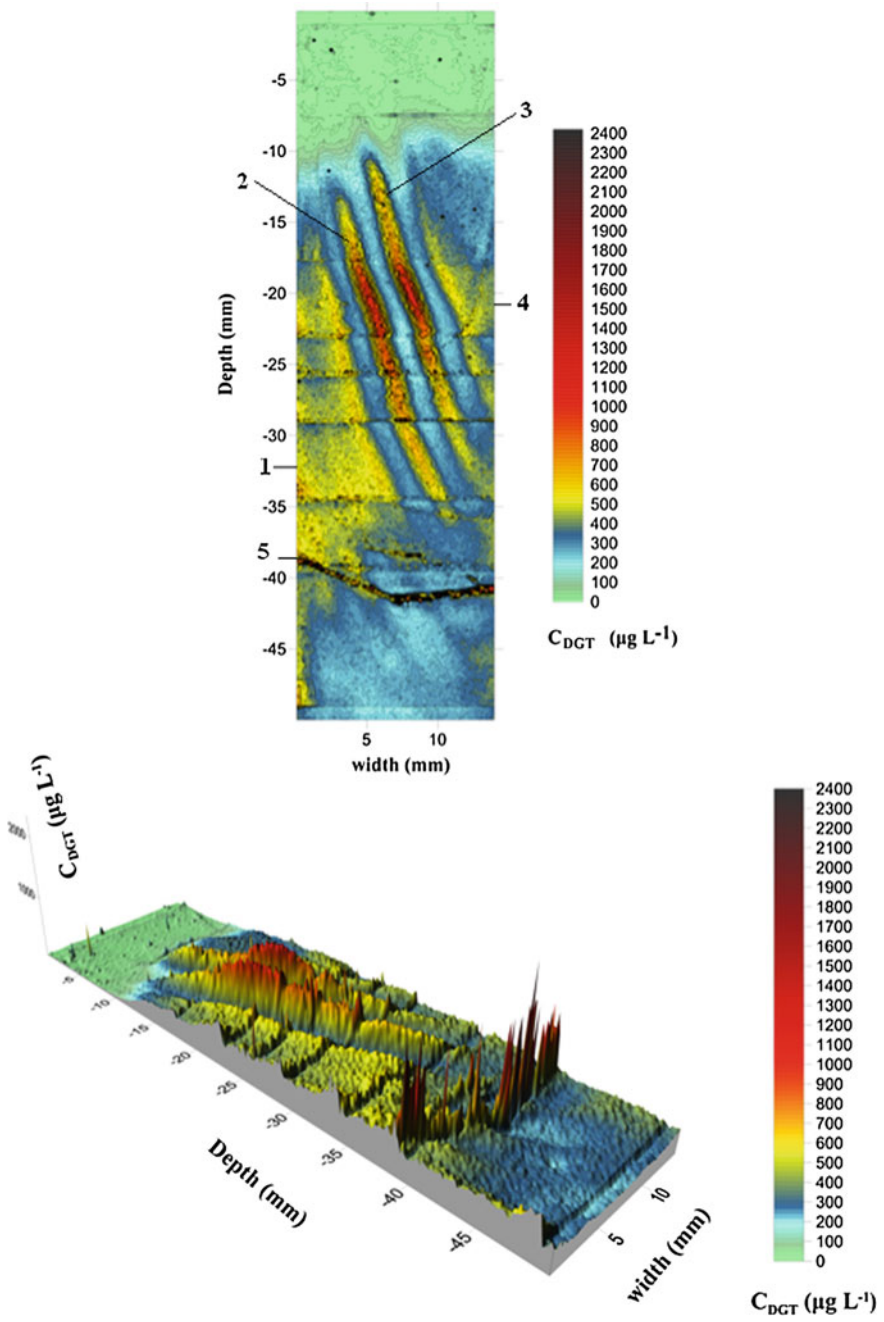

Fig. 6.2 2D images of C_{DGT}(Fe) (at depths between 0 and −49.98 mm) with zones

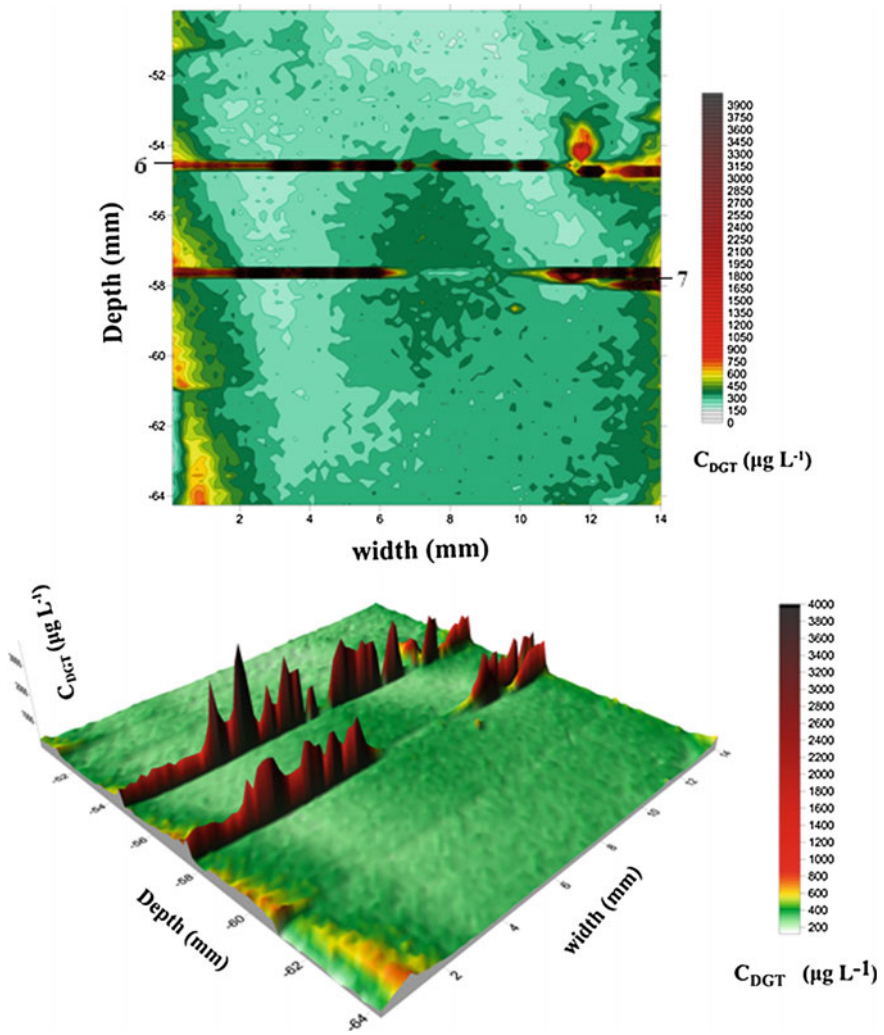

Fig. 6.3 2D images of C_{DGT}(Fe) (at depths between −50.15 and −64.26 mm) with zones (6 and 7)

6.2 DGT-Fe Distribution Character of Chemical Images

Zones (1–12) with a lot of "hot spots" with large C_{DGT}(Fe) values are indicated in Figs. 6.2, 6.3, 6.4, and 6.5. A lot of "hot spots" were distributed in zones (1–5) (Fig. 6.2-image 1). Zones (1 and 4) in yellow color were located at the left and right sides of the middle area, in turn; the rod-shaped zones (2 and 3) in red or yellow color were located in the middle of the image; the band-shaped zone (5) was located at the depth of about -40 mm and traversed image 1 in the horizontal direction.

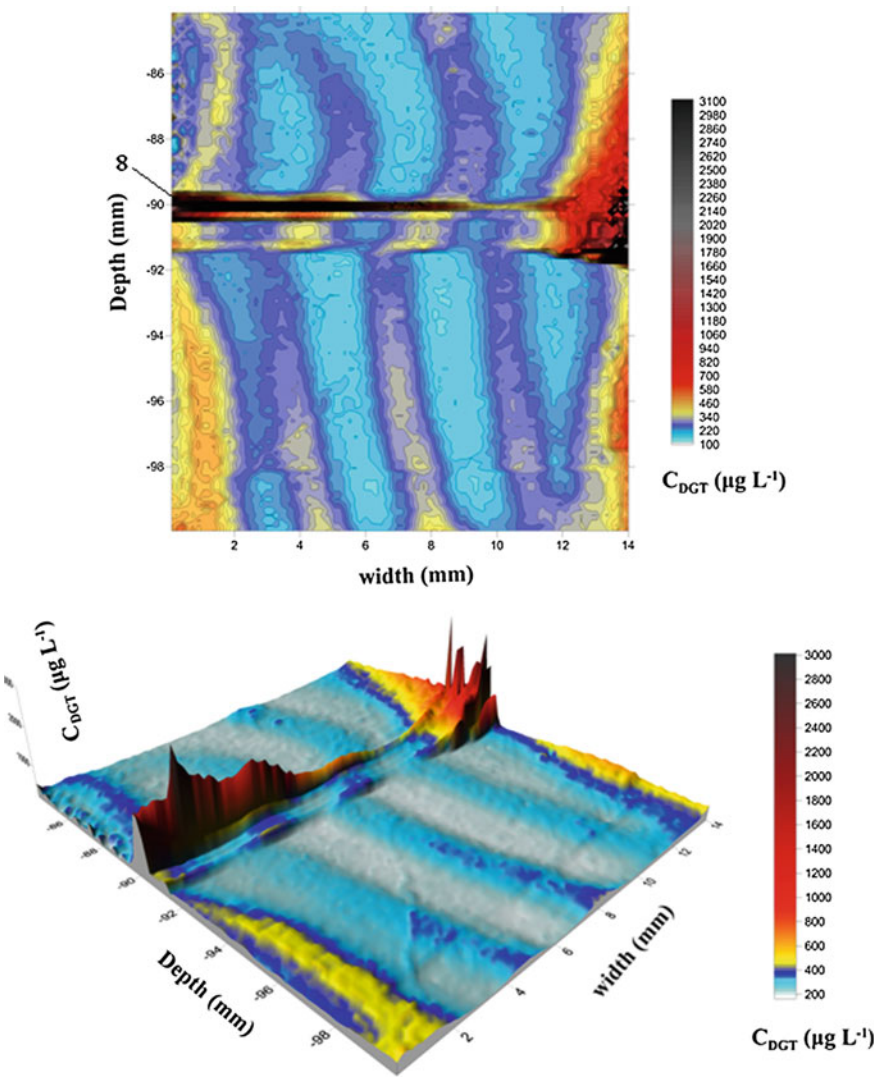

Fig. 6.4 2D images of C_{DGT}(Fe) (at depths between −84.15 and −99.96 mm) with zone 8

Zones (1, 2, 3, and 5) had a lot of C_{DGT}(Fe)-peak over 1000 μg L^{-1}, which are-given in Table 6.1. In this table, zone 1 had one C_{DGT}(Fe) peak with the value of 1229.3 μg L^{-1} at spot (0.26 mm, −26.18 mm), i.e., width and depth. In the following text, the exact position in the image is presented as this format; zone 2 had 26 C_{DGT}(Fe) peaks over 1000 μg L^{-1} with the largest value of 1093.0 μg L^{-1} (5.13 mm, −20.23 mm); zone 3 had 27 C_{DGT}(Fe) peaks over 1000 μg L^{-1} with the largest value of 1085.4 μg L^{-1} (7.74 mm, −19.38 mm); zone 5 had 39 C_{DGT}(Fe)

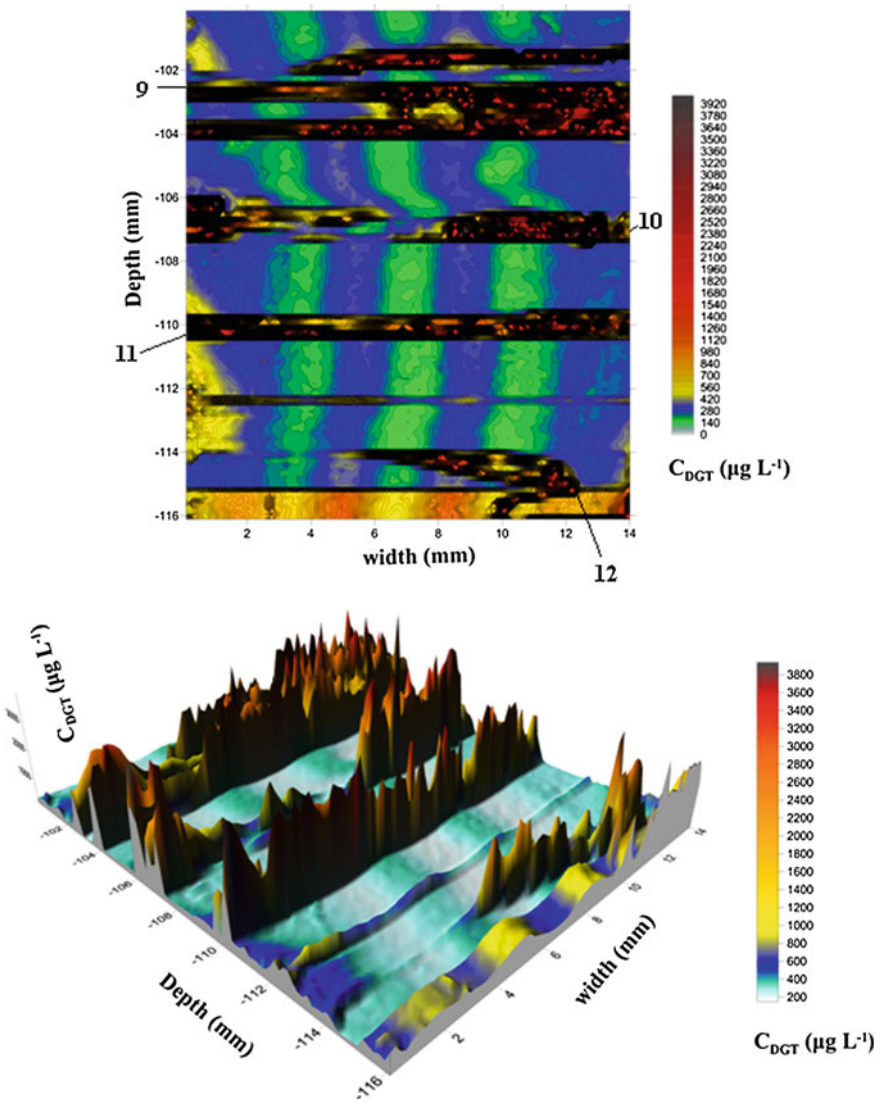

Fig. 6.5 2D images of C_{DGT}(Fe) (at depths between −100.13 and −116.11 mm) with zones (9–12)

peaks over 1000 μg L^{-1} with the largest value of 2341.4 μg L^{-1} (9.31 mm, −41.48 mm). Zone 4 had large C_{DGT}(Fe) values more than 500.0 μg L^{-1}, but those values did not exceed 800.0 μg L^{-1}. The largest value of 2341.4 μg L^{-1} (9.31 mm, −41.48 mm) in Fig. 6.2 was 10 times as much as the background value (230.0 μg L^{-1}) near this peak. Under the five zones (1–5) in vertical direction in Fig. 6.2, C_{DGT}(Fe) decreased until the end of this image.

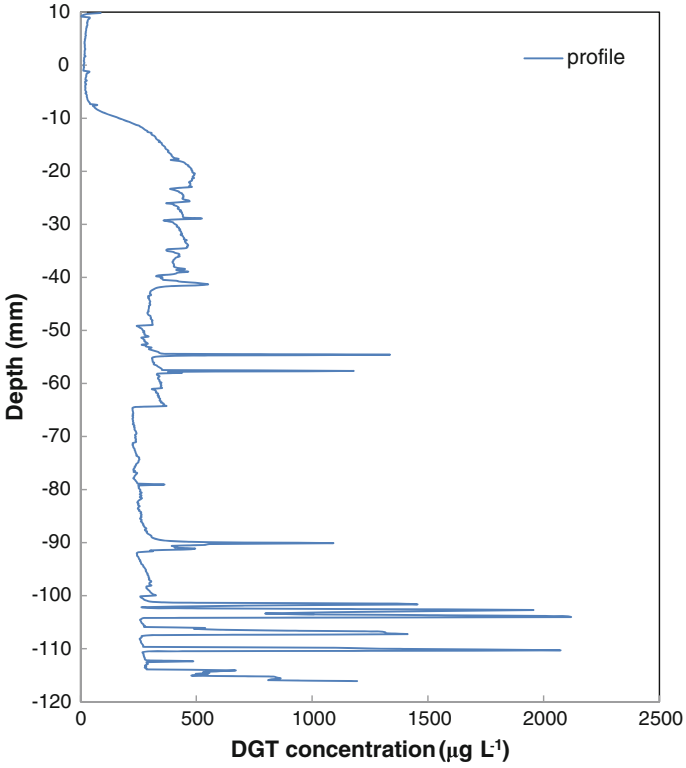

Fig. 6.6 1D DGT-Fe profile in vertical direction at SWI

In image 2 (Fig. 6.3), two zones (6 and 7) in red or black color were distributed in this image. Two band-shaped zones (6 and 7) with the large C_{DGT}(Fe) values were at the depths of about −54.50 and −57.50 mm, in turn, and they both traversed image 2 in the horizontal direction. Zone 6 had 56 C_{DGT}(Fe) peaks over 1000 μg L^{-1}, with the maximum value of 3897.3 μg L^{-1} (4.26 mm, −54.57 mm). In zone 6, there were 3 values over 3000 μg L^{-1}, 19 values between 2000 and 3000 μg L^{-1}, and 34 values between 1000 and 2000 μg L^{-1}. Zone 7 had 60 C_{DGT}(Fe) peaks over 1000 μg L^{-1}, with the maximum value of 2196.4 μg L^{-1} (2.70 mm, −57.63 mm). In zone 7, there were 9 values between 2000 and 3000 μg L^{-1} and 51 values between 1000 and 2000 μg L^{-1}.

In image 3 (Fig. 6.4), the average C_{DGT}(Fe) was 308.7 μg L^{-1}. One band-shaped zone (8) in red or black color with "hot spots" traversed the image in horizontal direction at the depth of about -90.0 mm. Zone 8 had 92 C_{DGT}(Fe) peaks over 1000 μg L^{-1}, with the maximum value of 3012.7 μg L^{-1} (13.83 mm, −89.59 mm). There were 1 value over 3000.0 μg L^{-1}, 9 values between 2000.0 and 3000.0 μg L^{-1}, and 82 values between 1000.0 and 2000.0 μg L^{-1}. There were four bar-shaped zones with the low C_{DGT}(Fe) (<220.0 μg L^{-1}) in vertical direction throughout

image 3. There were also some large values more than 400.0 μg L^{-1} on the left and right bottom of the image.

In image 4 (Fig. 6.5), the average C_{DGT}(Fe) of the whole image was 669.7 μg L^{-1}. Three band-shaped zones (9–11) and one irregular-shaped zone (12) in red or black color and with a lot of "hot spots" traversed image 4 in horizontal direction. Zone 9 was located at the depths between −100.13 and −104.55 mm with the largest value of 3862.8 μg L^{-1} (13.66 mm, −103.7 mm). Zone 9 had 512 C_{DGT}(Fe) peaks over 1000.0 μg L^{-1}, and among those values, there were 40 values over 3000.0 μg L^{-1}, 196 values between 2000.0 and 3000.0 μg L^{-1}, and 276 values between 1000.0 and 2000.0 μg L^{-1}. Zone 10 was located at the depths between −105.74 mm and −107.61 mm with the largest value of 3936.0 μg L^{-1} (0.26 mm, −106.08 mm). Zone 10 had 201 C_{DGT}(Fe) peaks over 1000.0 μg L^{-1}, and among those values, there were 31 values over 3000.0 μg L^{-1}, 99 values between 2000.0 and 3000.0 μg L^{-1}, and 71 values between 1000.0 and 2000.0 μg L^{-1}. Zone 11 was located at the depths between −109.31 and −110.67 mm with the largest value of 3922.2 μg L^{-1} (4.96 mm, −110.33 mm). Zone 11 had 275 C_{DGT}(Fe) peaks over 1000.0 μg L^{-1}, and among those values, there were 33 values over 3000.0 μg L^{-1}, 91 values between 2000.0 and 3000.0 μg L^{-1}, and 151 values between 1000.0 and 2000.0 μg L^{-1}. Zone 12 was located at the depths between −113.56 and −116.11 mm with the largest value of 3773.3 μg L^{-1} (11.57 mm, −114.58 mm). Zone 12 had 188 C_{DGT}(Fe) peaks over 1000.0 μg L^{-1}, and among those values, there were 4 values over 3000.0 μg L^{-1}, 39 values between 2000.0 and 3000.0 μg L^{-1}, and 145 values between 1000.0 and 2000.0 μg L^{-1}.

The sequence of the average C_{DGT}(Fe) value in 4 images (Figs. 6.2, 6.3, 6.4, and 6.5) was as follows: Fig. 6.5 (609.8 μg L^{-1}) > Fig. 6.3 (347.3 μg L^{-1}) > Fig. 6.2 (315.9 μg L^{-1}) > Fig. 6.4 (308.7 μg L^{-1}). The largest C_{DGT}(Fe) in the whole image is 3936.0 μg L^{-1} (0.26 mm, −106.08 mm).

The classification of the large C_{DGT}(Fe) (>1000 μg L^{-1}) in 11 zones is given in Table 6.1. The large C_{DGT}(Fe) values in zones (1–12) (Figs. 6.2, 6.3, 6.4, and 6.5) engendered the C_{DGT}(Fe) peaks in the 1D DGT profile, as follows: −20.40 mm (493.7 μg L^{-1}), −25.67 mm (470.5 μg L^{-1}), −28.90 mm (523.8 μg L^{-1}), −34.00 mm (464.6 μg L^{-1}), −38.93 mm (465.2 μg L^{-1}), −41.31 mm (551.3 μg L^{-1}), −54.57 mm (1336.6 μg L^{-1}), −57.63 mm (1179.6 μg L^{-1}), −90.10 mm (1092.1 μg L^{-1}), −101.66 mm (1450.3 μg L^{-1}), −102.68 mm (1930.1 μg L^{-1}), −104.04 mm (2116.9 μg L^{-1}), −107.27 mm (1404.1 μg L^{-1}), −110.33 mm (2039.9 μg L^{-1}), and −116.11 mm (1194.6 μg L^{-1}).

Particularly in image 4, there were 1176 values more than 1000.0 μg L^{-1} in 4 zones, engendering large peaks at depths between −100.13 and −116.11 mm in 1D DGT profile (Fig. 6.6). Figures 6.2, 6.3, 6.4, and 6.5 and Table 6.1 show the heterogenous distribution at two dimensions of labile Fe, and the "hot spots" engendered the large peaks in 1D profile (Fig. 6.6). The Fe-peaks and subpeaks of sediment porewater in 1D C_{DGT}-Fe profile (Fig. 6.6) and Fe-microniches in 2D DGT-Fe images (Figs. 6.2, 6.3, 6.4, and 6.5) reflected the intensive Fe-remobilization and Fe-R reactions in those zones.

Table 6.1 The large C_{DGT}(Fe) values over 1000 μg L^{-1} and the "contribution" of the large C_{DGT}(Fe)/flux (Fe) over 1000 μg L^{-1}/9.36 × 10^{-5} μg cm^{-2} s^{-1} in images

Image	Peak zone	Peak number				$\sum J \times A$	Contribution
		>1000 μg L^{-1}	2000–3000 μg L^{-1}	>3000 μg L^{-1}	1000–2000 μg L^{-1}	ng s^{-1}	%
1	1	1	0	0	1		
	2	26	0	0	26		
	3	27	0	0	27		
	5	39	1	0	38		
						3.059×10^{-3}	1.47
2	6	56	19	3	34		
	7	60	9	0	51		
						5.415×10^{-3}	8.27
3	8	92	9	1	82		
						3.775×10^{-3}	5.80
4	9	512	196	40	276		
	10	201	99	31	71		
	11	275	91	33	151		
	12	188	39	4	145		
						6.449×10^{-2}	49.62

6.3 The Proportion of DGT Flux Related to Fe-Microniche in "Hot Spots" of the Total DGT Flux in Microzone and the Implication

C_{DGT}-Fe zones (1–3 and 5–12) in Figs. 6.2, 6.3, 6.4, and 6.5 and C_{DGT}-Fe profile (Fig. 6.6) indicated large DGT concentrations (>1000.0 μg L^{-1}) focused on some microniches in sediment.

In order to evaluate the ratio between DGT flux (>9.36 × 10^{-5} μg cm^{-2} s^{-1}) corresponded with DGT concentration (>1000.0 μg L^{-1}) in n "hot spots" in images (1–4) and the total horizontal flux in the whole image, Eq. (6.1) was used to assess the parameter "contribution."

$$\text{Contribution} = \frac{\sum_{i=1}^{n} J_i^{\text{peak}} \times A_i^{\text{peak}}}{A_T \times J^{\text{ave}}} \tag{6.1}$$

where J_i^{peak} (μg cm^{-2} s^{-1}) is the peak flux of labile Fe for peak i; J^{ave} (μg cm^{-2} s^{-1}) is the average flux of the selected SPR-IDA gel; A_i^{peak} (cm^2) is the peak area for peak i; A_T (cm^2) is the total area of the studied SPR-IDA gel zone. This calculation method to quantify the ratio of Fe-microniche flux is similar with the other method

for the calculation of the proportion of sulfide microniche flux introduced in one reference (Widerlund and Davison 2007).

In order to derive the "contribution" value in zones (1–3 and 5–12) in Figs. 6.2, 6.3, 6.4, and 6.5, the DGT fluxes over 9.36×10^{-5} μg cm^{-2} s^{-1} (1000.0 μg L^{-1}) corresponded with microniche areas in the images were checked and derived with the aid of the softwares (Surfer 11 and Excel 2007). The total areas of those microniche peaks and the DGT-peak-flux values were used to calculate $A_T \times J^{ave}$. Similarly, the average flux of the selected SPR-IDA gel (and the total area of the studied gel zone (A_T)) was also calculated. The "contribution" of the large peak values over 1000.0 μg L^{-1} (>9.36×10^{-5} μg cm^{-2} s^{-1}) distributed in images (1–4) is shown in Table 6.1. The proportion of DGT-Fe fluxes over 9.36×10^{-5} μg cm^{-2} s^{-1} (1000.0 μg L^{-1}) related to Fe-microniche peaks of the total DGT-Fe flux in the corresponded microzone area (images 1–4) varied between 1.47 and 49.62 %. These values of "contribution" and large C_{DGT}-Fe in images (1–4) indicated the existence of Fe-microniches with the localized intense Fe-R reaction in anoxic sediment layers. The DGT measurement is usually lower than the real concentration in porewater because of the depletion of porewater concentration and the supply of Fe from solid phase, as liable Fe is removed by DGT device. However, the Fe-microniche flux can be observed by DGT image, and the main reason for the existent of Fe-microniches is the localized Fe-remobilization with intense flux in anoxic sediment microzone, which can be indicated as Eq. (6.2) (Stockdale et al. 2010).

$$4\mathrm{FeOOH} + \mathrm{OM} + 8\mathrm{H}^+ \longrightarrow \mathrm{K_{OM}}\Sigma\mathrm{CO_2}^{2-} + 0.1\mathrm{NH_4}^+ + 4\mathrm{Fe}^{2+} + 7\mathrm{H_2O} \quad (6.2)$$

The schematic graph of Fe-microniches related to Fe-flux is indicated in Fig. 6.7. Two microniche zones (a and b) selected from Fig. 6.2 were indicated as the areas of niche peaks, the edge of niche, and the background area. The DGT-Fe flux related to Fe-microniches indicated this Fe-reduction process. However, at the edge of Fe-microniches, DGT fluxes were depleted (Fig. 6.7). The dynamics of labile Fe and the formation of Fe-microniches are also controlled by the efficiency of Fe sinks, such as the availability of dissolved Fe and the precipitation of FeS. The AVS (acid-volatile sulfide) content in the sediment is indicated in Table 3.7 (Chap. 3). Most divalent metals form insoluble sulfides, such as pyrite, gregite, and amorphous Fe-monosulfide, which can immobilize the metals by transferring them to the sediment solid phase (Huerta-Diaz et al. 1998; Morse and Luther 1999). The low C_{DGT}-Fe values at the edge of Fe-microniches (Fig. 6.7) are due to the removal of Fe from solution by the precipitation of FeS (Motelica-Heino et al. 2003). Without the rapid removal process, the diffusion of Fe from closely spaced microniche sources could raise the general background concentration and diminish peak value.

In Fig. 6.8, sites (H, I, J, and K) with the low C_{DGT}-Fe values (no more than 280.0 μg L^{-1}) were adjacent to a lot of Fe-microniches with large C_{DGT}-Fe values (>1000.0 μg L^{-1}). The precipitation of FeS around Fe-microniches removed labile Fe from porewater and depleted the C_{DGT}-Fe values in those sites at the edge of

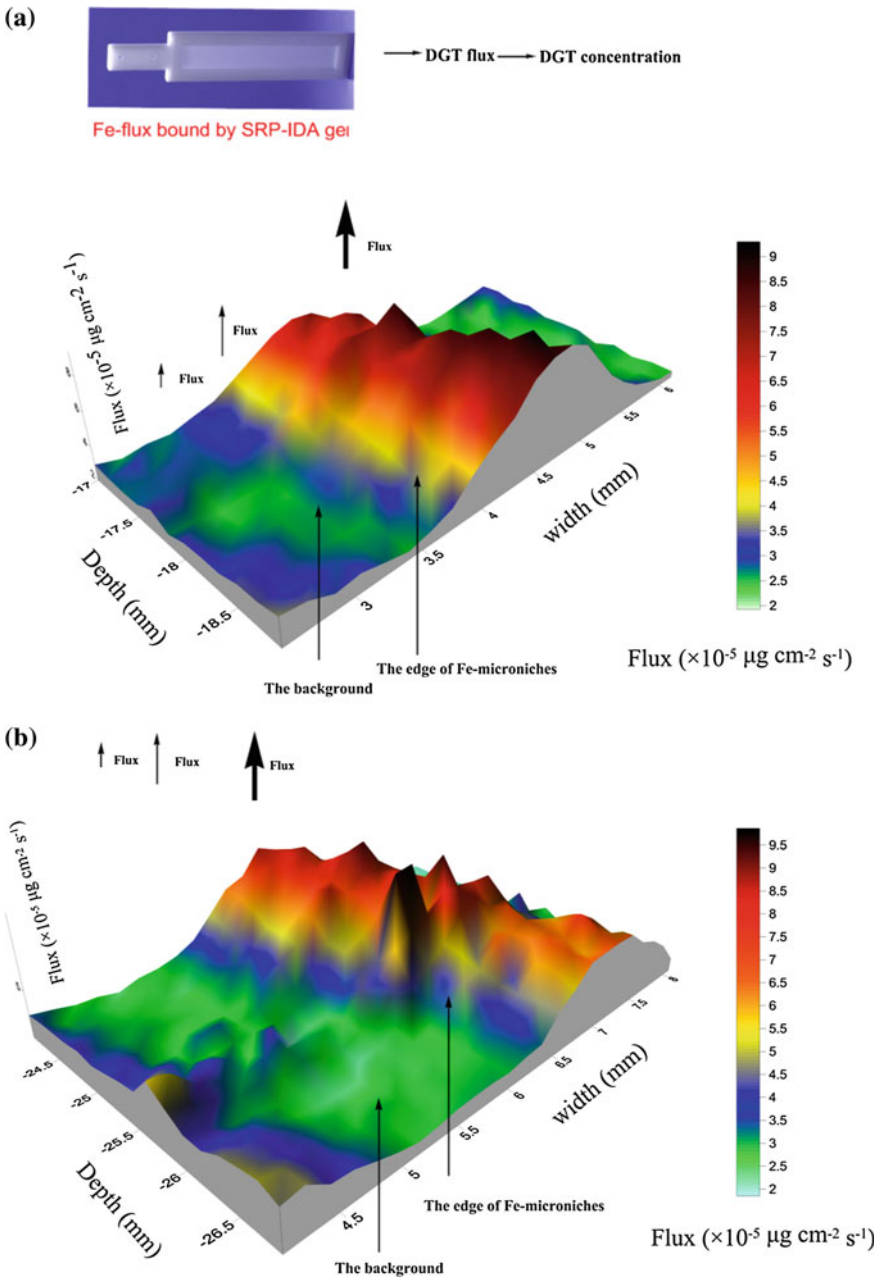

Fig. 6.7 The schematic graph of two Fe-microniche zones (**a** and **b**) related to Fe-flux, which was selected from zone 2 in Fig. 6.2 and converted to DGT flux

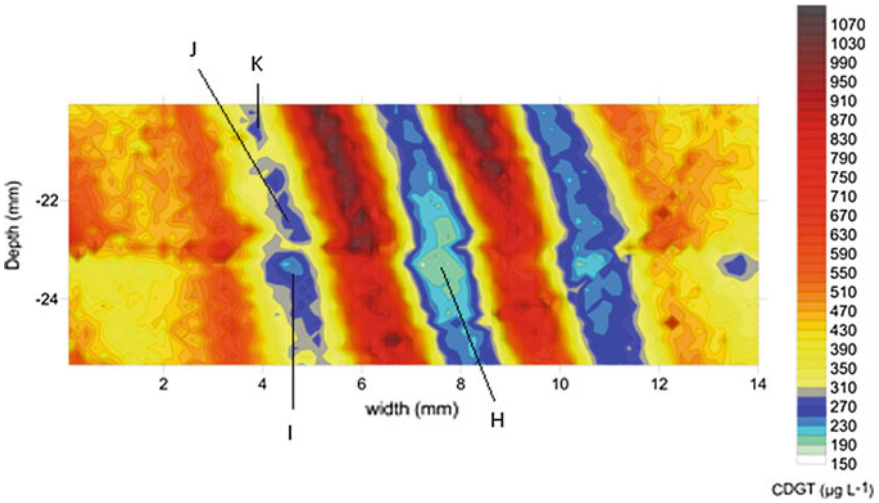

Fig. 6.8 The sites "H," "I," "J," and "K" in image 1 (Fig. 6.2) with low Fe values surrounded by large Fe-"hot spots"

Fe-microniches. Moreover, according to the 3D reaction-transport model for the formation of iron sulfide at fecal pellets and other microniches (Stockdale et al. 2010), sulfide microniches may exist in these sites (H, I, J, and K).

6.4 The Release of P and Trace Metals Predicted by Fe-Microniches

Anoxic conditions promote the reduction of insoluble FeOOH minerals to soluble Fe (II) resulting in the P-release from the surfaces and into the surrounding water (Böstrom and Pettersson 1982; Christophoridis and Fytianos 2006). In Chap. 4, the reduction of Fe oxide and P-release from Fe-bound P in anoxic sediment are the main mechanisms for P-release and "internal P-loading" of Dianchi Lake. In the research sites (sites A–G) near the sampling site (site H) for DGT/LA-ICP-MS measurement, the simultaneous release of Fe and P in sediment zone can engender many large C_{DGT}(Fe) values more than 1000 μg L^{-1} and C_{DGT}(P) over 200 μg L^{-1} at same depths in 1D DGT profiles (Fig. 4.3). According to Sect. 6.2, there were a lot of "hot spots" with large C_{DGT}(Fe) at zones (1–3 and 5–12) (Figs. 6.2, 6.3, 6.4, and 6.5 and Table 6.1), especially at zones (9–12) with many large Fe-peaks. Based on these large C_{DGT}(Fe) values in "hot spots" and abundant P-fractions in sediments (Table 3.8 in Chap. 3), P-release from Fe-bound P in sediment microzones can be predicted.

In anoxic sediments, the conversion of solid phase Fe to the reduced and dissolved forms of Fe^{2+} may liberate other trace metals absorbed or bound (Tessier

1992; Zhang et al. 1995; Wu et al. 2011, 2014). In one DGT research (Wu et al. 2015), the simultaneous release of Fe, Zn, Co, Cu, Cd, and Al in sediment porewater of Dianchi Lake (sites A-E) near the sampling site (site H) for DGT-Fe images was observed, and the good linear correlation in DGT profiles (Fe and trace metals) was obtained. So, in this DGT/LA-ICP-MS research, the large C_{DGT}(Fe) values in microzones with "hot spots" (Figs. 6.2, 6.3, 6.4, and 6.5 and Table 6.1) can engender the corelease of Fe and trace metals.

6.5 Summary

In this Chapter, DGT gel (SRP-IDA resin) and LA-ICP-MS instrument for the measurement of labile Fe at submillimeter spatial resolution in sediment porewater were researched and reported. Based the on chemical images of DGT-Fe, the heterogeneous distribution of DGT-Fe concentration at two dimensions is investigated. Fe-microniches related to highly localized Fe-R reaction at mm or submillimeter scale in anoxic sediment are revealed in sediment microzones. There are 902 C_{DGT}(Fe) values between 1000 and 2000 μg L^{-1}, 463 values between 2000 and 3000 μg L^{-1}, and 112 values over 3000 μg L^{-1} in the studied microzones caused by Fe-remobilization flux from "hot spots," i.e., Fe-flux related to Fe-microniche peaks. These "hot spots" in sediment microzones engendered large peaks at the same depths in the vertical 1D profile of C_{DGT}(Fe). The proportions of the large DGT-Fe fluxes (>9.36 × 10^{-5} μg cm^{-2} s^{-1}) related to Fe-microniche peaks in the studied microzones were in the range of 1.47–49.62 % of the total flux measured in the same image zones, which were due to the local source of the readily reactive Fe oxide and the dynamic biogeochemical reactions occurring at those microniches. The Fe-microniches may also engender the corelease of Fe and P or trace metals. The mechanisms for Fe-microniches were mainly due to the localized supply of labile Fe from solid phase and the precipitation of FeS at the edge of Fe-microniches. As the dynamics of the biogeochemical processes occurring at Fe-microniches is the key to improve our understanding of early diagenesis, 3D reaction-transport models should be developed to understand the complex reactions related to the rate constants of organic matter degradation, the formation of FeS and Fe-R process, P-release risk from Fe-microniche, sediment porosity, and niche lifetime.

In Part II (Chaps. 4–6), the P-release mechanism and kinetic P-release at SWI of Dianchi Lake were discussed. The DGT profiles of P/Fe/S(-II) at SWI indicated the main mechanism of P-remobilization from Fe-bound P during Fe-R process. The minor P-release mechanisms were due to the decomposition of algae biomass at the uppermost sediment and the coupled Fe–S–P geochemical reaction. The latter mechanism can be verified by the sulfide microniches in two segments of one DGT-S(-II) image and the corresponded DGT-P and -Fe concentrations at the same depths in sediment profile. 1D-DIFS model for P has revealed the R, T_C, and K_d values and how DGT parameters determine DGT curves of R and dissolved

concentration versus time/distance. DGT-S(-II) image at submillimeter scale indicates the distribution character of sulfide microniche, and the mechanisms were discussed in detail. DGT-Fe image at submillimeter scale was also derived by microchelex gel/LA-ICP-MS. The existence of Fe-microniche in sediment microzone was verified, and Fe-niche flux related to Fe-microniche peak was evaluated. The formation mechanisms of Fe-microniche were due to the localized Fe-remobilization with the intense flux in anoxic sediment microzone and the removal of Fe from solution by the precipitation of FeS at the edge of Fe-microniche. The Fe-microniche in sediment microzone can also be used to predict the release risk of P and trace metals. Moreover, the "internal P-loading" in Dianchi Lake was also quantified by DGT method. The above research results in this section indicate that DGT technique with multi-functions is a powerful tool for the measurement of P and related elements in sediment microzone and assessment of the mechanism of "internal P-loading."

References

Böstrom B, Pettersson K (1982) Different patterns of phosphorus release from lake-sediments in laboratory experiments. Hydrobiologia 91–2:415–429

Christophoridis C, Fytianos K (2006) Conditions affecting the release of phosphorus from surface lake sediments. J Environ Qual 35(4):1181–1192

Davison W, Fones GR, Grime GW (1997) Dissolved metals in surface sediment and a microbial mat at 100 um resolution. Nature 387(6636):885–888

Gao Y, van de Velde S, Williams PN, Baeyens W, Zhang H (2015) Two-dimensional images of dissolved sulfide and metals in anoxic sediments by a novel diffusive gradients in thin film probe and optical scanning techniques. Trac-Trend Anal Chem 66:63–71

Huerta-Diaz MA, Tesssier A, Carignan R (1998) Geochemical of trace metals associated with reduced sulfur in freshwater sediments. Appl Geochem 13:213–233

Liu YS, Hu ZC, Gao S, Günther D, Xu J, Gao CG, Chen HH (2008) In situ analysis of major and trace elements of anhydrous minerals by LA-ICP-MS without applying an internal standard. Chem Geol 257:34–43

Morse JW, Luther GW III (1999) Chemical influences on trace metal-sulfide interactions in anoxic sediments. Geochim Cosmochim Acta 63:3373–3378

Motelica-Heino M, Naylor C, Zhang H, Davison W (2003) Simultaneous release of metals and sulfide in Lacustrine sediment. Environ Sci Technol 37:4374–4381

Santner J, Prohaska T, Luo J, Zhang H (2010) Ferrihydrite containing gel for chemical imaging of labile phosphate species in sediments and soils using diffusive gradients in thin films. Anal Chem 82:7668–7674

Seltzer MD, Berry KH (2005) Laser ablation ICP-MS profiling and semiquantitative determination of trace element concentrations in desert tortoise shells: documenting the uptake of elemental toxicants. Sci Total Environ 339:253–265

Scally S, Davison W, Zhang H (2006) Diffusion coefficients of metals and metal complexes in hydrogels used in diffusive gradients in thin films. Anal Chem Acta 558:222–229

Scarpelli R, De Francesco AM, Gaeta M, Cottica D, Toniolo L (2015) The provenance of the Pompeii cooking wares: insights from LA-ICP-MS trace element analyses. Microchem J 119:93–101

Stockdale A, Davison W, Zhang H (2009) Micro-scale biogeochemical heterogeneity in sediments: a review of available technology and observed evidence. Earth-Sci Rev 92:81–97

Stockdale A, Davison W, Zhang H (2010) Formation of iron sulfide at faecal pellets and other microniches within suboxic surface sediment. Geochim Cosmochim Acta 74:2665–2676

Tessier A (1992) Sorption of trace elements on natural particles in oxic environments: environmental Particles. In: Buffle J, van Leeuwen HP (eds) Lewis, pp 425–453

Warnken KW, Zhang H, Davison W (2004) Analysis of polyacrylamide gels for trace metals using diffusive gradients in thin films and laser ablation inductively coupled plasma mass spectrometry. Anal Chem 76:6077–6084

Warnken KW, Zhang H, Davison W (2006) Accuracy of the diffusive gradients in thin-films technique: diffusive boundary layer and effective sampling area considerations. Anal Chem 78 (11):3780–3787

Widerlund A, Davison W (2007) Size and density distribution of sulfide-producing microniches in lake sediments. Environ Sci Technol 41:8044–8049

Wu B, Zoriy M, Chen YX, Becker JS (2009) Imaging of nutrient elements in the leaves of *Elsholtzia splendens* by laser ablation inductively coupled plasma mass spectrometry (LA-ICP-MS). Talanta 78:132–137

Wu ZH, He MC, Lin CY (2011) In situ measurements of concentrations of Cd Co, Fe and Mn in estuarine porewater using DGT. Environ Pollut 159:1123–1128

Wu ZH, Wang SR, Jiao LX, Wu FC (2014) The Simultaneous measurement of phosphorus, sulfide, and trace metals by ferrihydrite/AgI/chelex-100 DGT (diffusive gradients in thin films) probe at sediment/water interface (SWI) and remobilization assessment. Water Air Soil Pollut 225:2188–2194

Wu ZH, Wang SR, Jiao LX (2015) Geochemical behavior of metals-sulfide-phosphorus at SWI (sediment/water interface) assessed by DGT (Diffusive gradients in thin films) probes. J Geochem Explor 156:145–152

Zhang H, Davison W, Miller S, Tych W (1995) In situ high-resolution measurements of fluxes of Ni, Cu, Fe, and Mn and concentrations of Zn and Cd in porewaters by DGT. Geochim Cosmochim Acta 59:4181–4192

Part III
The P-behavior at the Interface of Sediment/Root of Aquatic Plants (Erhai Lake)

Chapter 7
The Uptake and Accumulation Mechanisms of P-Predicted by In Situ DGT Test at the Rhizosphere of Aquatic Plant

Aquatic plant can absorb N and P in water body by root and plays a key role in ecological restoration of lake eutrophication. On the other hand, the rhizosphere provides the necessary location and the good environmental condition for the survival of microorganisms and pollution degradation. *Zizania latifolia* is one kind of the emerged plant in lake, marsh, and river in South China. Some researchers have found that *Z. latifolia* can absorb N and P by root intensively. *Z. latifolia* can remove N and P on the premise of regular harvest. It can also recover vegetational community and improve biodiversity in waterbody. Submerged macrophyte-*Myriophyllum verticillatum* in China can act as an ecotone horizontally between land and water and vertically between sediments and the overlying water. Thus, this "underwater forest" can play an important role in nutrient cycling, especially in shallow lakes (Qiu et al. 2001). It is reported that the water quality can be significantly improved by reconstructing macrophytes (Blindow et al. 1993; Barko et al. 1991). The rhizosphere environment of aquatic plants is important for the interaction between sediment and plant, and P-removal. Plant root can influence the chemical condition in surrounding sediment solution, which is important for the P-transfer at the plant/porewater/sediment interface.

DGT technique has been used for the investigation of the dynamic process or bioavailability of elements in water, soil, or sediment. DGT resin can absorb element mass from sediment solution, and the resupply mass of element from sediment particle into porewater can be induced by the depletion of porewater concentration. The DGT can mimic element taken up by plant root, and DGT flux is determined by the element concentration in porewater, the diffusion rate, the resupply from complexes, the labile element-pool in sediment, and the release rate from sediment particle. The resupply ability of sediment is influenced by the content of element

S. Wang and Z. Wu, *DGT-based Measurement of Phosphorus in Sediment Microzones and Rhizospheres*, DOI 10.1007/978-981-10-0721-7_7

bound in sediment and the rate of desorption. DGT measurement involves embrace both element concentration in porewater and the capacity/kinetic exchange of sediment solid. When the uptake by root belongs to "diffusion limitation" type, DGT-measured parameters can generally correlate well with element content in plant tissues. However, there is no DGT measurement in rhizosphere of aquatic plants and the DGT method for the prediction of P-content in plant tissues. In this chapter, the aims of DGT research in rhizosphere of aquatic plants are as follows: (1) to develop DGT measurement method in the rhizosphere of aquatic plants, the calculation method for C_E—the effective concentration, and the measurement of P-concentrations in sediment/porewater/plant tissues; (2) to investigate the prediction for P-contents in plant tissues (root/stem/leaf) by C_{DGT} and C_E; and (3) to assess P-uptake ability of aquatic plants and the effect of macropytes on the ecological restoration of lake system.

7.1 P-Concentrations in Sediment–Porewater–Plant Samples and the DGT Measurement Results

The picture for the deployment of DGT piston in situ in the rhizosphere of *Z. latifolia* and *M. verticillatum* is shown in Fig. 7.1.

Firstly, the P-concentrations in sediment, porewater, root, stem, and leaf for in situ DGT test (*Z. latifolia*) were introduced as follows. The P-contents in root/stem/leaf were above the *LOD* (Table 3.2 in Chap. 3), and the values of them are given indicated in Fig. 7.2. The R_{diff} is calculated by 2D-DIFS model introduced in Sect. 3.3. 1, and the parameters such as C_0 (nmol ml^{-1}), T_c (10^{-10} s), K_D (10^{-10} cm^3 g^{-1}), Pc (g cm^{-3}), D_d (cm^2 s^{-1}), Ds (cm^2 s^{-1}), D_0 (cm^2 s^{-1}), pordif, porsed, C_0 (nmol ml^{-1}), and dg (cm) in accordance with the "diffusion-only" case were input into user's guide interface. Then, the R_{diff} was output, and C_E (effective concentration) was calculated using Eq. 1.3 in Chap. 1.

The input and output parameters for 2D-DIFS model are listed in Tables 7.1 and 7.2. The C_0 values, DGT concentrations, R_{diff}, and C_E in 10 sample sites (1–10) were in the ranges of 4.65–41.76 nmol ml^{-1}, 1.05–20.86 nmol ml^{-1}, 0.062–0.095, and 36–261.16 nmol ml^{-1}, in turn. Based on 1D-DIFS model introduced in Section 3.4 "The computer programs for DGT (DIFS, Visual MINTEQ, and ImageJ 1.38 e-softwares) and the operation/experiment methodology," the real R, K_D, and other DGT parameters can be input into the user's guide, and the real T_c can be calculated and output. The real R, K_D, the output parameter (T_c), and P-fraction (NH_4Cl-P + BD-P) in sediments are listed in Table 7.2. The R, T_c, and K_D values for 1D-DIFS were in the ranges of 0.226–0.717, 81–8500 s, and 60–558 cm^3 g^{-1}, respectively. Figure 7.3 shows the P-fraction in rhizosphere sediment (in situ DGT test for *Z. latifolia*).

Fig. 7.1 The insertion operation of DGT pistons into the rhizosphere of *Zizania caduciflora* and *Myriophyllum verticillatum*

Secondly, the P-concentrations in sediment, porewater, root, stem, and leaf for in situ DGT test (*M. verticillatum*) were introduced as following contents. The P-contents in root/stem/leaf were above the *LOD* (Table 3.2 in Chap. 3) and the values of them are indicated in Fig. 7.4. The input and output parameters for 2D-DIFS model are listed in Tables 7.3 and 7.4. The C_0 values, DGT values,

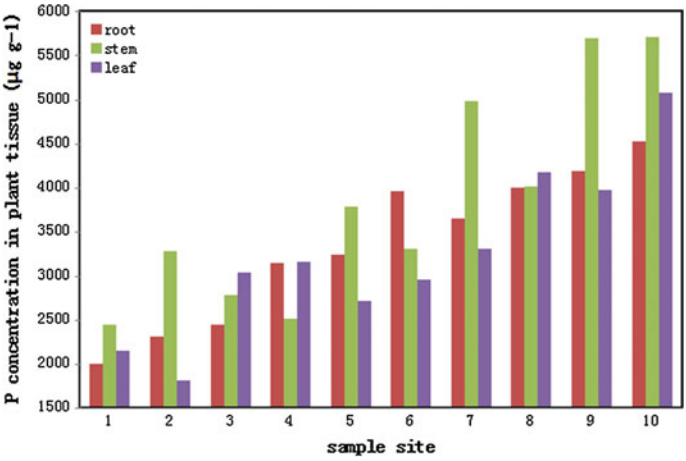

Fig. 7.2 The P-content in root/stem/leaf (in situ DGT test for *Zizania latifolia*)

R_{diff} and C_E in 10 sites (A–J) were in the ranges of 0.43–49.61 nmol ml^{-1}, 0.25–21. 44 nmol ml^{-1}, 060–0.079, 4.27–296.0 nmol ml^{-1}, in turn. The real R, K_D, the output parameter (T_c) for 1D-DIFS model and P-fraction (NH_4Cl-P + BD-P) in sediments were listed in Table 7.4. The R, T_c, and K_D values for 1D-DIFS were in the ranges of 0.318–0.661, 14–5069 s, and 166–1593 cm^3 g^{-1}. Figure 7.5 shows the P-fraction in sediment of rhizosphere (in situ DGT test for *M. verticillatum*).

7.2 The Linear Relationship Between DGT Measurement and P-Content in Plant Tissues for the Prediction of P-Uptake

Plots of C_{DGT} and C_E versus P-concentration (Figs. 7.6, 7.7 and 7.8) in plant tissue (*Z. latifolia*) in 10 sampling sites (1–10) displayed the significant linear relationship between them. For linear relationship between C_{DGT}, C_E, and P-content in plant tissue (C_{root}, C_{stem}, or C_{leaf}), R^2 values of 0.945, 0.780, and 0.823 (C_{DGT} and P-content in root, stem, and leaf, in turn) or 0.796, 0.917, and 0.736 (C_E and P-content in root, stem, and leaf, in turn) were obtained. The R^2 values for linear relationship between C_0 and P-content in plant tissues were 0.712 (root), 0.668 (stem), and 0.763 (leaf), in turn. The C_{DGT} can act as a better predictor for P-content in plant tissues, especially for root. However, C_E can only act as a better predictor for P-content in plant stem and root. DGT technique provides the good prediction of P-uptake in plant tissues, and the measurement encompasses resupply of P from sediment solid. The R values (resupply parameter) ranged from 0.23 to 0.72,

Table 7.1 The input parameters for the calculation of R_{diff} using 2D-DIFS model (in situ DGT test for *Zizania latifolia*)

Site	T_C (s)	K_d (cm^3 g^{-1})	P_c (g cm^{-3})	D_d (cm^2 s^{-1})	D_s (cm^2 s^{-1})	pordif	porsed	C_0 (nmol ml^{-1})	d_g (cm)	C_{DGT} (nmol ml^{-1})	R_{diff}	C_E (nmol ml^{-1})
1	1.00E+10	1.00E−10	0.2279	5.42	6.55	0.95	0.92	4.65	0.092	1.05	0.093	11.36
2	1.00E+10	1.00E−10	0.2379	5.42	6.51	0.95	0.92	6.64	0.092	1.87	0.092	20.26
3	1.00E+10	1.00E−10	1.0925	5.42	4.52	0.95	0.71	10.61	0.092	3.90	0.074	52.58
4	1.00E+10	1.00E−10	0.2201	5.42	6.58	0.95	0.92	15.88	0.092	4.58	0.093	49.29
5	1.00E+10	1.00E−10	0.8453	5.42	4.91	0.95	0.76	11.29	0.092	8.10	0.078	103.85
6	1.00E+10	1.00E−10	0.1553	5.42	6.85	0.95	0.94	16.98	0.092	9.98	0.095	104.79
7	1.00E+10	1.00E−10	0.8634	5.42	4.88	0.95	0.75	38.76	0.092	13.12	0.062	212.26
8	1.00E+10	1.00E−10	0.2731	5.42	6.38	0.95	0.91	35.97	0.092	15.32	0.091	167.82
9	1.00E+10	1.00E−10	0.9949	5.42	4.66	0.95	0.73	28.08	0.092	18.45	0.076	244.27
10	1.00E+10	1.00E−10	0.7442	5.42	5.11	0.95	0.78	41.76	0.092	20.86	0.080	261.16

Table 7.2 The output parameters for 1D-DIFS model and the P(NH_4Cl-P + BD-P) content in sediments (in situ DGT test for *Zizania latifolia*)

Site	T_C	K_D	R	NH_4Cl-P + BD-P (μmol g^{-1})
1	6449	303.9	0.226	1.41
2	1027	204.7	0.282	1.36
3	1912	178.3	0.368	1.89
4	8500	104.2	0.289	1.65
5	27.9	434.0	0.717	4.90
6	247	558.0	0.588	9.47
7	2211	60.0	0.338	2.33
8	837	96.7	0.426	3.48
9	81	313.5	0.657	8.80
10	201	102.3	0.500	4.27

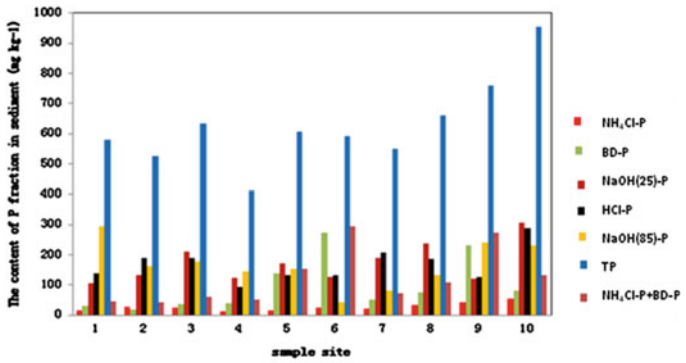

Fig. 7.3 The P-fraction in sediment (in situ DGT test for *Zizania latifolia*)

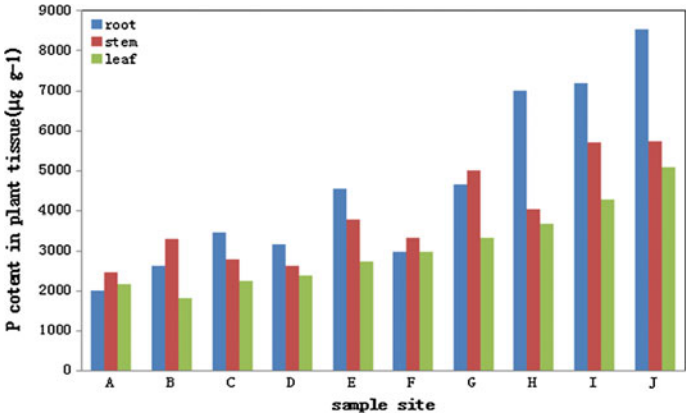

Fig. 7.4 The P-content in root/stem/leaf (in situ DGT test for *Myriophyllum verticillatum*)

Table 7.3 The input parameters for the calculation of R_{diff} using 2D-DIFS model (in situ DGT test for *Myriophyllum verticillatum*)

Site	T_C (s)	K_d (cm^3 g^{-1})	P_c (g cm^{-3})	D_d (×10-6 cm2 s-1)	D_s (×10^{-6} cm^2 s^{-1})	pordif	porsed	C_0 (nmol ml^{-1})	d_g (cm)	C_{DGT} (nmol ml^{-1})	R_{diff}	C_E (nmol ml^{-1})
A	1.00E+10	1.00E−10	1.03	5.42	4.60	0.95	0.72	0.43	0.092	0.25	0.060	4.27
B	1.00E+10	1.00E−10	0.93	5.42	4.77	0.95	0.74	1.08	0.092	0.59	0.077	7.68
C	1.00E+10	1.00E−10	1.05	5.42	4.58	0.95	0.72	2.90	0.092	0.78	0.075	10.42
D	1.00E+10	1.00E−10	0.95	5.42	4.73	0.95	0.74	1.59	0.092	0.97	0.076	12.71
E	1.00E+10	1.00E−10	0.89	5.42	4.83	0.95	0.75	4.25	0.092	1.35	0.077	17.44
F	1.00E+10	1.00E−10	0.91	5.42	4.80	0.95	0.74	3.10	0.092	1.92	0.077	24.94
G	1.00E+10	1.00E−10	0.80	5.42	5.00	0.95	0.77	5.85	0.092	3.70	0.079	46.91
H	1.00E+10	1.00E−10	1.10	5.42	4.50	0.95	0.71	12.54	0.092	7.65	0.074	103.5
I	1.00E+10	1.00E−10	1.00	5.42	4.65	0.95	0.73	20.60	0.092	13.62	0.075	180.5
J	1.00E+10	1.00E−10	1.21	5.42	4.36	0.95	0.69	49.61	0.092	21.44	0.072	296.0

Table 7.4 The output parameters and the P(NH_4Cl-P + BD-P) content in sediments (in situ DGT test for *Myriophyllum verticillatum*)

Site	T_C (s)	K_D ($cm^3\ g^{-1}$)	R	NH_4Cl-P + BD-P ($\mu mol\ g^{-1}$)
A	337	1593	0.593	0.68
B	508	1393	0.547	1.50
C	5069	772	0.268	2.24
D	298	1064	0.611	1.69
E	3545	379	0.318	1.61
F	206	422	0.619	1.31
G	90	264	0.632	1.55
H	14	166	0.610	2.08
I	75	326	0.661	6.71
J	844	208	0.432	10.34

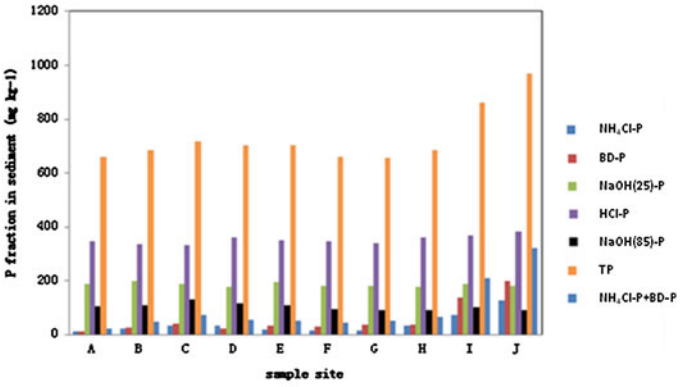

Fig. 7.5 The P-fraction in sediment (in situ DGT test for *Myriophyllum verticillatum*)

indicating that there was significant resupply of P from solid, especially at sites 5 and 9, but the resupply is insufficient to sustain fully porewater concentration.

Plots of C_{DGT} and C_E versus P-concentration (Figs. 7.9, 7.10, and 7.11) in plant tissue (*M. verticillatum*) in 10 sampling sites (A–J) displayed the significant linear correlations between them. For linear relationship between C_{DGT}, C_E, and P-content in plant tissue (C_{root}, C_{stem}, or C_{leaf}), R^2 values of 0.839, 0.718, and 0.892 (C_{DGT} and P-content in root, stem, and leaf, in turn) or 0.832, 0.702, and 0.892 (C_E and P-content in root, stem, and leaf, in turn) were obtained. The R^2 values for linear relationship between C_0 and P-content in plant tissues were 0.747 (root), 0.602 (stem), and 0.819 (leaf), in turn. The C_{DGT} can act as a better predictor for P-content in plant tissues, especially for root. However, C_E can only act as a better predictor for P-content C_{stem}(in situ *DGT test for* M. verticillatum), plant stem, and root. The R values (resupply parameter) ranged from 0.27 to 0.66, indicating that there was significant resupply of P from solid, especially at sites G and I, but the resupply is insufficient to sustain fully porewater concentration.

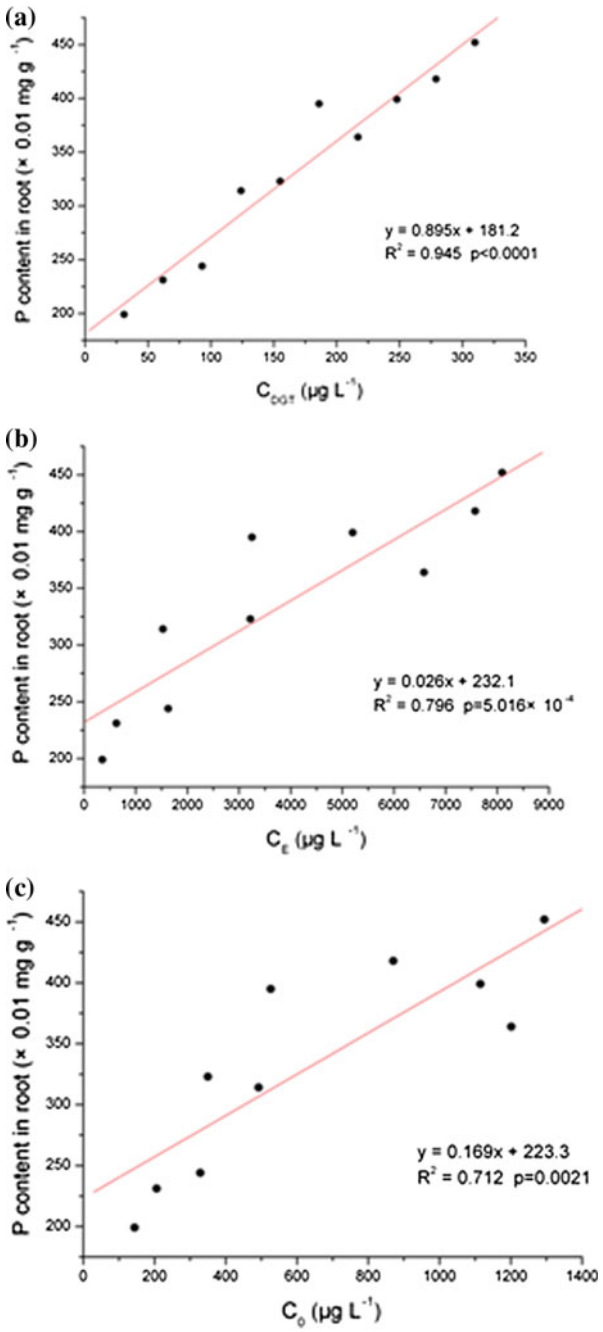

Fig. 7.6 The relationships between **a** C_{DGT} and C_{root}; **b** C_E and C_{root}; and **c** C_0 and C_{root} (in situ DGT test for *Zizania latifolia*)

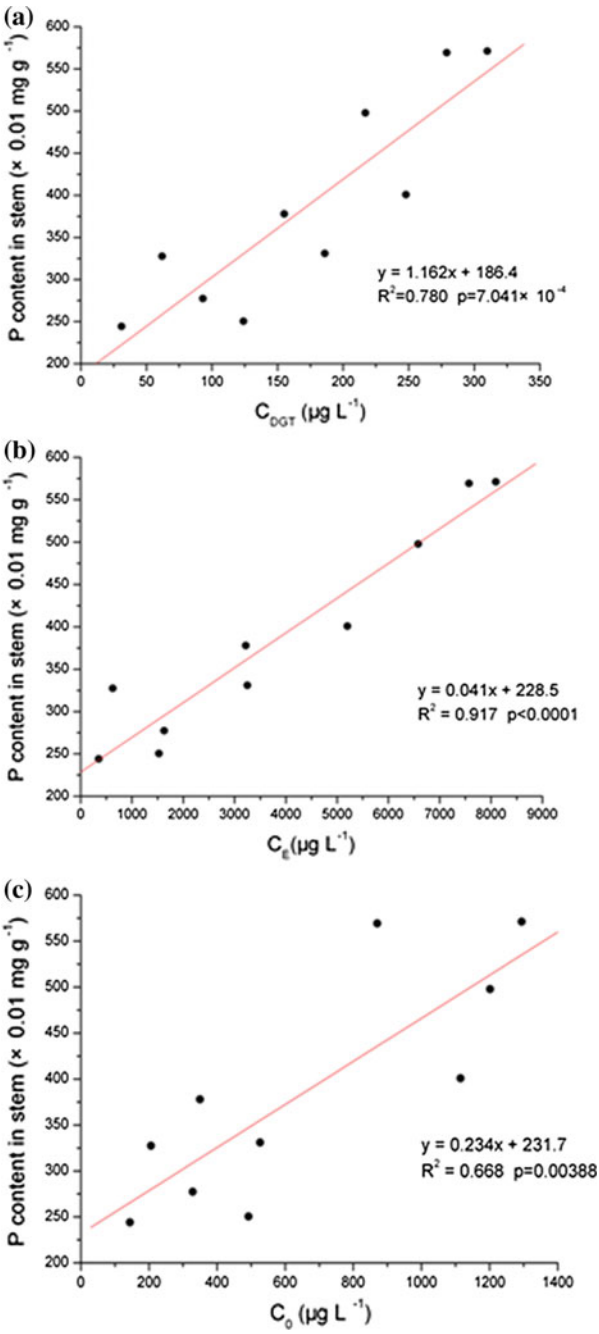

Fig. 7.7 The relationships between **a** C_{DGT} and C_{stem}; **b** C_E and C_{stem}; and **c** C_0 and C_{stem} (in situ DGT test for *Zizania latifolia*)

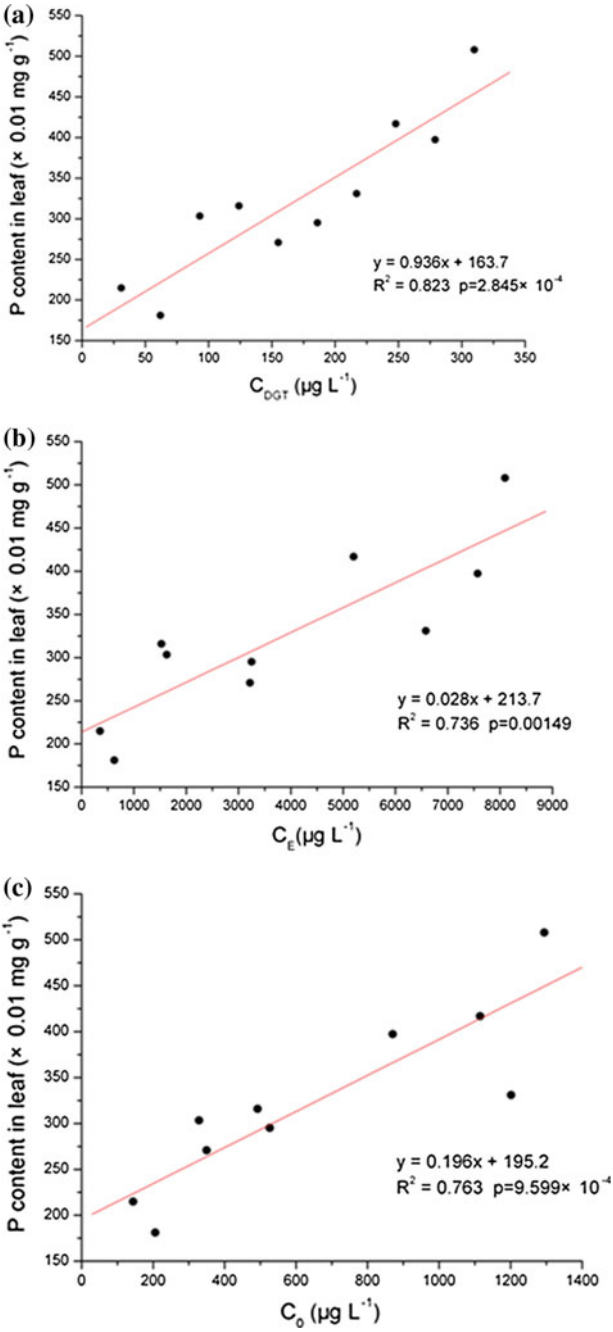

Fig. 7.8 The relationships between **a** C_{DGT} and C_{leaf}; **b** C_E and C_{leaf}; and **c** C_0 and C_{leaf} (in situ DGT test for *Zizania latifolia*)

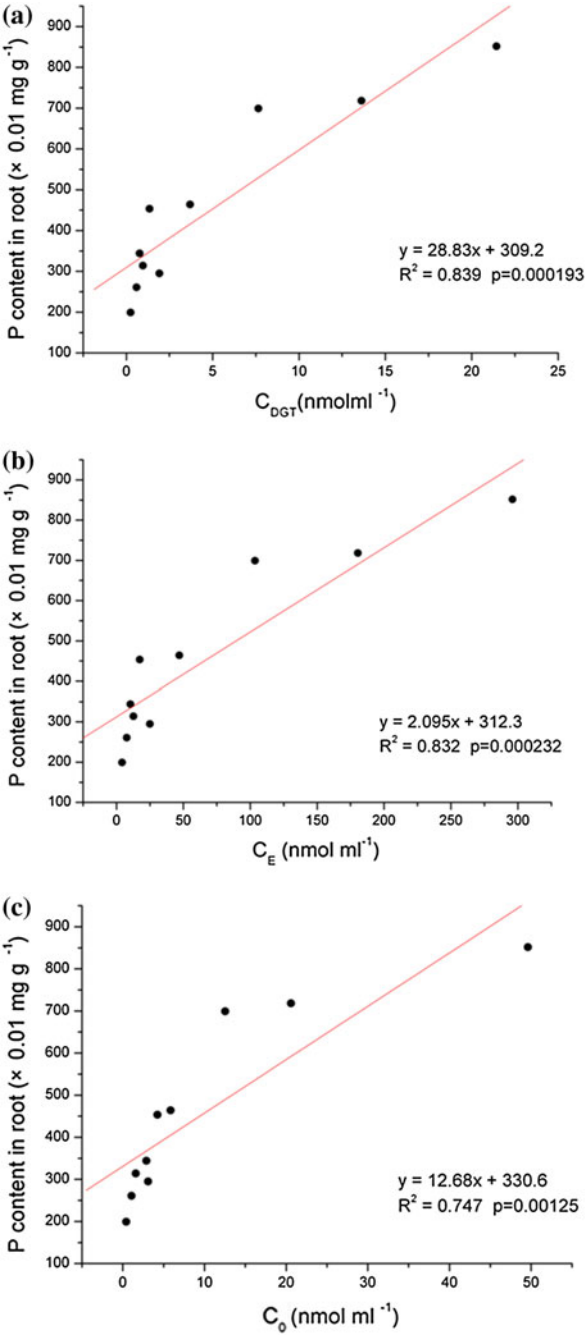

Fig. 7.9 The relationships between **a** C_{DGT} and C_{root}; **b** C_E and C_{root}; and **c** C_0 and C_{root} (in situ DGT test for *Myriophyllum verticillatum*)

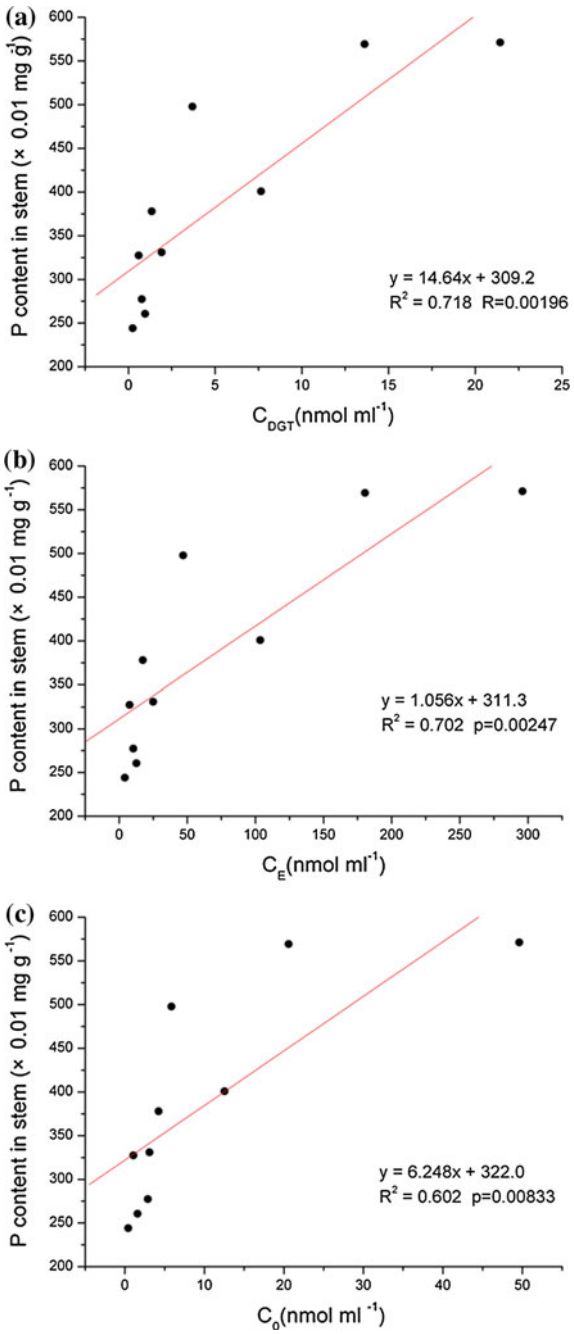

Fig. 7.10 The relationships between **a** C_{DGT} and C_{stem}; **b** C_E and C_{stem}; and **c** C_0 and C_{stem} (in situ DGT test for *Myriophyllum verticillatum*)

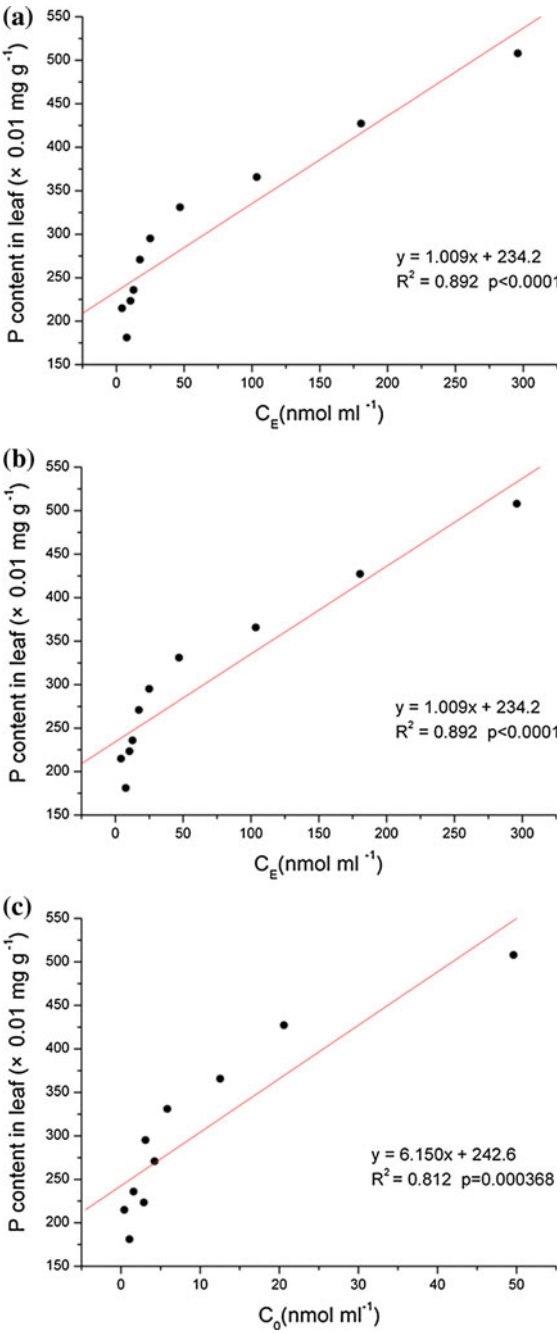

Fig. 7.11 The relationships between **a** C_{DGT} and C_{leaf}; **b** C_E and C_{leaf}; and **c** C_0 and C_{leaf} (in situ DGT test for *Myriophyllum verticillatum*)

P-fractions (NH_4Cl-P + BD-P) stand for the labile P-pool (loosely sorbed P- and Fe-bound P-phases) in sediment, which is used for 1D-DIFS simulation for T_c (Wu et al. 2015). So, the labile P-pool (NH_4Cl-P + BD-P) in sediment should maintain the resupply for depletion of sediment porewater and the P-uptake by root. The most important removal mechanism for P under neutral to slightly acidic conditions in sediment porewater is the sorption process of P onto Fe and Al sesquioxides (Holford and Patrick 1979; Khalid et al. 1977). The extractable Al is believed to be the most important reason for P adsorbed in freshwater wetlands (Richardson 1985). while the extractable Fe in sediment has been proved to be the other important sink for the P adsorption on sediment (Jacobsen 1977; Khalid et al. 1977). Fe:P molar ratios for minerals in sediments can also determine the mobility of P (Lijklema 1977; Jensen and Andersen 1990). The low Eh in sediment can also increase the P-concentration in sediment porewater. This is partially due to the reduction of Fe^{3+} to Fe^{2+} (Gotoh and Partrick 1972; Holford and Partrick 1979).

Figure 7.12 shows the schematic graphic for the P-desorption from sediment, P-uptake by plant root, and DGT uptake. DPUM (dynamic plant uptake model) has been developed to describe the element supply from a soil and kinetic uptake by root using kinetic and pool size parameters in a soil environment in which DGT device is deployed (Lehto et al. 2006). If the removal rate of element caused by

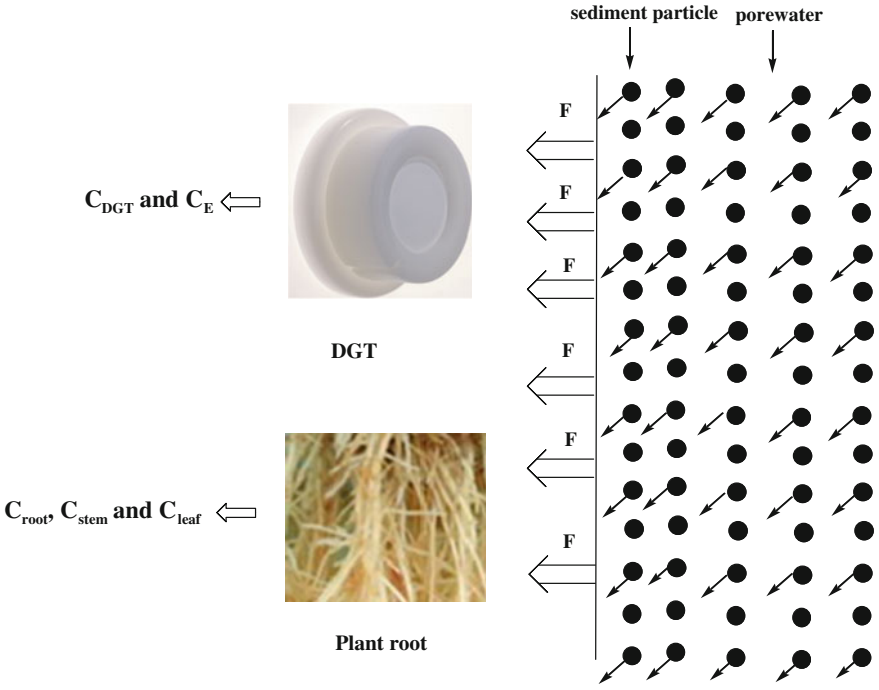

Fig. 7.12 The schematic graphic for P-desorption from sediment, the P-uptake by plant root, and the DGT test

plant root exceeds the diffusive resupply from the element in porewater, the element concentration in porewater immediately adjacent to root surface becomes depleted.

When it comes to P-uptake by root, this process leads to the P-resupply from solution and P-depletion in porewater. P-species in sediment porewater include total P (TP), dissolved total P (DTP), dissolved reactive P (DRP), and dissolved unreactive P (DUP). Moreover, P can be released from sediment particles and this process can cause P-depletion in porewater. In this situation, the concentration of total labile P in solution, its diffusional supply, the labile P resupplied from solid particle and the rate of the desorption from solid phase into solution can determine the supply of P to plant root. Like plant roots, DGT locally lowers P-concentrations in the sediment solution and responds to P resupplied from labile species in solution and the labile P-pool in the solid phase. The in situ DGT test in rhizosphere of two aquatic plants indicated the effect of a good surrogate for the assessment of the rates and extent to which P can be released from soil particles and supplied to biota. Moreover, the measured DGT flux of labile P in the sediment can be quantitatively related to a new term—C_E, indicating the sediment solution to supply the same mass of P accumulated by DGT in the "diffusion-only" case (b) (Fig. 1.5 in Chap. 1).

7.3 The Quantification for P-Uptake by Root of Aquatic Plant Using DGT Flux

The DGT-induced flux measured in the rhizosphere near the roots of aquatic plant can be used to derive DGT concentration and C_E value, based on Fick's diffusion law and 2D-DIFS model. DGT has been widely used as a reliable surrogate for the transport and metal release processes that affect plant uptake, and in one study (Lehto et al. 2006), the dynamic plant uptake model (DPUM) using soil parameters for micronutrients that are measured under similar conditions to those that apply during plant uptake was researched and compared with DGT and DIFS. In one study for P-uptake by wheat (Mason et al. 2010), DGT has been proved to be a robust technique that better assesses plant-available P and predicts the plant response to application of P, regardless of soil type and without recourse to further corrections or interpretation. In the DGT test in the rhizosphere of *Zizania caduciflora* or *M. verticillatum,* DGT concentration and C_E have been proved to be a good predictor for P-uptake by root and can be a better proxy of *Z. caduciflora* root. For the assessment of the P-uptake mass by *Z. caduciflora* or *M. verticillatum* roots and the function of ecological restoration using aquatic plants, the DGT flux determined in situ at the rhizosphere can be used to stand for P-mass taken up by root and to evaluate P-removal ability by aquatic plant root roughly.

The root biomass and its surface area for two plants are listed in Table 7.5. The DGT flux per area of DGT resin, P-mass accumulated on DGT resin (M/A),

Table 7.5 The root biomass and root surface area in the studying regions for two plants (*Zizania caduciflora* or *Myriophyllum verticillatum*)

Site	Root biomass (g plant^{-1})					Root surface area (cm^2 plant^{-1})			Total (cm^2 plant^{-1})
	d < 2 mm	2 < d<3 mm	d > 3 mm	rhizome	Total (g plant-1)	d < 2 mm	2 < d<3 mm	d > 3 mm	
Zizania caduciflora									
1	2.3	2.5	3	6	13.8	488	334	203	1025
2	2.6	2.3	3.3	7.3	15.5	496	313	234	1043
3	2.8	2.4	2.9	6.9	15	506	323	201	1030
4	3	2.4	3.1	6.1	14.6	532	322	228	1082
5	3.5	2.9	3.3	7.3	17	542	355	232	1129
6	2.4	2.9	2.8	6.6	14.7	490	468	195	1153
7	2.5	2.2	2.9	7.3	14.9	493	306	193	992
8	2.4	2.4	2.5	7.7	15	483	329	199	1011
9	2.8	2.3	2.8	6.9	14.8	513	319	123	955
10	2.8	2.5	2.9	6.7	14.9	521	335	142	998
Myriophyllum verticillatum									
A	1.3	1.5			2.8	188	134		322
B	1.6	1.3			2.9	196	123		319
C	1.8	1.4			3.2	206	103		309
D	1.5	2.0			3.5	232	126		358
E	1.9	1.8			3.7	192	155		347
F	2.1	1.9			4.0	190	168		358
G	2.0	1.8			3.8	193	206		399
H	2.2	1.7			3.9	183	219		402
I	2.2	2.1			4.3	213	179		392
J	2.3	1.9			4.2	221	184		405

Table 7.6 The DGT flux per area of DGT resin, P-mass accumulated on DGT resin (M/A), P-mass adsorbed by plant root, and P-mass removed by plant root in Erhai Lake (1 km^2) for *Zizania caduciflora* and *Myriophyllum verticillatum*

Site	DGT flux	Mass accumulated on resin (M/A)	Total	P adsorbed by plant root	P removed by roots in Erhai
ng cm^{-2} s^{-1}	ng cm^{-2} d^{-1}	cm^2 $plant^{-1}$	ng d^{-1}	mg d^{-1}	kg km^{-2} a^{-1}
Zizania caduciflora					
1	1.92E−03	166	1025	170,273	0.17
2	3.42E−03	296	1043	308,280	0.31
3	7.12E−03	615	1030	633,591	0.63
4	8.37E−03	723	1082	782,531	0.78
5	1.48E−02	1278	1129	1,442,362	1.44
6	1.82E−02	1575	1153	1,815,711	1.82
7	2.40E−02	2070	992	2,053,678	2.05
8	2.80E−02	2417	1011	2,443,975	2.44
9	3.37E−02	2911	955	2,780,268	2.78
10	3.81E−02	3292	998	3,284,973	3.28
Total (mg m^{-2} d^{-1})		15.72		2829	
Myriophyllum verticillatum					
A	4.65E−04	40	322	12,932	0.013
B	1.08E−03	93	319	29,633	0.030
C	1.42E−03	123	309	37,963	0.038
D	1.77E−03	153	358	54,710	0.055
E	2.46E−03	213	347	73,825	0.074
F	3.50E−03	303	358	108,348	0.108
G	6.75E−03	583	399	232,790	0.233
H	1.40E−02	1207	402	485,341	0.485
I	2.49E−02	2149	392	842,280	0.842
J	3.92E−02	3383	405	1,370,035	1.370
Total (mg m^{-2} d^{-1})		3.248		585	

P-mass adsorbed by plant root, and P-mass removed by two kinds of plant roots in Erhai Lake (1 km^2) are listed in Table 7.6. According to DGT flux (F, ng/(cm^2 s)), the mass accumulated on resin (M/A, ng cm^{-2}), the assumed equal P-mass adsorbed by plant root (ng $plant^{-1}$), P-mass adsorbed by plant root in 1 m^2 area (ten plants for *Z. caduciflora* or *M. verticillatum*), and the P-mass adsorbed by *Z. caduciflora* or *M. verticillatum* per year (180 d and 1 km^2-area) is calculated to be 2.83 or 0.58 tons km^{-2} a^{-1}. The "external P-loading" is about 74.49 tons a^{-1} (Zhang et al. 2011). If plant density of aquatic plants in Erhai Lake can be elevated to be 30 plants m^{-2}, the P-mass adsorbed by two plants per year should be 8.49 or 1.74 tons a^{-1}. The effects of *Z. caduciflora* or *M. verticillatum* on the P-removal ability can be used for controlling P-concentration in lake environment and the natural nutrient polishing systems.

7.4 Summary

Submerged and emerged macrophytes have been used for ecological restoration of water body under experimental conditions or by constructing wetland. The measurement of P-gradients at sediment/root interface is important to assess P bioavailability and kinetic P-uptake by plant root and the restoration ability of macrophytes for lake ecosystem. In this chapter, DGT measurement was made in the root/porewater/sediment interface for two plants (*Z. caduciflora* and *M. verticillatum*). DGT flux and concentration can reflect the P-process in rhizosphere, including the P-uptake by root, the depletion of P-concentration in porewater, the desorption of P from sediment, and the resupply from sediment into porewater. So, the DGT concentration contains both labile P-concentration in porewater and the P-content released from sediment. The effective concentration (C_E) is the hypothetical porewater concentration, which can be converted to the amount of P accumulated on DGT resin, if it belongs to "diffusional supply" case.

The calculation of C_E requires R_{diff} derived by 2D-DIFS calculation. The significant linear regression between DGT parameters and P-content in plant tissues indicates that DGT can act as a good proxy for macrophyte root because DGT measurement involves the resupply dynamics of P from solid phase to solution. So, DGT measurement can be used to predict P-mass uptake by aquatic plant, which indicates the P-removal performance of *Z. caduciflora* and *M. verticillatum.* The in situ DGT test in rhizosphere of aquatic plants indicates that DGT is an effective tool for the prediction of P-content in plant tissues and P-uptake ability of plant root for the ecological restoration of lake system.

References

Barko JW, Gunnison D, Carpenter SR (1991) Sediment interactions with submersed macrophyte growth and community dynamics. Aquat Bot 41:41–65

Blindow I, Andersson G, Haregy A (1993) Long-term pattern of alternative stable states in two shallow eutrophic lakes. Freshwater Biol. 30:1159–1167

Gotoh S, Partrick WH Jr (1972) Transformation of manganese in waterlogged soil as affected by redox potential and pH. Soil Sci Soc Am 36:738–742

Holford ICR, Pratick WH (1979) Effects of reduction and pH changes on phosphate sorption and mobility in an acid soil. Soil Sci Soc Am J 43:292–296

Jacobsen OS (1977) Sorption of phosphate by Danish lake sediments. Vatten 33:290–298

Jensen H, Andersen F (1990) Fosforbelastning i lavvandede eutrofe sØer. NPo-forskning fra MiljØstyrelsen. Nr.C4, 96 (In Danish)

Khalid RA, Patrick WH, Delaune RD (1977) Phosphorus sorption characteristics of flooded soils. Soil Sci Soc Am J 41:305–310

Lehto NJ, Davison W, Zhang H, Tych W (2006) Analysis of micro-nutrient behaviour in the rhizosphere using a DGT parameterised dynamic plant uptake model. Plant Soil 282:227–238

Lijklema L (1977) The role of iron in the exchange of phosphate between water and sediments. In: Golterman GL (ed) Interactions between sediments and freshwater. Dr. Junk, W. The Hague, pp 313–317

Mason S, McNeill A, McLaughlin MJ, Zhang H (2010) Prediction of wheat response to an application of phosphorus under field conditions using diffusive gradients in thin-films (DGT) and extraction methods. Plant Soil 337(1):243–258

Qiu DR, Wu ZB, Liu BY, Deng JQ, Fu GP, Feng H (2001) The restoration of aquatic macrophytes for improvingwater quality in a hypertrophic shallow lake in Hubei Province (in Chinese). China Ecol Eng 18:147–156

Richardson CJ (1985) Mechanisms controlling phosphorus retention capacity in freshwater wet lands. Science 228:1424–1427

Wu ZH, Wang SR, He MC (2015) Element remobilization, "internal P-loading" and sediment-P reactivity researched by DGT (diffusive gradients in thin films) technique. Environ Sci Pollut R 22:16173–16183

Zhang T (2011) Research on the spatio-teraporal distribution of the concentrations of nitrogen and phosphorus and exogenous fluxes in Erhai lake (2011) MA Thesis. Dali College, Dali, China

Chapter 8
The Uptake and Accumulation of P Assessed by DGT/Rhizobox Method

The rhizosphere zone includes the volume of soil or sediment interacting directly and indirectly with the plant roots and the microzone near root with the radial distance from nanometers to centimeters (Hiltner 1904). The rhizosphere environment is as complex as the aboveground part of the plant. The rhizosphere is the interface between root and mineral phases, which has the intricate ecological feedback, chemical interaction, and the interorganism communication. Rhizobox designs, as introduced by Youssef and Chino (1988) and Kuchenbuch and Jungk (1982), consist of a soil/root compartment and one or more adjacent soil compartments that are separated by porous membranes with a mesh width that allows for the exchange of solutes, but does not allow roots to penetrate from the soil/root into the soil compartments. Depending on the mesh width, root hairs may or may not grow into the soil compartment. In this chapter, a rhizobox with three compartments was designed and it was divided by membranes into narrow layers paralleling the root plane. The porous membranes (nylon or fiberglass) restrict particles passing through two layers and permit water and element exchange. DGT can be tested at the precise location in the rhizosphere of the cultivated aquatic plants in rhizoboxes. The DGT measurement and the related calculation can derive C_{DGT}, C_E, C_0, C_{root}, C_{stem}, C_{leaf}, and P-fractions in sediment, and the P-uptake mechanism by the plant root, and DGT as a proxy to mimic P taken up by plant root, can be investigated and assessed more thoroughly, compared with the results of in situ DGT test at plant rhizosphere in lake.

S. Wang and Z. Wu, *DGT-based Measurement of Phosphorus in Sediment Microzones and Rhizospheres*, DOI 10.1007/978-981-10-0721-7_8

8.1 P-Concentration in Sediment–Porewater–Plant Samples and the Derivation of C_E and R_{diff}

The DGT test in the rhizoboxes of two aquatic plants was conducted at the floating flat (Fig. 8.1) in Erhai Lake. After the test, DGT concentration (C_{DGT}), porewater concentration (C_0), the P-content in plant tissues (root, stem, and leaf), P-content in sediment, and the effective concentration (C_E) were determined or calculated.

Firstly, P-concentration in sediment, porewater, root, stem, and leaf: DGT concentration, the calculation of C_E, and R_{diff} for DGT test in rhizobox with *Zizania latifolia* are introduced in the following contents. The P-contents in root/stem/leaf were above the LOD (Table 3.2 in Chap. 3) and the values of them are indicated in Fig. 8.2. P-fractions in sediments of 15 rhizoboxes are indicated in Fig. 8.3. The P-concentration in porewater (C_0), C_{DGT}, and P-fraction (NH_4Cl-P + BD-P) in sediments for 2D-DIFS simulation are listed in Table 8.1. The R_{diff} is calculated by 2D-DIFS model introduced in Sect. 3.3.1, and the parameters, such as C_0 (nmol ml^{-1}), T_c (10^{10} s), K_d (10^{-10} cm^3 g^{-1}), P_c (g cm^{-3}), D_d (cm^2 s^{-1}), D_s (cm^2 s^{-1}), D_0 (cm^2 s^{-1}), pordif, porsed, C_0 (nmol ml^{-1}), and d_g (cm) in accordance with the "diffusion only" case, were input into user's guide interface. The R_{diff} and C_E were

Fig. 8.1 The picture of the floating flat in the north of Erhai Lake (Fig. 2.3 in Chap. 2) for DGT test in rhizoboxes of two aquatic plants. Thirty rhizoboxes for two kinds of plants were put into the water of floating flat for cultivation and subsequent DGT test

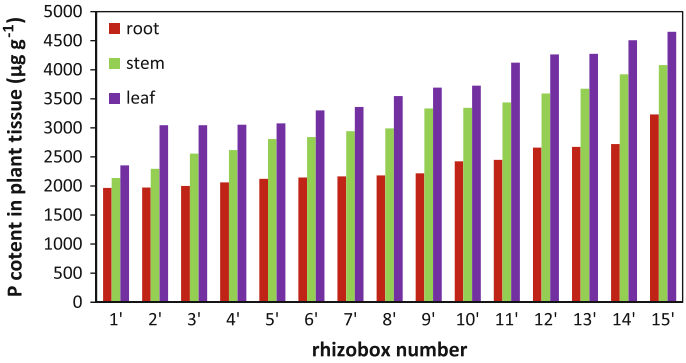

Fig. 8.2 The P-concentration in root/stem/leaf for DGT test in rhizobox (*Zizania latifolia*)

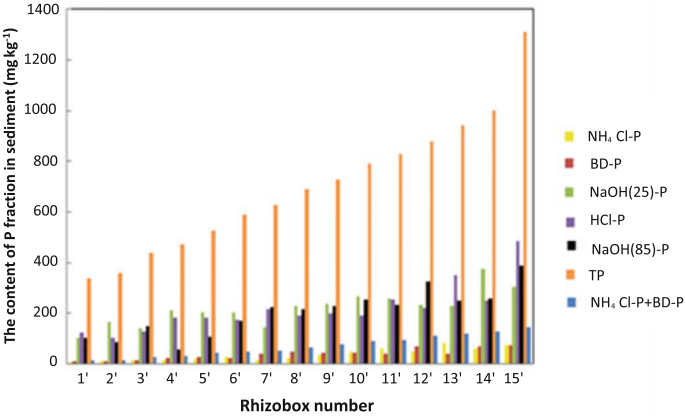

Fig. 8.3 The P-fraction in sediment of rhizobox (*Zizania latifolia)*

calculated by the method introduced in Sect. 6.1. The output parameters are also listed in Table 8.2. The C_0 values, DGT concentrations, R_{diff}, and C_E in 15 rhizoboxes were in the ranges 1.28–20.68 nmol ml^{-1}, 0.69–9.73 nmol ml^{-1}, 0.056–0.073, and 9.53–133.94 nmol ml^{-1}, in turn. Based on 1D-DIFS model introduced in Sect. 3.5, the real R, K_d, and other DGT parameters can be input into the user's guide and the real T_c can be output. The real R, K_d, the output parameter (T_c), and P-fraction (NH_4Cl-P + BD-P) in sediments are listed in Table 8.2. The R, T_c, and K_d values for 1D-DIFS were in the ranges 0.248–0.539, 320–2101 s, and 122.2–264.2 cm^3 g^{-1}.

Secondly, P-concentration in sediment, porewater, root, stem, and leaf, DGT concentration, the calculation of C_E, and R_{diff} for DGT test in rhizobox with *Myriophyllum verticillatum* are introduced in the following contents. The P-contents in root/stem/leaf were above the LOD (Table 3.2 in Chap. 3) and the values of them

Table 8.1 The input parameters for the calculation of R_{diff} using 2D-DIFS model (in rhizobox for *Zizania latifolia)*

Site	T_C (s)	K_d ($cm^3\ g^{-1}$)	P_c ($g\ cm^{-3}$)	D_d ($cm^2\ s^{-1}$)	D_s ($cm^2\ s^{-1}$)	Pordif	Porsed	C_0 (nmol ml^{-1})	d_g (cm)	C_{DGT} (nmol ml^{-1})	R_{diff}	C_E (nmol ml −1)
1′	1.E + 10	1E-10	1.22	5.42	4.34×10^{-6}	0.95	0.69	1.28	0.092	0.69	0.072	9.5
2′	1.E + 10	1E-10	3.39	5.42	2.88×10^{-6}	0.95	0.44	2.20	0.092	0.86	0.056	15.4
3′	1.E + 10	1E-10	3.27	5.42	2.93×10^{-6}	0.95	0.45	5.89	0.092	1.72	0.057	30.3
4′	1.E + 10	1E-10	1.32	5.42	4.22×10^{-6}	0.95	0.67	6.52	0.092	2.07	0.071	29.1
5′	1.E + 10	1E-10	1.35	5.42	4.19×10^{-6}	0.95	0.66	8.59	0.092	3.19	0.071	45.1
6′	1.E + 10	1E-10	1.47	5.42	4.05×10^{-6}	0.95	0.64	8.91	0.092	3.36	0.071	47.5
7′	1.E + 10	1E-10	2.91	5.42	3.07×10^{-6}	0.95	0.48	13.55	0.092	3.70	0.059	63.1
8′	1.E + 10	1E-10	1.42	5.42	4.10×10^{-6}	0.95	0.65	15.41	0.092	5.26	0.070	75.1
9′	1.E + 10	1E-10	2.29	5.42	3.40×10^{-6}	0.95	0.54	18.37	0.092	5.77	0.062	92.6
10′	1.E + 10	1E-10	1.99	5.42	3.60×10^{-6}	0.95	0.57	19.52	0.092	5.86	0.065	90.7
11′	1.E + 10	1E-10	2.32	5.42	3.38×10^{-6}	0.95	0.53	21.32	0.092	6.29	0.062	101.2
12′	1.E + 10	1E-10	2.99	5.42	3.04×10^{-6}	0.95	0.47	25.12	0.092	6.72	0.058	115.4
13′	1.E + 10	1E-10	2.46	5.42	3.30×10^{-6}	0.95	0.52	30.87	0.092	7.67	0.059	129.7
14′	1.E + 10	1E-10	2.10	5.42	3.52×10^{-6}	0.95	0.56	18.46	0.092	8.53	0.064	133.9
15′	1.E + 10	1E-10	1.19	5.42	4.37×10^{-6}	0.95	0.69	20.68	0.092	9.73	0.073	133.8

Table 8.2 The output parameters using 1D-DIFS and the P(NH_4Cl-P + BD-P) content in sediments (in rhizobox for *Zizania latifolia*)

Site	T_C (s)	K_d ($cm^3\ g^{-1}$)	R	NH_4Cl-P + BD-P (μmol g^{-1})
1′	320	264.2	0.539	0.338
2′	383	180.7	0.392	0.397
3′	930	128.2	0.293	0.754
4′	2454	140.0	0.317	0.914
5′	1234	149.6	0.371	1.285
6′	1080	156.0	0.377	1.390
7′	1308	120.0	0.273	1.626
8′	1536	131.4	0.341	2.025
9′	1195	127.5	0.314	2.341
10′	1609	141.7	0.300	2.767
11′	1397	141.2	0.295	3.011
12′	1339	139.6	0.268	3.506
13′	2101	122.2	0.248	3.772
14′	386	216.6	0.462	3.997
15′	601	219.0	0.471	4.531

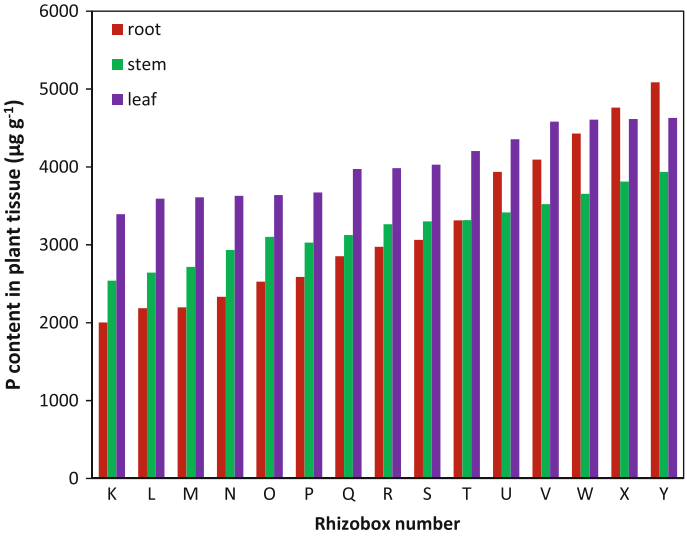

Fig. 8.4 The P-concentration in root/stem/leaf for DGT test in rhizobox *(Myriophyllum verticillatum)*

are indicated in Fig. 8.4. P-fractions in sediments of 15 rhizoboxes are indicated in Fig. 8.5. The P-concentration in porewater (C_0), C_{DGT}, and P-fraction (NH_4Cl-P + BD-P) in sediments for 2D-DIFS simulation are listed in Table 8.3.

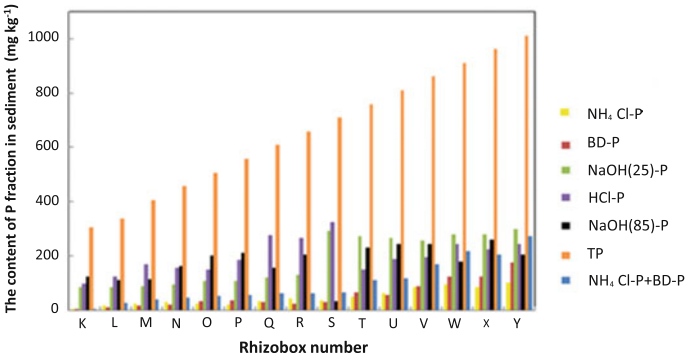

Fig. 8.5 The P-fraction in sediment of rhizobox *(Myriophyllum verticillatum)*

The real R, K_d, the output parameter (T_c), and P-fraction (NH_4Cl-P + BD-P) in sediments are listed in Table 8.4. The R, T_c, and K_d values for 1D-DIFS were in the ranges 0.207–0.741, 15–7237 s, and 80–1060 $cm^3\ g^{-1}$.

8.2 The Linear Regression of DGT Measurement Against P-Content in Plant Tissues for the Predictor of Bioavailability

Firstly, the linear regression curves of DGT concentration, P-concentration in porewater, the effective concentration against the P-contents in root, stem, and leaf for rhizobox *(Zizania latifolia)* are indicated in Figs. 8.6, 8.7, and 8.8, and the implication for P-uptake by root was introduced in the following content. Plots of C_{DGT} or C_E versus P-concentration in plant tissue in 15 rhizoboxes (Figs. 8.6, 8.7, and 8.8) indicated the significant correlations between DGT measurement and plant tissue. For linear relationship between C_{DGT} or C_E and P-content in plant tissue (C_{root}, C_{stem}, or C_{leaf}), R^2 values of 0.864, 0.980, 0.931 (C_{DGT} and P-content in root, stem, and leaf, in turn) or 0.808, 0.973, 0.941 (C_E and P-content in root, stem, and leaf, in turn) were obtained. The R^2 values for linear relationships between C_0 and P-content in plant tissues were 0.595 (root), 0.790 (stem), and 0.775 (leaf), in turn. The C_{DGT} and C_E can act as the better predictor than C_0 for P-content in plant tissues (root, stem, and leaf). DGT technique provides the good prediction of P-uptake by root and the P-content in plant tissues, and the measurement encompasses resupply of P from sediment solid. The R (resupply parameter) values ranged from 0.248 to 0.539, indicating that there was the significant resupply of P from solid, especially at rhizoboxes 1 and 10, but the resupply is insufficient to sustain fully porewater concentration. P-fractions (NH_4Cl-P + BD-P), which are used for

Table 8.3 The input parameters for the calculation of R_{diff} using 2D-DIFS model (in rhizobox for *Myriophyllum verticillatum*)

Site	T_C (s)	K_d (cm^3 g^{-1})	P_c (g cm^{-3})	D_d ($\times 10^{-6}$ cm^2 s^{-1})	D_s ($\times 10^{-6}$ cm^2 s^{-1})	Pordif	Porsed	C_0 (nmol ml^{-1})	d_g (cm)	C_{DGT} (nmolml^{-1})	R_{diff}	C_E (nmol ml^{-1})
K	1.0E + 10	1.0E-10	1.38	5.42	4.15	0.95	0.66	1.25	0.092	0.26	0.070	3.67
L	1.0E + 10	1.0E-10	1.39	5.42	4.14	0.95	0.66	0.77	0.092	0.32	0.070	4.58
M	1.0E + 10	1.0E-10	1.58	5.42	3.94	0.95	0.63	1.24	0.092	0.43	0.068	6.32
N	1.0E + 10	1.0E-10	1.66	5.42	3.87	0.95	0.61	2.04	0.092	0.86	0.067	12.77
O	1.0E + 10	1.0E-10	1.71	5.42	3.82	0.95	0.61	1.68	0.092	1.06	0.067	15.86
P	1.0E + 10	1.0E-10	1.85	5.42	3.71	0.95	0.59	2.83	0.092	1.29	0.066	19.65
Q	1.0E + 10	1.0E-10	2.15	5.42	3.48	0.95	0.55	4.60	0.092	1.72	0.063	27.20
R	1.0E + 10	1.0E-10	2.28	5.42	3.40	0.95	0.54	6.36	0.092	2.15	0.062	34.54
S	1.0E + 10	1.0E-10	3.28	5.42	2.92	0.95	0.45	6.02	0.092	3.84	0.057	67.62
T	1.0E + 10	1.0E-10	3.09	5.42	3.00	0.95	0.46	9.86	0.092	5.05	0.058	87.4
U	1.0E + 10	1.0E-10	3.02	5.42	3.03	0.95	0.47	9.30	0.092	6.89	0.058	118.6
V	1.0E + 10	1.0E-10	3.82	5.42	2.74	0.95	0.41	12.36	0.092	7.32	0.055	133.9
W	1.0E + 10	1.0E-10	4.10	5.42	2.66	0.95	0.39	14.60	0.092	9.22	0.054	171.6
X	1.0E + 10	1.0E-10	4.25	5.42	2.62	0.95	0.38	20.04	0.092	11.91	0.053	223.8
Y	1.0E + 10	1.0E-10	3.28	5.42	2.92	0.95	0.45	30.91	0.092	13.53	0.057	238.0

Table 8.4 The output parameters using 1D-DIFS and the P(NH_4Cl-P + BD-P) content in sediments (in rhizobox for *Myriophyllum verticillatum)*

Site	T_C (s)	K_D ($cm^3\ g^{-1}$)	R	NH_4Cl-P + BD-P (μmol g^{-1})
K	7237	80	0.207	0.10
L	964	1060	0.419	0.82
M	1515	998	0.347	1.24
N	761	719	0.423	1.46
O	163	997	0.631	1.68
P	536	631	0.456	1.79
Q	825	425	0.375	1.95
R	1039	312	0.339	1.99
S	58	340	0.638	2.05
T	188	358	0.512	3.53
U	15	403	0.741	3.75
V	85	436	0.593	5.39
W	58	476	0.631	6.95
X	64	327	0.594	6.55
Y	302	283	0.438	8.74

1D-DIFS simulation for C_E (Wu et al. 2015), should be the sediment pool for the resupply for depletion of sediment porewater and the P taken up by the root.

Secondly, the linear regression curves of DGT concentration, P-concentration in porewater, and the effective root against stem and leaf for rhizobox *(Myriophyllum verticillatum)* are indicated in Figs. 8.9, 8.10, and 8.11, and the implication for P-uptake by root was introduced in the following contents. Plots of C_{DGT} or C_E versus P-concentration in plant tissue in 15 rhizoboxes (Figs. 8.9, 8.10, and 8.11) indicated good correlations between DGT measurement and plant tissue. For linear relationship between C_{DGT}, C_E, and P-content in plant tissue (C_{root}, C_{stem}, or C_{leaf}), R^2 values of 0.971, 0.866, and 0.872 *(*C_{DGT} and P-content in root, stem, and leaf, in turn) or 0.967, 0.857, and 0.872 (C_E and P-content in root, stem, and leaf, in turn) were obtained. The R^2 values for linear relationships between C_0 and P-content in plant tissues were 0.885 (root), 0.804 (stem), and 0.751 (leaf), in turn. The C_{DGT} and C_E can act as the better predictor than C_0 for P-content in plant tissues (root, stem, and leaf). DGT technique provides the good prediction of P-uptake by root, the P-content in plant tissues and the measurement encompasses resupply of P from sediment solid. The R (resupply parameter) values ranged from 0.207 to 0.741, indicating that there was the significant resupply of P from solid, especially at rhizoboxes O, S, U, and W, but the resupply is insufficient to sustain fully porewater concentration.

The effective concentration (C_E) is the hypothetical porewater concentration that would be needed to accumulate the observed amount of labile P on the resin if there was only diffusional supply. The schematic graphic representation (Fig. 1.6 in Chap. 1) for the effective concentration (C_E) illustrates how the measured quantity,

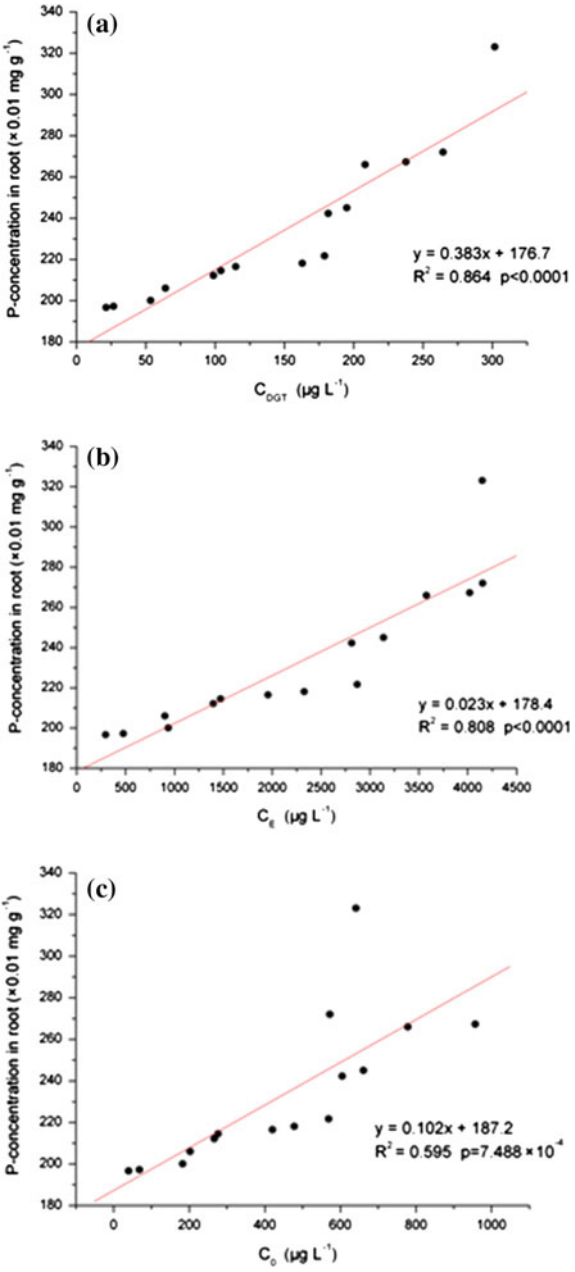

Fig. 8.6 The relationships between **a** C_{DGT} and C_{root}; **b** C_E and C_{root} **c** C_0 and C_{root} (in rhizobox for *Zizania latifolia)*

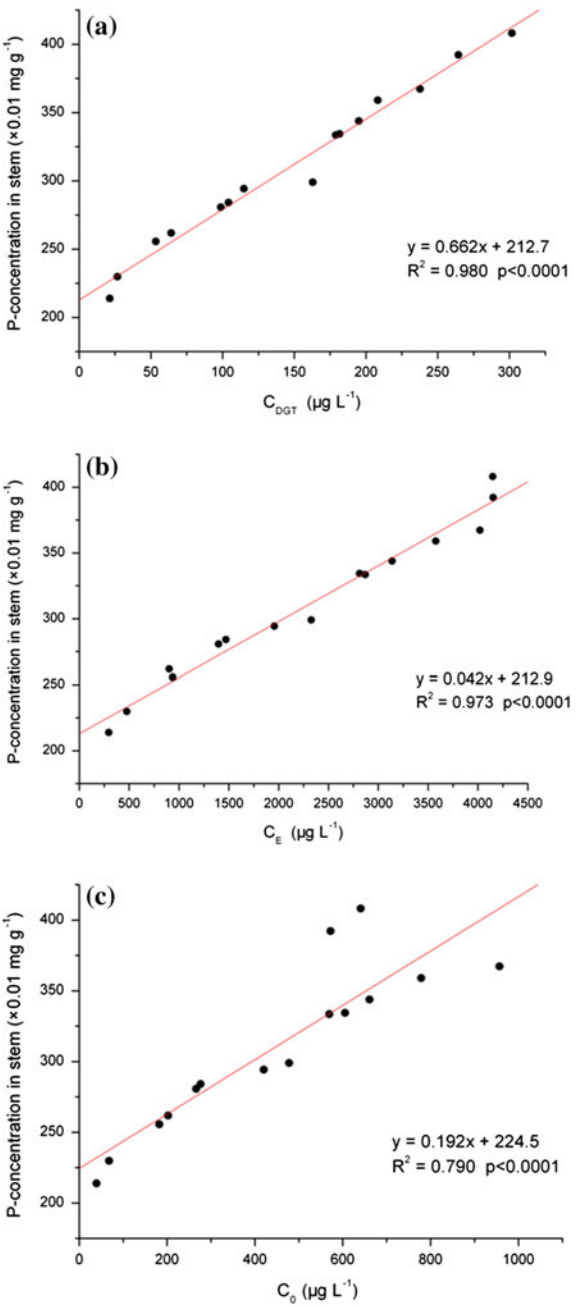

Fig. 8.7 The relationships between **a** C_{DGT} and C_{stem}; **b** C_E and C_{stem}; **c** C_0 and C_{stem} (in rhizobox for *Zizania latifolia)*

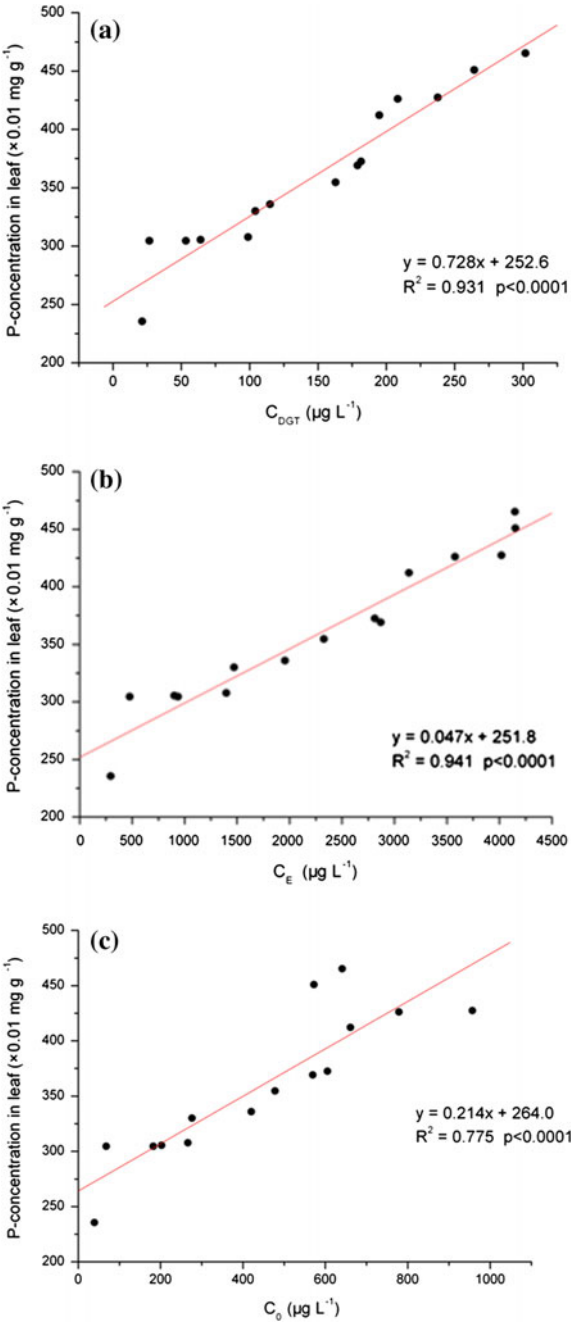

Fig. 8.8 The relationships between **a** C_{DGT} and C_{leaf}; **b** C_E and C_{leaf}; **c** C_0 and C_{leaf} (in rhizobox for *Zizania latifolia*)

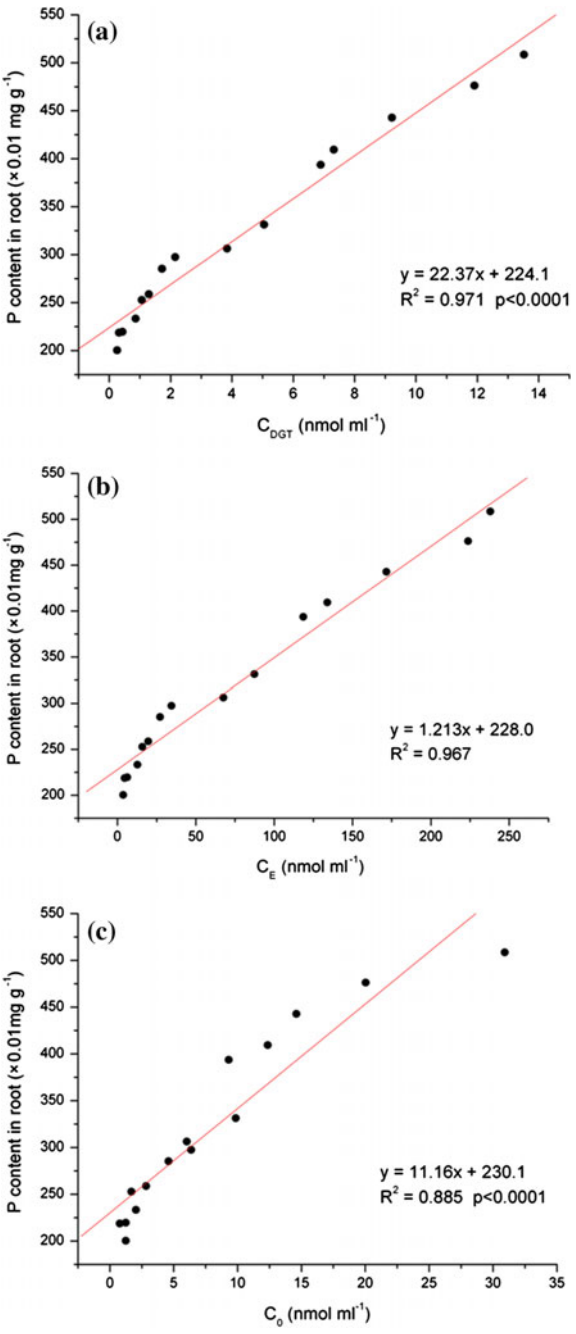

Fig. 8.9 The relationships between **a** C_{DGT} and C_{root}; **b** C_E and C_{root}; **c** C_0 and C_{root} (in rhizobox for *Myriophyllum verticillatum)*

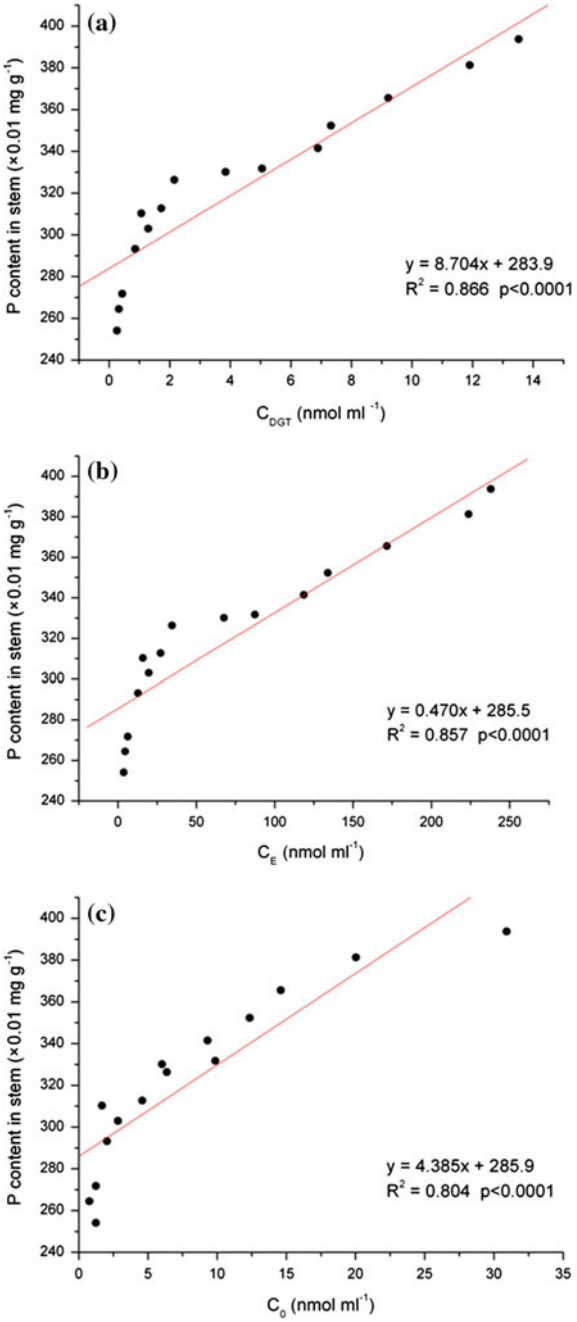

Fig. 8.10 The relationships between **a** C_{DGT} and C_{stem}; **b** C_E and C_{stem}; **c** C_0 and C_{stem} (in rhizobox for *Myriophyllum verticillatum)*

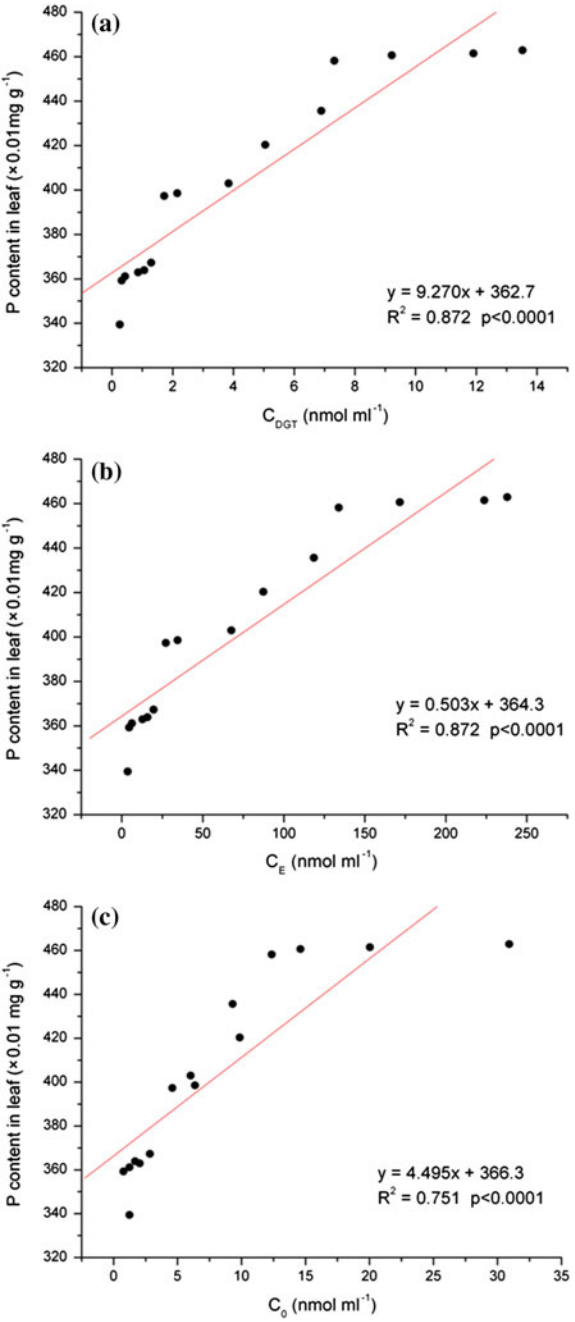

Fig. 8.11 The relationships between **a** C_{DGT} and C_{leaf}; **b** C_E and C_{leaf}; **c** C_0 and C_{leaf} (in rhizobox for *Myriophyllum verticillatum)*

C_{DGT}, relates to the effective concentration in the soil solution. The effective concentration differs from C_{DGT} with a factor that depends on the geometry of the device, deployment time, and sediment tortuosity. C_E, which can be derived by DGT device and 2D-DIFS model, is based on the understanding of diffusional plant uptake process. When the P-uptake by plant locally can cause the depletion of sediment concentration, C_E is believed to relate to plant uptake, directly. The case of transport-limited root uptake is the worst condition because element can be resupplied from both soil (sediment) and porewater. So, C_E provides an assessment parameter of the potential hazard of metals for one sediment type. For P-uptake in the rhizoboxes *(Zizania latifolia* and *Myriophyllum verticillatum), C_E* values in Tables 8.2 and 8.4 can be derived using 2D-DIFS model and provide a major step forward for assessing the hypothetical porewater concentration of P for P adsorbed by root.

8.3 The Significance of DGT as the Surrogate of Root for P-Uptake and the Implication for Ecological Restoration of Eutrophic Lake

Lake sediment zones within aquatic plants *(Zizania latifolia* and *Myriophyllum verticillatum*) with different levels of P in porewater and sediment produce plant tissues (root/stem/leaf) in field or in rhizobox. Little is known about P cycling in these sediments and the labile P relevant for plant uptake. Sediment porewater dynamics of field sediments for two kinds of plants were recreated under standardized laboratory conditions to investigate the mobility of P, in relation to P-content in plant tissues, using the dynamic sampling technique-diffusive gradients in thin films (DGT) and 2D-DIFS model. Based on the good linear relations between DGT-derived parameter-C_E (effective concentration) or C_{DGT} and P-contents in two plants, DGT can be used as a surrogate for P-uptake by root and predict the P-contents in root, stem, and leaf. This function of DGT has been verified by two kinds of DGT tests (in situ and in rhizobox) and the minor difference between two kinds of tests is that the value of R^2 for rhizobox is larger than that for in situ. The reason is that the conformation of rhizobox can allow DGT test at the precise location in the rhizosphere and the mixing procedure for sediment and sand according to certain proportion can make the physicochemical property in rhizobox homogeneous. Moreover, based on DGT-induced flux determined in situ in rhizosphere, the P-uptake ability by plant roots can be estimated, roughly. This estimation is significant for ecosystem restoration of lake system using aquatic plants. DGT test integrates a wider range of sediment properties, which impact on P-diffusion/P-release/P-adsorption than other single measurement approaches (sediment porewater or chemical extraction technique). DGT method also considers the dominant processes occurring in sediments during root uptake by lowering the

porewater concentration locally and engendering diffusive supply and release from complexes and the solid phase. So, DGT test in rhizosphere can reflect the "real" kinetic P-process across sediment/root interface and P taken up by root in lake.

8.4 Summary

Element uptake by aquatic plants is governed by element transfer at the sediment/root interface. If a plant root removes element from the sediment more slowly than the resupply by diffusion process, then the element concentration in porewater can govern the element content (free-ion activity) in plant tissue (root/stem/leaf) due to the negligible depletion of element at sediment/root interface. Uptake model based on free-ion activity such as BLM (Biotic Ligand Model) can explain this case and the significant relationships between concentrations in plant tissues and in sediment porewater. If uptake of element by plant root is fast relative to diffusional supply, then free ion is depleted at the interface of root/sediment, and diffusional transport to the root, the sediment pool, and the kinetics of release from sediment particle to porewater can be expected. In this case, the dynamic plant uptake model (DPUM) and DGT measurement at rhizosphere of aquatic plant can describe or reflect the behavior of elements in the rhizosphere, particularly with respect to interactions between solid and solution compartment. In particular, DGT, like plant roots, can locally lower the element concentrations in porewater and respond to the resupply from labile element in solution and sediment pool.

In Part III, the DGT test, in situ and in rhizobox, for two aquatic plants *(Zizania latifolia* and *Myriophyllum verticillatum*) was conducted in order to investigate the mechanism of P-uptake by aquatic plants, predict P-concentrations in plant tissues, and quantify P-uptake by root for the assessment of the effect of plant root on ecological restoration of lake systems. Both the in situ and in rhizobox DGT tests indicated the significant relationship (R^2) between C_E or C_{DGT} and P-contents in plant tissues (C_{root}, $C_{stem,}$ or C_{leaf}). For in situ DGT measurement *(Zizania latifolia),* R^2 between them were 0.945, 0.780, 0.823 *(*C_{DGT} and P-content in root, stem, and leaf, in turn) or 0.796, 0.917, 0.736 (C_E and P-content in root, stem, and leaf, in turn); for in rhizobox DGT measurement *(Zizania latifolia),* R^2 values between them were 0.864, 0.980, 0.931 *(*C_{DGT} and P-content in root, stem, and leaf, in turn) or 0.808, 0.973, 0.941 (C_E and P-content in root, stem, and leaf, in turn). For in situ DGT measurement *(Myriophyllum verticillatum),* R^2 values between them were 0.839, 0.718, 0.892 *(*C_{DGT} and P-content in root, stem, and leaf, in turn) or 0.832, 0.702, 0.892 (C_E and P-content in root, stem, and leaf, in turn); for in rhizobox DGT measurement (*Myriophyllum verticillatum),* R^2 values between them were 0.971, 0.866, 0.872 *(*C_{DGT} and P-content in root, stem, and leaf, in turn) or 0.967, 0.857, 0.872 (C_E and P-content in root, stem, and leaf, in turn), while the R^2 values

between C_0 and plant tissues for in situ or in rhizobox DGT tests were not as good as the R^2 of C_{DGT} or C_E versus P-contents in plant tissues. So, DGT measurement parameter (C_{DGT} or C_E) is a reliable tool for predicting P-content in plant tissues, especially for root. C_E, which was derived by DGT test and 2D-DIFS model, included both P-concentration in sediment porewater and a concentration which presents P-resupply from solid particle. When plant uptake locally lowered porewater concentration, C_E can be related directly to P-uptake by plants. The kinetically labile solid phase pool of P clearly plays an important role in the plant uptake and is included in the DGT measurement. The in rhizobox DGT test indicated more predicting function for P-contents in plant tissues than that in situ test due to the more accurate DGT test in the designed rhizobox. The P-transfer mechanism in rhizosphere included the P-release from sediment-P pool (NH_4Cl-P + BD-P) to porewater and the depletion of P-concentration in porewater due to P-uptake by root. Moreover, based on in situ DGT test, P-uptake ability of plant root for *Zizania caduciflora* or *Myriophyllum verticillatum* per year (180 d and 1 km^2 area) is calculated to be 3.74 or 2.92 tons a^{-1}.

Altogether, DGT test for aquatic plant indicates that DGT is a good predictor for P-content in plant tissues and it can act as a better proxy of plant root for the investigation of the P-resupply dynamics from the solid phase to solution and dynamic P-uptake by root. Furthermore, DGT-induced flux determined in rhizosphere can also be used to predict P removal ability of root to assess the function of aquatic plants to restore lake systems from the eutrophic status.

References

Hiltner L (1904) Uber neuere Erfahrungen und Probleme auf dem Gebiet der Bodenbakteriologie und unter besonderer Beriicksichtigung der Griindiingung und Brache. Arbeiten der Deutschen Landwirtschafts Gesellschafi 98:59–78

Kuchenbuch R, Jungk A (1982) A method for determining concentration profiles at the soil–root interface by thin slicing rhizosphere soil. Plant Soil 68:391–394

Wu ZH, Wang SR, He MC (2015) Element remobilization, “internal P-loading” and sediment-P reactivity researched by DGT (diffusive gradients in thin films) technique. Environ Sci Pollut R 22:16173–16183

Youssef RA, Chino M (1988) Development of a new rhizobox system to study the nutrient status in the rhizosphere. Soil Sci Plant Nutr 34:461–465

Chapter 9
Conclusion and Prospect

P-loading to lake systems comes from external or internal sources. When the "external P-loading" is reduced or controlled, the "internal P-loading" becomes more important because of the P-release from sediment to surrounding water and the related biogeochemical process. So, it is important to develop one kind of technique for the in situ research of P-process at SWI, including the quantification method for kinetic P-exchange at solid/water interface, the coupled geochemical reactions for P and related elements (Fe and sulfide) in sediment microzones, and the quantification method for Fe- or S(-II)-microniches related to P-release in sediments. Moreover, the aquatic plants can restore ecological system of lake water body through P-removal by plant roots. The in-situ and –rhizobox DGT tests at sediment/root interface are also important to investigate P-transfer in rhizosphere and assess P taken up by plant roots. DGT and the related techniques (CID, DIFS, LA-ICP-MS, and DGT measurement methods at SWI or sediment/root interface) can achieve the last aims. The DGT investigations for P-measurement and P-transfer at environmental interfaces of Dianchi and Erhai lakes as two case studies have solved and revealed the last questions.

9.1 The DGT and Related Techniques for Lake Research

The schematic graphic of the layout of the P and related elements measured by DGT, the conclusion about the P-transfer across SWI or sediment/root interface, and the further research for DGT measurement is indicated in Fig. 9.1.

In the research for P-transfer across SWI or sediment/root interface, and the P-release mechanism, a series of new DGT techniques and related methods have been developed in this book. In order to reveal the geochemical reactions for

S. Wang and Z. Wu, *DGT-based Measurement of Phosphorus in Sediment Microzones and Rhizospheres*, DOI 10.1007/978-981-10-0721-7_9

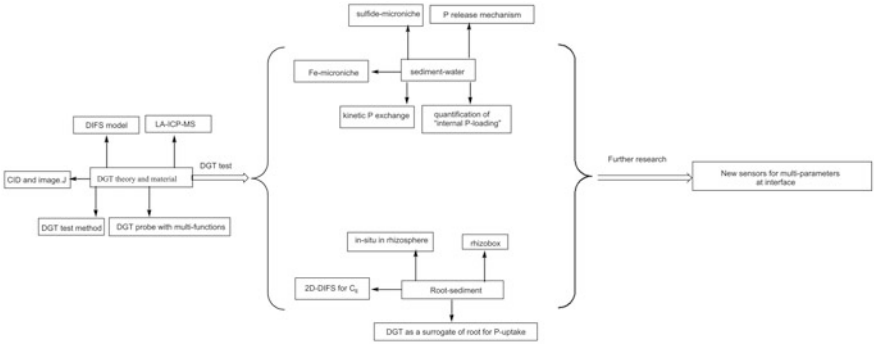

Fig. 9.1 The schematic graphic of the layout of the P and related elements measured by DGT, the main conclusion, and future research

P-release, the multi-layer-binding gel DGT probe, the twin DGT probes, the definition of the diffusive layer thickness, and the deployment method were designed for test. These DGT probes with new types included ferrihydrite/AgI/Chelex-100 DGT, AgI/Chelex-100 DGT, AgI/Chelex-100 DGT versus ferrihydrite DGT (back to back), and Chelex-100 DGT versus ferrihydrite DGT (back to back). By these kinds of DGT probes, P and related elements (S(-II) and Fe) can be measured at the same location in sediment porewater. The retrieved DGT resin can be analyzed for DGT profile or image. In order to investigate the kinetic P-process across DGT/porewater/sediment interface, the liable P-pool (NH_4Cl-P + BD-P) in anoxic sediment of Dianchi Lake was used for the calculation of DGT parameter K_D, which can be input into user's interface of 1D-DIFS model for the output parameter T_C and the DGT curves. CID for S(-II) analysis in sediment porewater was used for the AgI gel in ferrihydrite/AgI/Chelex-100 and AgI/Chelex-100 DGT probes, and DGT-S(-II) image with the spatial resolution of 42 μm can be used for the sulfide microniche research. The method used in the LA-ICP-MS instrument for the microchelex gel analysis at submillimeter scale was investigated for the distribution of Fe-microniche and the prediction of P-release. For the investigation of P-transfer across root/sediment interface, DGT as a surrogate of root was used for the in-situ or –rhizobox test, and 2D-DIFS model for the calculation of R_{diff} and C_E was developed for two aquatic plants (*Zizania latifolia* and *Myriophyllum verticiilaturn*) in Erhai Lake. In this book, the software programs (Visual MINTEQ, ImageJ. 1.38 e, and 1D/2D-DIFS) were used for the DGT image and data processing. Those DGT techniques with multi-functions can be utilized to reveal the P-release and kinetic P-process in lake sediment or rhizosphere at fine scale.

9.2 The Environmental Process of P and Related Elements in Sediment or Rhizosphere Revealed by DGT Technique and the Significance

9.2.1 The Mechanism and Release Intensity of "Internal P-Loading" and Kinetic Exchange of P at DGT/Porewater/Sediment Interface

DGT probes and pistons have been used for the measurement of labile P, Fe, and S (-II) in sediment porewater at mm or even submillimeter spatial resolutions. Based on the character of DGT-P/Fe-profiles and S(-II) images in seven sampling sites (A–G) at two seasons, the P-release mechanisms were mainly due to the reduction process of Fe (III) hydroxyoxide and subsequent P-release from Fe-bound P in anoxic sediments. The minor reasons were the breakdown of algae biomass in the uppermost sediment layer, and the formation of FeS(s) and the subsequent P-release from Fe-bound P. Based on diffusive flux across SWI, the "internal P-loading" in Dianchi Lake with the value of 17.01 t a^{-1} was derived.

The kinetic P-process for diffusion/desorption/adsorption at DGT/sediment interface (nine surface sediments in Dianchi Lake) can be researched by 1D-DIFS model. The sediment-P-pool was the total fraction of NH_4Cl-P and BD-P due to the P-release mechanism and was used for the calculation of K_d distribution ratio (134.7–1536 cm^3g^{-1}) for the input parameter. The output parameter T_C-response time (33–56,060 s), resupply parameter R (0.189–0.743), derived parameters-K_1 (1.51–2609 d^{-1}) and K_{-1} (0.03–13.13 d^{-1}), and the output curves for the *dissolved* concentration versus time/distance, and R value versus time at the DGT/porewater/sediment interface, were used to investigate how those parameters determined the dynamic process of P-exchange across DGT/sediment interface and to assess the release risk.

9.2.2 Sulfide Microniche for the Coupled Fe–S–P Biogeochemical Process and the Chemical Image of Labile Fe for the Prediction of P-Release

In this book, DGT/CID technique was used for the S(-II) images with the spatial resolutions of 42 μm, and sulfide microniche distribution, and the DGT flux related to niche peak can be quantified and assessed by the ImageJ. 1.38 e software. Circularity, area, peak flux, and R_{JM} can be used for the assessment of sulfide microniches due to the localized elevated sulfide formed as a result of oxidation of reactive organic matter, decaying organisms, algae aggregates, fecal pellets, and localized pyrite at the edges of the niches. Furthermore, at one site of sediment profile (site A), a plenty of sulfide microniches are distributed in two segments of AgI gel, which were corresponded to

the low DGT-Fe-concentrations and the distinct P-release at the same depth in sediment profile. The coupled Fe–S–P geochemical process can be observed to explain this mechanism for P-release. If Fe- and P-images at submillimeter spatial resolutions at the same position of sulfide microniches can also be determined, this mechanism can be explained more visually.

DGT/LA-ICP-MS has been investigated to measure labile Fe at submillimeter spatial resolutions with two dimensions. The derived DGT-Fe-images can be used to verify the existence of Fe-microniches and quantify DGT flux from "hot spots" ($> 9.36 \times 10^{-5}$ μg cm^{-2} s^{-1}) related to Fe-microniche peak in sediment microzone. The mechanism of Fe-microniche was mainly due to the localized supply of labile Fe from solid phase and the precipitation of FeS at the edge of Fe-microniche. Moreover, the Fe-"hot spots" or Fe-microniches in sediment microzone can engender the simultaneous release of Fe, and P or trace metals.

9.2.3 DGT as a Prediction Tool for P-Bioavailability and Transfer at the Sediment/Root Interface

Aquatic plants are commonly used for the environmental engineering for the controlling of lake eutrophication, and roots play an important role in the P-uptake and the P-exchange at sediment/water interface in lakes. In this book, the DGT tests in situ and in rhizobox for roots of two plants (*Z. latifolia* and *M. verticiilaturn*) were researched. For in situ and rhizobox tests, C_{DGT} and C_E derived by 2D-DIFS, C_0 (porewater concentration), and P-contents in plant tissues (root, stem, and leaf) can be quantified to study P-uptake mechanism by root. Both C_{DGT} and C_E can predict P-contents in plant tissues with the good linear regression parameter ($R^2 > 0.70$) between C_{DGT} or C_E and P-contents in tissues. P-transfer model across sediment/root (DPUM—dynamic plant uptake model) has also indicated the similar P-uptake character with that derived by DGT test in sediment/root microzones. The kinetic perturbation of solute concentrations by DGT in the sediment system is most likely similar to that occurring during plant uptake. So, DGT should be a reliable surrogate for the transport and P-release processes that affect the P-uptake by aquatic plants. Moreover, DGT flux during in situ test at the rhizosphere of *Zizania caduciflora* or *M. verticiilaturn* can be used to evaluate P-uptake capability by roots, roughly. The P-masses adsorbed by *Z. caduciflora* or *M. verticiilaturn* per year (180 d and 1 km^2 area) in Erhai Lake were calculated to be, respectively, 2.83 or 0.58 t km^{-2} a^{-1}.

9.2.4 The Significance for DGT Technique as the Ecological Indicator for P-Process at Sediment or Rhizosphere in Lakes

Environmental processes in sediments are central for large-scale P and other element cycling and ultimately regulate the ecological risk of them in the lake environment. Sediments store organic material (OM), nutrients, and redox-sensitive minerals (Fe and S(-II)), and the upper sediment horizons represent sites of intense remineralization and biogeochemical activity. Microbial communities regenerate organic material and nutrients, and the associated redox and pH dynamics regulate the mobility of many important trace elements (P, Fe, and S(-II)). The intense biogeochemical activity in lake sediment typically induces steep concentration gradients of the involved redox species. In the lake research, the requirement for the high-resolution measurement techniques for resolving these intense biogeochemical dynamics led to the development of microsensors. Traditional methods, mainly chemical extraction, can provide a simple differentiation of the labile and inert forms of P or other elements in sediments, but they are developed based on an operationally defined response to chemical reagents rather than on a true reflection of the liability of P or other elements. The thin-layer sampler DGT (diffusive gradients in thin films) is expected to be superior to extraction techniques by responding to the kinetic solid–solution interaction of P rather than a pseudo-equilibrium between the extractant and sediment. Furthermore, the P-uptake by DGT can mimic the uptake and migration of labile P in the root and sediment. Due to their similarity, DGT has also been successfully applied to assess the bioavailability and predict P-content in the plant tissues.

In order to reveal the mechanisms for "internal P-loading" of sediments, the geochemical reactions causing P-release in sediment microzone, the kinetic exchange of P at the sediment/porewater interface, the chemical image at submillimeter scale in two dimensions of Fe and S(-II) for the quantification of Fe- or S(-II)-microniches, the prediction for P-release related to Fe- or S(-II)-microniches, the assessment of P-transfer across sediment/root interface, and DGT techniques with multi-functions as the ecological indicator, have been developed to achieve the last aims.

The DGT probes with the multi-binding-gel layers have been developed to determine labile P, Fe, and S(-II) at the same position at the sampling site (Dianchi Lake). DGT profiles of labile P/Fe/S(-II) and DGT-S(-II) image at two dimensions can be researched for the P-release mechanisms, including the P-release from Fe-bound P, the coupled Fe/S(-II)/P biogeochemical reaction, and the breakdown of algae biomass in the uppermost sediment. Based on the vertical diffusive flux across SWI, the "internal P-loading" in lake sediments (Dianchi Lake) can be quantified. Furthermore, the solubility of Fe sulfide can be assessed by saturation index (SI) derived by the DGT profiles of Fe/S(-II) and Visual MINTEQ ver. 3.0 software. DGT pistons and 1D-DIFS have been developed to derive reaction and transport parameters and the curves of dissolved concentrations versus distance/time and

R versus time. The effect of the reaction/transport parameters on the P-transfer across DGT/sediment interface (Dianchi Lake) can be investigated in detail.

Microniches give us information about the geochemical processes occurring, but with a low resolution of a few mm, many of the microniches remain invisible. A significant advantage of DGT is the capability of the high-resolution measurement of the labile elements at the 2D scale, and the DGT-measured concentration is sensitive to the changes in the local increase or decrease of solution concentration as well as the solid-phase resupply. In this book, the DGT/CID has been used for the sulfide-image and DGT/LA-ICP-MS has been developed for Fe-image, both at spatial resolutions of submillimeters in two dimensions. The sulfide- and Fe-microniches in Dianchi Lake have been quantified according to the niche peak flux and the percentage of DGT flux related to microniche peak to the total DGT flux at the studied DGT resin. The formation mechanisms for Fe- or S(-II)-microniches were researched, and their effect on P-release in sediment microzones has also been revealed.

The P-uptake mechanism by roots of two aquatic plants in Erhai Lake has been researched by DGT test in situ and in rhizobox. C_E (the effective concentration) has been calculated by 2D-DIFS model. Both C_{DGT} and C_E indicated the good linear relationships with P-contents in plant tissues, indicating DGT as a predictor for the P-accumulation in plant tissues and a surrogate for the P-uptake by plant roots in sediments. DGT flux can be used for the quantification of P-uptake capability by roots and the assessment of the restoration effect on eutrophic lake.

DGT and the related techniques, including DIFS, CID, LA-ICP-MS, and DGT test methods in sediment or rhizosphere, have been developed for the "internal P-loading," the kinetic P-exchange at solid/water interface, the quantification of DGT fluxes related to microniches, and the P-transfer at sediment/root interface. The DGT methods applied in two lakes as case studies, the P-mobilization mechanisms and the quantification/calculation results for DGT parameters, indicate DGT is an effective indicator for the P-transfer and release risk in microzones (sediment or rhizosphere).

9.3 Further Work—the New Technique Coupled with DGT for Sediment Microzone or Rhizosphere

In this book, the DGT probes with multi-functions, DGT piston, and related techniques have been used for the DGT-P distribution in sediment porewater at fine scale, kinetic P-exchange across DGT/porewater/sediment, and P-transfer across sediment/root interface. "Internal P-loading" of Dianchi Lake and P-uptake mechanism by plant root in Erhai Lake has been revealed. However, the technique of LA-ICP-MS for Fe-image in sediment porewater is expensive and several DGT images cannot be obtained to research the comprehensive information about geochemical process in the whole lake. Moreover, the pH/O_2 at the similar spatial resolution with that of DGT image should also be tested because the geochemical

reaction at submillimeter scale is related to redox potential and pH distribution at the same location.

As the dynamics of the biogeochemical processes occurring at sediment microniches is the key to improve our understanding of early diagenesis, further works should also be done to develop sensing techniques such as DGT-optode sandwich sensors for the images with multi-parameters and to investigate biogeochemical process under complex redox and pH dynamics in sediment microzone or rhizosphere. The dual-layer "sandwich" sensors that combine planar optodes and DGT gels can be applied for the simultaneous determination of trace elements and pH/O_2. The very thin DGT gels are required to minimize blurring of the optode. The simultaneous measurement of elements (P or trace metals) and pH/O_2 for chemical map at the fine scale is required to be developed to investigate the complex biogeochemical processes for P-release in sediment microzone or the P-transfer across sediment/root coupled with multiple solute species (trace metals or sulfide) under complex microenvironmental conditions (pH and O_2).

9.4 Summary

This chapter mainly summed up the DGT techniques (DGT probes with new types, the deployment method for DGT at SWI or sediment/root interface, DIFS model, CID, LA-ICP-MS, software programs—Visual MINTEQ and ImageJ. 1.38 e) for the measurement of P and the research of P-transfer/P-release. The main conclusions about the mechanism of "internal P-loading" and the kinetic exchange of P in sediment microzone in Dianchi Lake and the P taken up by roots of aquatic plants in Erhai Lake were also indicated and discussed. The significance of DGT as an ecological indicator or a surrogate for the investigation of P-transfer or P-uptake at lake interfaces was also remarked. The research in this book tried to develop DGT technique for the measurement of P and related elements at lake interfaces and to reveal the environment processes (P-transfer and P-release) and geochemical reactions with a new perspective, compared with conventional methods (chemical extraction, linear distribution coefficient (K_d), a nonlinear adsorption isotherm, or "bulk" analysis method). Based on DGT profile/ DGT image and DIFS simulation, the theme about "internal P-loading" in Dianchi Lake was discussed. The mechanisms for P-release from sediment were as follows: P-release from Fe-bound P during the reduction of Fe (III) hydroxyoxide in anoxic sediment, the decomposition of algae biomass in the uppermost sediment layer, and the coupled Fe–S–P geochemical reaction. The "internal P-loading" in Dianchi Lake was about 17.01 t a^{-1} and accounted for 2.6 % of the total "entering P-loading" (648 t a^{-1}). The DIFS model for nine sites in Dianchi Lake can derive kinetic parameter T_C (33–56,060 s), distribution coefficient K_d (134.7–1536 cm^3 g^{-1}), and resupply parameter R (0.189–0.743). The DIFS curves of dissolved concentration and R value at the DGT/porewater/sediment interface during DGT measurement were used to research how kinetic parameter and sediment-P-pool determine the P-release character at this interface. Sulfide microniches on the

submillimeter scale were determined using CID and assessed according to distribution, area, shape, and niche peak flux. Microchelex gel and LA-ICP-MS can derive DGT-Fe-image at two dimensions on submillimeter scales, which can be used to reveal the existence of Fe-microniche and the prediction of P-release from Fe-microniche. DGT test in the rhizosphere of aquatic plants (*Z. latifolia* and *M. verticiilaturn*) in Erhai Lake indicated that DGT can act as a surrogate of root for P-uptake and predict P-content in plant tissues. In order to achieve the aim for the further research of element dynamics and biogeochemical reactions at lake microzones (sediment microzone or rhizosphere), the multi-sensor techniques should be developed to derive chemical images with multi-parameters (solutes, pH, or O_2) at submillimeter scale.